# University of Alberta

## Kinetic Model for a Platinum Diesel Oxidation Catalyst

by

Carolina Sola Quiroz

A thesis submitted to the Faculty of Graduate Studies and Research
in partial fulfillment of the requirements for the degree of

Master of Science

in

Chemical Engineering

Department of Chemical and Materials Engineering



Fall 2011
Edmonton, Alberta

## Abstract

Using data from artificial gas mixtures, global kinetic models for a platinum diesel oxidation catalyst are developed. The modelling of CO and $C_3H_6$ was inspired by the classical work of Voltz et al.[1], while the modelling of NO and $C_3H_6$ was based on the earlier work of Pandya[2], Mulla et al.[3], Bhatia et al.[4] and Hauff et al.[5]. The creation of the model was performed piecewise, starting from experiments on single reactants. A new model is proposed to account for the formation of $N_2O$. A global model is developed that is able to correlate with reasonable accuracy the results from the complete gas mixture. The model is not, however, able to correlate all of the data from feeds containing the complete set of reactants and those with single or dual reactants present.

## Acknowledgements

Special Thanks,

- to Professor Dr. R.E. Hayes who mentored, supported and inspired me with his passion, wisdom and knowledge.
- to Auto21 for providing the financial support
- to Umicore AG for providing the catalyst monolith.
- to Ali Abedi from the University of Waterloo for taking the data.
- to Jason Boddez, Dallin Bullock, Prof. Dr. D. Checkel and Dr. J. Olfert from the Department of Mechanical Engineering of the University of Alberta, for all their help, assistance and support obtaining data from a real engine exhaust.
- to Dr. Joe Mmbaga and Teng-Wang Nien for their continuous help and support, and for making the lab ambience always pleasant.
- to Italo San Martin for taking the chance and have believed on this. For taking care of me, and supporting me every since day one, with his love, patience and comprehension becoming on the best roommate, the best friend and the best partner I could ever have asked for.
- to my parents Yolanda and Alberto, my brother Andres, my cousin Sebastian, my grandparents and family, for believing in me, have continuously given me their unconditional love and being always so close to me despite the distance.
- to the San Martin family and Marina, who have become in my second family, and have treated me back just as if I would really be part of theirs.
- to Hector De la Hoz, Rosa Rueda, Carolina Figueroa, Mariangel Rivolta, Roberto Fedon, Lina Parra, Alfonso Garcia and Venkat Nadadoor, “classmates” and close friends, who were always there to help me and support me, with their friendship, love and wisdom.

# Table of Contents

## List of Tables

## List of Figures

## List of Symbols

| Symbol | Units | Description |
|---|---|---|
| $C$ | $mol/m^3$ | Concentration |
| CPSI | $units/in^2$ | Channels per square inch |
| STP | - | Standard conditions for temperature and pressure |
| $u_m$ | $mol/m^3$ | Bulk molar concentration |
| $Y_j$ | - | Mol fraction of species $j$ |
| $(-R_j)$ | $mol/m^2 \cdot s$ | Rate of disappearance of species $j$ |
| $z$ | m | Length of reactor |
| $V_W$ | $m^3$ | Washcoat volume |
| $V_C$ | $m^3$ | Channel volume |
| $D_{WC}$ | m | Diameter of circular cylinder before washcoat |
| $D_H$ | m | Diameter of circular cylinder after washcoat |
| $O_i$ | - | Objective function of the optimization |
| $X_{exp}$ | - | Experimental data |
| $X_{pred}$ | - | Predicted data |
| $k_i$ | $mol^{1-n} \cdot m^{3(n-1)} \cdot s^{-1}$ | Kinetic constant / Rate coefficient for a reaction of order "n" |
| $A_i$ | $mol^{1-n} \cdot m^{3(n-1)} \cdot s^{-1}$ | Pre-exponential factor of the Arrhenius equation for the kinetic constant $i$ |
| $E_i$ | J/mol | Activation energy for the kinetic constant for the kinetic constant $i$ |
| $R_g$ | $J/(mol \cdot K)$ | Gas constant |
| $T$ | K or °C | Temperature |
| $K_j$ | $mol^{1-n} \cdot m^{3(n-1)} \cdot s^{-1}$ | Adsorption equilibrium constant / Rate coefficient for a reaction of order "n" |
| $B_j$ | $mol^{1-n} \cdot m^{3(n-1)} \cdot s^{-1}$ | Pre-exponential factor of the Arrhenius equation for the adsorption constant $j$ |
| $H_j$ | J/mol | Activation energy for the kinetic constant for the adsorption constant $j$ |
| $\beta$ | - | Equilibrium term |
| $P$ | bar | Pressure |
| $K_{eq}$ | - | Equilibrium constant |

# 1 Introduction

During the 1960's, with air pollution becoming a major concern, especially in the large population centres, automotive emissions became a major concern to the population due its negative effect on human health. Gasoline and diesel engines produce emissions such as hydrocarbons (HC), carbon monoxide (CO), nitrogen oxides ($NO_X$) and particular matter (PM or soot), that in high level emissions can cause, among other things, brain damage, respiratory problems, lung tissue damage, reduction of cardiovascular function, and even coma or death [6, 7].

For these reasons the reduction of these kinds of emissions was imperative, and today, the most effective solution is called catalytic converter. There are different kinds of catalytic converters, but what all have in common is the ability of converting some of the original emissions into others that are less harmful using a catalyst. The most popular kind of catalytic converter used for mobile sources uses a monolithic honeycomb type core usually made of cordierite, which is covered with a washcoat of Alumina ($Al_2O_3$) that contains particles of a catalyst metal such as Platinum (Pt), Palladium (Pd), Rhodium (Rh), or a combination of them. The catalytic reactions occur within this thin washcoat layer.

For gasoline engines the most common converter type is the three way converter, which requires a stoichiometric fuel air ratio to obtain the required conversion. In lean burn engines, such as Diesels, the process of conversion is more complicated than for regular gasoline engines, because the emissions contain an excess of oxygen. The excess of oxygen facilitates the oxidation of CO and HC's, but in consequence, the reduction of NO is hampered, because it needs to compete for the hydrocarbons before they oxidized in order to do so [2]. Normally a separate reactor is used to reduce the $NO_X$.

## 1.1. State of the Problem

Computer simulation of the catalytic converter can be a useful design tool that reduces the cost of development. A requirement of a computer model is a kinetic model for each of the reactions. Because the kinetic parameters are unique for each catalyst, it is also desirable to have an efficient and rapid methodology for determining such parameters for a new catalyst. Kinetic trials for new catalytic configurations are time consuming. Furthermore, the strong mass and heat transfer become a big issue while experimenting under realistic operating conditions, because it is very difficult to achieve isothermal conditions due to the large heat of reaction produced during the process [8].

Based on these facts, a method to predict kinetic parameters accurate enough for design purposes is wanted. To achieve this goal, the investigation of the kinetics in the reactors is necessary. The final objective is to be able to simulate through a kinetic model that represents the process, the same conditions found in practice. The underlying mechanisms of the process do not need to be necessarily correct, but must represent the process accurately [8].

Voltz published in 1973 [1] a model for the CO and $C_3H_6$ oxidation in the presence or absence of NO. In this paper experiments with real and synthesis gas mixtures were compared, and so pellets and monolith type of catalysts. The work done in that research has been widely used by many investigators until today, with many changes and subtle variations, becoming the start point for many studies in this area of research, and also for this investigation.

## 1.2. Thesis Objective

This project focused on finding a model that is able to reproduce the behaviour of the conversion of the gases found in a Diesel exhaust in a piece

wise way, for a platinum diesel oxidation catalyst. Through this process, values for the kinetic parameters are found. Since the kinetic model is not necessarily mechanistically correct, the values only have a mathematical meaning. The research studied variations of the models proposed by Voltz [1], Pandya [2], Mulla [9], Bhatia [4] and Hauff [5]. The model proposed is evaluated using experimental data obtained at the University of Waterloo, all with different initial concentration and combination of the gases. These data were used to test various kinetic models using appropriate reactor models and optimization software.

## 1.3. Layout of the Thesis

The thesis starts with an introduction of the work that will be developed, followed by the background information, which involves the emissions coming from a motor vehicle and more specifically, from a diesel engine vehicle. Information about how the emission regulations are treated in Canada is complemented with the impact that these emissions have on our health and our environment. A general description of ways to control exhaust emissions and a small section dedicated exclusively to diesel oxidations catalysts is also included, to finalize with the explanation of the data collecting process, the models tested and the results of the modelling process applied.

# 2 Background

## 2.1. Emissions

### 2.1.1. Motor Vehicle Emissions

Motor vehicles have become an indispensable tool for our daily life. They are with us everywhere, used to shorten travel times, to protect us from the harshness of weather, to help us move objects, etc. But there is a trade off. All motor vehicles produce harmful emissions that put in risk our health and the well being of the planet we live in. Gases emitted by motor vehicles such as $CO_2$, $CH_4$ and $N_2O$, [10] contribute to global warming, and gases such as CO, $CO_2$, NOx, $O_3$ and $SO_2$ can produce serious damage to our health.

The main toxic emissions generated by cars, trucks and off-road vehicles are CO, HC's and NOx, and its respective contribution to the total amount of these pollutants in most of the urban areas of developed countries, can be represented as a generality by the following proportions [11]:

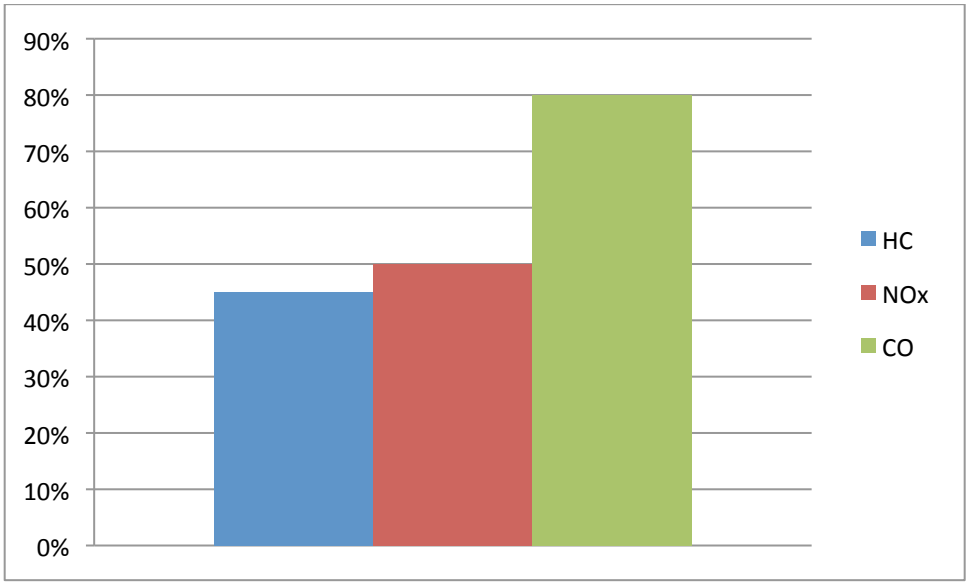


**Figure 1:** Cars, trucks and off-road vehicles % contribution to the total amount of CO, HC and $NO_X$ in developed countries urban areas.

The hydrocarbons found in the exhaust can be the result of unburned fuel that was trapped in small places within the engine cylinder such as crevices, where the flame could not penetrate. An initial solution to this problem is to make these crevices as small as possible, but this effort is not sufficient.

The $NO_X$ is produced primarily due to the high temperatures achieved in the cylinder during the air-fuel combustion process, so a solution is to try to decrease the temperature within the cylinder. One way of achieving this purpose is to recirculate a portion of the exhaust gas to the intake to dilute the fuel-air mixture, thus decreasing the temperature of the combustion.

The amount of CO produced depends on whether the engine is running stoichiometric, with excess of fuel (rich), or with excess of air (lean). When the engine is running lean, the amount of oxygen is enough to oxidize in the process most of the CO into $CO_2$. That is the case in Diesel engine vehicles. But modern Spark-Ignition (SI) vehicles run in a close-to-stoichiometric point, which means that a fair amount of CO is still emitted.

For all these reasons, an exhaust control system capable of reducing the amount of these three different kinds of pollutants is necessary, and that is exactly the role played by the catalytic converter [11].

**Diesel Engine Emission**

For the particular case of Diesel engines, the emissions are divided into three different kinds [12], solids, liquids and gaseous emissions, consisting of CO, HC's, $NO_X$ and particular matter. The particulate matter (PM) is considered a combination of the solid and liquid emissions, formed by:

- Organic liquids, also called SOF (soluble organic fraction) or VOF (volatile organic fraction), composed of unburned fuel and lubricating oils;
- Inorganic oxides, such as sulphates, that will turn into $H_2SO_4$, after reacting with the moisture in the exhaust;

- Dry carbon or soot.

Diesel engines may emit lower amounts of noxious emissions compared than gasoline engines. However, because of the excess oxygen present in the exhaust, the elimination of $NO_X$ poses a bigger challenge.

### 2.1.2. Emissions and Regulation in Canada

In Canada the regulation of emissions produced by internal combustion engines is under the authority of *Transport Canada* and *Environment Canada*. *Transport Canada* is responsible of regulating railway locomotives, aircraft and commercial marine vessels, while *Environment Canada* regulates the rest of the emissions related to engines.

In 1971, for the first time, and under the *Motor Vehicle Safety Act*, Canada stared regulating the amount of emissions produced by on-road vehicles. During those days, the only entity in charge of controlling emissions was *Transport Canada*. It wasn't until 2000 with the Canadian Environmental Protection Act 1999 (CEPA 1999) that *Environment Canada* took control of off-road and some of the on-road vehicle emission standards.

Since 1988 the on-road vehicle emission standards have been aligned with the U.S. Environment Protection Agency (EPA) federal standards as much as possible, and in 2001 with the *Federal Agenda on Cleaner Vehicles, Engines and Fuels* it was extended to off-road vehicles emission standards and fuel standards as well [13].

The current governing regulations standards for Light-Duty-Vehicles (LDV) initiated with the creation of two set of standards that the EPA stated in the Clean Air Act Amendments (CAAA) in 1990. These standards are:

- Tier 1 standards, with a period of completion between 1994 and 1997.
- Tier 2 standards, with a period of completion between 2004 and 2009.

Tier 1 standards were applied to all new light-duty vehicles (LDV) and separate its standards into two groups according to the weight of the vehicles, “light LDV’s” and “heavy LDV’s”.

Tier 2 standards have more strict emission limits compared to Tier 1, and they are applied to all LDV’s, plus medium-duty passenger vehicles (MDPV). A major difference between Tier 1 and Tier 2, is that Tier 2 does not make a difference by weight. It includes heavier vehicles, so that every vehicle considered to belong to this group, regardless of the fuel that it uses, has to meet the same limits.

Tier 2 also brought restrictions for the sulfur content of fuels, demanding a reduction in the amount of sulfur present in gasoline and diesel fuel. This requirement was necessary to allow more advanced aftertreatment devices.

Tier 2 is divided in 8 different certificates called “Bins”. All of the vehicles regulated under Tier 2 have to meet the limits specified by one of the 8 different bins. Starting with the 2009 model cars, not only all the LDV and MDPV vehicles have to choose among the 8 bins to be certified by one of them, but also, the entire LDV or MDPV fleet sold by each manufacturer has to meet the average $NO_X$ standard of 0.07 g/mi.

During the phase-in period, 3 additional temporary certification bins were included. The bins 9, 10 and 11 were more relaxed in limitations to allow ease the process for achieving the goal emissions, but that period expired with the 2008 model year [13].

Examples of the Tier 2 for intermediate life and full useful life, are shown in tables 1 and 2:

**Table 1:** Tier 2 Emission Standards, Federal Test Procedure, g/mi, for Intermediate life (information taken from [13])

| Bin# | Intermediate life (5 years / 50,000 mi) | | | | |
|---|---|---|---|---|---|
| | NMOG * | CO | NOx | PM | HCHO |
| 8 | 0.100 (0.125) | 3.4 | 0.14 | - | 0.015 |
| 7 | 0.075 | 3.4 | 0.11 | - | 0.015 |
| 6 | 0.075 | 3.4 | 0.08 | - | 0.015 |
| 5 | 0.075 | 3.4 | 0.05 | - | 0.015 |
| 4 | - | - | - | - | - |
| 3 | - | - | - | - | - |
| 2 | - | - | - | - | - |
| 1 | - | - | - | - | - |

* Only for Diesel fueled vehicles

**Table 2:** Tier 2 Emission Standards, Federal Test Procedure, g/mi, for full useful life (information taken from [13])

| Bin# | Full useful life | | | | |
|---|---|---|---|---|---|
| | NMOG* | CO | Nox | PM | HCHO |
| 8 | 0.125 (0.156) | 4.2 | 0.2 | 0.02 | 0.018 |
| 7 | 0.09 | 4.2 | 0.15 | 0.02 | 0.018 |
| 6 | 0.09 | 4.2 | 0.1 | 0.01 | 0.018 |
| 5 | 0.09 | 4.2 | 0.07 | 0.01 | 0.018 |
| 4 | 0.07 | 2.1 | 0.04 | 0.01 | 0.011 |
| 3 | 0.055 | 2.1 | 0.03 | 0.01 | 0.011 |
| 2 | 0.01 | 2.1 | 0.02 | 0.01 | 0.004 |
| 1 | 0 | 0 | 0 | 0 | 0 |

* Only for Diesel fueled vehicles

### 2.1.3. Emissions Impact in Health

Since we are exposed to various kinds of pollutants simultaneously, it is difficult to define the responsibility of each one in our health while developing a disease, particularly because many illnesses are the result of being exposed chronically to these toxic gases. An effective way of reducing these risks, is by controlling and regulating the air quality that we are surrounded by [7].

**Carbon Monoxide (CO)**

CO is produced by incomplete combustion of carbon-containing materials. It is a very light and odourless gas that is rapidly absorbed by the lungs. Thus, the CO easily binds with the hemoglobin in the red blood cells, decreasing the capacity of the hemoglobin to transport $O_2$, carrying the CO instead. This way, tissues with high demand of $O_2$, such as brain and parts of the nervous system, are first affected by CO intoxication.

Early signs of intoxication are among others, dizziness, confusion, short of breath, headache, and lack of motor coordination. Final states may include loss of consciousness and death [7].

**Carbon Dioxide ($CO_2$)**

$CO_2$ is odourless and heavier than air. It is produced by burning carbon-containing materials and it also is an end-product of a metabolic process in the body. Very high concentrations of $CO_2$ in the air can replace the amount of oxygen necessary for the body, producing hyperventilation, headache and sweating, followed in extreme cases by loss of consciousness by asphyxia and death [7].

**Nitrogen Oxides ($NO_X$)**

Within the family of nitrogen oxides, the production of nitrogen dioxide ($NO_2$) is particularly harmful. It is a gas with a very irritating odour that can affect the bronchioles and alveoli. In high concentrations it may produce a pulmonary edema, problems related with lack of oxygen in tissues (for a similar reason than CO), or even death [7]. $NO_2$ also is an absorber of UV light, which makes it promote the formation of ozone according to the reactions:

$$NO_2 \xrightarrow{UV} NO + O \tag{2.1}$$

$$O + O_2 \rightarrow O_3 \quad (2.2)$$

**Ozone ($O_3$)**

Ozone ($O_3$) is a strong oxidant that may cause chest discomfort, dryness of the throat, eyes irritation and cough under low concentrations exposure. Under higher concentrations, it may produce pulmonary edema, and it could contribute to develop emphysema for some people [7].

**Sulphur Dioxide ($SO_2$)**

$SO_2$ is a very irritating gas that in fairly low concentrations can be smelled and even tasted. Its solubility in water is remarkable, being easily absorbed by the airways and mucous membranes of the body, producing a quick response and irritation in mouth, nose, eyes and upper respiratory track. High exposure to this gas could produce laryngeal spasm or pulmonary edema, both with possibility to be fatal [7].

### 2.1.4. Emissions Impact in Greenhouse Effect

It has been observed in the past century, an increase of 0.5°C in the Earth's surface temperature. A natural global warming cycle is known to happen every few thousands of years. But at these rates, and considering the amount of agents that human activities developed mainly during the 1900's that have been released to the atmosphere, and that are proven to affect and enhance the greenhouse effect, seem to indicate that we could be facing a most dramatic climate change. There are many theories supporting and opposing the fact that these changes may or may not be the result of human activities.

Some of the most important greenhouse gases emitted by engine vehicles are, carbon dioxide ($CO_2$), water vapour, nitrous oxides ($N_2O$) and ozone ($O_3$)

[14]. The reason why these gases produce the greenhouse effect, is because they have the capacity to permit the passage of radiation when it comes from the sun. When the radiation is reflected by the Earth, these gases capture the reflected energy because of the shift in its wavelength thus potentially increasing the Earth surface temperature [15].

Diesel engines offer a friendly alternative to address these issues. It presents good fuel efficiency, which means less unburned HC's that are precursors of photochemical smog, and low emissions of $CO_2$ and NOx [14].

Black soot produced due to the incomplete combustion in aerosols, is believed to be an important global warming agent due its capacity of adsorbing sunlight and heating of the lower atmosphere. This same black soot is a product in the diesel engine exhaust, but it is one of the emissions also controlled by the exhaust emissions control devices [14].

## 2.2. Exhaust Emissions Control

Even though Diesel compression-ignition (CI) engine vehicles are becoming increasingly popular, spark-ignition (SI) engine vehicles fueled with gasoline still represent the majority.

### 2.2.1. Spark-Ignition (SI) Engines Exhaust Control

The catalytic converter used by SI vehicles is the Three Way Catalyst (TWC) which successfully removes a large portion of the three main pollutant emissions, CO, HC and $NO_X$.

TWC works with stoichiometric air-fuel exhaust gas, which means that for its proper performance, is necessary to control of the air fuel ratio, to ensure that the correct mixture is used. To do so, oxygen sensors are placed in the exhaust manifold, and with that feedback, the control system is able to regulate the

quantity of fuel injected. The stoichiometric operation is necessary because HC and CO require an oxidizing environment and $NO_X$ requires a reducing environment to be removed, and stoichiometric exhaust gas provides a window where this two environments exist simultaneously, giving effective removal of all emissions [11].

### 2.2.2. Compression-Ignition (CI) Engine Exhaust Control

The most popular kind of vehicles that use compression-ignition (CI) engine, are diesel vehicles. They work with vaporized fuel that mixes with the high-temperature air within the cylinder chamber, and as a result of the compression of the piston, the mixture spontaneously ignites, without the necessity of a spark. The main exhaust gases to be treated are, as before, CO, HC and $NO_X$, however, they are now in a lean environment with excess of oxygen, plus a new and complex problem, particulates or soot.

Diesel emissions are relatively low in HC and CO due their almost complete combustion, which is a result of the excess oxygen in the system. But since the combustion temperatures are high and the quantity of NOx emissions produced is directly proportional to it, the reduction of NOx becomes one of the major challenges along with the soot that also adsorbs high molecular weight HC's.

$NO_X$ and particulate emission control has been improved by modifying the combustion process that allows an increase in the air-fuel mixing rate. Better control of the lubricant has reduced the high molecular weight HC particulate component that is adsorbed on the soot. In addition, the control of the inlet air temperature has helped to reduce the amount of $NO_X$ [11].

TWC is not an option to treat this kind of exhaust due the excess of oxygen in it, so different and complementary solutions have had to be developed.

**External Exhaust Gas Recirculation (EGR)**

Exhaust Gas Recirculation is a method that consists in taking a fraction of the exhaust gas back to the intake in order to decrease the oxygen concentration, reducing the partial pressure, which allows slowing down the combustion process and in consequence decreases the combustion temperature, which directly affects the production of $NO_X$.

EGR is one of the most effective methods to meet the $NO_X$ emission standards. In the case of diesel engines, it is possible to recirculate as much as 50% of the exhaust gas without affecting significantly the combustion stability, which is one of the major concerns [16, 17].

There is, however, a trade-off when decreasing the temperature of the exhaust. At lower temperature the amount of $NO_X$ is reduced, but due to the combustion temperature has been decreased, the formation of Particular Matter (PM) increases [12].

**Selective Catalytic Reduction (SCR)**

Selective Catalytic Reduction is a method to reduce the amount of $NO_X$ in the exhaust in a lean environment, and is thus appropriate for a Diesel engine. Notice that, once again the cleanness of the fuel plays a very important role; metals and sulphur content in the fuel deactivates the catalysts quickly. [18]

There are two kinds of SCR systems, those using ammonia and those using hydrocarbons. In both cases, the reactor has a honeycomb shape with a washcoat layer of catalyst.

*SCR by ammonia ($NH_3$)*

This method of $NO_X$ reduction has been widely used in large scale applications, such as power generation plants, and has recently seen adoption in automobiles. Ammonia ($NH_3$) is injected into the exhaust stream, where it reacts

over a suitable catalyst with $NO_X$ to produce $N_2$ and $H_2O$. This reaction has to be carried out at a temperature between 320 and 400 °C, depending on the amount of $SO_X$, to avoid plugging the catalyst and to have a good efficiency. [18]. Typically both NO and $NO_2$ react according to: [18]

$$4NO + 4NH_3 + O_2 \rightarrow 4N_2 + 6H_2O \quad (2.3)$$

$$6NO_2 + 8NH_3 \rightarrow 7N_2 + 12H_2O \quad (2.4)$$

In a vehicle the ammonia is usually carried as a solution of urea. The urea has to be converted in ammonia through the following possible reactions: [18]

$$CO(NH_2)_2 + H_2O \rightarrow CO_2 + 2NH_3 \quad (2.5)$$

Or:

$$CO(NH_2)_2 + H_2O \rightarrow HNCO + NH_3 \quad (2.6)$$

$$HNCO + H_2O \rightarrow CO_2 + NH_3 \quad (2.7)$$

*SCR by hydrocarbons*

In SCR by hydrocarbons the $NO_X$ reacts with hydrocarbons in the exhaust to form $N_2$ and $H_2O$. One problem with this method is the competitive oxidation and reduction reactions involving hydrocarbons. The ratio between NO and $NO_2$ is not an issue for the conversion. There are tight temperature constraints for the SCR by hydrocarbons.

Because of the limitations of SCR by hydrocarbons, a development of this method is the $NO_X$ trap. In this application, BaO is added to the catalyst, which reacts with $NO_2$ to form $BaNO_3$. After all of the BaO has reacted, the engine runs rich to produce hydrocarbons, which then react with the $BaNO_3$ to produce $N_2$ and $H_2O$. [14, 19]

**Diesel Particulate Filter (DPF)**

As previously mentioned, one of the most difficult emissions of a diesel exhaust to process, is the particular matter. As the name suggests, this is a device that filters the particular matter by blocking them within the channels. Since the particular matter accumulates in these channels, a method to regenerate the traps is needed. Using oxygen requires temperatures close to 600°C, which is excessively high for a diesel exhaust. Using $NO_2$ requires much lower temperatures to oxidize the accumulated particular matter. But 275°C it is still too high for light duty diesel engines. The solution to this problem is to increase the temperature through fuel injection to oxidize the soot, regenerating periodically the diesel particulate filter [14], [19].

**Diesel Oxidation Catalyst (DOC)**

In a Diesel exhaust system, the first catalyst is usually a diesel oxidation catalyst (DOC). The DOC oxidizes CO, hydrocarbons, and NO. Over a narrow temperature window, some SCR by the hydrocarbon may occur. Different metals have been tested in efforts to reach better efficiency at low temperatures. Some metals such as copper and nickel are poisoned too easily. Thus, the best proven metals to be used in the diesel oxidation catalyst are platinum and palladium.

The distance of the diesel oxidation catalyst to the engine is very important due because it will affect the temperature of the gases coming into it. For this reason among all the catalysts that form the system, the diesel oxidation catalyst is the closest one to the engine but also, at a reasonable distance so there is no potential thermal damage.

The material used for the monoliths is usually Cordierite due to its low porosity and superior strength. A washcoat covers the monolith surface in a thin layer so the catalyst metal can be dispersed on it. Alumina, silica, and zeolites are the most common washcoat materials, and each of them contributes different properties. [19]

# 3 Experimental Procedures

The work reported in this thesis required (1) a comprehensive set of experimental data, (2) an appropriate reactor model, and (3) an optimizer for determining the best fit parameters in the proposed kinetic models. These three aspects are defined in this chapter.

## 3.1. Experimental Data

All of the experimental data used in this investigation were performed at the University of Waterloo, under the guidance of Professor William Epling. The data were taken by graduate student Meshari AL-Harbi. The catalyst used was supplied by Umicore AG in the form of washcoated monolith. The samples supplied had been aged by Umicore by flowing under air at 650 °C for ten hours. The sample contains 95 $g/ft^3$ (based on total monolith volume) platinum (Pt) supported on $Al_2O_3$. A sample of size 0.9" diameter with a length of 2.4" was cut from a monolith block that had a cell density of 400 CPSI. The sample was placed in a horizontal quartz tube, which was then inserted into a Lindberg Mini-mite temperature-controlled furnace. To ensure that no gas slipped around the sample, the catalyst was wrapped with 3M insulation material to seal the catalyst in the quartz tube. Six K-type thermocouples were placed along the catalyst length for temperature measurement purposes. The locations of the thermocouples in the tube reactor are shown in Table 3. The reactor assembly was installed in a flow system which controlled the composition of the inlet gases, and an analysis system to measure the concentrations of the effluent gases.

**Table 3:** Thermocouples location within the catalytic converter

| Thermocouple | Location |
|---|---|
| 0 | Upstream |
| 1 | 0 cm (Middle) |
| 2 | 2 cm (Top) |
| 3 | 2 cm (Middle) |
| 4 | 2 cm (bottom) |
| 5 | 4 cm |
| 6 | 6 cm (Middle) |

## 3.2. Experimental Procedure

In all experiments, the feed stream was introduced to the reactor at temperatures below 80˚C, to avoid reaction before ramping. The temperature of the reactor was ramped at approximately 3 °C/min. When complete oxidation was achieved, the reactor was cooled by decreasing the furnace temperature to below 80 °C. The base feed stream consisted of 10 % $O_2$, 10 % $H_2O$, 10 % $CO_2$, 300 ppm or 1% He, appropriate reactant gases, with $N_2$ as the balance. Reactants were added to this stream as required. The total gas flow rate was 9.34 L/min referenced to 298 K and 1 atm pressure. The space velocity is 20,520 $h^{-1}$ at STP (273 K and 1 atm).

The outlet gas composition was measured using a MultiGas 2030 FTIR analyzer (MKS) and an HPR20 mass spectrometer (MS). Before running any experiment, a test with $N_2$ only (no reactant) was performed to check the temperature difference between the front and the back of the catalyst as well as the radial direction. The test showed that the maximum difference was less than 5 °C between the front and the back and 4 °C in the radial direction (which occurred at high temperature).

### 3.2.1. Summary of Experiments

Thirty three experiments were performed at the University of Waterloo. The basis of the experiments was to perform tests with each reactant separately, and then combinations of pairs of reactants, and then runs with all reactants included. For each reactant, a low, medium and high concentration was assigned, based on typical values that might be found in real exhaust. Experiments were performed with CO, NO and $C_3H_6$ separately at each of these concentrations. In all runs reported here with CO, hydrogen was added at an amount equal to 1/3 of the CO concentration, which is a typical amount found in engine exhaust. Then selected pairs of concentrations were studied, and finally a series of runs was done with all three reactants present. Waterloo provided the results for 33 experiments, although some of these were not used because of problems with thermocouple recording during operation. Furthermore, some runs were performed with CO alone without hydrogen, and these runs were not used in the modelling. The original experiment numbering is used in this thesis.

The data provided by Waterloo were extensive, with data points collected every second or so. To reduce the number of points for the optimization and parameter estimation, only selected data points were taken from the master set provided. These selected data are felt to be sufficient to describe the curves. The method to select the data was to take points at every delta conversion of the order of 5 %, or temperature change of 5 degrees, whichever was smaller. The figures that follow show the plots of the experiments and data points used for the optimization.

The description of the inlet concentrations for each experiment/run, are shown in the following, along with their respective plots and analysis. The concentrations quoted in these tables are the nominal value. The actual values used are given in a Table 10 at the end of this section.

**CO Oxidation with $H_2$**

The temperature was ramped from 60 to 160 °C for three experiments with different inlet concentrations of CO and a third of that value of $H_2$. The concentrations are shown in the Table 4 and the ignition curves in Figure 2. The hydrogen conversion is not shown in the plots. However, the hydrogen reacts shortly after the CO is converted. The general observation is that the light-off point of CO (the temperature at which 50 % conversion is observed) increases with increasing CO concentration. This effect is well documented at Voltz et. al. [1] and Salomons et. al. [20].

**Table 4:** CO inlet concentration

| Exp. | CO [ppm] | $H_2$ [ppm] |
|---|---|---|
| 1 | 500 | 167 |
| 2 | 1000 | 333 |
| 3 | 2000 | 666 |

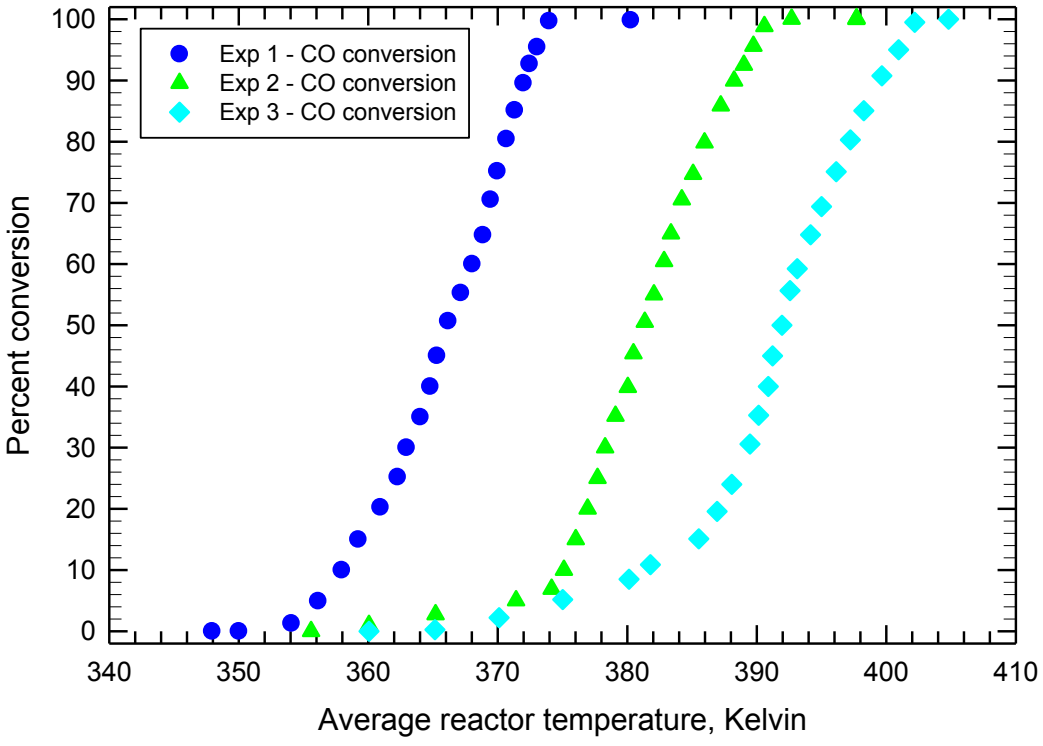


**Figure 2:** Data used for optimization, experiments 1, 2 and 3.

**Propene Oxidation**

The temperature was ramped from 80 to 200°C for three $C_3H_6$ concentrations. The concentrations are given in Table 5 and the ignition plots in Figure 3. The light-off is displaced to the right when the concentration increases. This shows that $C_3H_6$ exhibits self-inhibition as well.

**Table 5:** Propene inlet concentration

| Exp | Propene [ppm] |
|---|---|
| 7 | 250 |
| 8 | 500 |
| 9 | 750 |

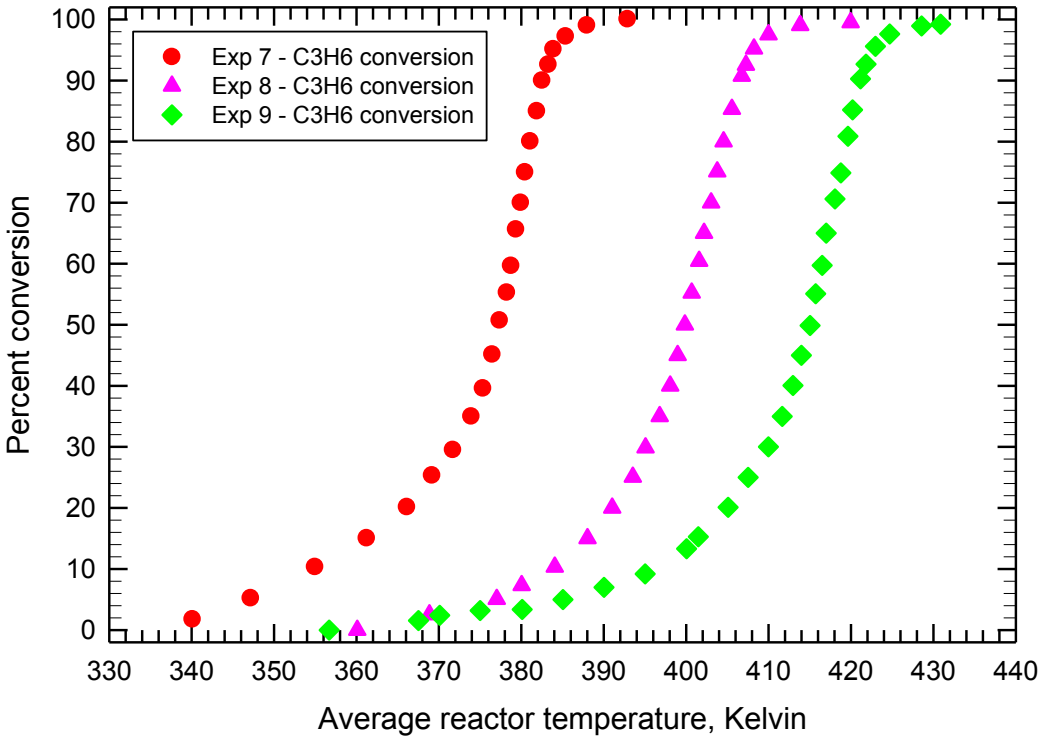


**Figure 3:** Data used for optimization, experiments 7, 8 and 9.

**NO Oxidation**

The temperature was ramped from 80 to 350°C for three different NO inlet concentrations. Table 6 shows the feed concentrations used, and Figure 4 the ignition plots. NO also shows self-inhibition, demonstrated through the light-off displacement to the right when the concentration is increased. At high temperatures the reaction is equilibrium limited, and the conversion decreases with increasing temperature.

**Table 6:** NO inlet concentration

| Exp | NO [ppm] |
|---|---|
| 10 | 150 |
| 11 | 300 |
| 12 | 600 |

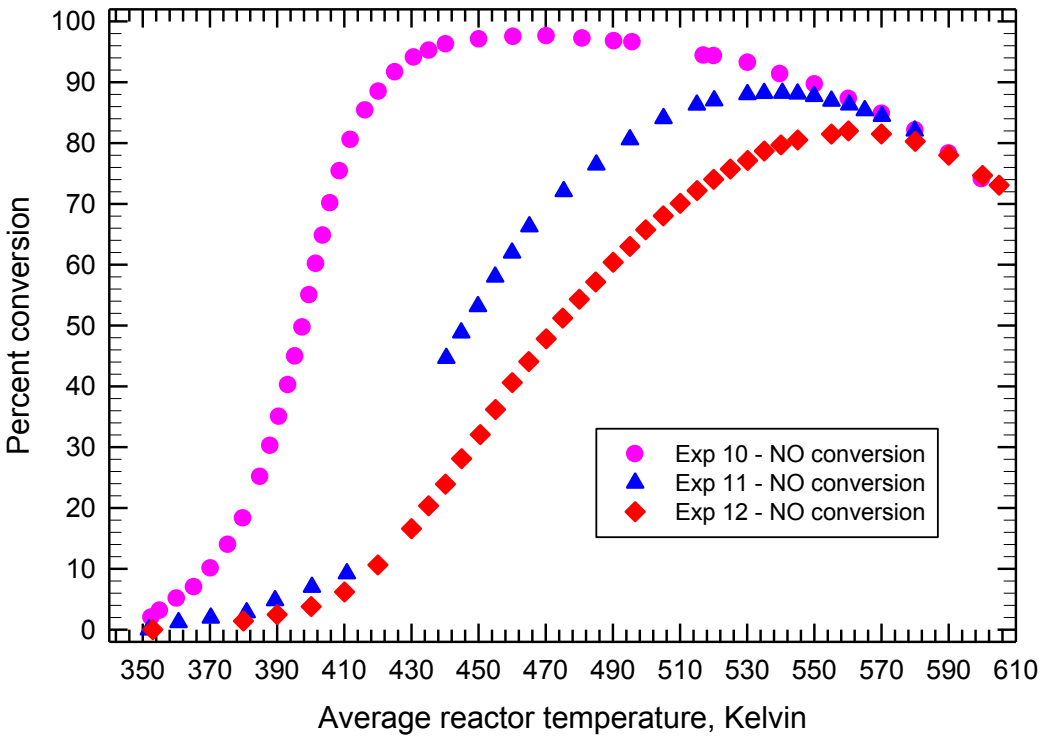


**Figure 4:** Data used for optimization, experiments 10, 11 and 12.

**Mixture of NO and $C_3H_6$**

The temperature was ramped from 80 to 320°C for experiments with a constant propene concentration, but different NO inlet concentration. The inlet concentrations are given in Table 7 and the ignition curves for the species in Figures 5 – 7. Note that the reactions of NO are more complex than with NO alone. Initially NO is reduced by hydrocarbon, either to $N_2O$ or $N_2$, and as the temperature increases, the NO is oxidized to $NO_2$. The graphs show the conversion to $N_2$ (which is represented as $NO_X$ conversion), to $N_2O$ and to $NO_2$.

**Table 7:** Propene inlet concentration

| Exp | Propene [ppm] | NO [ppm] |
|---|---|---|
| 13 | 500 | 150 |
| 14 | 500 | 300 |
| 15 | 500 | 600 |

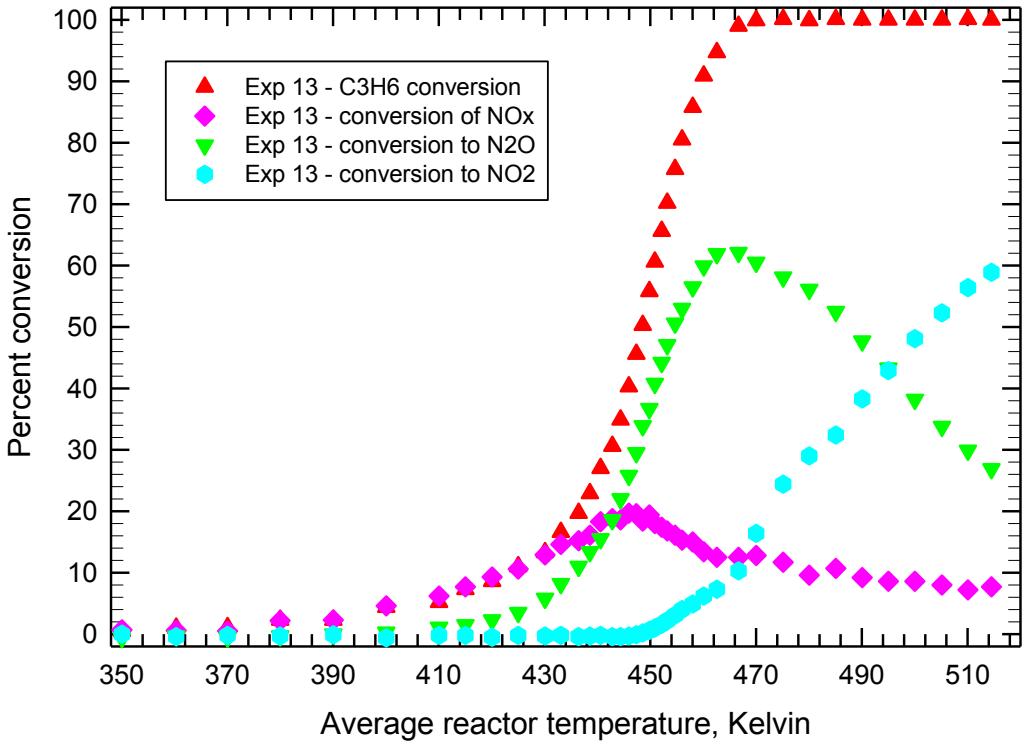


**Figure 5:** Data used for optimization, experiment 13.

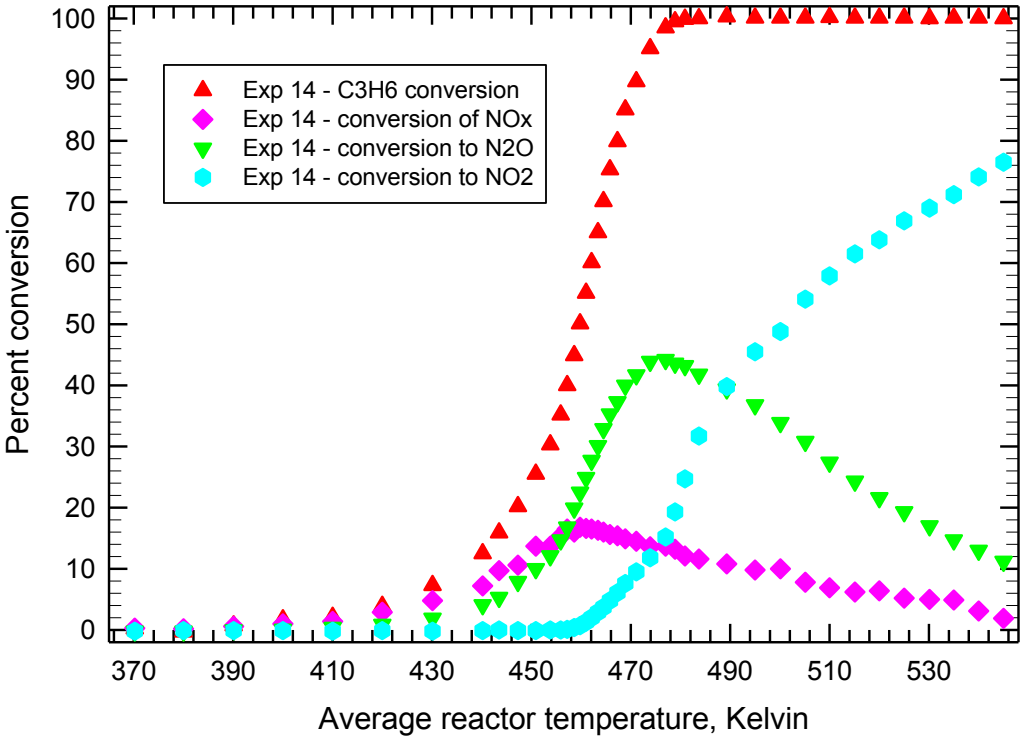


**Figure 6:** Data used for optimization, experiment 14.

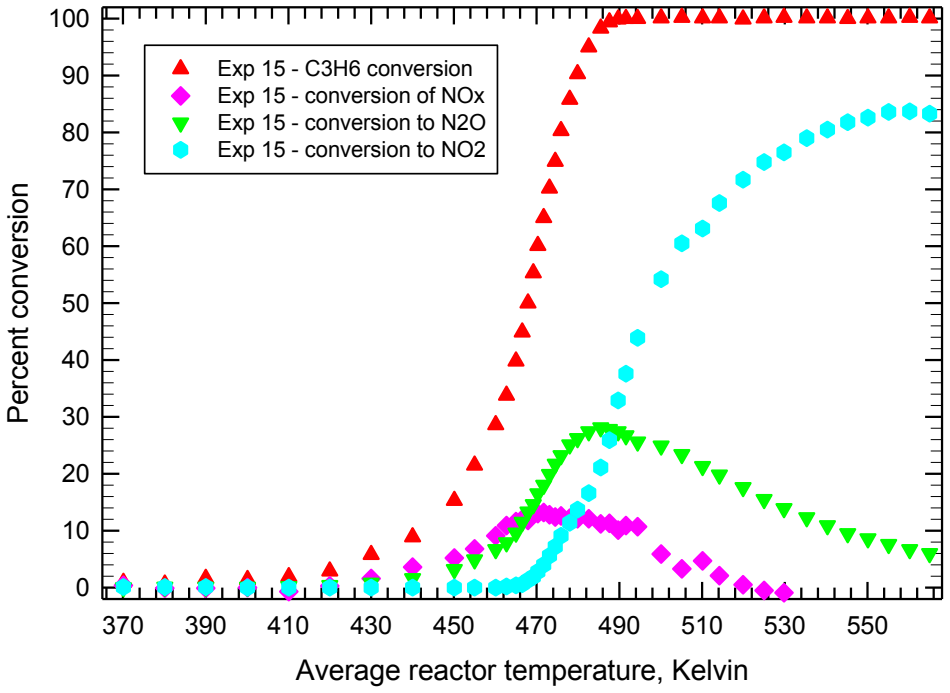


**Figure 7:** Data used for optimization, experiment 15.

**Mixture of CO, $H_2$ and $C_3H_6$**

The temperature was ramped from 80 to 200°C for experiments with the same propene concentration, different CO inlet concentration, and $H_2$ present at 1/3 of the CO. Table 8 shows the inlet concentrations. Figures 8, 9 and 10 show the ignition curves. From these it can be inferred that the concentration of CO not only has a self-inhibition effect, but also inhibits the $C_3H_6$, which light-off increase along with the increase of CO inlet concentration.

**Table 8:** CO and Propene mixture inlet concentration

| Exp | CO [ppm] | $H_2$ [ppm] | Propene [ppm] |
|---|---|---|---|
| 17 | 500 | 167 | 250 |
| 18 | 1000 | 333 | 250 |
| 19 | 2000 | 666 | 250 |

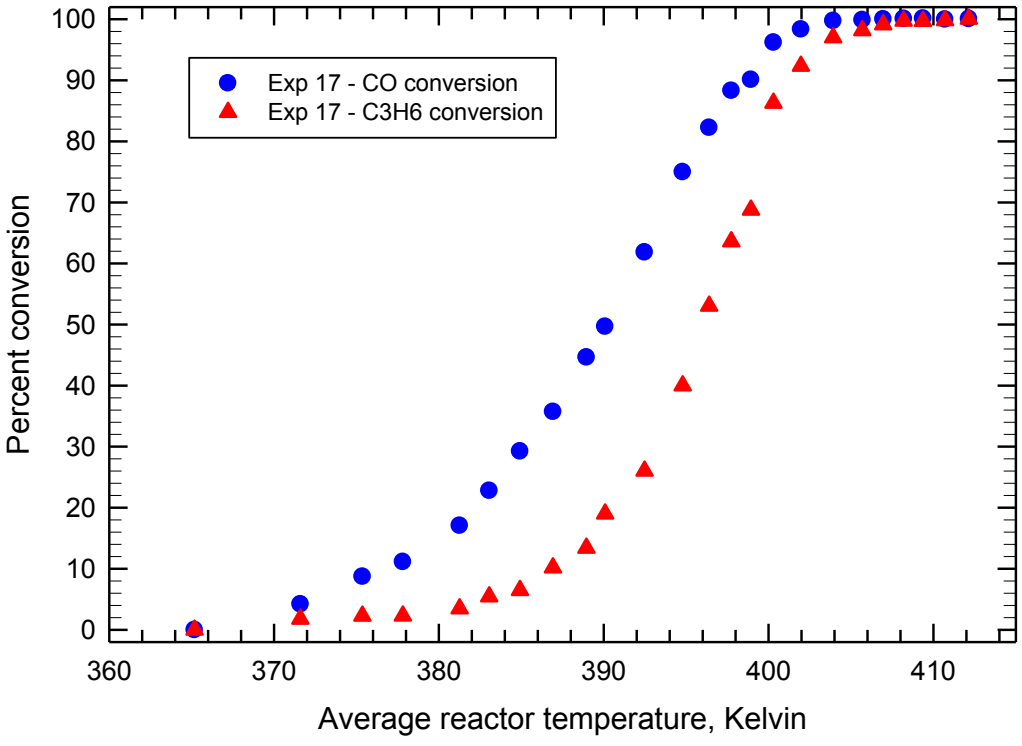


**Figure 8:** Data used for optimization, experiment 17.

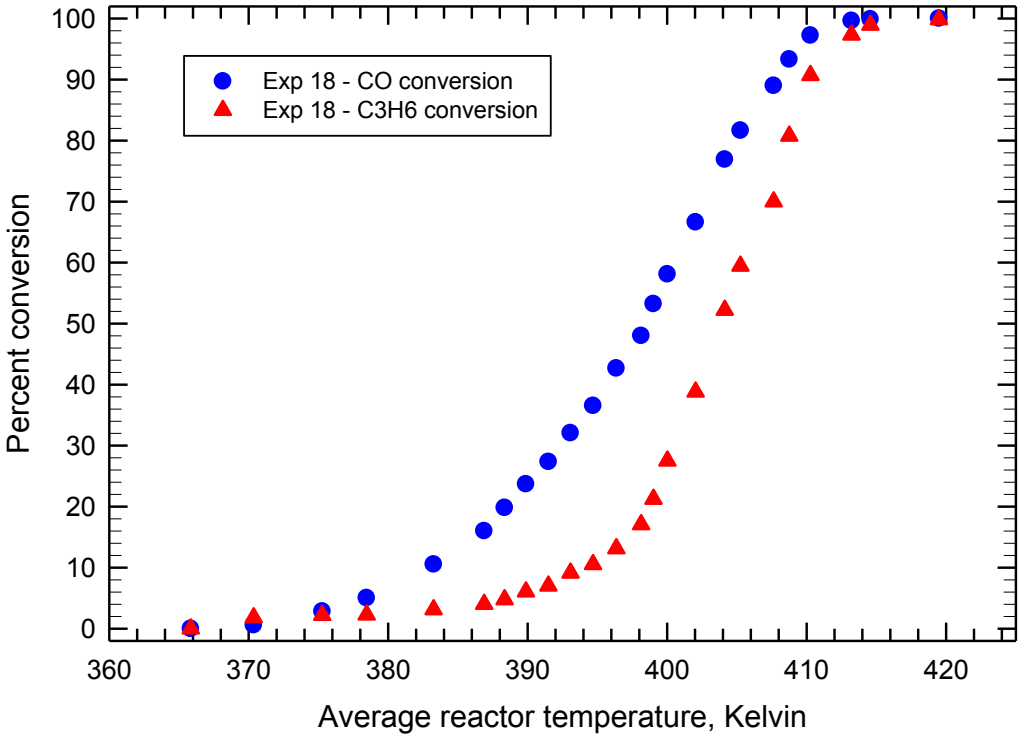


**Figure 9:** Data used for optimization, experiment 18.

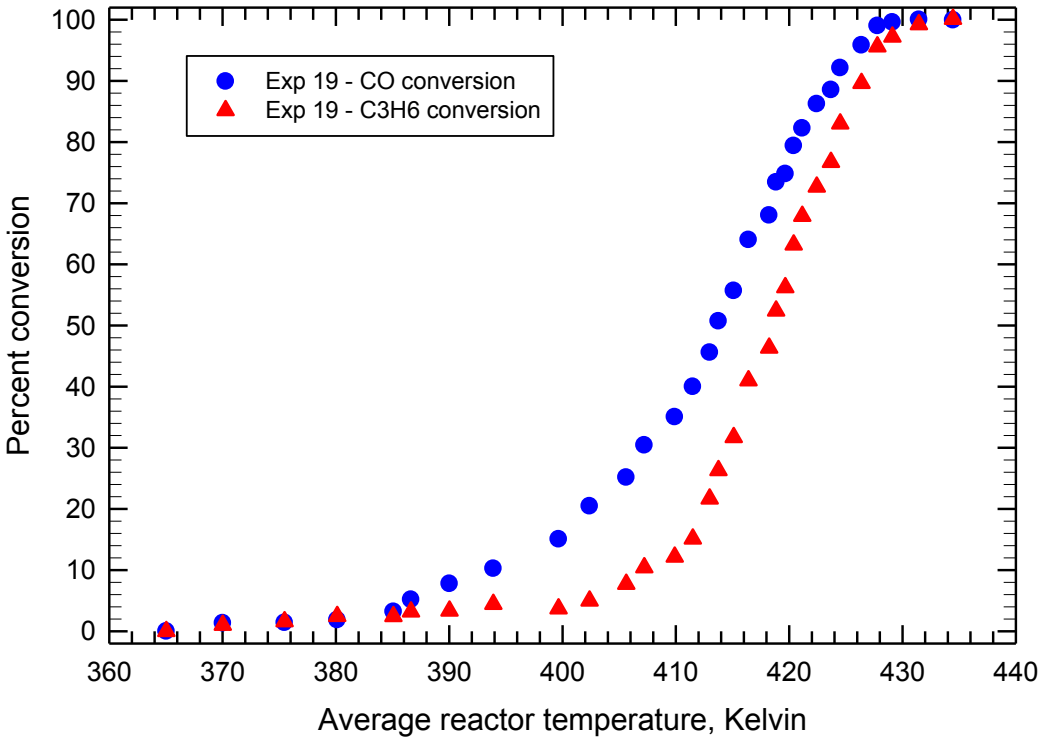


**Figure 10:** Data used for optimization, experiment 19.

**Mixture of CO, $H_2$, NO and $C_3H_6$**

Ten usable experiments were available for the complete mixture, in which the temperature was ramped from 80 to 260°C. The concentrations used are given in Table 9. Experiments 23 to 28 had constant C3H6 and NO concentrations, and variable CO. The remaining five experiments had variations in all concentrations. The ignition curves are given in Figures 11 to 20. As for the experiments with $C_3H_6$ and NO, it is seen that the NO is reduced to $N_2$, and $N_2O$, as well as being oxidized to $NO_2$.

From Figures 11 to 15, which show only the experiments where CO is varied, it can be inferred that (as seen in the case of CO-$C_3H_6$ mixture), CO not only has a self-inhibition effect, but also inhibits $C_3H_6$ and NO.

**Table 9:** CO, Propene and NO mixture inlet concentration

| Exp | CO [ppm] | $H_2$ [ppm] | Propene [ppm] | NO [ppm] |
|---|---|---|---|---|
| 23 | 500 | 167 | 500 | 150 |
| 24 | 750 | 250 | 500 | 150 |
| 26 | 1250 | 417 | 500 | 150 |
| 27 | 1500 | 500 | 500 | 150 |
| 28 | 2000 | 666 | 500 | 150 |
| 29 | 500 | 167 | 250 | 300 |
| 30 | 750 | 250 | 750 | 300 |
| 31 | 1000 | 333 | 750 | 600 |
| 32 | 1500 | 417 | 750 | 600 |
| 33 | 2000 | 666 | 750 | 600 |

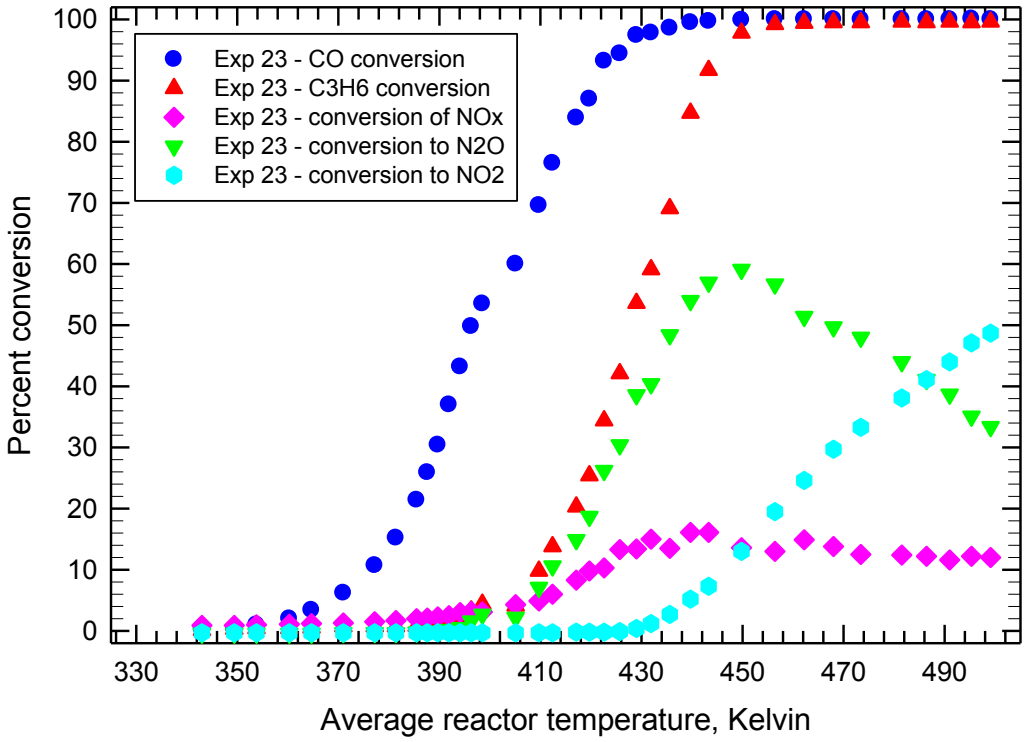


**Figure 11:** Data used for optimization, experiment 23.

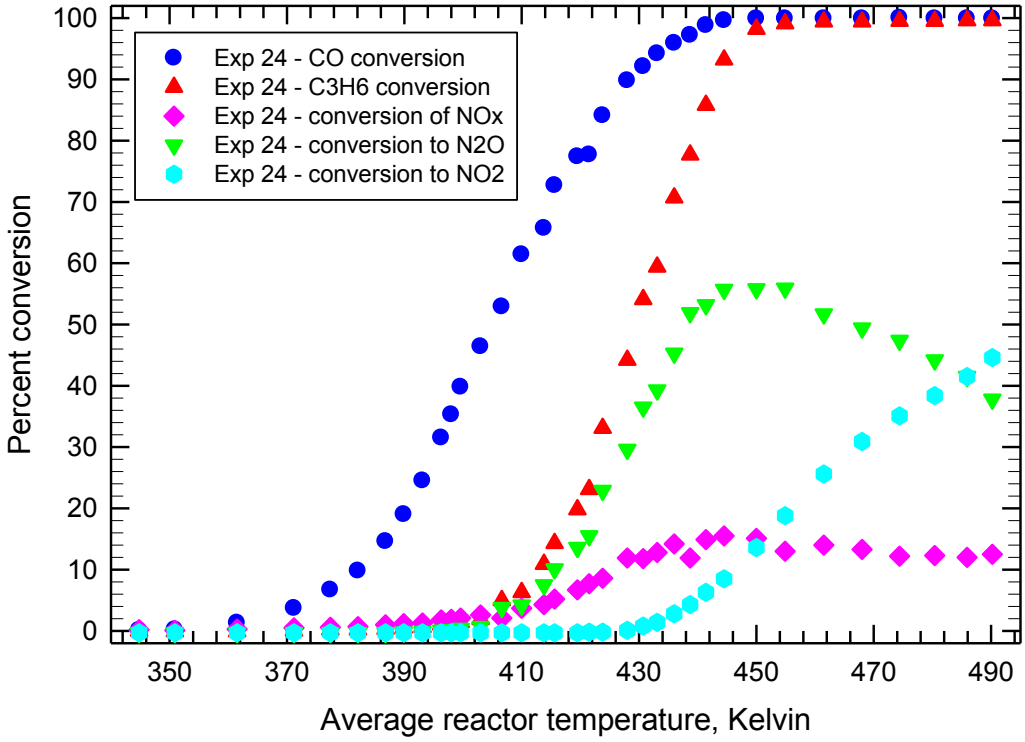


**Figure 12:** Data used for optimization, experiment 24.

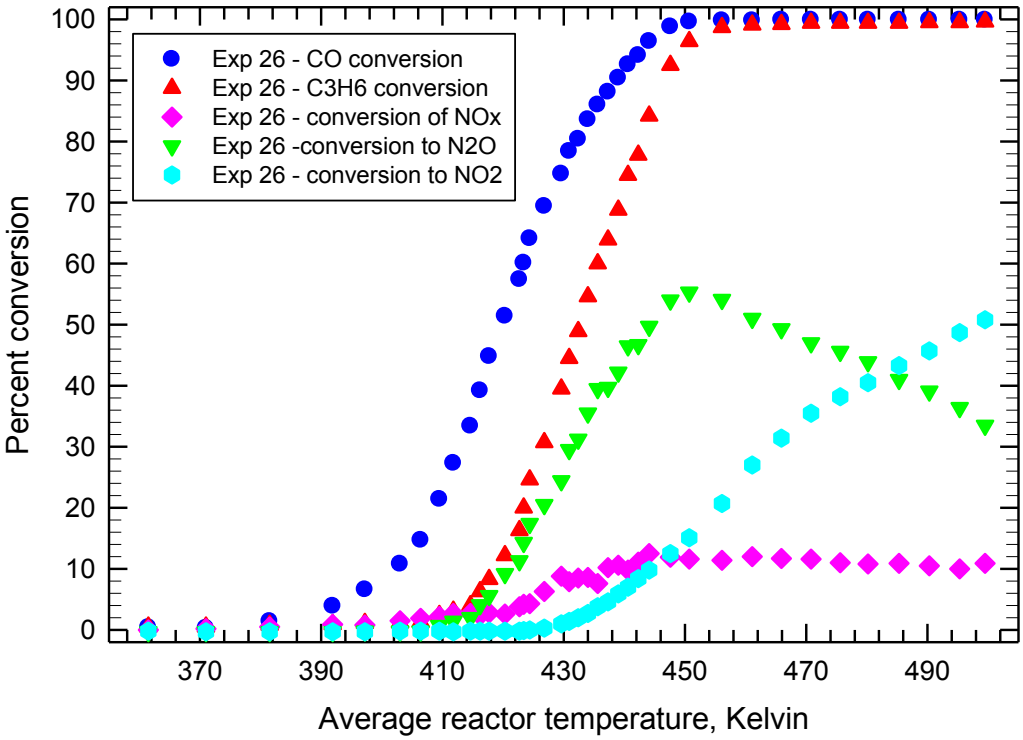


**Figure 13:** Data used for optimization, experiment 26.

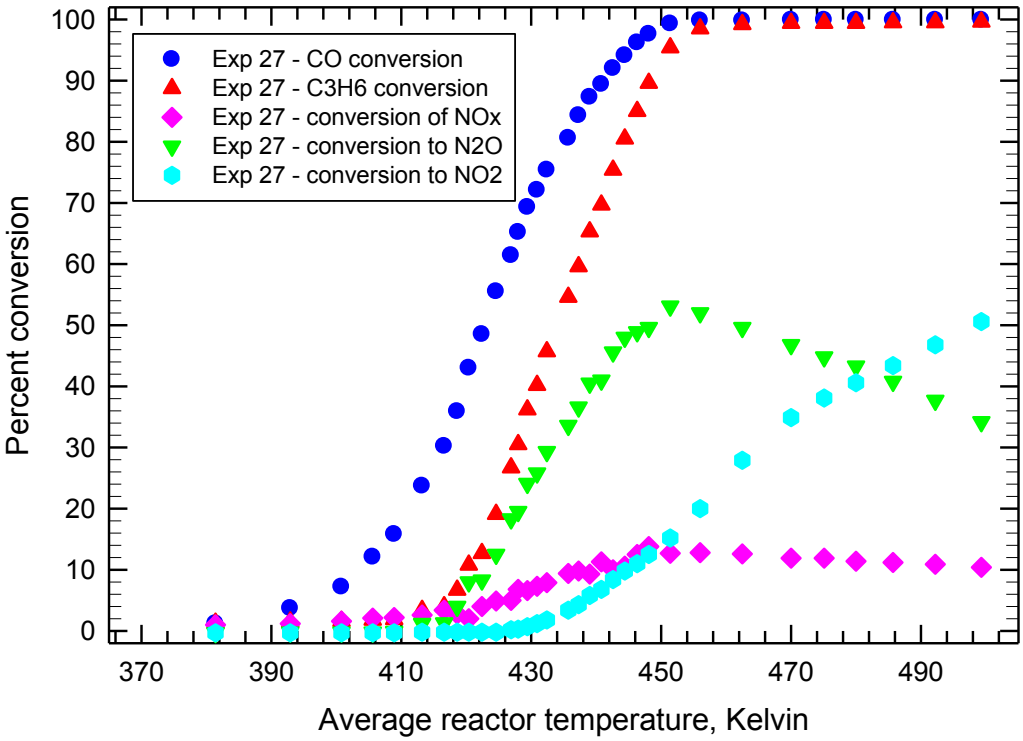


**Figure 14:** Data used for optimization, experiment 27.

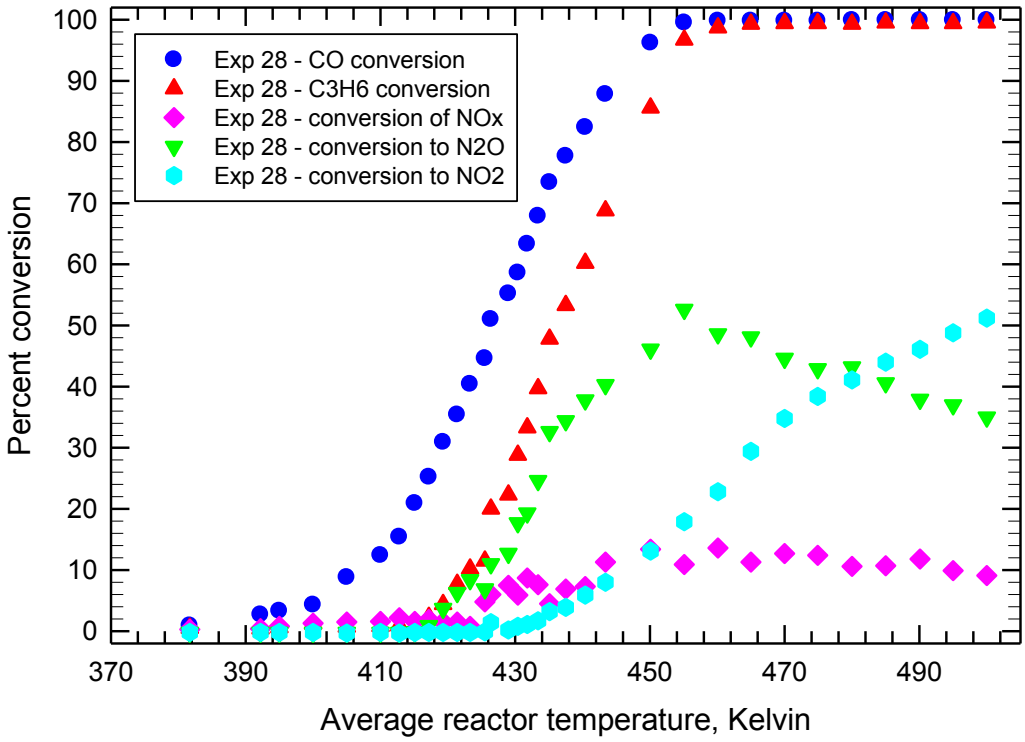


**Figure 15:** Data used for optimization, experiment 28.

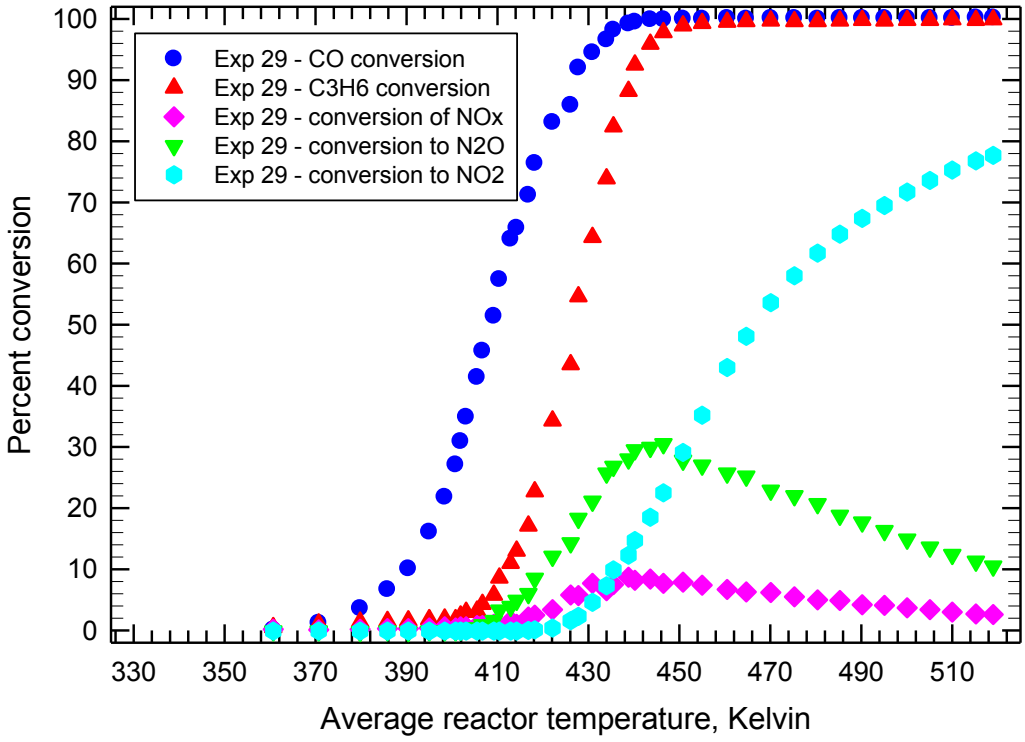


**Figure 16:** Data used for optimization, experiment 29.

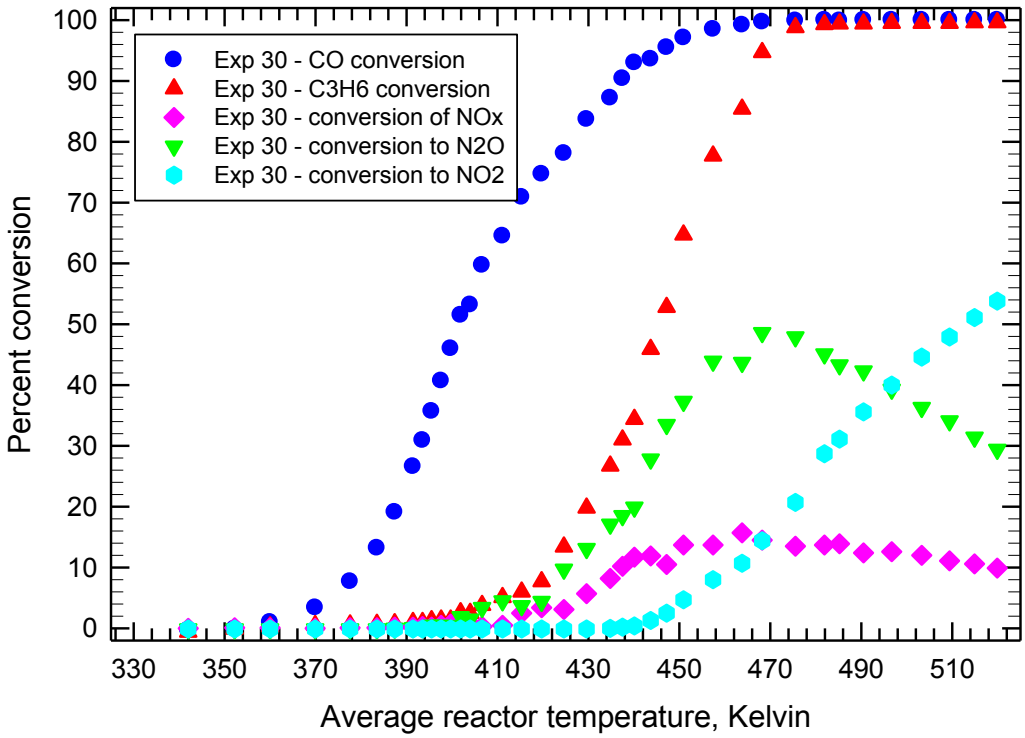


**Figure 17:** Data used for optimization, experiment 30.

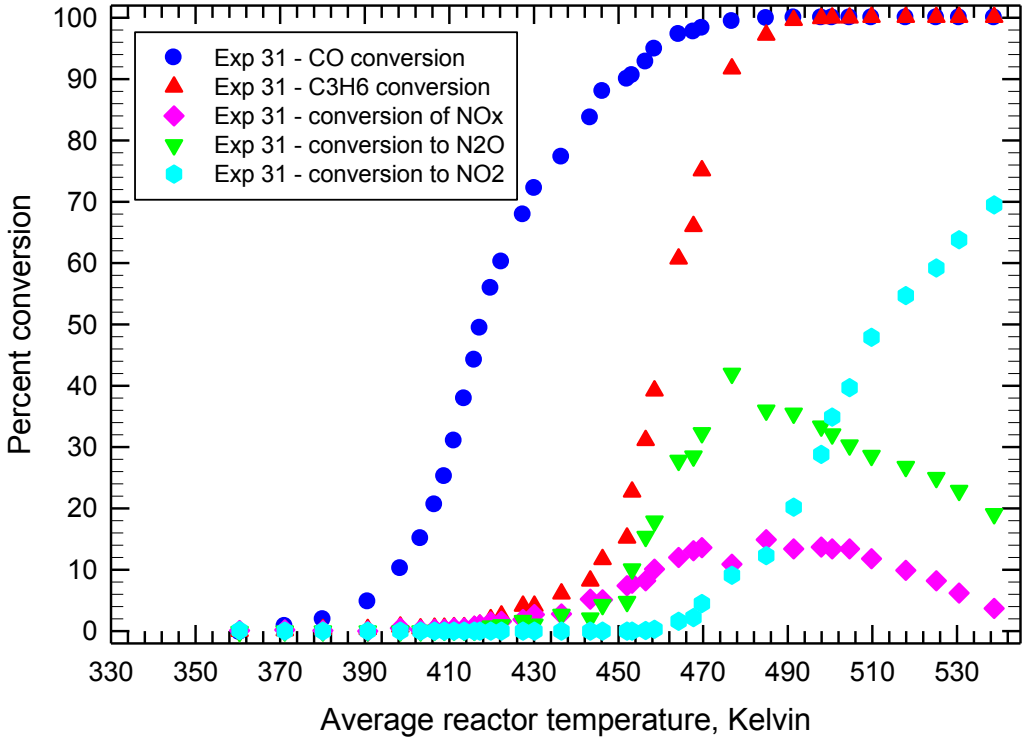


**Figure 18:** Data used for optimization, experiment 31.

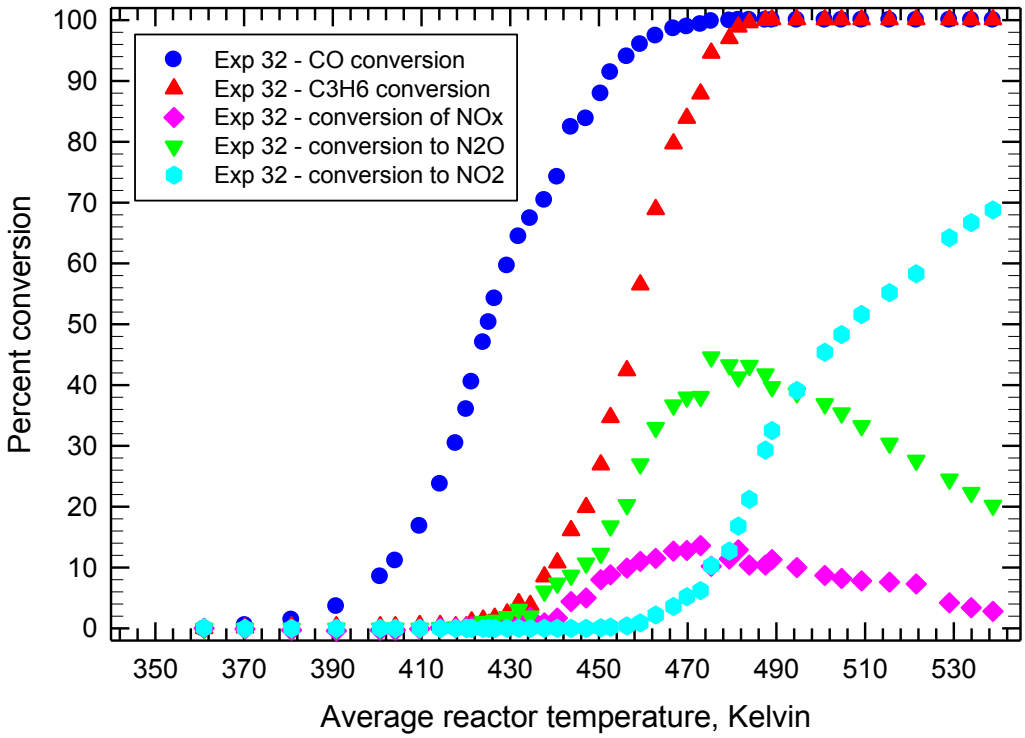


**Figure 19:** Data used for optimization, experiment 32.

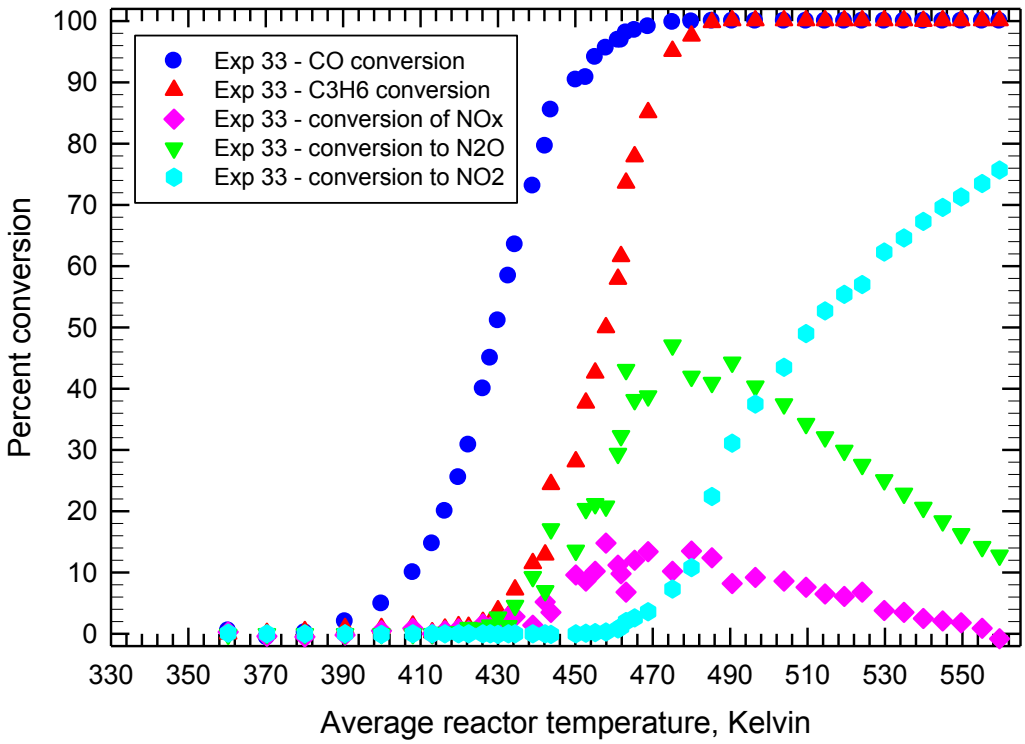


**Figure 20:** Data used for optimization, experiment 33.

**Table 10:** Summary of the experimental initial concentrations:

| Run | CO [ppm] | Propene [ppm] | NO [ppm] |
|---|---|---|---|
| 1 | 426 | 0 | 0 |
| 2 | 1061 | 0 | 0 |
| 3 | 2124 | 0 | 0 |
| 7 | 0 | 227 | 0 |
| 8 | 0 | 440 | 0 |
| 9 | 0 | 695 | 0 |
| 10 | 0 | 0 | 150 |
| 11 | 0 | 0 | 301 |
| 12 | 0 | 0 | 596 |
| 13 | 0 | 549 | 151 |
| 14 | 0 | 547 | 304 |
| 15 | 0 | 549 | 604 |
| 17 | 520 | 275 | 0 |
| 18 | 1006 | 278 | 0 |
| 19 | 1994 | 281 | 0 |
| 23 | 579 | 524 | 166 |
| 24 | 790 | 523 | 166 |
| 26 | 1296 | 519 | 163 |
| 27 | 1545 | 526 | 165 |
| 28 | 2055 | 520 | 164 |
| 29 | 577 | 271 | 305 |
| 30 | 823 | 731 | 305 |
| 31 | 1077 | 790 | 603 |
| 32 | 1649 | 786 | 600 |
| 33 | 2197 | 788 | 603 |

## 3.3. Reactor Model

There are several mathematical model possibilities to choose from when simulating a monolith reactor. In a single channel model, all of the monolith channels are assumed to behave in the same way, and hence a single channel is assumed to represent the entire monolith reactor. When modelling the single channel, it is also necessary to choose whether or not a heterogeneous or a homogeneous model is used. In a heterogeneous model, the fluid and solid phases are modelled separately, and are coupled using the appropriate heat and mass transfer coefficients. In a pseudo-homogeneous model the fluid and solid concentrations are assumed to be the same, and the gas phase concentrations are used in the model. Finally, the diffusion in the catalytic washcoat may be significant. However, modelling the washcoat requires a large expense in terms of computer resources. The overriding requirement for doing this optimization study was that the model (simulator) executes extremely quickly, and therefore the simplest model, consistent with obtaining useful information, was selected.

The reactor model chosen was a one dimensional pseudo-homogeneous steady state plug flow model. Only the appropriate mass conservation equations are solved, and not the energy balance. The reactor temperature at each time step is imposed based on the experimental profiles measured during the experiments. It is not possible to include the energy balance, because the reactor is not adiabatic and the rates of heat transfer to and from the reactor are not known. Since the temperature along the centre line of the reactor is known at four locations, the simulator uses these four temperatures to impose a temperature profile along the reactor. Temperatures between the experimental data points were obtained by linear interpolation.

Even though the experiments are transient, it is acceptable to use a steady state model. The residence time in the reactor is very small, of the order of 0.02 s. The temperature change of the solid is much slower, so in effect the gas is

always in a pseudo-steady state with the wall temperature. Because the temperature is measured, the steady state model will give a good solution. The ignition curve was constructed by performing a sequence of steady state simulations with increasing reactor temperatures, based on the experimental values.

The plug flow mole balance equation is written for each species of interest. For species *j* the equation is:

$$-Cu_m \frac{dY_j}{dz} + \left(-R_j\right)\frac{V_W}{V_C} = 0 \tag{3.1}$$

The mean velocity in the channel is denoted $u_m$ and the bulk molar concentration of the gas is *C*, which is specified by the ideal gas law. Usually the reaction rate for a catalytic converter is based on the washcoat volume, and therefore it must be converted to a basis of channel volume for the homogeneous model. Thus the ratio of washcoat volume ($V_W$) and the channel volume ($V_C$) are included to provide the correct basis for the reaction rate. If we assume that the channel can be represented as a right circular cylinder of a length of *z*, diameter $D_H$, and that the washcoat occupies an annular ring of outside diameter $D_{WC}$, then with the appropriate substitution, we obtain:

$$-Cu_m \frac{dY_j}{dz} + \left(-R_j\right)_V \frac{\left(D_{WC}{}^2 - D_H{}^2\right)}{D_H{}^2} = 0 \tag{3.2}$$

The equation can be explicitly arranged to give:

$$\frac{dY_j}{dz} = \frac{\left(-R_j\right)_V}{Cu_m}\frac{\left(D_{WC}{}^2 - D_H{}^2\right)}{D_H{}^2} \tag{3.3}$$

This model was available in existing software. The resulting kinetic parameters are therefore global, in that they include all heat and mass transfer effects implicitly, and are not necessarily intrinsic rate constants.

Because the plug flow model is used, the solution of the reactor model requires the solution of a coupled set of ordinary differential equations (ODE). The general purpose solver VODE is used, in the double precision version written in Fortran 77 (DVODE). This software is public domain code written by Sandia labs and was downloaded from their website.

The execution of the simulator can result in the execution of the solution for a single experiment or multiple experiments. For each experiment, the simulator calculates the value of the residual for each ignition curve for each reacting component in feed, the combined (total) residual for all of the ignition curves in the experiment, and, if more than one experiment is simulated, the total residual for all of the experiments.

## 3.4. Optimization Routine

The optimisation was performed with the Matlab optimisation toolbox, using a General Pattern Search (GPS) algorithm. The adjustable parameters are the pre-exponential factors and the activation energies for each constant in the kinetic model. For the optimization process, the search range for each parameter was set based on literature values and was adjusted during the optimization process. This methodology is further explained in Chapter 4.

There are several advantages of the GPS method over more traditional gradient based methods. The first is that gradient based methods will become trapped in a local minimum, whilst the GPS allows the movement away from such a state. Although finding a global minimum is never certain, the chances are higher with the GPS. The next advantage is that the computation of gradients is

not required, only the computation of the appropriate objective function. This makes the method ideal for a “black box” solver, whose only role is to provide the objective function for a given set of parameter values. Another advantage is that if a certain set of parameter values produces a non-tenable solution (such as a division by zero), the optimization procedure is not halted, because the parameter set can simply be discarded.

In this work, an experiment could contain up to five ignition curves, for the oxidation of CO, oxidation of $C_3H_6$, oxidation of NO to $NO_2$, the conversion of NO to $N_2$, and the conversion of NO to $N_2O$. An objective function was calculated for each curve according to:

$$O_i = \frac{1}{2}\sum_{i=1}^{n}(X_{\exp} - X_{pred})^2 \qquad (3.4)$$

The objective function for any experiment was defined as the sum of the objective functions for all of the relevant reactions for that experiment. When more than one experiment was used for the optimization, then the objective function was the sum of the objective functions for each experiment.

# 4 Modelling the Diesel Oxidation Catalyst

## 4.1. Kinetic models

When selecting a kinetic model for the catalytic converter, the choice must be made between a global model, which is in essence an empirical model, and a so-called mechanistic model. The latter model type contains many steps and attempts to mimic the actual mechanism of the chemical reactions. The global model, typified by the Langmuir-Hinschelwood-Hougen-Watson form, on the other hand represents a simplified approach that results in a more empirical model. Both model types are extensively used in industrial practice, although global models are by far the most common. These models are most widely used in the catalytic converter field, and thus were used in this study.

The models tested are introduced in the sections that follow, however, all model parameters (kinetic constants) have an Arrhenius type form, thus inherently require two terms. The parameters are labeled as follows. A lower case *k* represents a "kinetic" constant, whilst an upper case *K* represents an adsorption equilibrium constant. Each of these constants has two parameters, corresponding to the pre-exponential factor and the activation energy.

All parameters had the general Arrhenius form:

$$k_i = A\exp\left(\frac{-E}{R_g T}\right) \tag{4.1}$$

To reduce the range of the parameters, the optimization was performed on the following version of the Arrhenius equation:

$$k_i = \exp\left(A' - \frac{-E}{R_g}\left[\frac{1}{T} - \frac{1}{450}\right]\right) \tag{4.2}$$

Writing the equation in this way reduces the effective search range of the optimizer, and thus makes the solution more stable and more rapid. Notwithstanding the equation used, the values of the pre-exponential factor reported in the all of the results corresponds to the equation:

$$k_i = A'' \exp\left(\frac{-E}{R_g}\left[\frac{1}{T} - \frac{1}{450}\right]\right) \tag{4.3}$$

The modelling study was performed piecewise. That is, the modeling of the individual species and the combinations of two reactants was studied first, followed by a study of the complete mixture. This approach was felt to offer a better model discrimination opportunity, and also allowed the evaluation of some common ideas found in the literature.

## 4.2. Models and Results

### 4.2.1. The oxidation of CO and $C_3H_6$

One of the earliest papers that reported on kinetic models for catalytic converters is the classical work of Voltz et al., which appeared in 1973 [4]. The model has been adopted and adapted by many investigators in the automotive catalytic converter world, with many changes and subtle variations. It has been extended to three-way catalysis with extensive modifications. As of August 2011, the original paper had 259 citations (based on information obtained from the Web of Science), although many of these have referred to the model only in passing. This model was intended for the oxidation of CO and $C_3H_6$ in the presence or absence of NO. NO was considered to be an adsorbing but non-reacting species. Hydrogen is present but not specifically modelled. The global reactions for the oxidation of reactions are:

$$CO + \frac{1}{2}O_2 \rightarrow CO_2 \quad (4.4)$$

$$C_3H_6 + \frac{9}{2}O_2 \rightarrow 3CO_2 + 3H_2O \quad (4.5)$$

$$H_2 + \frac{1}{2}O_2 \rightarrow H_2O \quad (4.6)$$

The catalytically active ingredient was platinum and both catalyst pellets and typical crushed monolith samples were compared. Also, both synthesis gas mixtures and real exhaust gas were used. As mentioned above, NO was considered to be non-reacting. The concentrations ran to relatively high levels of CO and $C_3H_6$ , with up to 7000 ppm CO, 800 ppm $C_3H_6$ and 500 ppm NO. Oxygen was varied from 3% to 10%. Both CO and $C_3H_6$ were observed to inhibit the reaction, as well as NO.

The basic model for the simultaneous oxidation of CO and $C_3H_6$ is based on a Langmuir-Hinshelwood type mechanism with the surface reaction between two adsorbed species being the rate determining step. The rate was expressed in terms of mole fractions (or a variant thereof). Thus we can consider the basic kinetic model as:

$$\left(-R_{CO}\right) = \frac{k_1 Y_{CO} Y_{O_2}}{R_I} \quad (4.7)$$

and:

$$\left(-R_{C_3H_6}\right) = \frac{k_3 Y_{C_3H_6} Y_{O_2}}{R_I} \quad (4.8)$$

In these equations $R_I$ is the adsorption inhibition term, given by:

$$R_I = \left(1 + K_5 Y_{CO} + K_6 Y_{C_3H_6}\right)^2 \quad (4.9)$$

This model was reported to give a reasonable fit to the experimental data, except at higher concentrations of CO and $C_3H_6$, and for this latter situation another term was added to the denominator, to give:

$$R_{\mathrm{I}} = \left(1 + K_5 Y_{\mathrm{CO}} + K_6 Y_{\mathrm{C_3H_6}}\right)^2 \left(1 + K_7 \left(Y_{\mathrm{CO}} Y_{\mathrm{C_3H_6}}\right)^2\right) \quad (4.10)$$

A term for NO inhibition was added, and justified in terms of NO being an adsorbed non-reacting species. The final inhibition term reported is thus:

$$R_{\mathrm{I}} = \left(1 + K_5 Y_{\mathrm{CO}} + K_6 Y_{\mathrm{C_3H_6}}\right)^2 \left(1 + K_7 \left(Y_{\mathrm{CO}} Y_{\mathrm{C_3H_6}}\right)^2\right)\left(1 + K_8 \left(Y_{\mathrm{NO}}\right)^{0.7}\right) \quad (4.11)$$

This model was reported to give a good correlation with the experimental data for both synthesis gas mixtures and real exhaust, and also for both the catalyst pellets and the crushed monolith. In the latter case, the pre-exponential factor was adjusted to account for the change in the number of active sites.

Since its publication, the Voltz model [1] has been used by many workers. A common practice is to use the adsorption parameters, and often the activation energies, reported by Voltz and to adjust the pre-exponential factors to fit the experimental data. The parameter values from Voltz, adjusted so that all concentrations are expressed in mole fractions, and disregarding the pre-exponential factors for the kinetic terms, are:

$$k_1 = A_1 \exp\left(\frac{-104387}{R_g T}\right) \quad (4.12)$$

$$k_3 = A_3 \exp\left(\frac{-121015}{R_g T}\right) \quad (4.13)$$

Note that the gas constant is 8.314 J/(mol·K), and the activation energies have units of J/mol. The units of the pre-exponential factor will depend on the basis that is used to derive them, and the values also depend on the Pt loading and dispersion. The original adsorption constants are:

$$K_5 = 65.5 \exp\left(\frac{7990}{R_g T}\right) \tag{4.14}$$

$$K_6 = 2080 \exp\left(\frac{3001}{R_g T}\right) \tag{4.15}$$

$$K_7 = 3.98 \exp\left(\frac{96534}{R_g T}\right) \tag{4.16}$$

$$K_8 = 4.79 \times 10^5 \exp\left(\frac{-31036}{R_g T}\right) \tag{4.17}$$

As noted, many have used the Voltz model. It is interesting to discuss a few early uses, because they introduce some significant changes into subsequent works. There were a number of publications up to 1980 that used the Voltz CO oxidation model, but these were mainly theoretical studies that just used the Voltz model to represent a “typical” LHHW type system. Oh et al. (1980)[21] is apparently the first to use the Voltz system for some real data. They modelled a single pellet system and used recycle reactor data which it is inferred from the paper that they obtained. The model used was a simplification of the full Voltz model, and concentrations were used instead of mole fractions. They state that the adsorption parameters and the activation energies were those of Voltz, but the values quoted in the paper are actually different from those of Voltz. Of especial note is that they used a negative “heat of adsorption” for $C_3H_6$. The rate equations were:

$$\left(-R_{CO}\right) = \frac{k_1 Y_{CO} Y_{O_2}}{\left(1 + K_5 Y_{CO} + K_6 Y_{C_3H_6}\right)^2} \quad (4.18)$$

$$\left(-R_{C_3H_6}\right) = \frac{k_3 Y_{C_3H_6} Y_{O_2}}{\left(1 + K_5 Y_{CO} + K_6 Y_{C_3H_6}\right)^2} \quad (4.19)$$

In a later paper, Oh and Cavendish (1982) [22], introduced a significant variation of the Voltz model, one that is widely used in later papers. An additional temperature was introduced into the adsorption inhibition term, giving:

$$R_I = T\left(1 + K_5 Y_{CO} + K_6 Y_{C_3H_6}\right)^2 \left(1 + K_7 \left(Y_{CO} Y_{C_3H_6}\right)^2\right)\left(1 + K_8 \left(Y_{NO}\right)^{0.7}\right) \quad (4.20)$$

In that paper, they used mole fractions and the adsorption parameters and the activation energies were indeed those of Voltz. The pre-exponential factors were tuned using recycle reactor data, although it is not clear if these were the same data used in the earlier paper. There is no explanation given for the introduction of the temperature into the denominator. This work has been cited by others who have used the temperature in the denominator, and appears to be the origin of this version of the Voltz model. The next paper from Oh and Cavendish (1985)[23] with the Voltz model used the original form of term for adsorption proposed by Voltz, but with concentrations rather than mole fractions:

$$R_I = \left(1 + K_5 Y_{CO} + K_6 Y_{C_3H_6}\right)^2 \left(1 + K_7 \left(Y_{CO} Y_{C_3H_6}\right)^2\right)\left(1 + K_8 \left(Y_{NO}\right)^{0.7}\right) \quad (4.21)$$

They used the parameters from Oh et al. (1980)[21]. The 1985 paper was titled as part 2 of the 1980 paper, so it is normal that the same parameters

would be used. The paper states that the same recycle reactor data used in Oh and Cavendish (1982)[22] was used to tune the pre-exponential factors in the kinetic terms. There is clearly some inconsistency in these papers.

For this work, the Voltz model has been adopted as a starting point, and its ability to predict the data has been tested. In this first part of the analysis the work has been restricted to experiments that contain only CO and $C_3H_6$, along with hydrogen, water and carbon dioxide. Because at this point a system containing NO is not considered, the denominator becomes:

$$R_{\mathrm{I}} = \left(1 + K_5 Y_{\mathrm{CO}} + K_6 Y_{\mathrm{C_3H_6}}\right)^2 \left(1 + K_7 \left(Y_{\mathrm{CO}} Y_{\mathrm{C_3H_6}}\right)^2\right) \tag{4.22}$$

Because of the common usage in the literature, also tested was the denominator with added temperature terms, thus:

$$R_{\mathrm{I}} = T\left(1 + K_5 Y_{\mathrm{CO}} + K_6 Y_{\mathrm{C_3H_6}}\right)^2 \left(1 + K_7 \left(Y_{\mathrm{CO}} Y_{\mathrm{C_3H_6}}\right)^2\right) \tag{4.23}$$

$$R_{\mathrm{I}} = T^2\left(1 + K_5 Y_{\mathrm{CO}} + K_6 Y_{\mathrm{C_3H_6}}\right)^2 \left(1 + K_7 \left(Y_{\mathrm{CO}} Y_{\mathrm{C_3H_6}}\right)^2\right) \tag{4.24}$$

The model contains ten adjustable parameters, as shown in Table 11.

Preliminary optimization studies indicated that there was no significant difference in the goodness of fit of the various models tested when temperature term in the denominator has a power of 0, 1 or 2. This observation was generally true for all of the tests made with the CO and $C_3H_6$ mixtures. To stay with the popular trend in the literature, it was therefore decided to retain the temperature to the first power in the denominator. All results presented hereafter will use this form of the adsorption term.

**Table 11:** Parameter's description for CO and $C_3H_6$ experiments

| **Parameter** | | **Description of parameter** |
|---|---|---|
| $k_1$ | $A_1$ | pre-exponential factor, CO oxidation rate constant |
| | $E_1$ | activation energy, CO oxidation rate constant |
| $k_3$ | $A_3$ | pre-exponential factor, $C_3H_6$ oxidation rate constant |
| | $E_3$ | activation energy, $C_3H_6$ oxidation rate constant |
| $K_5$ | $B_5$ | pre-exponential factor, CO adsorption inhibition term |
| | $H_5$ | activation energy, CO adsorption inhibition term |
| $K_6$ | $B_6$ | pre-exponential factor, $C_3H_6$ adsorption inhibition term |
| | $H_6$ | activation energy, $C_3H_6$ adsorption inhibition term |
| $K_7$ | $B_7$ | pre-exponential factor, CO/$C_3H_6$ mixture adsorption inhibition term |
| | $H_7$ | activation energy, CO/$C_3H_6$ mixture adsorption inhibition term |

*Optimization of CO oxidation curves*

The first optimization study used experiments 1, 2 and 3. The effective model being used is thus:

$$\left(-R_{\mathrm{CO}}\right) = \frac{k_1 Y_{\mathrm{CO}} Y_{\mathrm{O_2}}}{T\left(1 + K_5 Y_{\mathrm{CO}}\right)^2} \tag{4.25}$$

For the first optimization test, each of experiments 1, 2 and 3 was optimized individually. Only the pre-exponential factor on the kinetic constant in the numerator was allowed to vary, and the activation energy and adsorption parameters were fixed to the values proposed by Voltz [1]. The best fit curves to the experimental points are given in Figure 21, and the parameter values and residual for each experiment in Table 12.

The agreement between the model and experiments is not extremely good, although might be considered acceptable by some. However, the parameter $A_1$ is significantly different in each case, suggesting that the model is not sufficient. This is confirmed by optimizing the three experiments together. The result is shown in Figure 22, and the parameter values and residual are given in Table 13. Clearly, it is not sufficient to optimize only the pre-exponential factor.

The next step is to adjust both the pre-exponential factor and the activation energy in the kinetic constant, $k_1$, and optimizing the three experiments together. The results from these optimization trials are given in Figure 23, and the parameter values in Table 14. Although the fit is superior (the residual is a bit lower), it does not really give an acceptable correlation. Therefore, it can be concluded that the practice of assuming the Voltz values will not be successful, and this approach was not used further in this work.

Finally, all four parameters were allowed to adjust, with the three experiments optimized together. The result is shown in Figure 24 and the parameter values and residual are given in Table 15.

From these results it is concluded that the best fit when optimizing 3 experiments simultaneously is obtained when varying all 4 parameters.

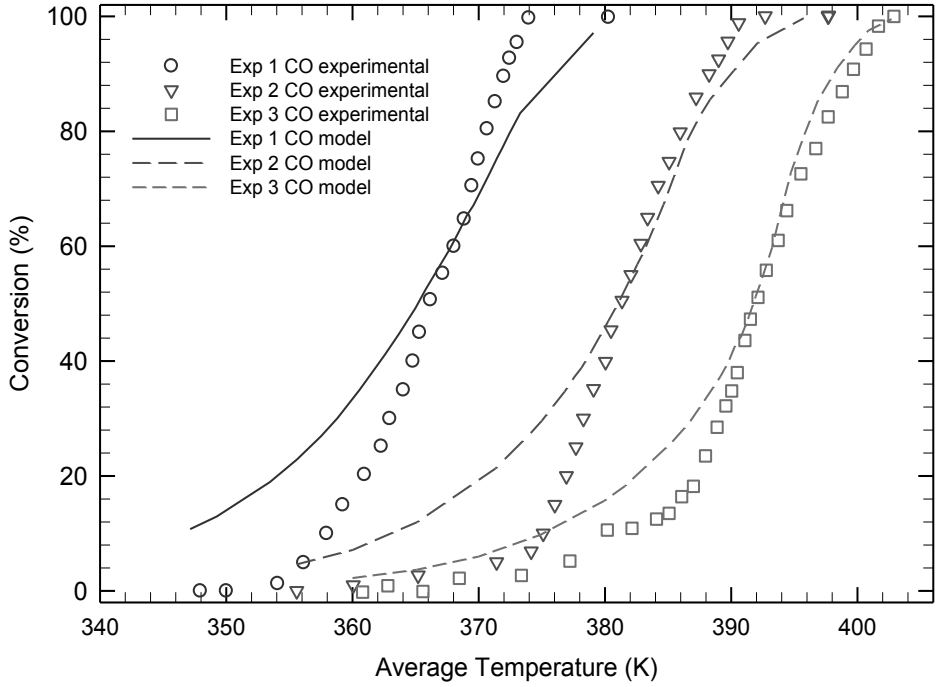


**Figure 21:** CO model results when optimizing individually each experiment and varying only one parameter out of four.

**Table 12:** Values of Parameters related to the individual modelling of CO

| Parameter | | Experiment 1 | Experiment 2 | Experiment 3 |
|---|---|---|---|---|
| $k_1$ | $A_1$ | 5,251,082,065 | 2,194,675,420 | 1,539,155,921 |
| | $E_1$ | 104,387 | 104,387 | 104,387 |
| $K_5$ | $B_5$ | 554.28 | 554.28 | 554.28 |
| | $H_5$ | -7,990 | -7,990 | -7,990 |
| Residual | | 139 | 91 | 25 |

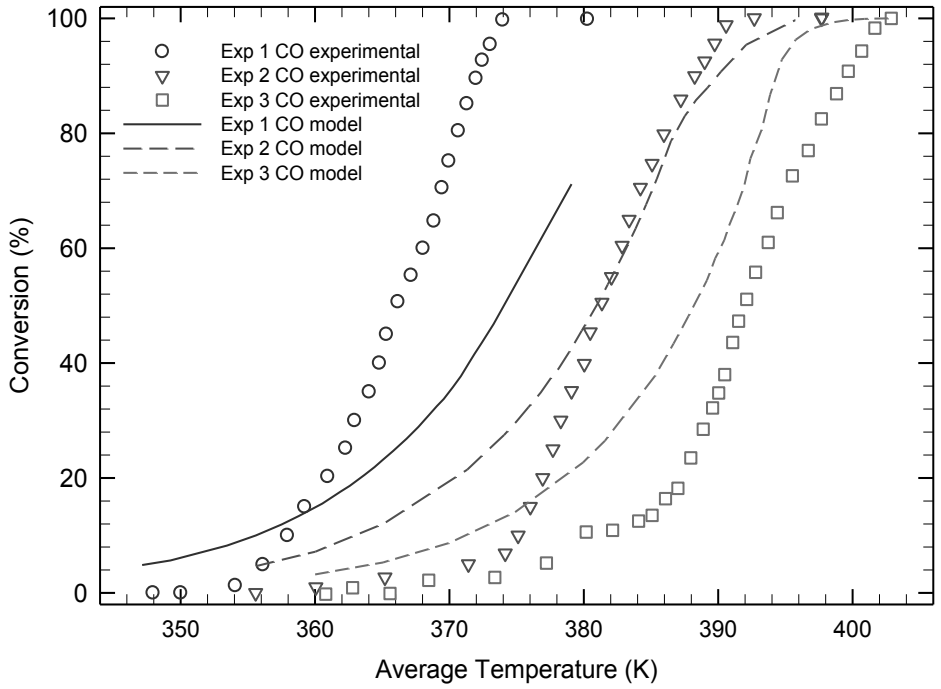


**Figure 22:** CO model results when simultaneously optimizing 3 experiments and varying only one parameter out of four.

**Table 13:** Value of the parameters and residuals the simultaneous modelling of CO varying one parameter

| Parameter | | Experiment 1 | Experiment 2 | Experiment 3 |
|---|---|---|---|---|
| $k_1$ | $A_1$ | 2,209,871,044 | | |
| | $E_1$ | 104,387 | | |
| $K_5$ | $B_5$ | 554.28 | | |
| | $H_5$ | -7,990 | | |
| Residual | | 950 | 92 | 254 |
| Total residual | | 1,296 | | |

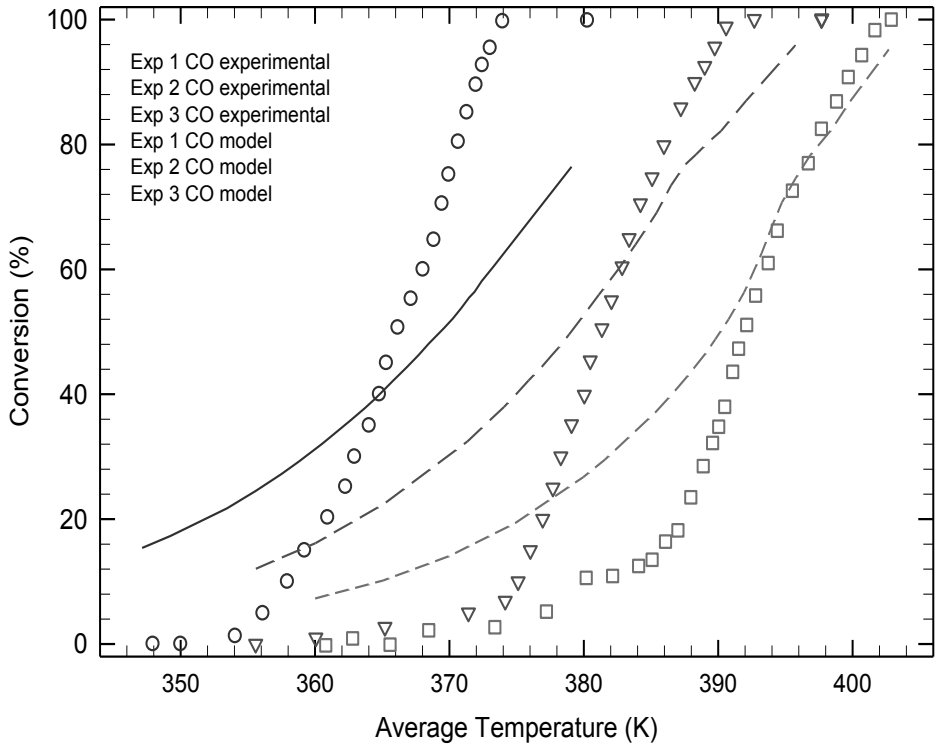


**Figure 23:** CO model results when simultaneously optimizing 3 experiments and varying 2 parameters out of four.

**Table 14:** Value of the parameters and residuals the simultaneous modelling of CO experiments varying 2 parameters

| Parameter | | Experiment 1 | Experiment 2 | Experiment 3 |
|---|---|---|---|---|
| $k_1$ | $A_1$ | 393,463,947 | | |
| | $E_1$ | 66,303 | | |
| $K_5$ | $B_5$ | 554.28 | | |
| | $H_5$ | -7,990 | | |
| Residual | | 464 | 265 | 138 |
| Total residual | | 867 | | |

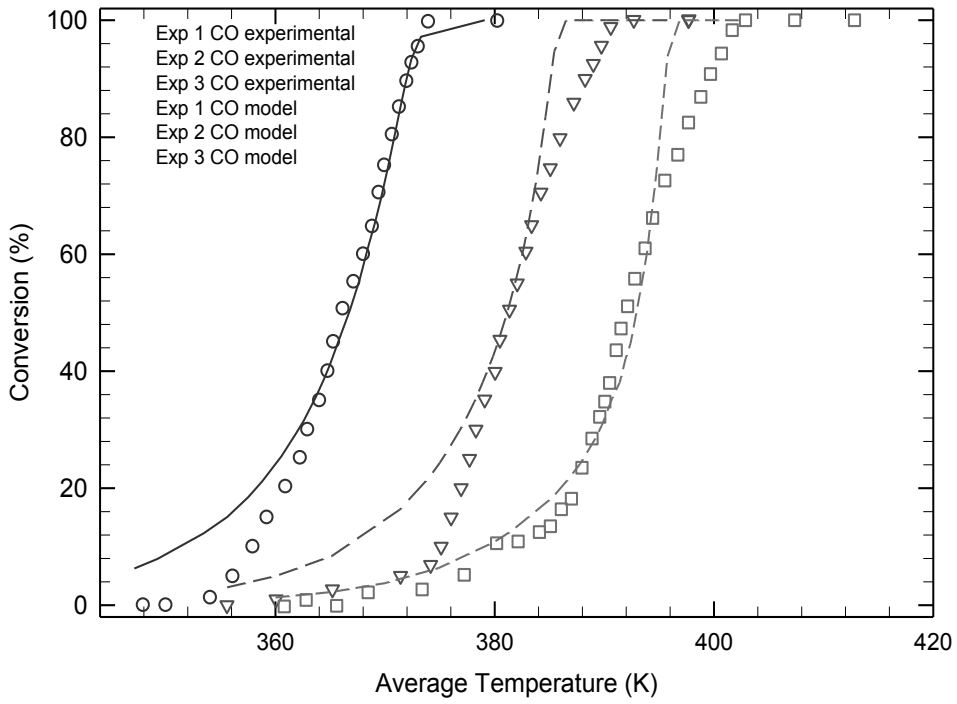


**Figure 24:** Results when optimizing 3 experiments and varying all four parameters.

**Table 15:** Value of the parameters and residuals the simultaneous modelling of CO experiments varying all 4 parameters

| Parameter | | Experiment 1 | Experiment 2 | Experiment 3 |
|---|---|---|---|---|
| $k_1$ | $A_1$ | 25,964,602,369 | | |
| | $E_1$ | 102,894 | | |
| $K_5$ | $B_5$ | 3,926 | | |
| | $H_5$ | -9,627 | | |
| Residual | | 30 | 58 | 58 |
| Total residual | | 146 | | |

*Optimization of $C_3H_6$ oxidation curves*

The second optimization study used experiments 7, 8 and 9. The model being used is thus:

$$\left(-R_{C_3H_6}\right) = \frac{k_3\, Y_{C_3H_6}\, Y_{O_2}}{T\left(1 + K_6\, Y_{C_3H_6}\right)^2} \tag{4.26}$$

A similar set of tests was conducted as used for the optimization of experiments 1, 2 and 3. That is, the model was optimized by varying only one and then two parameters. The result was very similar to that observed with the CO oxidation; therefore the results are not shown. The best result obtained for the simultaneous optimization of the three experiments was again found when optimizing the four parameters together. The parameter values are given in Table 16 and the curves are shown in Figure 25. It is seen that a reasonable agreement is achieved.

**Table 16:** Value of the parameters and residuals the simultaneous modelling of $C_3H_6$ experiments

| Parameter | | Experiment 7 | Experiment 8 | Experiment 9 |
|---|---|---|---|---|
| $k_3$ | $A_3$ | 87,220,043,666 | | |
| | $E_3$ | 64,884 | | |
| $K_6$ | $B_6$ | 99,708 | | |
| | $H_6$ | -5,079 | | |
| Residual | | 62 | 126 | 17 |
| Total residual | | 205 | | |

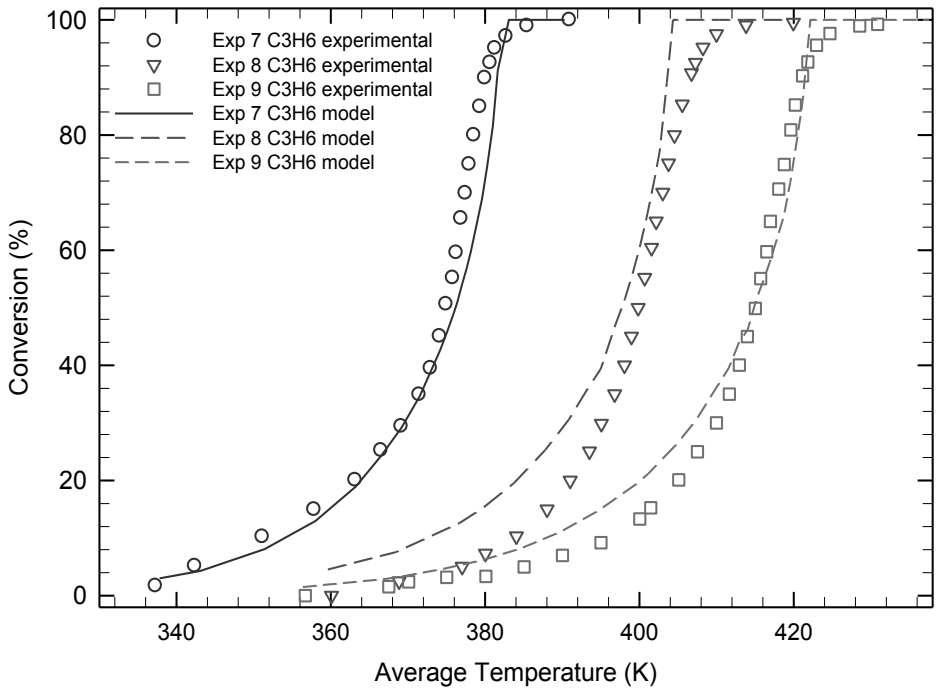


**Figure 25:** $C_3H_6$ model results when simultaneously optimizing 3 experiments and varying all four parameters.

*Optimization of combined CO and $C_3H_6$ oxidation curves*

In the previous section it was seen that when the triplets representing the results from a single oxidation reaction were optimized, it was possible to obtain reasonable fits to the experimental data. The next logical step was then to extend the study to experiments that included a mixture of CO and $C_3H_6$. These experiments are 17, 18 and 19. The Voltz model in this case can be written:

$$\left(-R_{\mathrm{CO}}\right) = \frac{k_1 Y_{\mathrm{CO}} Y_{\mathrm{O_2}}}{T\left(1 + K_5 Y_{\mathrm{CO}} + K_6 Y_{\mathrm{C_3H_6}}\right)^2 \left(1 + K_7 \left(Y_{\mathrm{CO}} Y_{\mathrm{C_3H_6}}\right)^2\right)} \tag{4.27}$$

$$\left(-R_{\mathrm{C_3H_6}}\right) = \frac{k_3 Y_{\mathrm{C_3H_6}} Y_{\mathrm{O_2}}}{T\left(1 + K_5 Y_{\mathrm{CO}} + K_6 Y_{\mathrm{C_3H_6}}\right)^2 \left(1 + K_7 \left(Y_{\mathrm{CO}} Y_{\mathrm{C_3H_6}}\right)^2\right)} \tag{4.28}$$

The first test was to use the values of the parameters obtained for the individual experiments for CO and $C_3H_6$ and to see if they would fit the results of the combined runs. Thus, the values of $A_1$, $E_1$, $A_3$, $E_3$, $B_5$, $H_5$, $B_6$ and $H_6$ were fixed to the values obtained when the CO and $C_3H_6$ oxidation experiments were optimized previously, and, in the first instance, the value of $K_7$ was set to zero. This test was performed because Voltz et al. [1] had postulated that this term was only needed at high concentrations. Therefore, there are no further parameters to fit. The results are shown in Figure 26 for the CO oxidation and in Figure 27 for the $C_3H_6$ oxidation. The predictions using these parameters were not satisfactory at all; indeed, the light-off for $C_3H_6$ occurred earlier than the light-off for CO. The total residual was 4853. As a second step, the parameters in constant $K_7$ were then set to the values quoted by Voltz [1]. These results are shown in Figures 28 and 29. Although the residual improved, it only decreased to 2726. Finally, the parameters in constant $K_7$ were allowed to vary. The lowest achievable residual was 2518, which was still unsatisfactory. These final results are shown in Figures 30 and 31.

At this point a few observations are warranted. If the model is mechanistic meaningful and correct, then it should be possible to build the final model using a set of experiments using individual reactions. The fact that this is not possible here does not necessarily invalidate the approach, although it does point to some weaknesses. During the optimization of the individual reactions, it was observed that there were several sets of parameters that would give similar residual values, and therefore we could conclude that three experiments are not sufficient to determine the best set of parameters over all ranges. Another possibility is that there are additional interactions between CO and $C_3H_6$ that are not accounted for in the model.

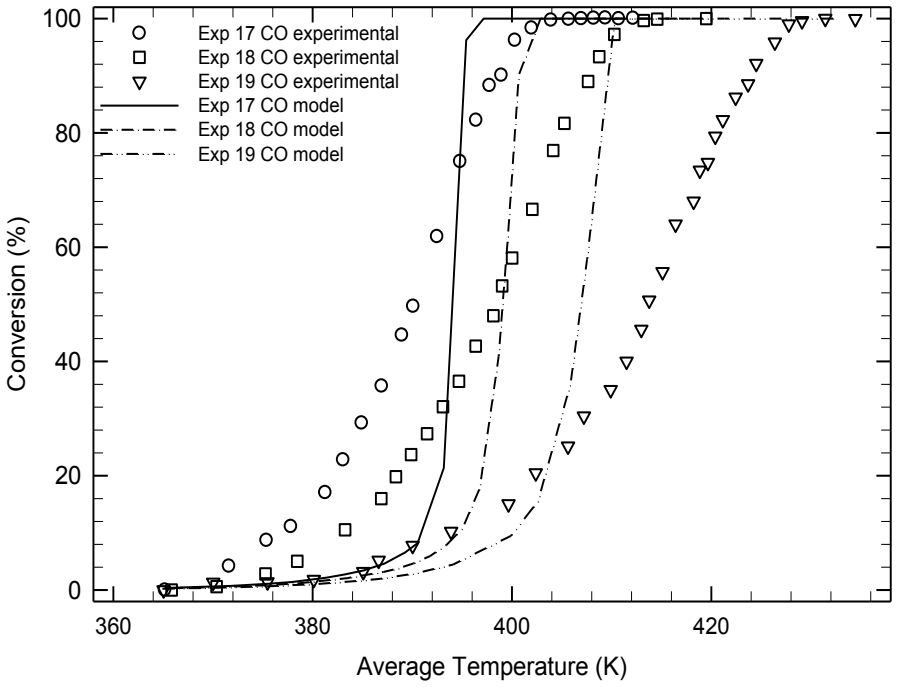


**Figure 26:** CO model results for the CO and $C_3H_6$ mixture experiments when setting previous best parameters found for individual CO and $C_3H_6$ experiments. $K_7$ set to zero.

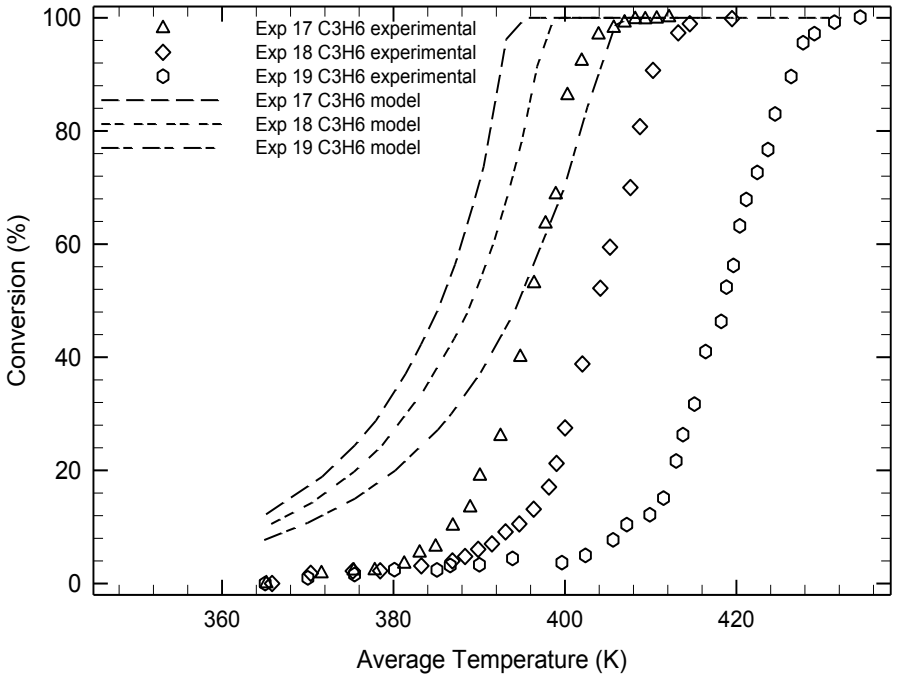


**Figure 27:** $C_3H_6$ model results for the CO and $C_3H_6$ mixture experiments when setting previous best parameters found for individual CO and $C_3H_6$ experiment. $K_7$ set to zero.

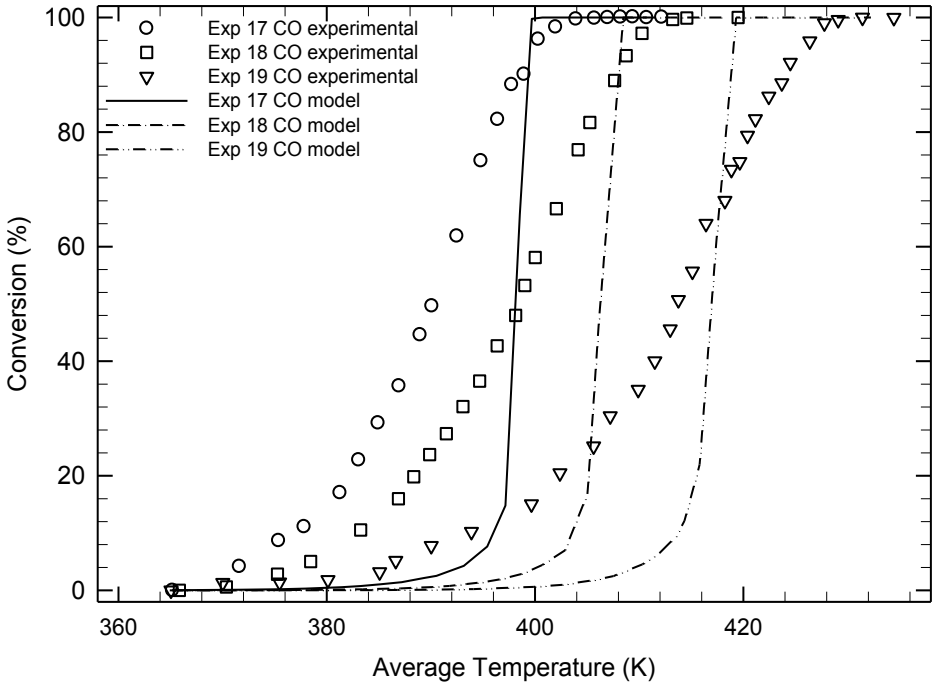


**Figure 28:** CO model results for the CO and $C_3H_6$ mixture experiments when setting previous best parameters found for individual CO and $C_3H_6$ experiment. $K_7$ optimized.

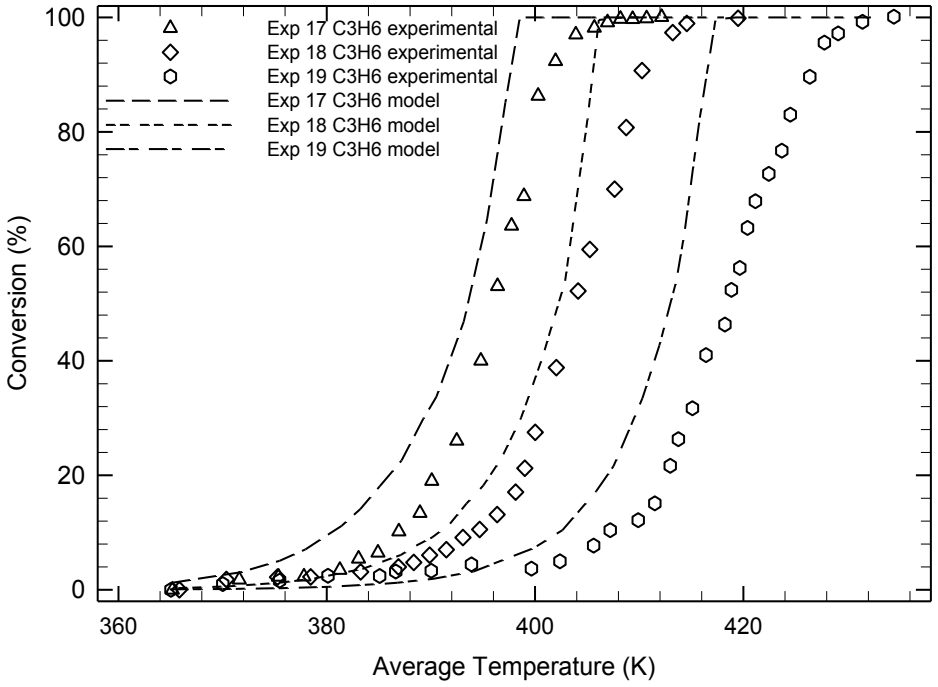


**Figure 29:** $C_3H_6$ model results for the CO and $C_3H_6$ mixture experiments when setting previous best parameters found for individual CO and $C_3H_6$ experiment. $K_7$ optimized.

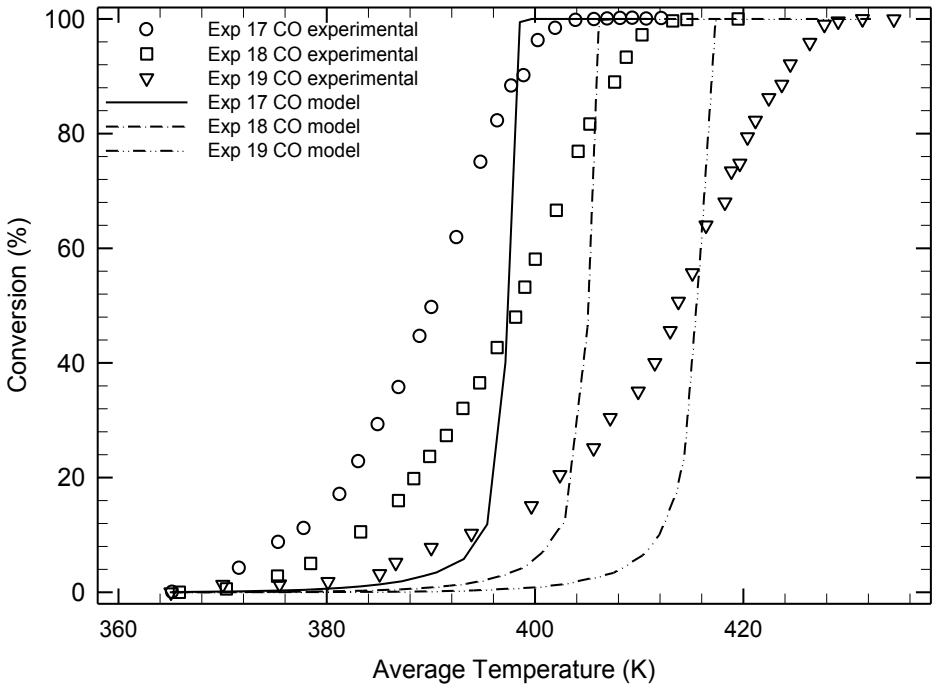


**Figure 30:** CO model results for the CO and $C_3H_6$ mixture experiments when setting previous best parameters found for individual CO and $C_3H_6$ experiment. $K_7$ set to SPV value.

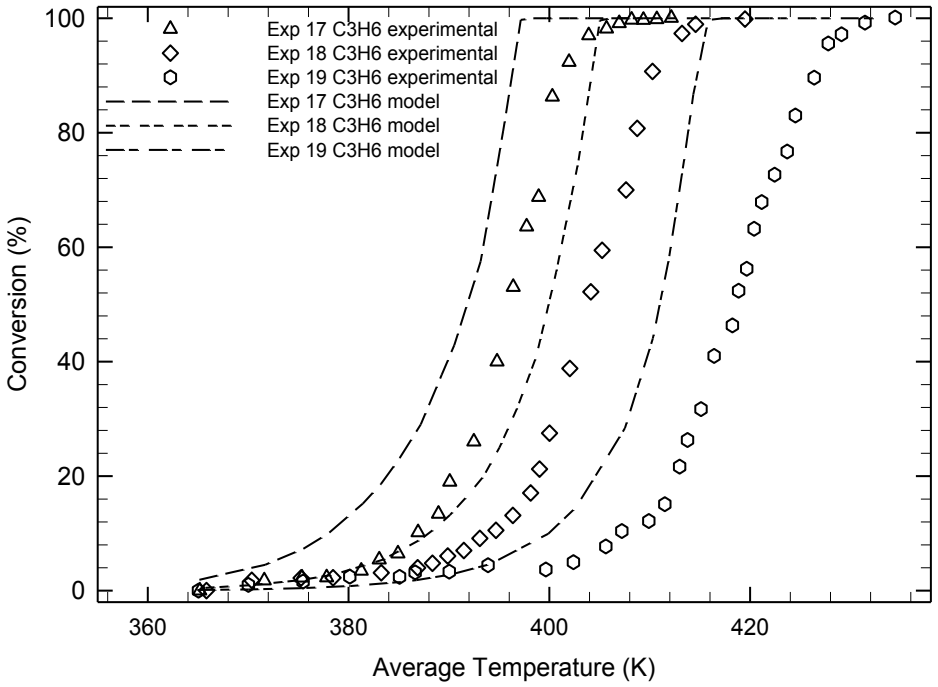


**Figure 31:** $C_3H_6$ model results for the CO and $C_3H_6$ mixture experiments when setting previous best parameters found for individual CO and $C_3H_6$ experiment. $K_7$ set to its SPV value.

Because the previously found parameters are not satisfactory, the next step was to optimize the three experiments (17 – 19) and allowing all of the parameters to vary. In the first instance, the parameters $A_1$, $E_1$, $A_3$, $E_3$, $B_5$, $H_5$, $B_6$ and $H_6$ were adjusted. Three tests were performed. In the first the value of $K_7$ was set to zero, in the second the value was set to the values reported by Voltz (SVP)[1], and finally it was allowed to find the optimal value, thus giving ten parameters to fit. All of the parameter values and residuals are given in Table 17. The graphs are shown in Figures 32 and 33, 34 and 35, and 36 and 37 respectively.

**Table 17:** Value of the parameters and residuals the simultaneous modeling of CO and $C_3H_6$ mixture when $K_7$ is set to zero and SVP values, and finally is allowed to adjust

| Parameter | | $K_7$ = zero | | | $K_7$ = SVP | | | $K_7$ = optimised | | |
|---|---|---|---|---|---|---|---|---|---|---|
| | | 17 | 18 | 19 | 17 | 18 | 19 | 17 | 18 | 19 |
| $k_1$ | $A_1$ | 1,905,861,549 | | | 316,426,011 | | | 1,334,336,498 | | |
| | $E_1$ | 92,220 | | | 63,659 | | | 82,410 | | |
| $k_3$ | $A_3$ | 1,040,742,253 | | | 259,898,059 | | | 1,095,963,805 | | |
| | $E_3$ | 100,227 | | | 78,336 | | | 102,913 | | |
| $K_5$ | $B_5$ | 2,958 | | | 862 | | | 2,431 | | |
| | $H_5$ | -6,618 | | | -6,649 | | | -8,948 | | |
| $K_6$ | $B_6$ | 759 | | | 575 | | | 1,067 | | |
| | $H_6$ | -7,732 | | | -9,374 | | | -6,764 | | |
| $K_7$ | $B_7$ | 1 | | | 6.39E+11 | | | 127,910,930,094 | | |
| | $H_7$ | 0 | | | -96,534 | | | -75,624 | | |
| Residual | | 33 | 47 | 101 | 40 | 35 | 92 | 40 | 35 | 92 |
| Total residual | | 181 | | | 226 | | | 167 | | |

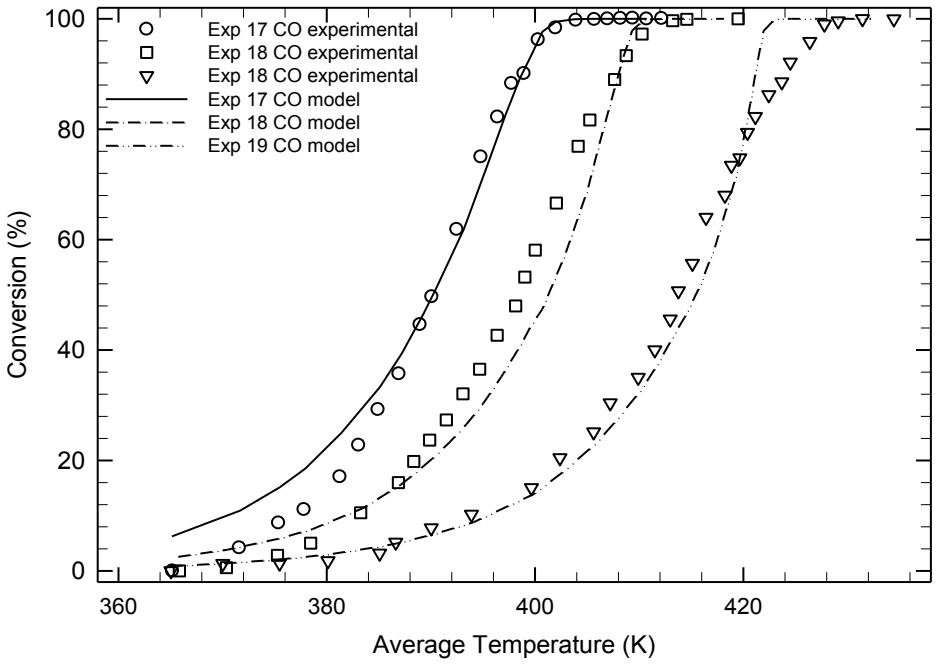


**Figure 32:** CO model results when simultaneously optimizing 3 experiments and varying 8 parameters of CO and $C_3H_6$ mixture. $K_7$ set zero.

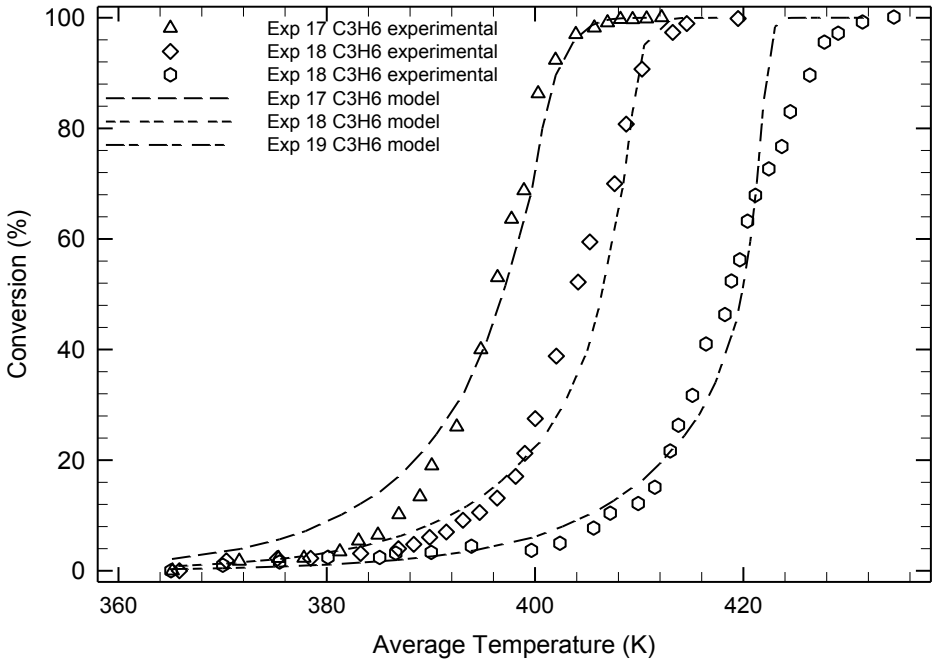


**Figure 33:** $C_3H_6$ model results when simultaneously optimizing 3 experiments and varying 8 parameters of CO and $C_3H_6$ mixture. $K_7$ set zero.

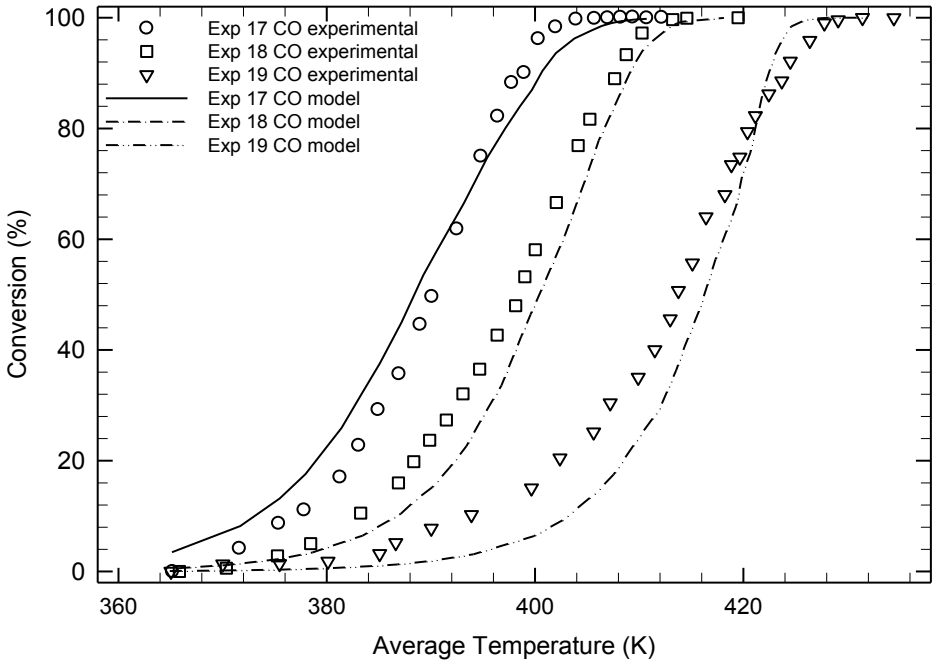


**Figure 34:** CO model results when simultaneously optimizing 3 experiments and varying 8 parameters of CO and $C_3H_6$ mixture. $K_7$ set to its SPV value.

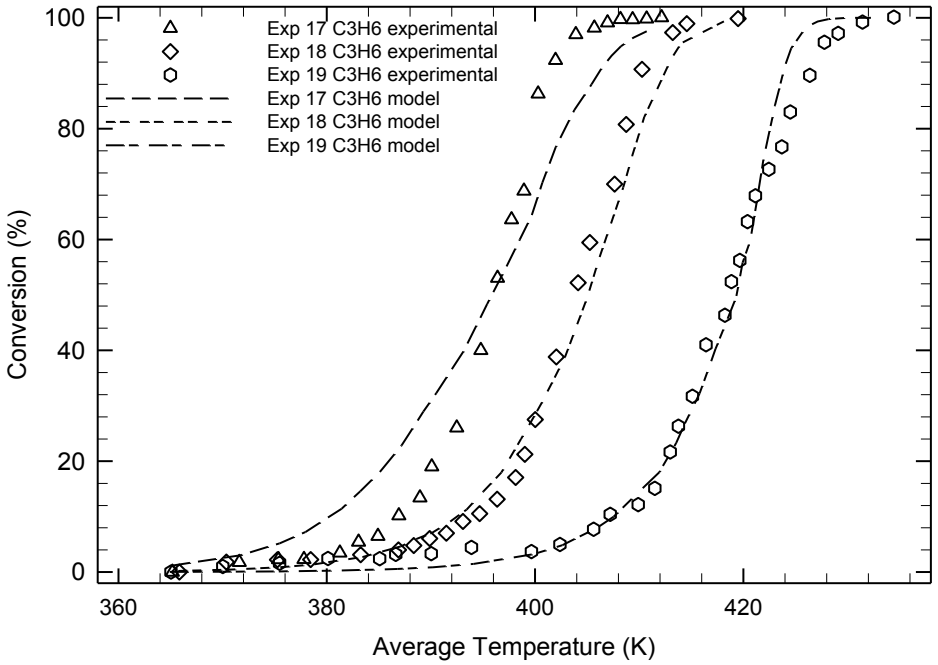


**Figure 35:** CO model results when simultaneously optimizing 3 experiments and varying 8 parameters of CO and $C_3H_6$ mixture. $K_7$ set to its SPV value.

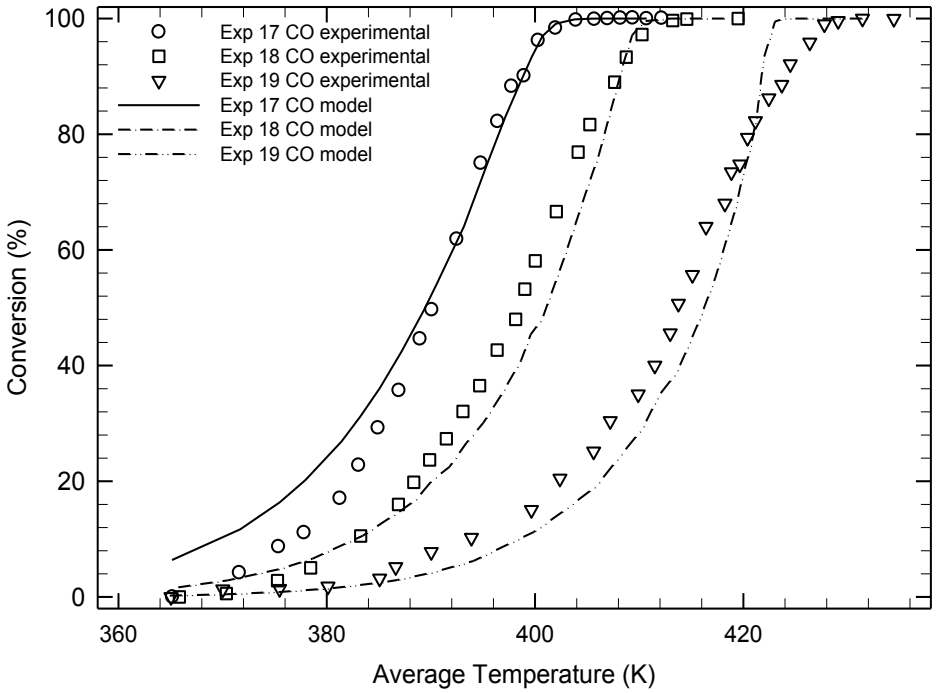


**Figure 36:** CO model results when simultaneously optimizing 3 experiments and varying all 10 parameters of CO and $C_3H_6$ mixture.

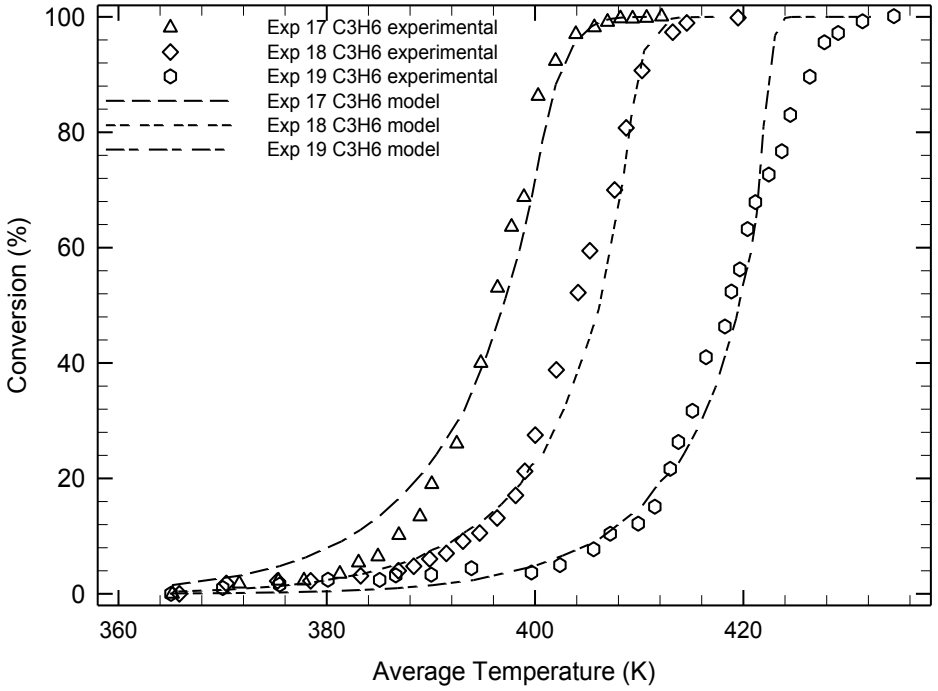


**Figure 37:** $C_3H_6$ model results when simultaneously optimizing 3 experiments and varying all 10 parameters of CO and $C_3H_6$ mixture.

It is seen that the best result is obtained when $K_7$ is included and adjusted. This result is not surprising, because additional parameters should result in a better fit. The interesting point is that the result when $K_7$ is not used is superior to that when it is included with the standard Voltz values [1].

As noted earlier, the parameters obtained when fitting the CO and $C_3H_6$ oxidation experiments (1-3, and 7-9) did not give a good solution for the optimization of the combined oxidation experiments, experiments 17-19. Similarly, when the parameters from the optimization of experiments 17-19 were used to predict the results of experiments 1, 2, 3, 7, 8 and 9, the results were also not very good. Therefore, all nine experiments were optimized together, whilst fitting the ten parameters. The best parameters are given in Table 18, and the graphs in Figures 38 to 41.

Although the residual is clearly higher by a noticeable amount, the fits of the model are still reasonable.

**Table 18:** Value of the parameters and residuals the simultaneous modeling of all 9 experiments of CO, $C_3H_6$ and their mixture, varying all 10 parameters

| Parameter | | Exp 1 | Exp 2 | Exp 3 | Exp 7 | Exp 8 | Exp 9 | Exp 17 | Exp 18 | Exp 19 |
|---|---|---|---|---|---|---|---|---|---|---|
| $k_1$ | $A_1$ | 14,265,359,174 | | | | | | | | |
| | $E_1$ | 89,663 | | | | | | | | |
| $k_3$ | $A_3$ | 3,293,774,472 | | | | | | | | |
| | $E_3$ | 62,634 | | | | | | | | |
| $K_5$ | $B_5$ | 4,000 | | | | | | | | |
| | $H_5$ | -9,996 | | | | | | | | |
| $K_6$ | $B_6$ | 19,499 | | | | | | | | |
| | $H_6$ | -2,017 | | | | | | | | |
| $K_7$ | $B_7$ | 933,213,646,196 | | | | | | | | |
| | $H_7$ | -75,012 | | | | | | | | |
| Residual | | 65 | 56 | 138 | 118 | 135 | 35 | 75 | 144 | 212 |
| Total residual | | 978 | | | | | | | | |

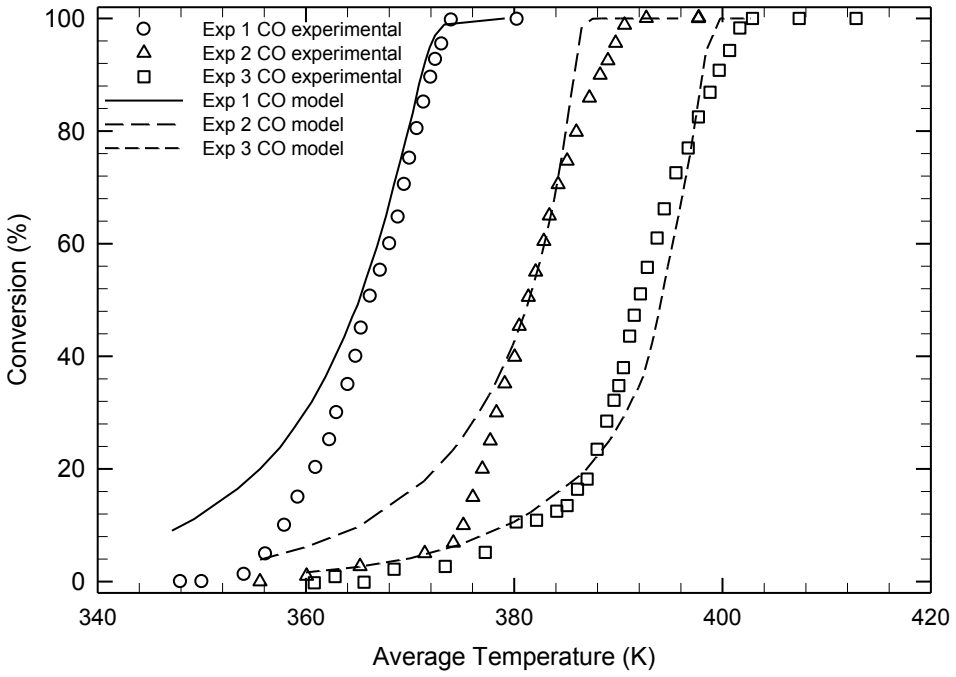


**Figure 38:** CO model results when simultaneously optimizing all 9 experiments of CO, $C_3H_6$ and mixture, and varying all 10 parameters.

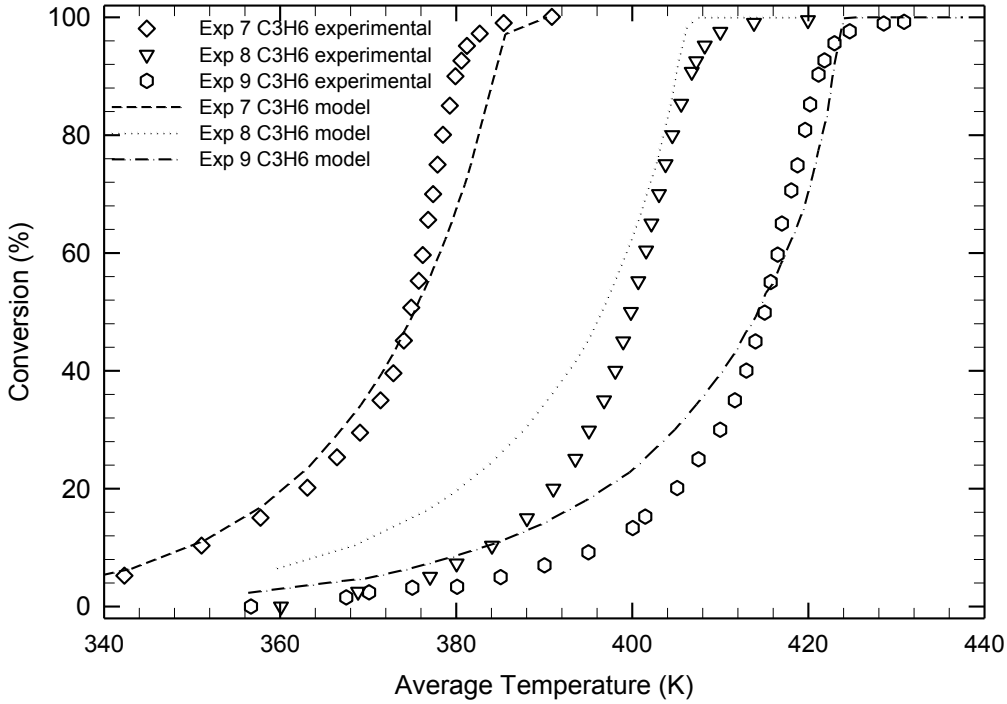


**Figure 39:** $C_3H_6$ model results when simultaneously optimizing all 9 experiments of CO, $C_3H_6$ and mixture, and varying all 10 parameters.

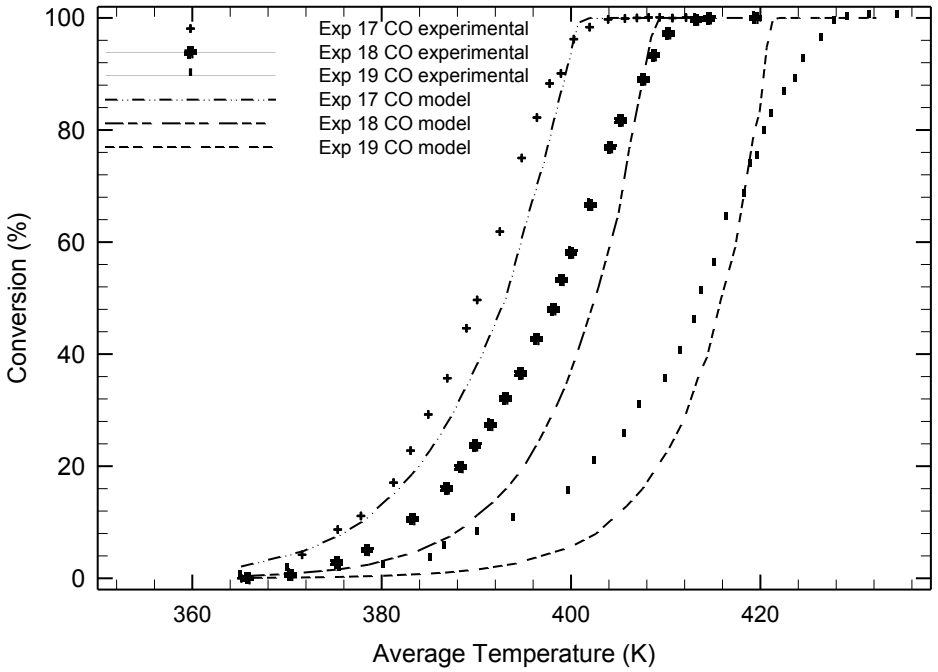


**Figure 40:** CO in mix model results when simultaneously optimizing all 9 experiments of CO, $C_3H_6$ and mixture, and varying all 10 parameters.

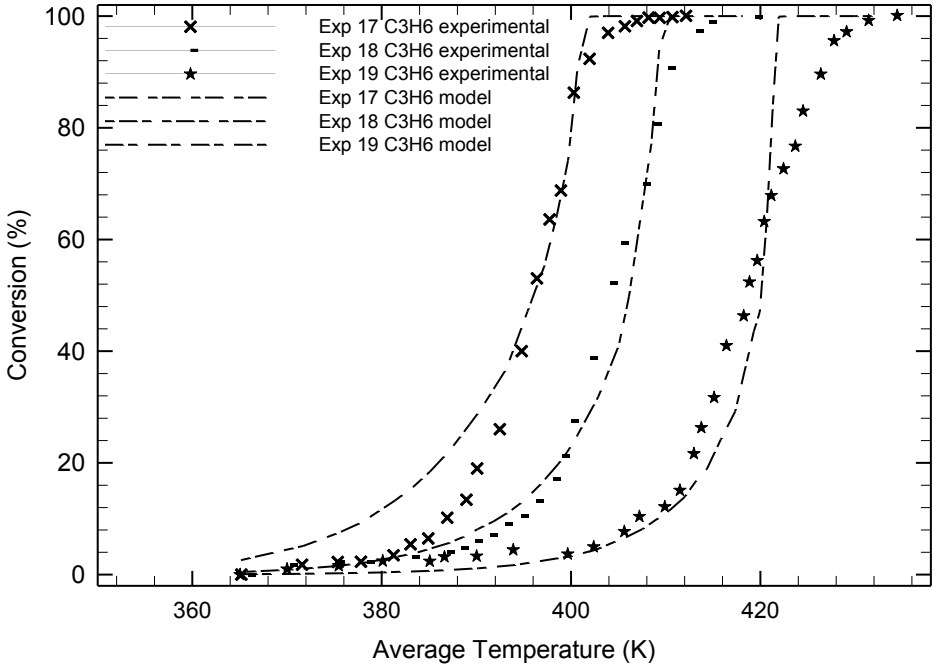


**Figure 41:** $C_3H_6$ in mix model results when simultaneously optimizing all 9 experiments of CO, $C_3H_6$ and mixture, and varying all 10 parameters.

### 4.2.2. The oxidation of NO and $C_3H_6$

**Model for Oxidation of NO**

There is a lot of work reported in the literature that deals with the oxidation of NO on platinum catalyst. A key feature of the oxidation of NO is that it is constrained by equilibrium at higher temperatures. The global reaction may be represented by:

$$\mathrm{NO} + \frac{1}{2}\mathrm{O_2} \rightarrow \mathrm{NO_2} \tag{4.29}$$

The key global models presented in the literature have been reviewed by Hauptmann et al. [24] and the main ones that have been reported are given in the following. The first model presented is based on a form used by Sampara et al. [25] and Pandya [2]:

$$\left(-R_{\mathrm{NO}}\right) = \frac{k_4\, Y_{\mathrm{NO}} Y_{\mathrm{O_2}}^{0.5}}{\left(1 + K_8 Y_{\mathrm{NO}}\right)}\left(1 - \beta\right) \tag{4.30}$$

where the equilibrium term is:

$$\beta = \left[\frac{1}{K_{\mathrm{eq}}}\frac{1}{\sqrt{P}}\frac{Y_{\mathrm{NO_2}}}{Y_{\mathrm{NO}}\left(Y_{\mathrm{O_2}}\right)^{0.5}}\right] \tag{4.31}$$

The pressure, *P*, has units of bar. Many papers do not include the pressure, however, most investigations are carried out at or near one bar pressure. The equilibrium constant as a function of temperature is given by:

$$K_{\mathrm{eq}} = \exp\left(\begin{array}{l} 5.045 + \dfrac{6.344\times10^{3}}{T} - 2.3\ln(T) + \\ 3.031\times10^{-3}T - 8.281\times10^{-7}T^{2} + 1.142\times10^{-10}T^{3} \end{array}\right) \tag{4.32}$$

Mulla et al. [9] developed a model that can be written as:

$$\left(-R_{\mathrm{NO}}\right) = \frac{k_4 Y_{\mathrm{O_2}}}{\left(1 + K_8 \dfrac{Y_{\mathrm{NO_2}}}{Y_{\mathrm{NO}}}\right)}(1-\beta) \tag{4.33}$$

This model was claimed to be consistent with experimental data that showed an inhibition effect by $NO_2$. Bhatia et al. [4] reported the following model:

$$\left(-R_{\mathrm{NO}}\right) = \frac{k_4 Y_{\mathrm{O_2}}}{\left(1 + K_8\, Y_{\mathrm{NO}} + K_{10} \dfrac{Y_{\mathrm{NO_2}}}{Y_{\mathrm{NO}}}\right)}\left(1-\beta^2\right) \tag{4.34}$$

In this work, it is proposed to use this model in slightly modified form, with the equilibrium expression raised to the power one, in keeping with common practice.

$$\left(-R_{\mathrm{NO}}\right) = \frac{k_4 Y_{\mathrm{O_2}}^{0.5}}{\left(1 + K_8\, Y_{\mathrm{NO}} + K_{10} \dfrac{Y_{\mathrm{NO_2}}}{Y_{\mathrm{NO}}}\right)}(1-\beta) \tag{4.35}$$

Hauff et al. [5] proposed a slightly different rate equation as part of a general model for a diesel oxidation catalyst:

$$\left(-R_{\mathrm{NO}}\right) = \frac{k_4\, Y_{\mathrm{NO}} Y_{\mathrm{O_2}}^{0.5}}{\left(1 + K_8 Y_{\mathrm{NO}} + K_{10} Y_{\mathrm{NO_2}}\right)^2}(1-\beta) \tag{4.36}$$

It should be noted that the model of Hauff et al. [2, 5] did not allow for inhibition by hydrocarbons, even when used as part of the DOC model. Slight variations have been made on these reported equations to develop five models for testing. In keeping with the common Voltz [1] type assumption, the

temperature has been included in the denominator, although this actually had no significant effect (although obviously the parameter values are different). Also note that oxygen has been put to the 0.5 in the Bhatia model [4].

The five tested models are summarized below:

**Model 1:**
$$\left(-R_{\mathrm{NO}}\right) = \frac{k_4\, Y_{\mathrm{NO}} Y_{\mathrm{O_2}}^{0.5}}{T\left(1 + K_8 Y_{\mathrm{NO}}\right)}\left(1 - \beta\right) \tag{4.37}$$

**Model 2:**
$$\left(-R_{\mathrm{NO}}\right) = \frac{k_4 Y_{\mathrm{O_2}}}{T\left(1 + K_8 \dfrac{Y_{\mathrm{NO_2}}}{Y_{\mathrm{NO}}}\right)}\left(1 - \beta\right) \tag{4.38}$$

**Model 3:**
$$\left(-R_{\mathrm{NO}}\right) = \frac{k_4 Y_{\mathrm{O_2}}^{0.5}}{T\left(1 + K_8\, Y_{\mathrm{NO}} + K_{10} \dfrac{Y_{\mathrm{NO_2}}}{Y_{\mathrm{NO}}}\right)}\left(1 - \beta^2\right) \tag{4.39}$$

**Model 4:**
$$\left(-R_{\mathrm{NO}}\right) = \frac{k_4 Y_{\mathrm{O_2}}^{0.5}}{T\left(1 + K_8\, Y_{\mathrm{NO}} + K_{10} \dfrac{Y_{\mathrm{NO_2}}}{Y_{\mathrm{NO}}}\right)}\left(1 - \beta\right) \tag{4.40}$$

**Model 5:**
$$\left(-R_{\mathrm{NO}}\right) = \frac{k_4\, Y_{\mathrm{NO}} Y_{\mathrm{O_2}}^{0.5}}{T\left(1 + K_8 Y_{\mathrm{NO}} + K_{10} Y_{\mathrm{NO_2}}\right)^2}\left(1 - \beta\right) \tag{4.41}$$

The models contain up to six adjustable parameters, as shown in the Table 19:

**Table 19:** Parameter's description for NO experiments

| Parameter | | Description of parameter |
|---|---|---|
| $k_4$ | $A_4$ | pre-exponential factor, NO oxidation rate constant |
| | $E_4$ | activation energy, NO oxidation rate constant |
| $K_8$ | $B_8$ | pre-exponential factor, NO adsorption inhibition term |
| | $H_8$ | activation energy, NO adsorption inhibition term |
| $K_{10}$ | $B_{10}$ | pre-exponential factor, $NO_2$ adsorption inhibition term |
| | $H_{10}$ | activation energy, $NO_2$ adsorption inhibition term |

*Oxidation of NO alone*

This optimization study used experiments 10, 11 and 12 to test the 5 models. As previously seen, when fitting the parameters in the CO and HC models, it was relatively easy to obtain a very good fit for any of the models when fitting a single experiment. However, as before, there is a wide difference in the parameter values for each experiment. All of the following results were obtained when the three curves were fit simultaneously.

From the plots, it can be inferred that models 3, 4 and 5 gave the best fitting of the curves. Model 3 will not be deeper studied, because of disagreements with the structure of the model. Therefore, models 4 and 5 were evaluated for the mixture concentrations of NO and $C_3H_6$, along with model 1 for historical purposes.

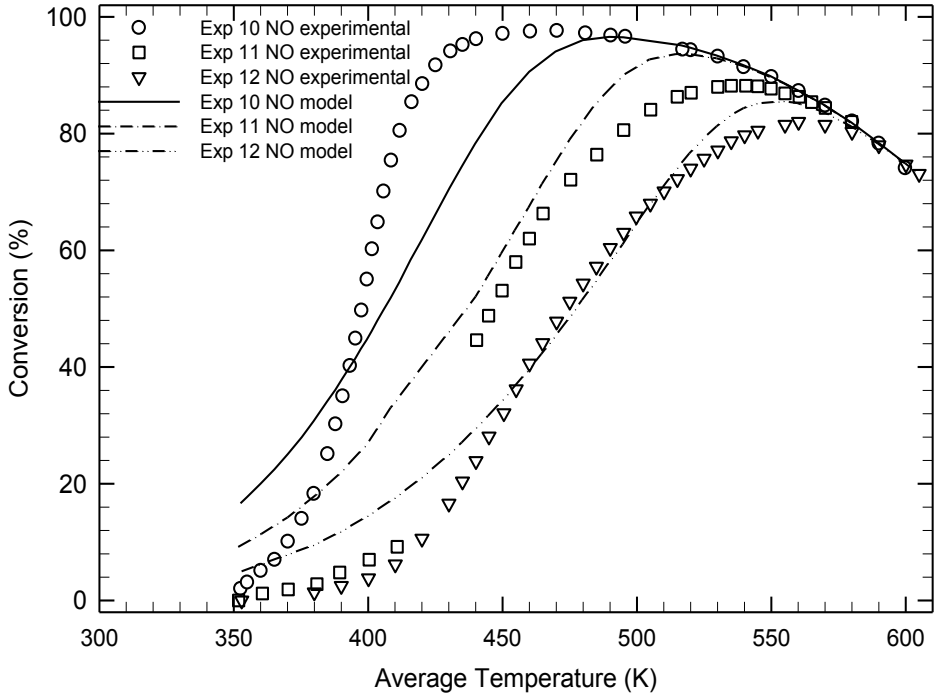


**Figure 42:** NO model results when simultaneously optimizing 3 experiments and varying all four parameters. Model 1.

**Table 20:** Value of the parameters and residuals the individual modelling of NO for Model 1

| Parameter | | Experiment 10 | Experiment 11 | Experiment 12 |
|---|---|---|---|---|
| $k_4$ | $A_4$ | 13,048,712 | | |
| | $E_4$ | 25,034 | | |
| $K_8$ | $B_8$ | 19,975 | | |
| | $H_8$ | -5,014 | | |
| Residual | | 183 | 86 | 24 |
| Total residual | | 293 | | |

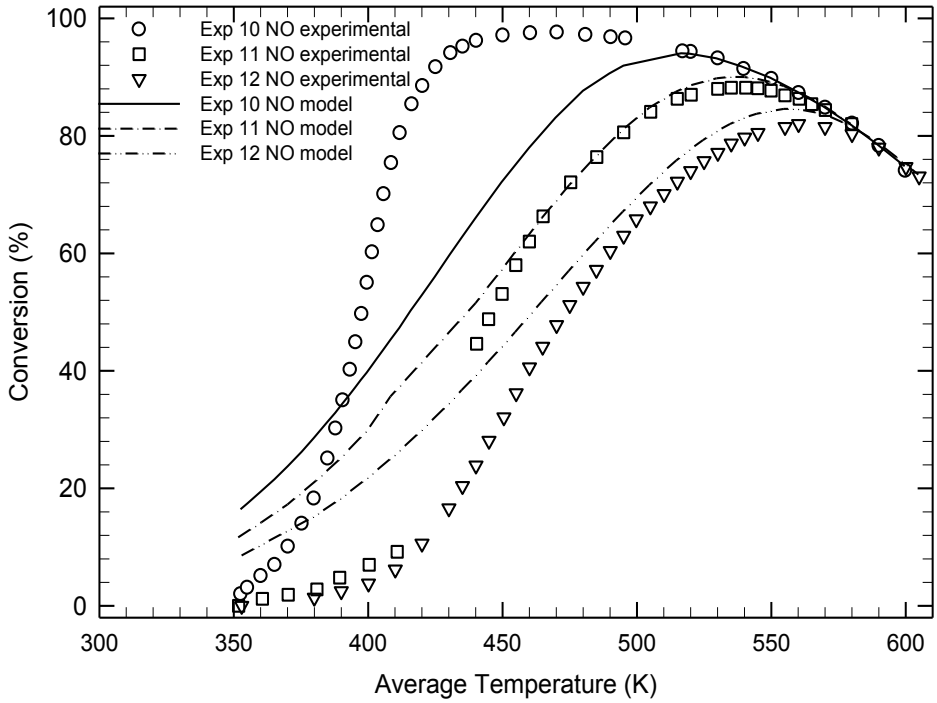


**Figure 43:** NO model results when simultaneously optimizing 3 experiments and varying all four parameters. Model 2.

**Table 21:** Value of the parameters and residuals the individual modelling of NO for Model 2

| Parameter | | Experiment 10 | Experiment 11 | Experiment 12 |
|---|---|---|---|---|
| $k_4$ | $A_4$ | 3,558,679 | | |
| | $E_4$ | 43,496 | | |
| $K_8$ | $B_8$ | 14,658 | | |
| | $H_8$ | -8,567 | | |
| Residual | | 333 | 91 | 88 |
| Total residual | | 512 | | |

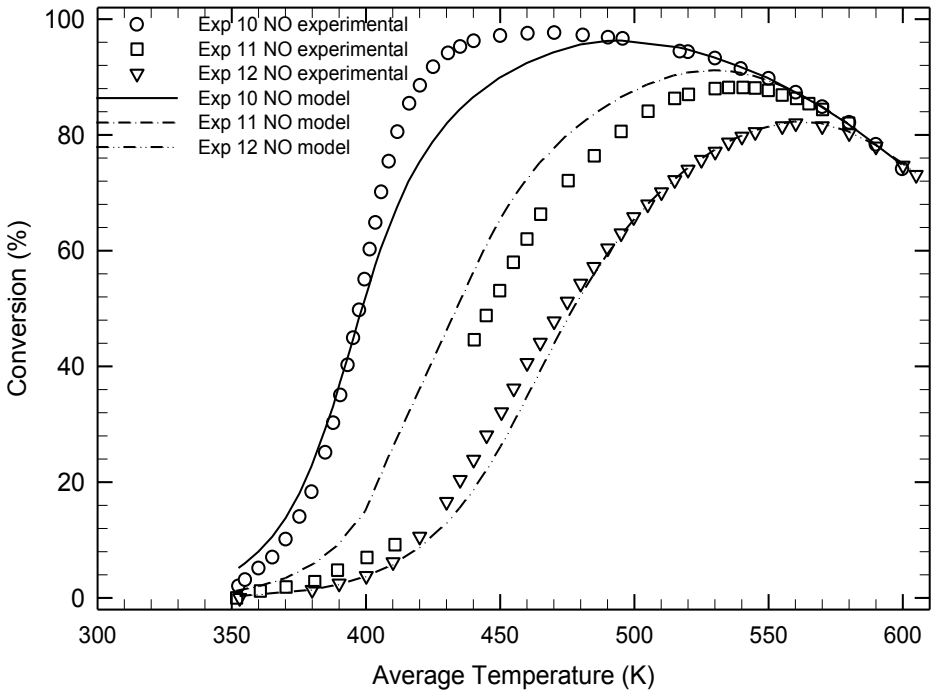


**Figure 44:** NO model results when simultaneously optimizing 3 experiments and varying all four parameters. Model 3.

**Table 22:** Value of the parameters and residuals the individual modelling of NO for Model 3

| Parameter | | Experiment 10 | Experiment 11 | Experiment 12 |
|---|---|---|---|---|
| $k_4$ | $A_4$ | 5,391 | | |
| | $E_4$ | 25,037 | | |
| $K_8$ | $B_8$ | 19,197 | | |
| | $H_8$ | -38,127 | | |
| $K_{10}$ | $B_{10}$ | 7.19 | | |
| | $H_{10}$ | -7.25 | | |
| Residual | | 39 | 44 | 8 |
| Total residual | | 91 | | |

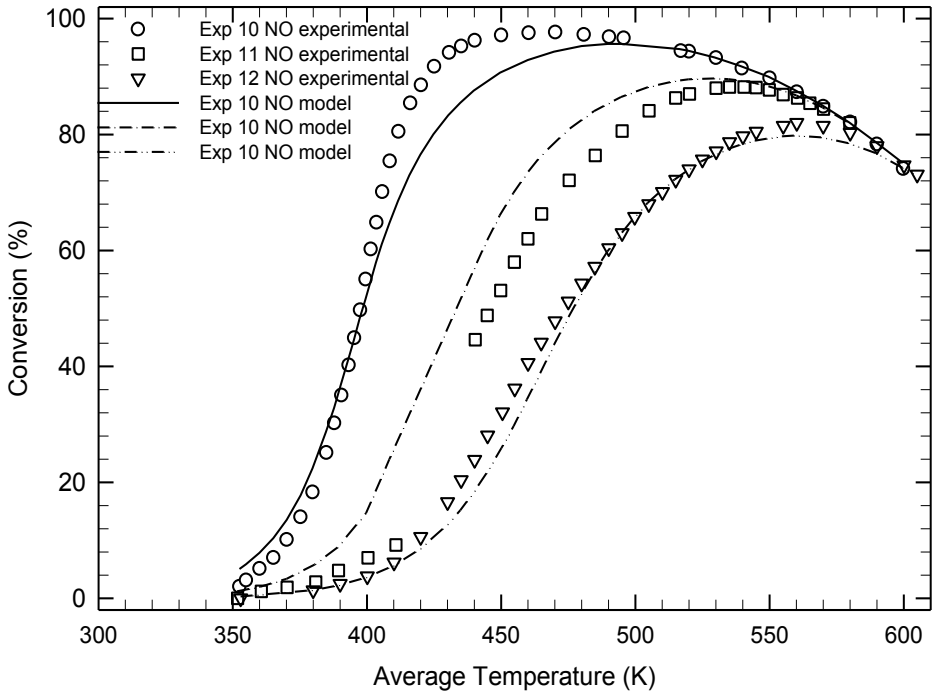


**Figure 45:** NO model results when simultaneously optimizing 3 experiments and varying all four parameters. Model 4.

**Table 23:** Value of the parameters and residuals the individual modelling of NO for Model 4

| Parameter | | Experiment 10 | Experiment 11 | Experiment 12 |
|---|---|---|---|---|
| $k_4$ | $A_4$ | 5,473 | | |
| | $E_4$ | 25,029 | | |
| $K_8$ | $B_8$ | 19,927 | | |
| | $H_8$ | -38,130 | | |
| $K_{10}$ | $B_{10}$ | 6.73 | | |
| | $H_{10}$ | -0.31 | | |
| Residual | | 33 | 47 | 9 |
| Total residual | | 89 | | |

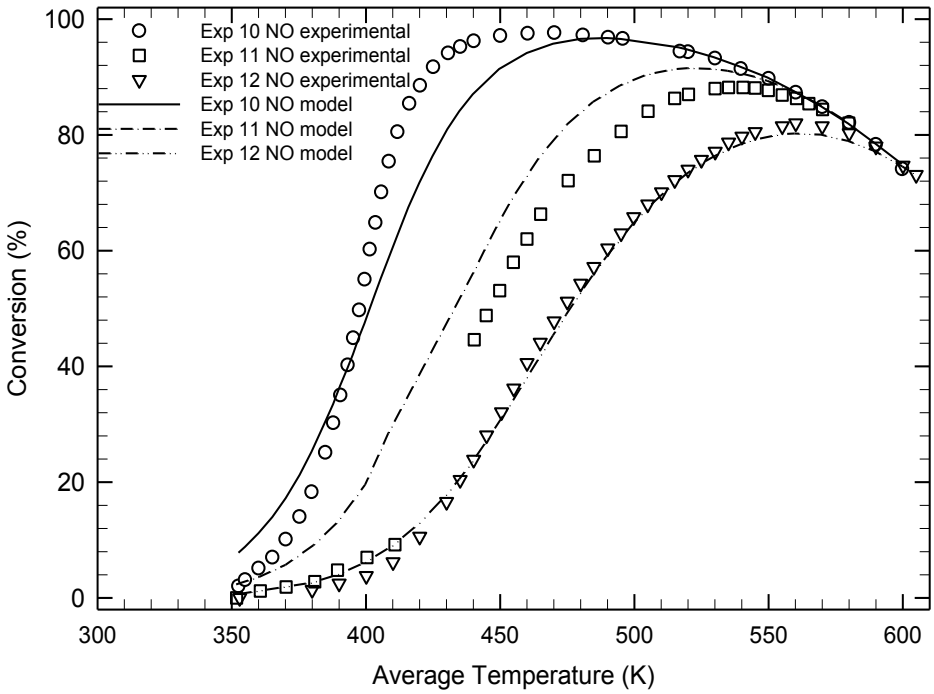


**Figure 46:** NO model results when simultaneously optimizing 3 experiments and varying all four parameters. Model 5.

**Table 24:** Value of the parameters and residuals the individual modelling of NO for Model 5

| Parameter | | Experiment 10 | Experiment 11 | Experiment 12 |
|---|---|---|---|---|
| $k_4$ | $A_4$ | 26,770,203 | | |
| | $E_4$ | 25,007 | | |
| $K_8$ | $B_8$ | 7,007 | | |
| | $H_8$ | -17,754 | | |
| $K_{10}$ | $B_{10}$ | 5,579 | | |
| | $H_{10}$ | -3.23 | | |
| Residual | | 68 | 61 | 2 |
| Total residual | | 131 | | |

**Oxidation of NO in the presence of $C_3H_6$**

There has been much work done on SCR catalysts for hydrocarbons. With a feed of HC and NO in an excess of oxygen both will be oxidized. However, over a small temperature range, some NO will be reduced by the HC. Alternatively, it has been proposed that the NO is first oxidized, and then the $NO_2$ reacts with the HC. The consensus in the literature seems to be that over Pt catalysts, the reduction of NO occurs by the reaction of NO with partial oxidation products of $C_3H_6$ to form $N_2$ and $N_2O$. If $NO_2$ reacts with $C_3H_6$ then it simply forms NO. Over other acid catalysts, it has been proposed that the reduction reaction occurs between $C_3H_6$ and $NO_2$. The competing pathways for propene conversion under oxidizing conditions can be represented by the following global reactions:

$$C_3H_6 + 2NO + \frac{7}{2}O_2 \rightarrow N_2 + 3H_2O + 3CO_2 \quad (4.42)$$

$$C_3H_6 + 2NO + 4O_2 \rightarrow N_2O + 3H_2O + 3CO_2 \quad (4.43)$$

$$C_3H_6 + \frac{9}{2}O_2 \rightarrow 3H_2O + 3CO_2 \quad (4.44)$$

The reaction between $NO_2$ and propene can be written:

$$C_3H_6 + NO_2 + 4O_2 \rightarrow NO + 3H_2O + 3CO_2 \quad (4.45)$$

For the SCR of $NO_X$ present in the exhaust from a lean burn diesel engine, the paper by Ansell et al. (1996)[26] is a significant work. It is a good starting point for the development of a global kinetics models for the prediction of light-off performance of SCR catalysts. The rate expressions that they proposed for propene and $NO_X$ conversion are:

$$\left(-R_{C_3H_6}\right) = A_{C_3H_6} \exp\left(-\frac{E_{C_3H_6}}{R_g T}\right) \frac{C_{C_3H_6} C_{O_2}}{\left(1 + X\, C_{C_3H_6}\right)\left(1 + Y\, C_{NO}\right)} \tag{4.46}$$

$$\left(-R_{NO}\right)_{reduce} = \left(-R_{C_3H_6}\right) \frac{k_{NO}\, C_{NO}}{\left(1 + K_{NO} \exp\left(-\frac{E_{O_2}}{R_g T}\right) C_{O_2}\right)} \frac{1}{\left(1 + Z\, C_{NO}\right)} \tag{4.47}$$

The rate expressions were derived using LHHW principles, and assume that adsorption of propene and NO inhibit the rate. The mechanistic study as well as experimental observation strongly implied that the rate of NO reduction depends on the rate of propene oxidation. It was also observed that at higher catalyst temperatures $O_2$ competes with NO for catalyst sites, which favours HC oxidation. This caused a decline in NO conversion to $N_2$. An exponential temperature dependent term for the adsorption of $O_2$ was included in the denominator of Equation (4.47). This exponential temperature dependent term increases the surface coverage of $O_2$ at high temperature, and acts to decrease the NO conversion by HC at higher temperature. At these temperatures, NO is oxidised to $NO_2$. They used the model to predict the performance for different conditions and some correlation between experimental and predicted values was obtained.

The model used by Ansell [26] does not give a very good result for the propene oxidation, but Pandya [2] used his idea to couple propene oxidation to NO reduction with a measure of success. His model for the oxidation of $C_3H_6$ with NO was based more on the classical Voltz [2] model:

Oxidation of $C_3H_6$:
$$\left(-R_{C_3H_6}\right) = \frac{k_3\, Y_{C_3H_6}\, Y_{O_2}}{T\left(1 + K_6\, Y_{C_3H_6}\right)^2 \left(1 + K_8 Y_{NO}\right)} \tag{4.48}$$

Oxidation of NO:
$$\left(-R_{\mathrm{NO}}\right) = \frac{k_4 Y_{\mathrm{NO}}\, Y_{\mathrm{O_2}}^{0.5}\left[1-\beta\right]}{T\left(1+K_6\, Y_{\mathrm{C_3H_6}}\right)^2\left(1+K_8 Y_{\mathrm{NO}}\right)} \qquad (4.49)$$

Reduction of NO:
$$\left(-R_{\mathrm{NO}}\right)_{\mathrm{reduce}} = \frac{\left(-R_{\mathrm{C_3H_6}}\right)k_2\, Y_{\mathrm{NO}}}{\left(1+K_9 Y_{\mathrm{O_2}}\right)} \qquad (4.50)$$

Note that the reduction rate equation was a slightly simplified version of the one proposed by Ansell [26]. Pandya [2] used this model as part of a model for a DOC, and thus CO was included. The model gave a reasonable agreement between experiments and predictions for a limited set of experimental data.

When the NO alone experiments were optimized, it was seen that the best models for the oxidation of NO were those of Bhatia [4] (in modified form) and Hauff [5]. These models are used here as a basis for the remaining models to be tested. Note that for the models based on those of Hauff [5], it is necessary to add an inhibition term for the hydrocarbon. The models to be tested are summarized below:

**Model C1**:

The Model C1 is inspired on the basic model of Pandya [2]. Note that it was seen earlier that this model was not very good for the low concentrations of NO, therefore it is not expected a good fit when all nine runs are included. The rate equations are:

Oxidation of $C_3H_6$:
$$\left(-R_{\mathrm{C_3H_6}}\right) = \frac{k_3\, Y_{\mathrm{C_3H_6}}\, Y_{\mathrm{O_2}}}{T\left(1+K_6\, Y_{\mathrm{C_3H_6}}\right)^2\left(1+K_8 Y_{\mathrm{NO}}\right)} \qquad (4.51)$$

Oxidation of NO:
$$\left(-R_{\mathrm{NO}}\right) = \frac{k_4 Y_{\mathrm{NO}}\, Y_{\mathrm{O_2}}^{0.5}\left[1-\beta\right]}{T\left(1+K_6\, Y_{\mathrm{C_3H_6}}\right)^2\left(1+K_8 Y_{\mathrm{NO}}\right)} \qquad (4.52)$$

Two versions of the model were tested. In the first, called **Model C1a**, the reduction rate equations are written:

Reduction of NO to $N_2$:
$$\left(-R_{\mathrm{NO}}\right)_{\mathrm{r1}} = \frac{\left(-R_{\mathrm{C_3H_6}}\right) k_2 \, Y_{\mathrm{NO}}}{\left(1 + K_9 Y_{\mathrm{O_2}}\right)} \tag{4.53}$$

Reduction of NO to $N_2O$:
$$\left(-R_{\mathrm{NO}}\right)_{\mathrm{r2}} = \frac{\left(-R_{\mathrm{C_3H_6}}\right) k_{11} \, Y_{\mathrm{NO}}}{\left(1 + K_9 Y_{\mathrm{O_2}}\right)} \tag{4.54}$$

Model C1b is a variation of the Model 1. An equation for the reduction of $NO_2$ by hydrocarbon was added. This reduction reaction uses the same for as NO, but the rate is ten times higher. Thus:

Reduction of $NO_2$:
$$\left(-R_{\mathrm{NO_2}}\right)_{\mathrm{r3}} = \frac{\left(-R_{\mathrm{C_3H_6}}\right) 10 \, k_2 \, Y_{\mathrm{NO_2}}}{\left(1 + K_9 Y_{\mathrm{O_2}}\right)} \tag{4.55}$$

**Model C4:**

The next set of models is based on the NO oxidation model of Bhatia [4]. There are several variations that can be tried. In the first, Oxidation of $C_3H_6$ is based on the classical Voltz type for the NO inhibition:

$$\left(-R_{\mathrm{C_3H_6}}\right) = \frac{k_3 \, Y_{\mathrm{C_3H_6}} \, Y_{\mathrm{O_2}}}{T\left(1 + K_6 \, Y_{\mathrm{C_3H_6}}\right)^2 \left(1 + K_8 Y_{\mathrm{NO}}\right)} \tag{4.56}$$

For the oxidation of NO the modified Bhatia model was used (called Model 4 in section under NO oxidation), but it is necessary to add a term for the $C_3H_6$ inhibition. The rate of oxidation of NO is thus written:

$$\left(-R_{NO}\right) = \frac{k_4 Y_{O_2}}{T\left(1 + K_6 Y_{C_3H_6} + K_8 Y_{NO} + K_{10}\frac{Y_{NO_2}}{Y_{NO}}\right)}(1-\beta) \quad (4.57)$$

The reduction of NO is taken the same as for model C1. Again, two variations were considered, with and without the reduction of $NO_2$ by propene. These variations were called C4a and C4b respectively.

**Model C5**:

The modified Hauff model [5] is called model C5. There are also two variations on the model. In both cases the two oxidation reactions are:

$$\left(-R_{C_3H_6}\right) = \frac{k_3 Y_{C_3H_6} Y_{O_2}}{T\left(1 + K_6 Y_{C_3H_6} + K_8 Y_{NO}\right)^2} \quad (4.58)$$

$$\left(-R_{NO}\right) = \frac{k_4 Y_{NO} Y_{O_2}^{0.5}}{T\left(1 + K_6 Y_{C_3H_6} + K_8 Y_{NO} + K_{10} Y_{NO_2}\right)^2}(1-\beta) \quad (4.59)$$

Model C5a did not include the reaction between $NO_2$ and propene, while model C5b did.

The models potentially contain up to sixteen adjustable parameters, as shown in Table 24. Note that the activation energies of the $k_2$ and $k_{11}$ parameter were always set to zero, following the results of Pandya [2], leaving a maximum of 14 adjustable parameters.

**Table 25:** Parameter's description for NO and $C_3H_6$ experiments

| Parameter | | Description of parameter |
|---|---|---|
| $k_2$ | $A_2$ | pre-exponential factor, NO reduction rate constant ($N_2$ ) |
| | $E_2$ | activation energy, NO reduction rate constant ($N_2$ ) |
| $k_3$ | $A_3$ | pre-exponential factor, $C_3H_6$ oxidation rate constant |
| | $E_3$ | activation energy, $C_3H_6$ oxidation rate constant |
| $k_4$ | $A_4$ | pre-exponential factor, NO oxidation rate constant |
| | $E_4$ | activation energy, NO oxidation rate constant |
| $K_6$ | $B_6$ | pre-exponential factor, $C_3H_6$ adsorption inhibition term |
| | $H_6$ | activation energy, $C_3H_6$ adsorption inhibition term |
| $K_8$ | $B_8$ | pre-exponential factor, NO adsorption inhibition term |
| | $H_8$ | activation energy, NO adsorption inhibition term |
| $K_9$ | $B_9$ | pre-exponential factor, $O_2$ adsorption inhibition term |
| | $H_9$ | activation energy, $O_2$ adsorption inhibition term |
| $K_{10}$ | $B_{10}$ | pre-exponential factor, $NO_2$ adsorption inhibition term |
| | $H_{10}$ | activation energy, $NO_2$ adsorption inhibition term |
| $k_{11}$ | $A_{11}$ | pre-exponential factor, NO reduction rate constant ($N_2O$ ) |
| | $E_{11}$ | activation energy, NO reduction rate constant ($N_2O$ ) |

In the first test performed the $C_3H_6$ parameters were set to the values found previously for the mixture CO/$C_3H_6$, and varying the rest of the parameters. As seen before, this method did not give acceptable results, showing that the $C_3H_6$ curves are shifted to the left of the experimental results.

The best fit curves were obtained when varying all of the parameters involved in each case. The curves and the experimental points for models C1a, C1b, C4a, C4b, C5a and C5b are given in the following figures, with the parameter values given in a table after each figure.

**Model C1a**

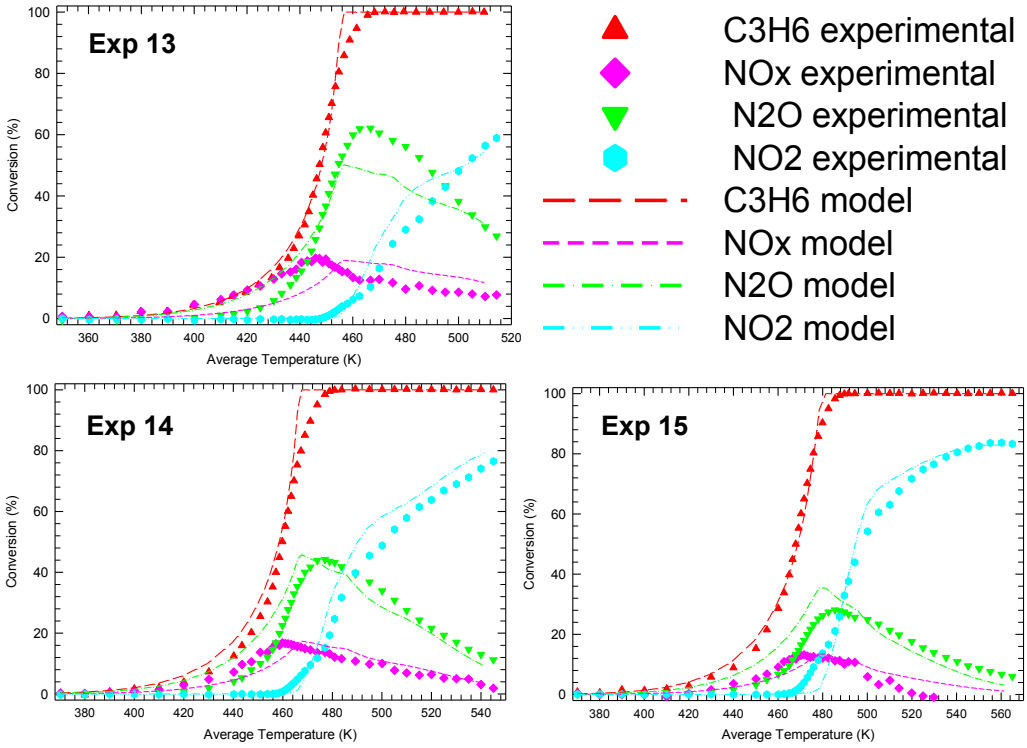


**Figure 47:** NO, $C_3H_6$ and NOx model results when simultaneously optimizing 3 experiments and varying 13 parameters. Model C1a.

**Table 26:** Value of the parameters and residuals for the modelling of NO and $C_3H_6$ mixture for Model C1a

| Parameter | | Experiment 13 | Experiment 14 | Experiment 15 |
|---|---|---|---|---|
| $k_2$ | $A_2$ | 703 | | |
| | $E_2$ | 0 | | |
| $k_3$ | $A_3$ | 1,224,134,622 | | |
| | $E_3$ | 59,111 | | |
| $k_4$ | $A_4$ | 2,396,213 | | |
| | $E_4$ | 99,340 | | |
| $K_6$ | $B_6$ | 18,047 | | |
| | $H_6$ | -4,317 | | |
| $K_8$ | $B_8$ | 19,218 | | |
| | $H_8$ | -11,171 | | |
| $K_9$ | $B_9$ | 0.18 | | |
| | $H_9$ | 148,607 | | |
| $K_{10}$ | $B_{10}$ | 1 | | |
| | $H_{10}$ | 0 | | |
| $k_{11}$ | $A_{11}$ | 1,853 | | |
| | $E_{11}$ | 0 | | |
| Residual | | 99 | 60 | 75 |
| Total residual | | 233 | | |

**Model C1b**

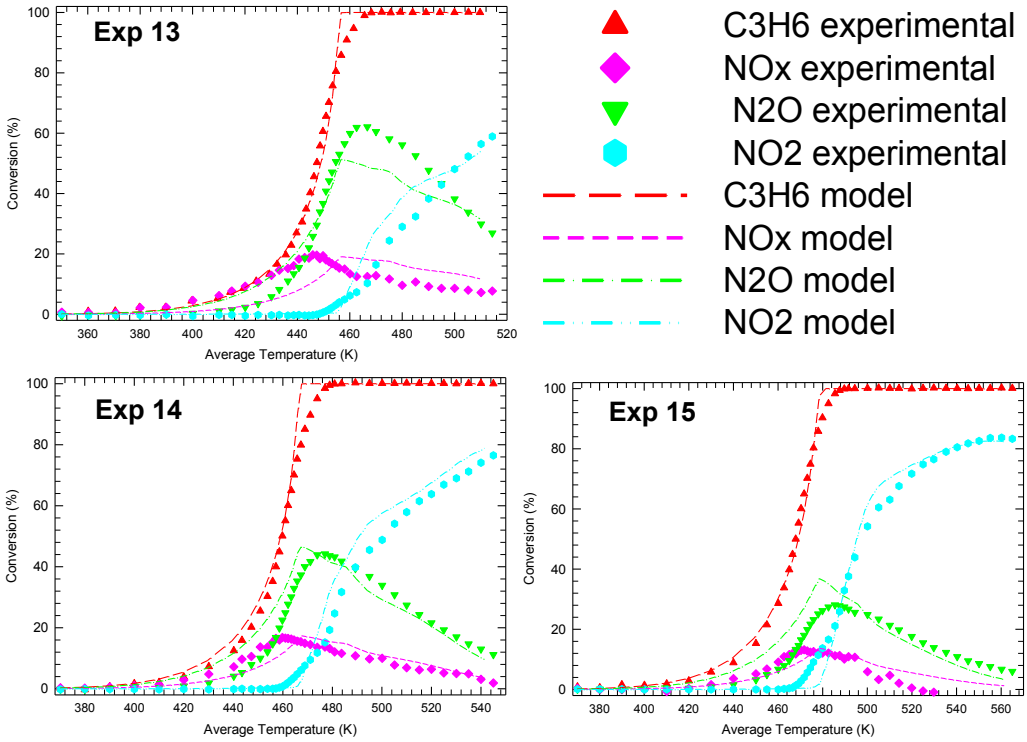


**Figure 48:** NO, $C_3H_6$ and $NO_X$ model results when simultaneously optimizing 3 experiments and varying 13 parameters. Model C1b.

**Table 27:** Value of the parameters and residuals for the modelling of NO and $C_3H_6$ mixture for Model C1b

| Parameter | | Experiment 13 | Experiment 14 | Experiment 15 |
|---|---|---|---|---|
| $k_2$ | $A_2$ | 727 | | |
| | $E_2$ | 0 | | |
| $k_3$ | $A_3$ | 1,192,001,901 | | |
| | $E_3$ | 63,351 | | |
| $k_4$ | $A_4$ | 6,168,708 | | |
| | $E_4$ | 66,432 | | |
| $K_6$ | $B_6$ | 18,091 | | |
| | $H_6$ | -2,054 | | |
| $K_8$ | $B_8$ | 19,928 | | |
| | $H_8$ | -13,967 | | |
| $K_9$ | $B_9$ | 0.20 | | |
| | $H_9$ | 146,841 | | |
| $K_{10}$ | $B_{10}$ | 1 | | |
| | $H_{10}$ | 0 | | |
| $k_{11}$ | $A_{11}$ | 1,959 | | |
| | $E_{11}$ | 0 | | |
| Residual | | 101 | 59 | 79 |
| Total residual | | 239 | | |

**Model C4a**

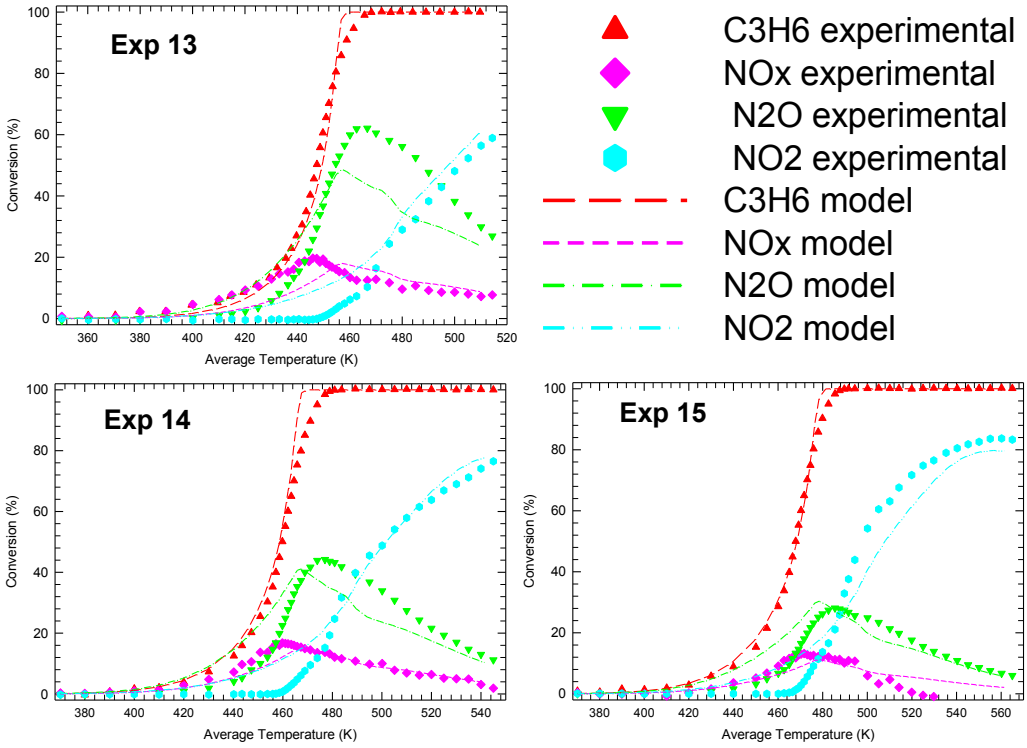


**Figure 49:** NO, $C_3H_6$ and NOx model results when simultaneously optimizing 3 experiments and varying 15 parameters. Model C4a.

**Table 28:** Value of the parameters and residuals for the modelling of NO and $C_3H_6$ mixture for Model C4a

| Parameter | | Experiment 13 | Experiment 14 | Experiment 15 |
|---|---|---|---|---|
| $k_2$ | $A_2$ | 1,707 | | |
| | $E_2$ | 0 | | |
| $k_3$ | $A_3$ | 315,762,214 | | |
| | $E_3$ | 90,103 | | |
| $k_4$ | $A_4$ | 23,066 | | |
| | $E_4$ | 100,000 | | |
| $K_6$ | $B_6$ | 8,653 | | |
| | $H_6$ | -2,153 | | |
| $K_8$ | $B_8$ | 23,073 | | |
| | $H_8$ | -2,324 | | |
| $K_9$ | $B_9$ | 6.38 | | |
| | $H_9$ | 76,582 | | |
| $K_{10}$ | $B_{10}$ | 7,640 | | |
| | $H_{10}$ | -49,932 | | |
| $k_{11}$ | $A_{11}$ | 4,621 | | |
| | $E_{11}$ | 0 | | |
| Residual | | 162 | 111 | 131 |
| Total residual | | 403 | | |

**Model C4b**

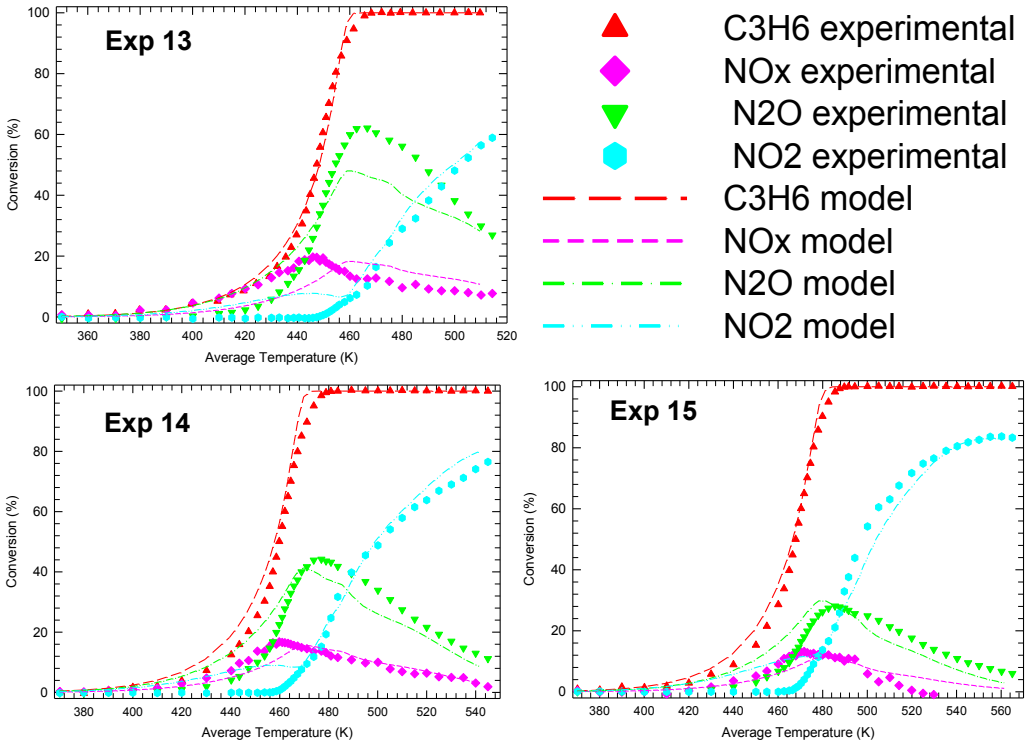


**Figure 50:** NO, $C_3H_6$ and NOx model results when simultaneously optimizing 3 experiments and varying 15 parameters. Model C4b.

**Table 29:** Value of the parameters and residuals for the modelling of NO and $C_3H_6$ mixture for Model C4b

| Parameter | | Experiment 13 | Experiment 14 | Experiment 15 |
|---|---|---|---|---|
| $k_2$ | $A_2$ | 881 | | |
| | $E_2$ | 0 | | |
| $k_3$ | $A_3$ | 286,973,375 | | |
| | $E_3$ | 58,347 | | |
| $k_4$ | $A_4$ | 180,142 | | |
| | $E_4$ | 99,922 | | |
| $K_6$ | $B_6$ | 8,009 | | |
| | $H_6$ | -2,659 | | |
| $K_8$ | $B_8$ | 21,585 | | |
| | $H_8$ | -8,653 | | |
| $K_9$ | $B_9$ | 0.20 | | |
| | $H_9$ | 135,286 | | |
| $K_{10}$ | $B_{10}$ | 20,068 | | |
| | $H_{10}$ | -34,823 | | |
| $k_{11}$ | $A_{11}$ | 2,319 | | |
| | $E_{11}$ | 0 | | |
| Residual | | 124 | 76 | 93 |
| Total residual | | 293 | | |

**Model C5a**

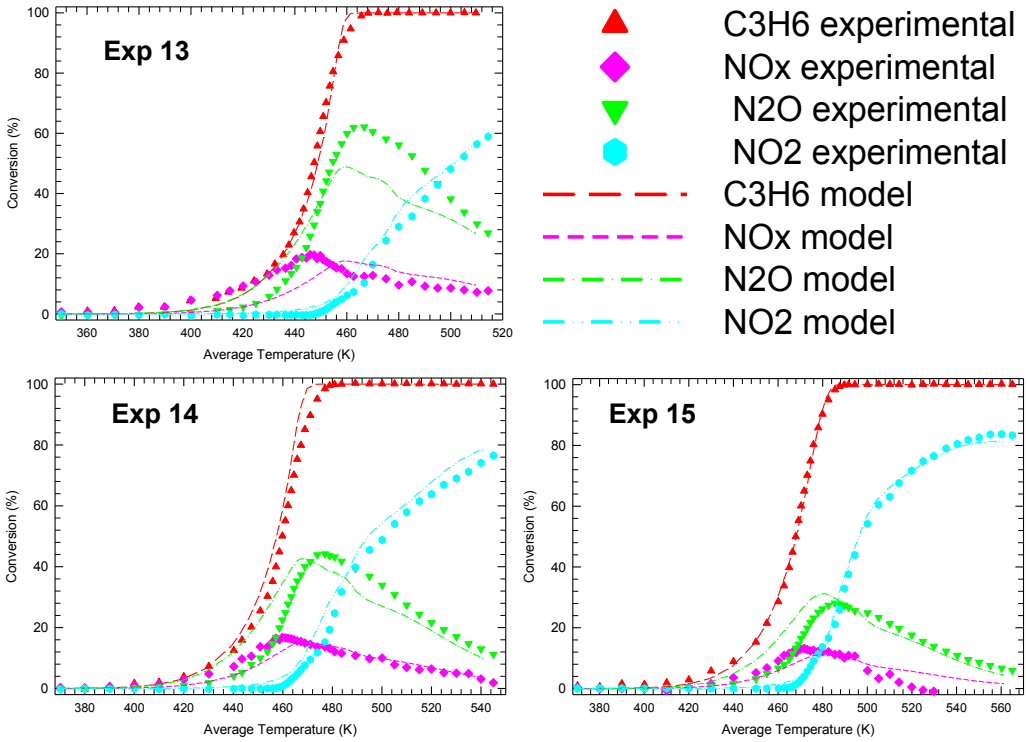


**Figure 51:** NO, $C_3H_6$ and NOx model results when simultaneously optimizing 3 experiments and varying 15 parameters. Model C5a.

**Table 30:** Value of the parameters and residuals for the modelling of NO and $C_3H_6$ mixture for Model C5a

| Parameter | | Experiment 13 | Experiment 14 | Experiment 15 |
|---|---|---|---|---|
| $k_2$ | $A_2$ | 885 | | |
| | $E_2$ | 0 | | |
| $k_3$ | $A_3$ | 290,234,565 | | |
| | $E_3$ | 69,031 | | |
| $k_4$ | $A_4$ | 6,492,771 | | |
| | $E_4$ | 90,857 | | |
| $K_6$ | $B_6$ | 9,812 | | |
| | $H_6$ | -2,162 | | |
| $K_8$ | $B_8$ | 24,205 | | |
| | $H_8$ | -36,563 | | |
| $K_9$ | $B_9$ | 1.20 | | |
| | $H_9$ | 109,387 | | |
| $K_{10}$ | $B_{10}$ | 4.65 | | |
| | $H_{10}$ | -49,995 | | |
| $k_{11}$ | $A_{11}$ | 2,460 | | |
| | $E_{11}$ | 0 | | |
| Residual | | 99 | 66 | 52 |
| Total residual | | 217 | | |

**Model C5b**

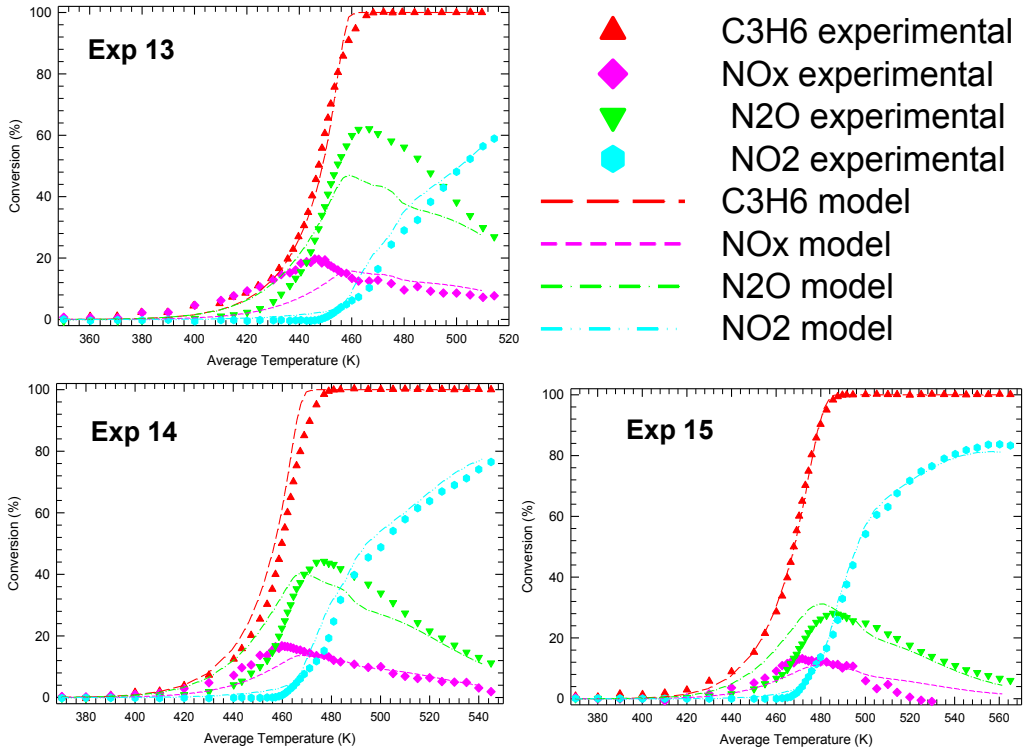


**Figure 52:** NO, $C_3H_6$ and NOx model results when simultaneously optimizing 3 experiments and varying 15 parameters. Model C5b.

**Table 31:** Value of the parameters and residuals for the modelling of NO and $C_3H_6$ mixture for Model C5b

| Parameter | | Experiment 13 | Experiment 14 | Experiment 15 |
|---|---|---|---|---|
| $k_2$ | $A_2$ | 934 | | |
| | $E_2$ | 0 | | |
| $k_3$ | $A_3$ | 290,234,565 | | |
| | $E_3$ | 79,825 | | |
| $k_4$ | $A_4$ | 10,731,565 | | |
| | $E_4$ | 98,682 | | |
| $K_6$ | $B_6$ | 10,393 | | |
| | $H_6$ | -2,349 | | |
| $K_8$ | $B_8$ | 22,825 | | |
| | $H_8$ | -22,390 | | |
| $K_9$ | $B_9$ | 1.59 | | |
| | $H_9$ | 98,098 | | |
| $K_{10}$ | $B_{10}$ | 7.830 | | |
| | $H_{10}$ | -49,999 | | |
| $k_{11}$ | $A_{11}$ | 2,547 | | |
| | $E_{11}$ | 0 | | |
| Residual | | 102 | 67 | 52 |
| Total residual | | 221 | | |

From the plots and results, it can be inferred that the best result was obtained with the model C5a which shows a residual value of 217, followed very close by model C5b with a residual value of 221. Models C1a and C1b showed residual values of 233 and 239 respectively, and models C4a and C4b presented residuals of 403 and 293.

Next, the 9 tests involving $C_3H_6$ and NO are optimized simultaneously. The graphs and the parameter values are given in the following pages.

**Model C1a**

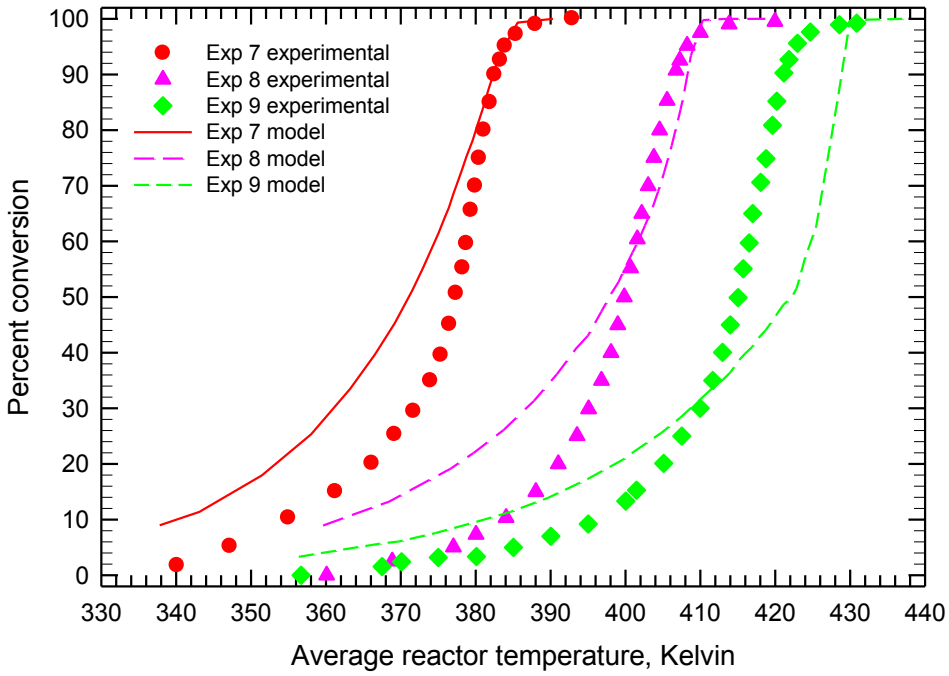


**Figure 53:** $C_3H_6$ model results when simultaneously optimizing all 9 experiments and varying 13 parameters. Model C1a.

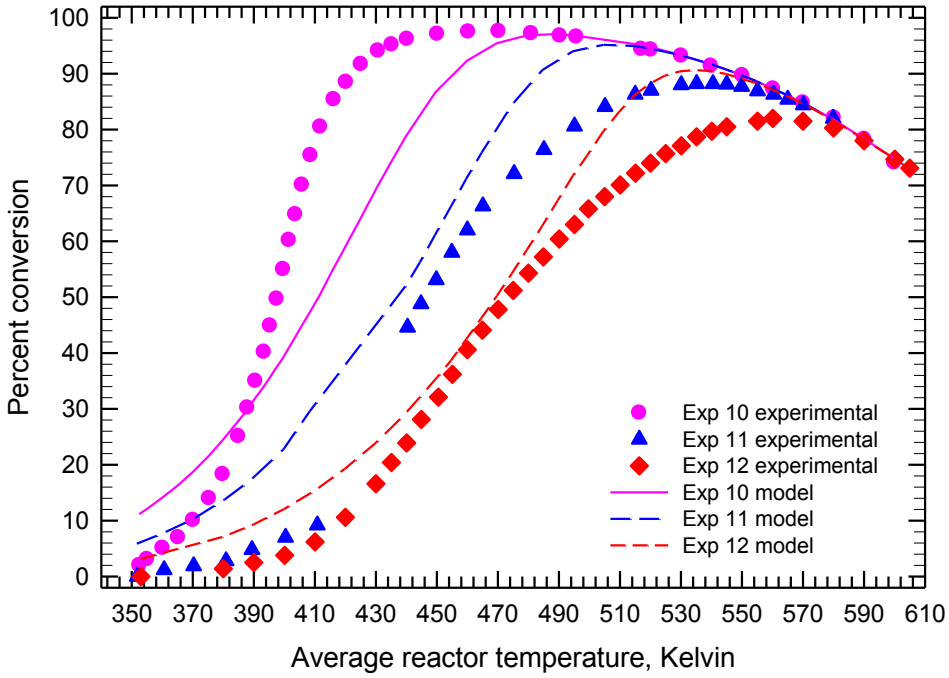


**Figure 54:** NO model results when simultaneously optimizing all 9 experiments and varying 13 parameters. Model C1a.

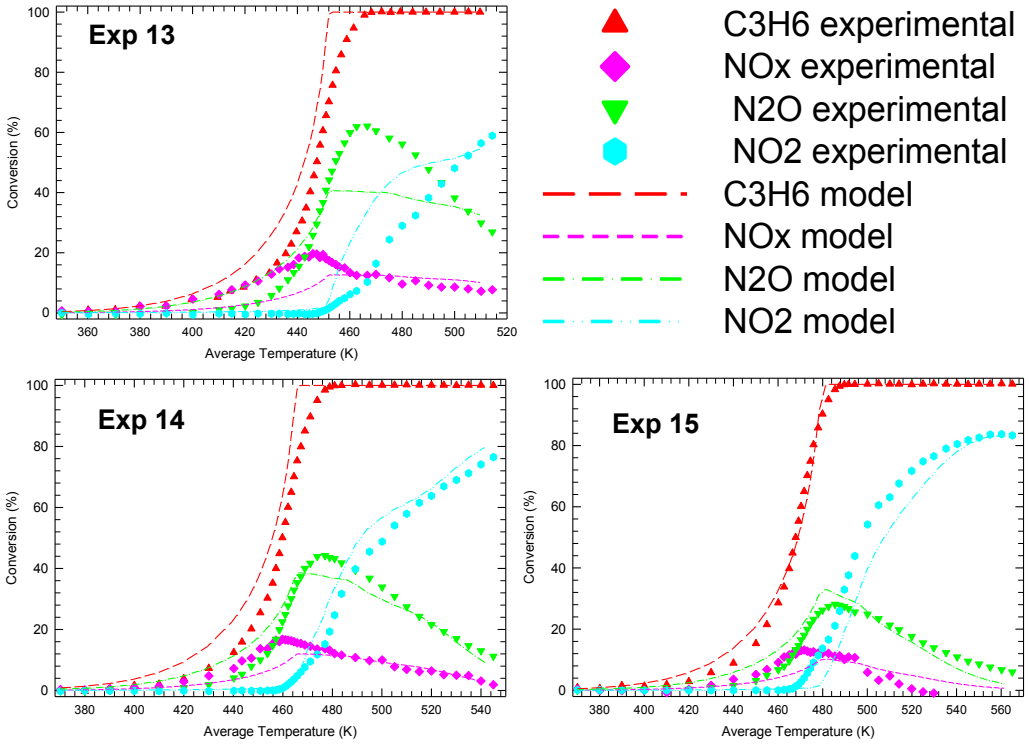


**Figure 55:** NO, $C_3H_6$ and NOx model results when simultaneously optimizing 9 experiments and varying 13 parameters. Model C1a.

**Table 32:** Value of the parameters and residuals for the modelling of NO, $C_3H_6$, and their mixture for Model C1a

| Parameter | | Exp 7 | Exp 8 | Exp 9 | Exp 10 | Exp 11 | Exp 12 | Exp 13 | Exp 14 | Exp 15 |
|---|---|---|---|---|---|---|---|---|---|---|
| $k_2$ | $A_2$ | 365 | | | | | | | | |
| | $E_2$ | 0 | | | | | | | | |
| $k_3$ | $A_3$ | 2,052,655,176 | | | | | | | | |
| | $E_3$ | 50,098 | | | | | | | | |
| $k_4$ | $A_4$ | 13,539,204 | | | | | | | | |
| | $E_4$ | 25,014 | | | | | | | | |
| $K_6$ | $B_6$ | 19,880 | | | | | | | | |
| | $H_6$ | -2,000 | | | | | | | | |
| $K_8$ | $B_8$ | 20,000 | | | | | | | | |
| | $H_8$ | -12,143 | | | | | | | | |
| $K_9$ | $B_9$ | 0.01 | | | | | | | | |
| | $H_9$ | 199,243 | | | | | | | | |
| $K_{10}$ | $B_{10}$ | 1 | | | | | | | | |
| | $H_{10}$ | 0 | | | | | | | | |
| $k_{11}$ | $A_{11}$ | 1,171 | | | | | | | | |
| | $E_{11}$ | 0 | | | | | | | | |
| Residual | | 89 | 94 | 385 | 204 | 82 | 61 | 350 | 105 | 149 |
| Total residual | | 1,519 | | | | | | | | |

**Model C1b**

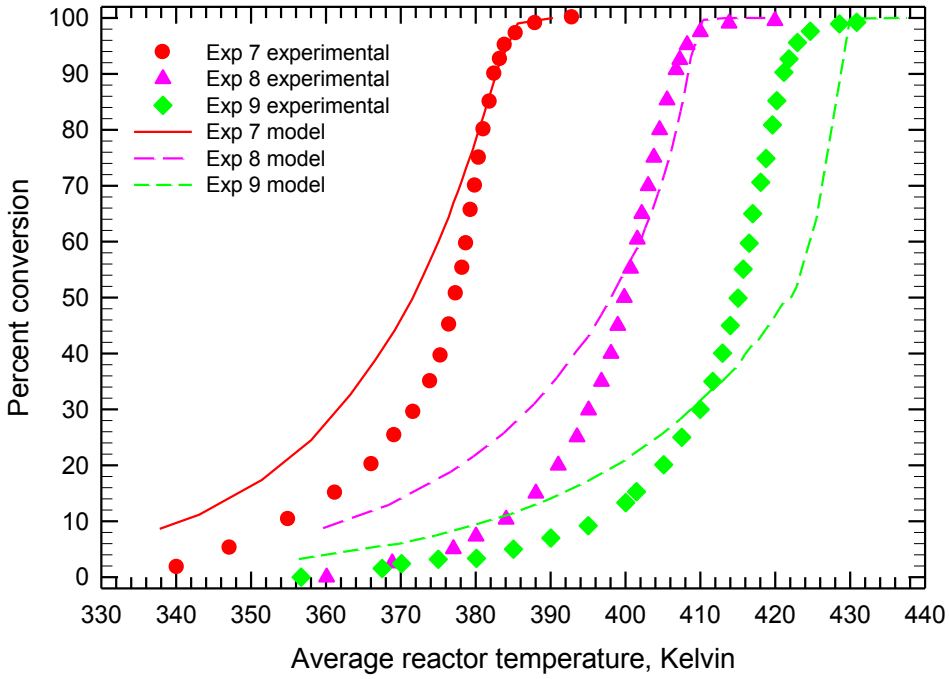


**Figure 56:** $C_3H_6$ model results when simultaneously optimizing all 9 experiments and varying 13 parameters. Model C1b.

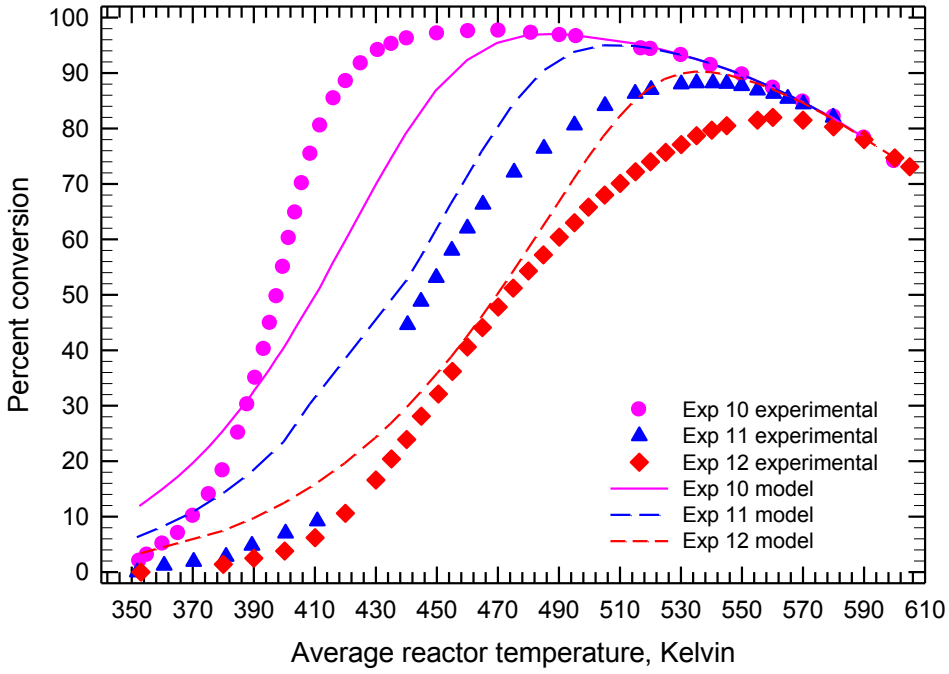


**Figure 57:** NO model results when simultaneously optimizing all 9 experiments and varying 13 parameters. Model C1b.

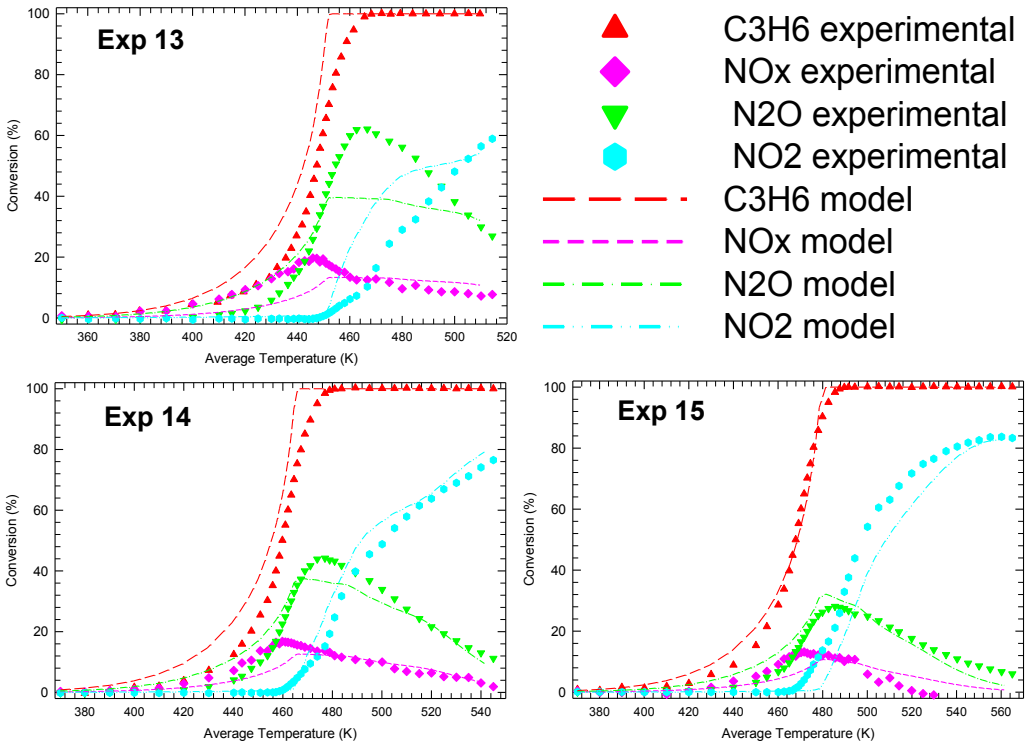


**Figure 58:** NO, $C_3H_6$ and NOx model results when simultaneously optimizing 9 experiments and varying 13 parameters. Model C1b.

**Table 33:** Value of the parameters and residuals for the modelling of NO, $C_3H_6$, and their mixture for Model C1b

| Parameter | | Exp 7 | Exp 8 | Exp 9 | Exp 10 | Exp 11 | Exp 12 | Exp 13 | Exp 14 | Exp 15 |
|---|---|---|---|---|---|---|---|---|---|---|
| $k_2$ | $A_2$ | 381 | | | | | | | | |
| | $E_2$ | 0 | | | | | | | | |
| $k_3$ | $A_3$ | 2,054,092,538 | | | | | | | | |
| | $E_3$ | 50,632 | | | | | | | | |
| $k_4$ | $A_4$ | 13,578,524 | | | | | | | | |
| | $E_4$ | 25,007 | | | | | | | | |
| $K_6$ | $B_6$ | 19,736 | | | | | | | | |
| | $H_6$ | -2,021 | | | | | | | | |
| $K_8$ | $B_8$ | 19,982 | | | | | | | | |
| | $H_8$ | -11,182 | | | | | | | | |
| $K_9$ | $B_9$ | 0.01 | | | | | | | | |
| | $H_9$ | 199,826 | | | | | | | | |
| $K_{10}$ | $B_{10}$ | 1 | | | | | | | | |
| | $H_{10}$ | 0 | | | | | | | | |
| $k_{11}$ | $A_{11}$ | 1,132 | | | | | | | | |
| | $E_{11}$ | 0 | | | | | | | | |
| Residual | | 83 | 91 | 376 | 193 | 85 | 56 | 372 | 113 | 153 |
| Total residual | | 1,523 | | | | | | | | |

**Model C4a**

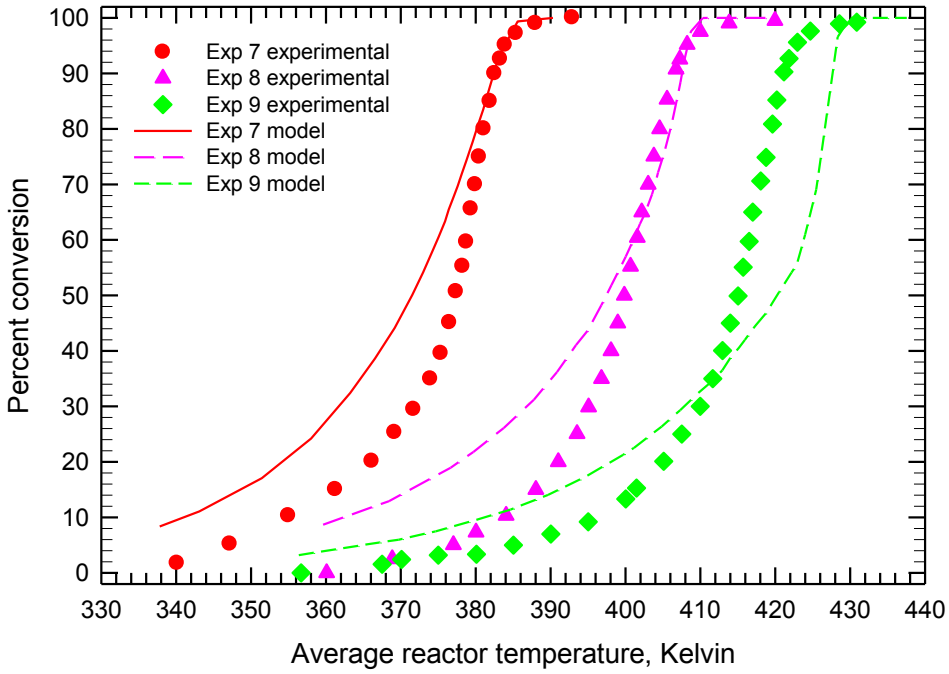


**Figure 59:** $C_3H_6$ model results when simultaneously optimizing all 9 experiments and varying 15 parameters. Model C4a.

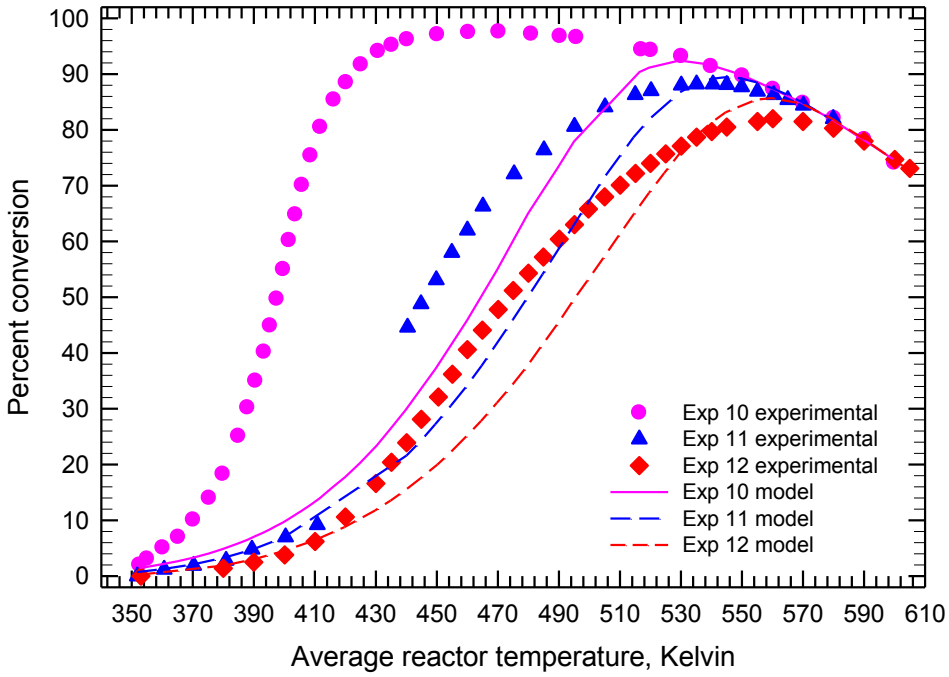


**Figure 60:** NO model results when simultaneously optimizing all 9 experiments and varying 15 parameters. Model C4a.

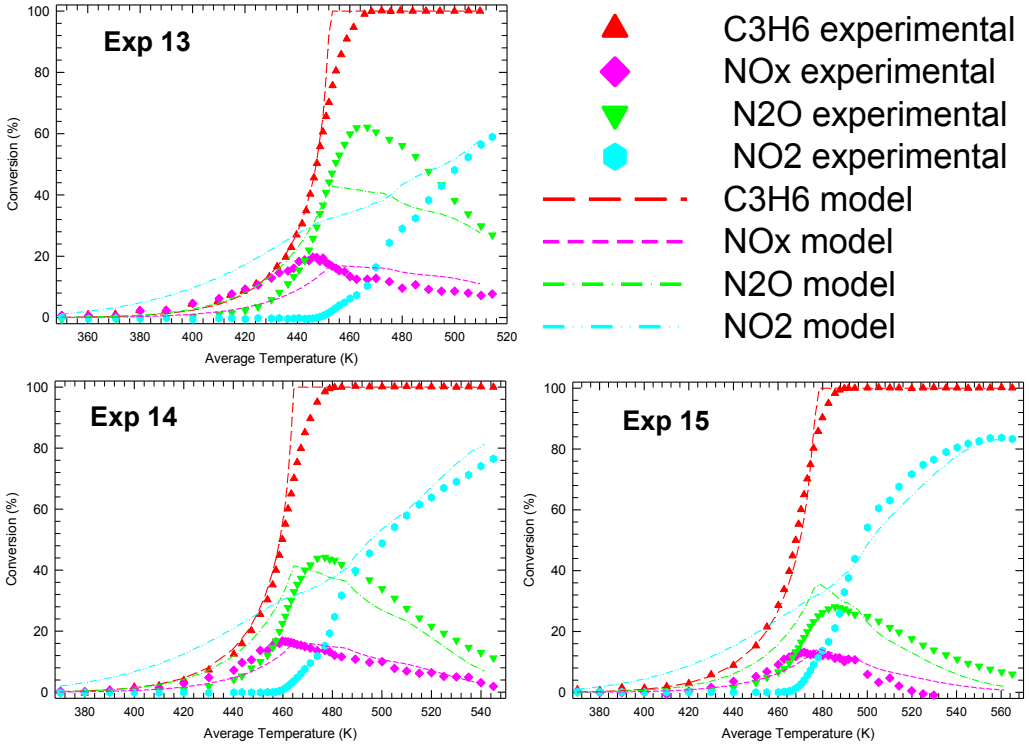


**Figure 61:** NO, $C_3H_6$ and NOx model results when simultaneously optimizing 9 experiments and varying 15 parameters. Model C4a.

**Table 34:** Value of the parameters and residuals for the modelling of NO, $C_3H_6$, and their mixture for Model C4a

| Parameter | | Exp 7 | Exp 8 | Exp 9 | Exp 10 | Exp 11 | Exp 12 | Exp 13 | Exp 14 | Exp 15 |
|---|---|---|---|---|---|---|---|---|---|---|
| $k_2$ | $A_2$ | 1,154 | | | | | | | | |
| | $E_2$ | 0 | | | | | | | | |
| $k_3$ | $A_3$ | 2,198,629,393 | | | | | | | | |
| | $E_3$ | 51,411 | | | | | | | | |
| $k_4$ | $A_4$ | 369,830 | | | | | | | | |
| | $E_4$ | 83,922 | | | | | | | | |
| $K_6$ | $B_6$ | 19,832 | | | | | | | | |
| | $H_6$ | -2,170 | | | | | | | | |
| $K_8$ | $B_8$ | 49,021 | | | | | | | | |
| | $H_8$ | -25,489 | | | | | | | | |
| $K_9$ | $B_9$ | 0.09 | | | | | | | | |
| | $H_9$ | 171,854 | | | | | | | | |
| $K_{10}$ | $B_{10}$ | 9263 | | | | | | | | |
| | $H_{10}$ | -5627.49 | | | | | | | | |
| $k_{11}$ | $A_{11}$ | 2,904 | | | | | | | | |
| | $E_{11}$ | 0 | | | | | | | | |
| Residual | | 80 | 91 | 303 | 1,573 | 205 | 85 | 618 | 421 | 310 |
| Total residual | | 3,684 | | | | | | | | |

**Model C4b**

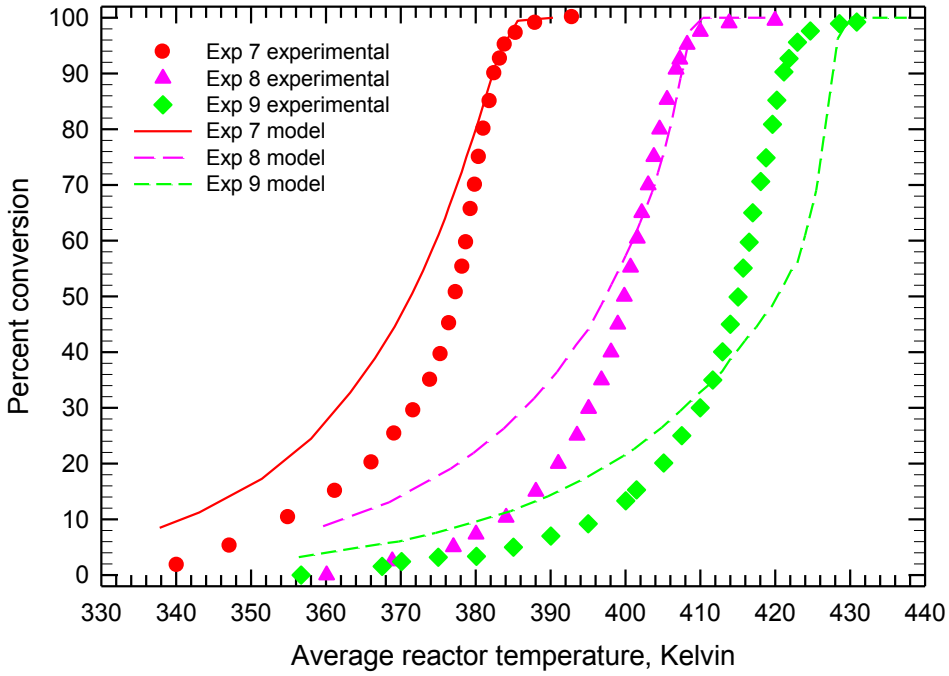


**Figure 62:** $C_3H_6$ model results when simultaneously optimizing all 9 experiments and varying 15 parameters. Model C4b.

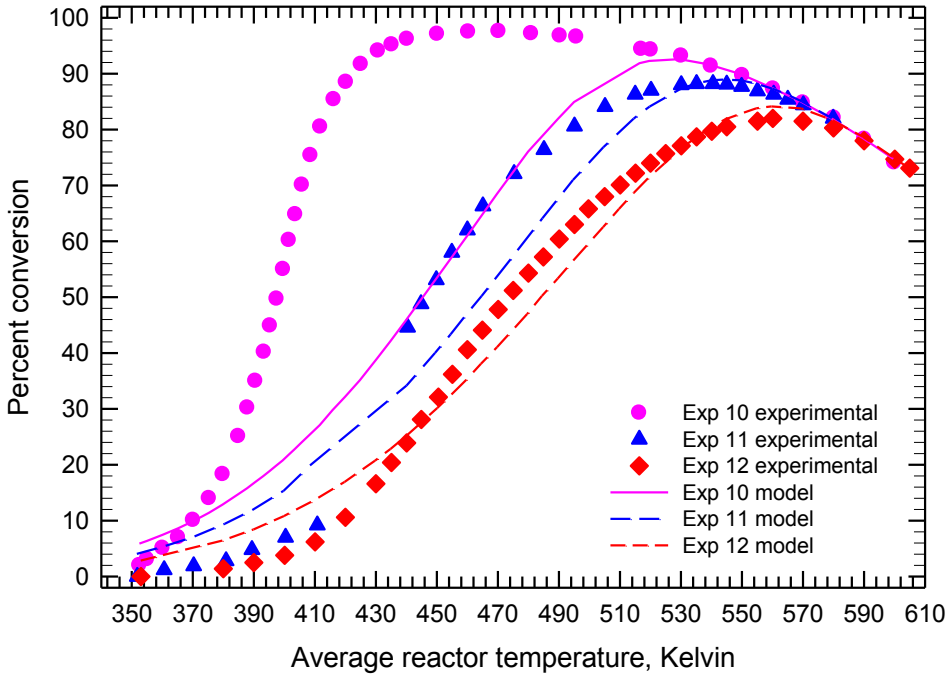


**Figure 63:** NO model results when simultaneously optimizing all 9 experiments and varying 15 parameters. Model C4b.

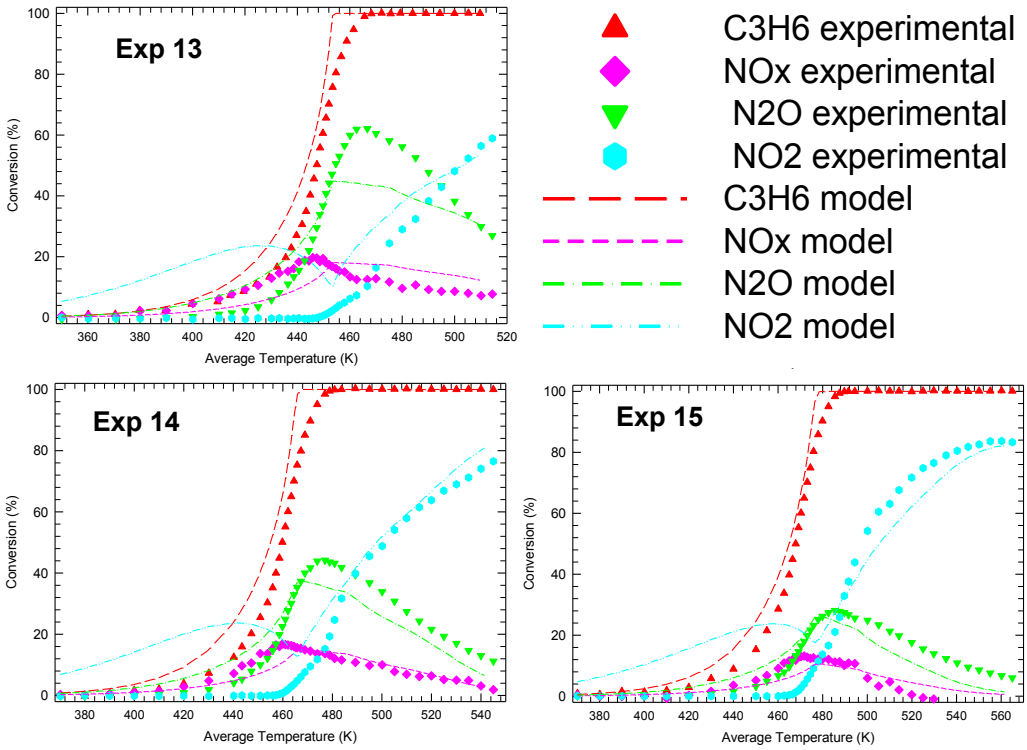


**Figure 64:** NO, $C_3H_6$ and NOx model results when simultaneously optimizing 9 experiments and varying 14 parameters. Model C4b.

**Table 35:** Value of the parameters and residuals for the modelling of NO, $C_3H_6$, and their mixture for Model C4b

| Parameter | | Exp 7 | Exp 8 | Exp 9 | Exp 10 | Exp 11 | Exp 12 | Exp 13 | Exp 14 | Exp 15 |
|---|---|---|---|---|---|---|---|---|---|---|
| $k_2$ | $A_2$ | 1,034 | | | | | | | | |
| | $E_2$ | 0 | | | | | | | | |
| $k_3$ | $A_3$ | 2,198,629,393 | | | | | | | | |
| | $E_3$ | 51,383 | | | | | | | | |
| $k_4$ | $A_4$ | 1,301,984 | | | | | | | | |
| | $E_4$ | 64,844 | | | | | | | | |
| $K_6$ | $B_6$ | 19,866 | | | | | | | | |
| | $H_6$ | -2,075 | | | | | | | | |
| $K_8$ | $B_8$ | 49,971 | | | | | | | | |
| | $H_8$ | -2,334 | | | | | | | | |
| $K_9$ | $B_9$ | 0.02 | | | | | | | | |
| | $H_9$ | 189,642 | | | | | | | | |
| $K_{10}$ | $B_{10}$ | 13280 | | | | | | | | |
| | $H_{10}$ | -3595.55 | | | | | | | | |
| $k_{11}$ | $A_{11}$ | 2,567 | | | | | | | | |
| | $E_{11}$ | 0 | | | | | | | | |
| Residual | | 82 | 93 | 302 | 914 | 69 | 20 | 431 | 289 | 242 |
| Total residual | | 2,443 | | | | | | | | |

**Model C5a**

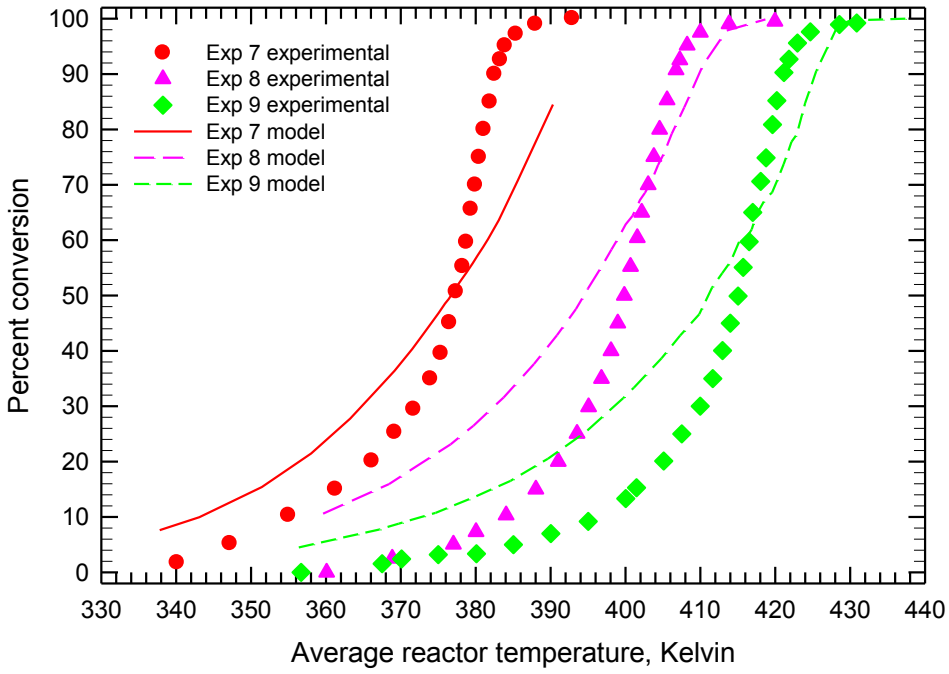


**Figure 65:** $C_3H_6$ model results when simultaneously optimizing all 9 experiments and varying 14 parameters. Model C5a.

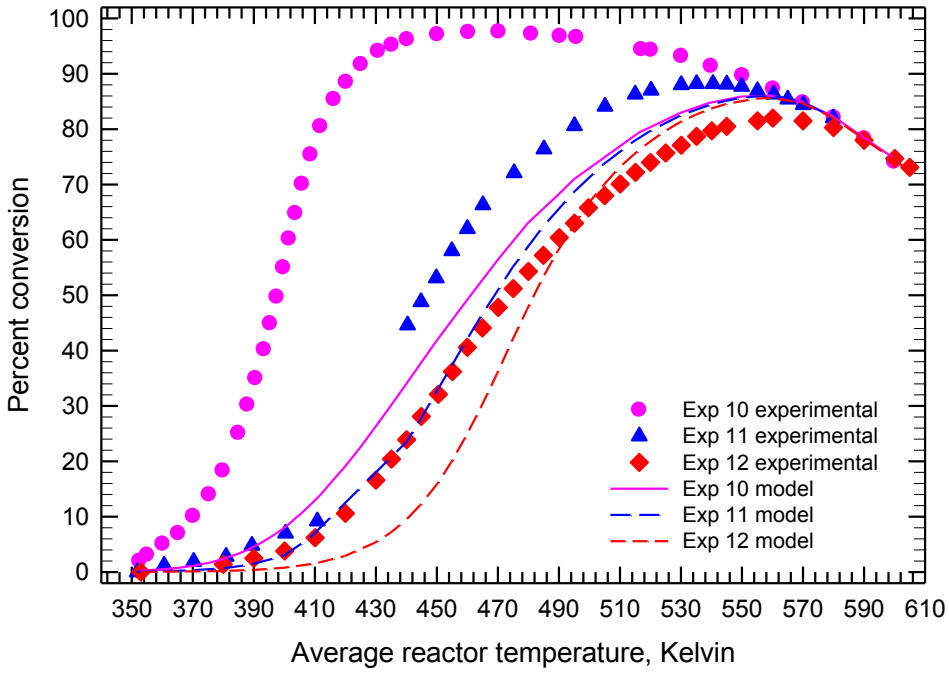


**Figure 66:** NO model results when simultaneously optimizing all 9 experiments and varying 14 parameters. Model C5a.

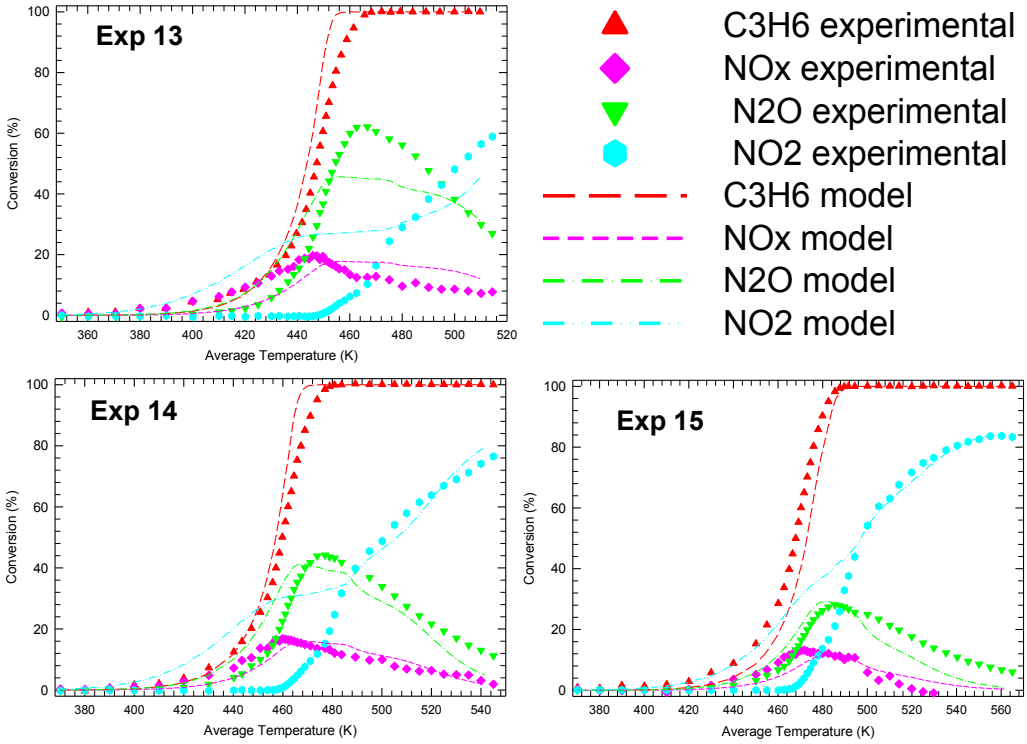


**Figure 67:** NO, $C_3H_6$ and NOx model results when simultaneously optimizing 9 experiments and varying 14 parameters. Model C5a.

**Table 36:** Value of the parameters and residuals for the modelling of NO, $C_3H_6$ and their mixture for Model C5a

| Parameter | | Exp 7 | Exp 8 | Exp 9 | Exp 10 | Exp 11 | Exp 12 | Exp 13 | Exp 14 | Exp 15 |
|---|---|---|---|---|---|---|---|---|---|---|
| $k_2$ | $A_2$ | 1,110 | | | | | | | | |
| | $E_2$ | 0 | | | | | | | | |
| $k_3$ | $A_3$ | 301,385,279 | | | | | | | | |
| | $E_3$ | 50,030 | | | | | | | | |
| $k_4$ | $A_4$ | 413,223,844 | | | | | | | | |
| | $E_4$ | 25,095 | | | | | | | | |
| $K_6$ | $B_6$ | 4,980 | | | | | | | | |
| | $H_6$ | -3,898 | | | | | | | | |
| $K_8$ | $B_8$ | 46,850 | | | | | | | | |
| | $H_8$ | -36,344 | | | | | | | | |
| $K_9$ | $B_9$ | 0.05 | | | | | | | | |
| | $H_9$ | 199,996 | | | | | | | | |
| $K_{10}$ | $B_{10}$ | 29 | | | | | | | | |
| | $H_{10}$ | -43,068 | | | | | | | | |
| $k_{11}$ | $A_{11}$ | 2,852 | | | | | | | | |
| | $E_{11}$ | 0 | | | | | | | | |
| Residual | | 361 | 194 | 126 | 1,575 | 124 | 63 | 559 | 405 | 397 |
| Total residual | | 3,803 | | | | | | | | |

**Model C5b**

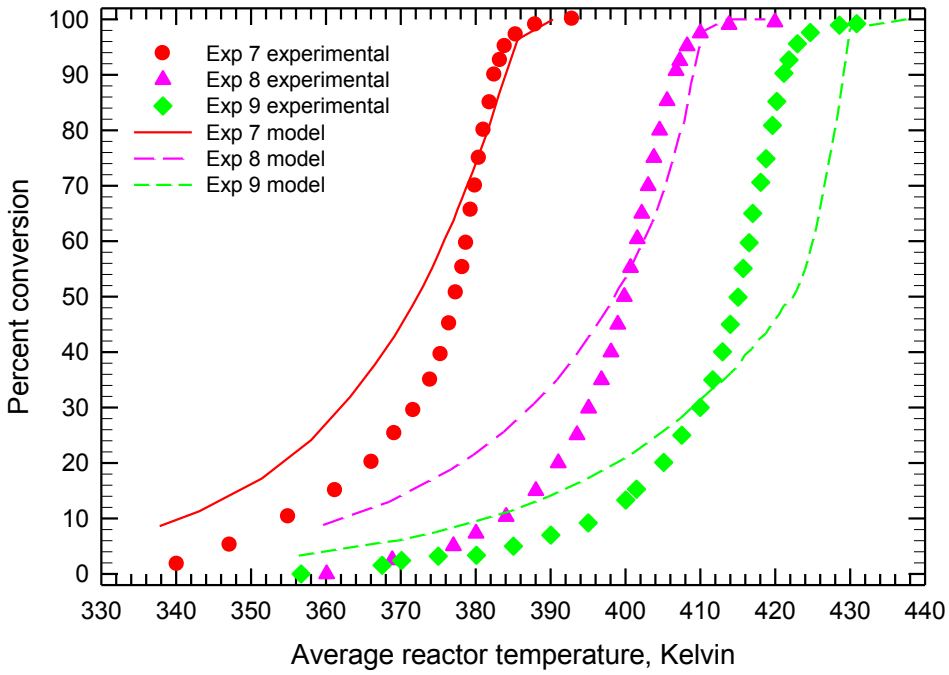


**Figure 68:** $C_3H_6$ model results when simultaneously optimizing all 9 experiments and varying 15 parameters. Model C5b.

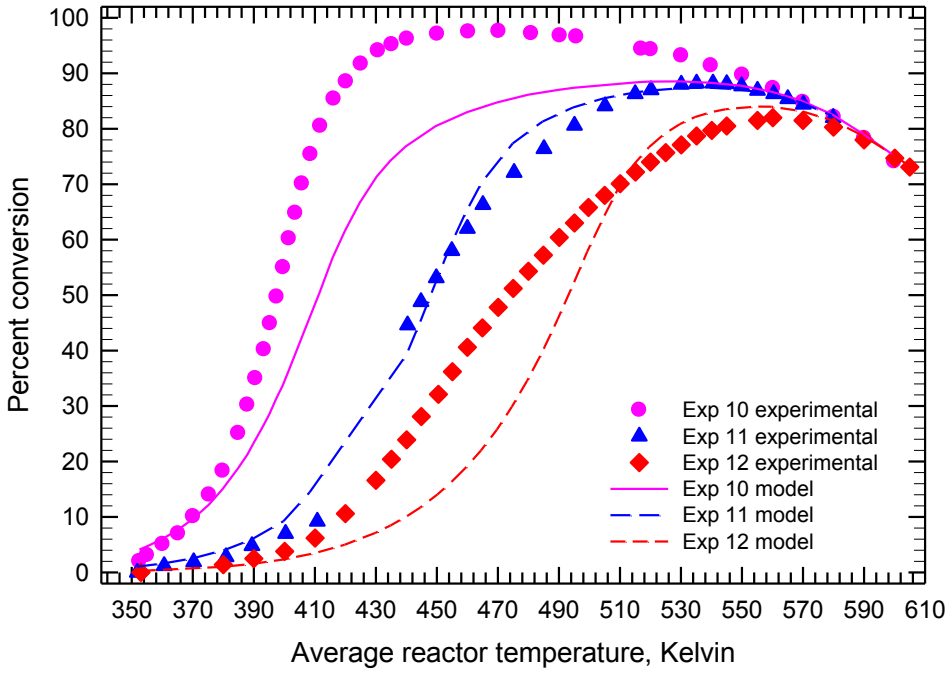


**Figure 69:** NO model results when simultaneously optimizing all 9 experiments and varying 14 parameters. Model C5b.

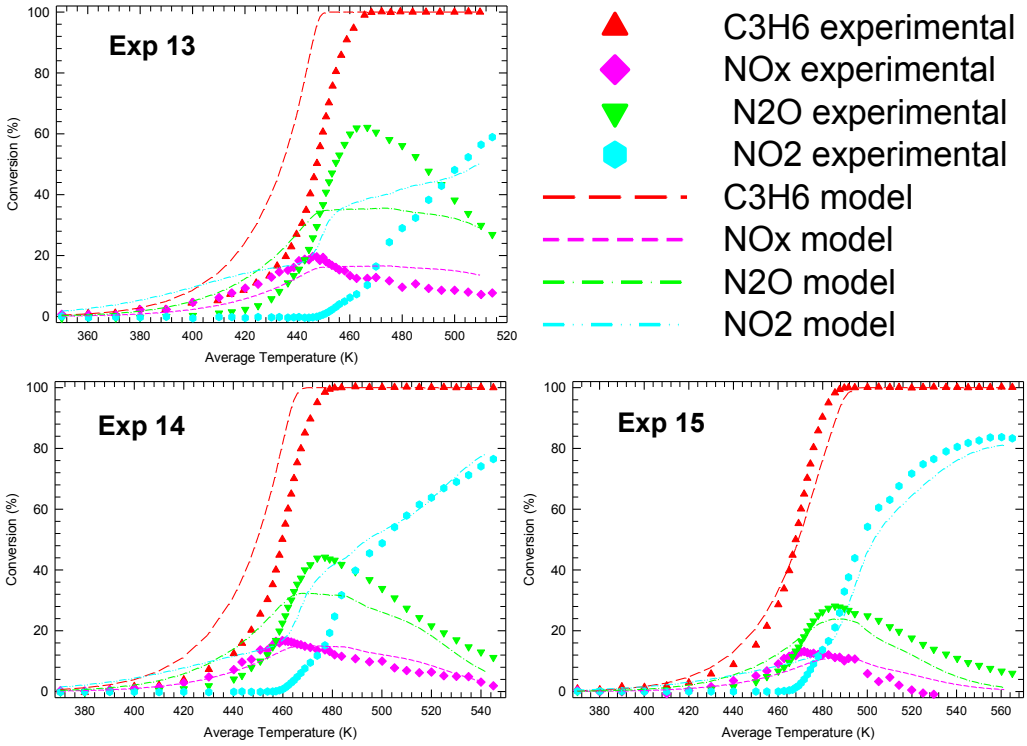


**Figure 70:** NO, $C_3H_6$ and NOx model results when simultaneously optimizing 9 experiments and varying 15 parameters. Model C5b.

**Table 37:** Value of the parameters and residuals for the modelling of NO, $C_3H_6$ and their mixture for Model C5b

| Parameter | | Exp 7 | Exp 8 | Exp 9 | Exp 10 | Exp 11 | Exp 12 | Exp 13 | Exp 14 | Exp 15 |
|---|---|---|---|---|---|---|---|---|---|---|
| $k_2$ | $A_2$ | 639 | | | | | | | | |
| | $E_2$ | 0 | | | | | | | | |
| $k_3$ | $A_3$ | 1,605,016,702 | | | | | | | | |
| | $E_3$ | 50,248 | | | | | | | | |
| $k_4$ | $A_4$ | 358,270,914 | | | | | | | | |
| | $E_4$ | 25,071 | | | | | | | | |
| $K_6$ | $B_6$ | 17,404 | | | | | | | | |
| | $H_6$ | -2,004 | | | | | | | | |
| $K_8$ | $B_8$ | 49,886 | | | | | | | | |
| | $H_8$ | -15,600 | | | | | | | | |
| $K_9$ | $B_9$ | 0.02 | | | | | | | | |
| | $H_9$ | 199,640 | | | | | | | | |
| $K_{10}$ | $B_{10}$ | 2 | | | | | | | | |
| | $H_{10}$ | -2,004 | | | | | | | | |
| $k_{11}$ | $A_{11}$ | 1,371 | | | | | | | | |
| | $E_{11}$ | 0 | | | | | | | | |
| Residual | | 97 | 99 | 403 | 241 | 6 | 123 | 1,118 | 449 | 144 |
| Total residual | | 2,680 | | | | | | | | |

When considering the 9 experiments regarding $C_3H_6$, NO and their mixture, the models that show better results are model C1a (residual value of 1,519) and model C1b (residual value of 1,523) in plots and numbers. Those best results were followed by models C4b and C5b, with a total residual value of 2,443 and 2,680 respectively. None of the parameter sets was really satisfactory.

### 4.2.3. The oxidation of CO, $C_3H_6$ and NO combined

The final challenge was to fit the experiments that included all of the reactants. There were 10 experiments used from the set comprising 23 to 33. Based on the results found for the models in the NO and $C_3H_6$ optimization, it was determined to test models C1b, C4b and C5b for the runs 23-33 that involve CO, $C_3H_6$ and NO. Model C1b was included for historical reasons, in that it was the one used by Pandya[2].

**Model C1b**

As we had seen with earlier optimization runs, any model was generally able to fir a single experiment. For illustration purposes, the result of optimizing experiment 23 using Model C1b is shown in Figure 71. It is seen that there is a good match obtained. The parameter values are given in Table 38.

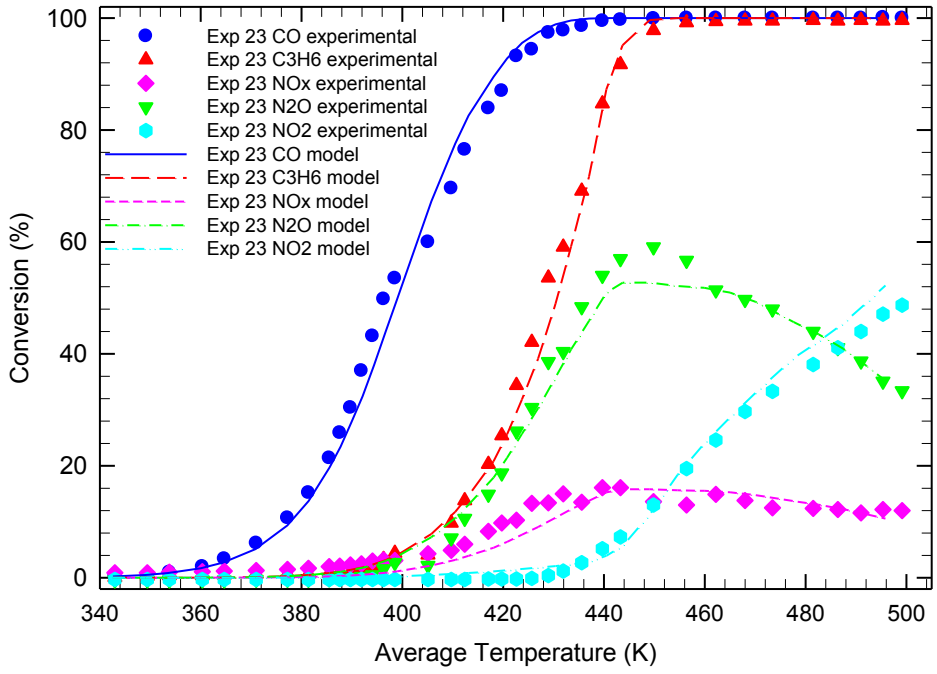


**Figure 71:** Experiment 23 optimized with Model 1b.

**Table 38:** Value of the parameters and total residual for the modelling of CO, $C_3H_6$ and NO mixture when optimizing only one experiment for Model C1b

| Parameter | | Exp 1 |
|---|---|---|
| $k_1$ | $A_1$ | 359,311,407 |
| | $E_1$ | 50,481 |
| $k_2$ | $A_2$ | 692 |
| | $E_2$ | 0 |
| $k_3$ | $A_3$ | 69,789,910 |
| | $E_3$ | 91,213 |
| $k_4$ | $A_4$ | 2,365,027 |
| | $E_4$ | 98,047 |
| $K_5$ | $B_5$ | 8 |
| | $H_5$ | -4,240 |
| $K_6$ | $B_6$ | 1,363 |
| | $H_6$ | -2,000 |
| $K_8$ | $B_8$ | 6,848 |
| | $H_8$ | -1,359 |
| $K_9$ | $B_9$ | 0.52 |
| | $H_9$ | 180,470 |
| $K_{10}$ | $B_{10}$ | 93 |
| | $H_{10}$ | -51,813 |
| $k_{11}$ | $A_{11}$ | 2,308 |
| | $E_{11}$ | 0 |
| Total residual | | 23 |

Experiments 23-28 all had the same inlet concentration of NO and $C_3H_6$, with only the CO concentration changing. These experiments were optimized together, and the resulting curves are shown in Figure 72, with the parameter values being given in Table 39. The agreement between the model and experiments is very good in this case.

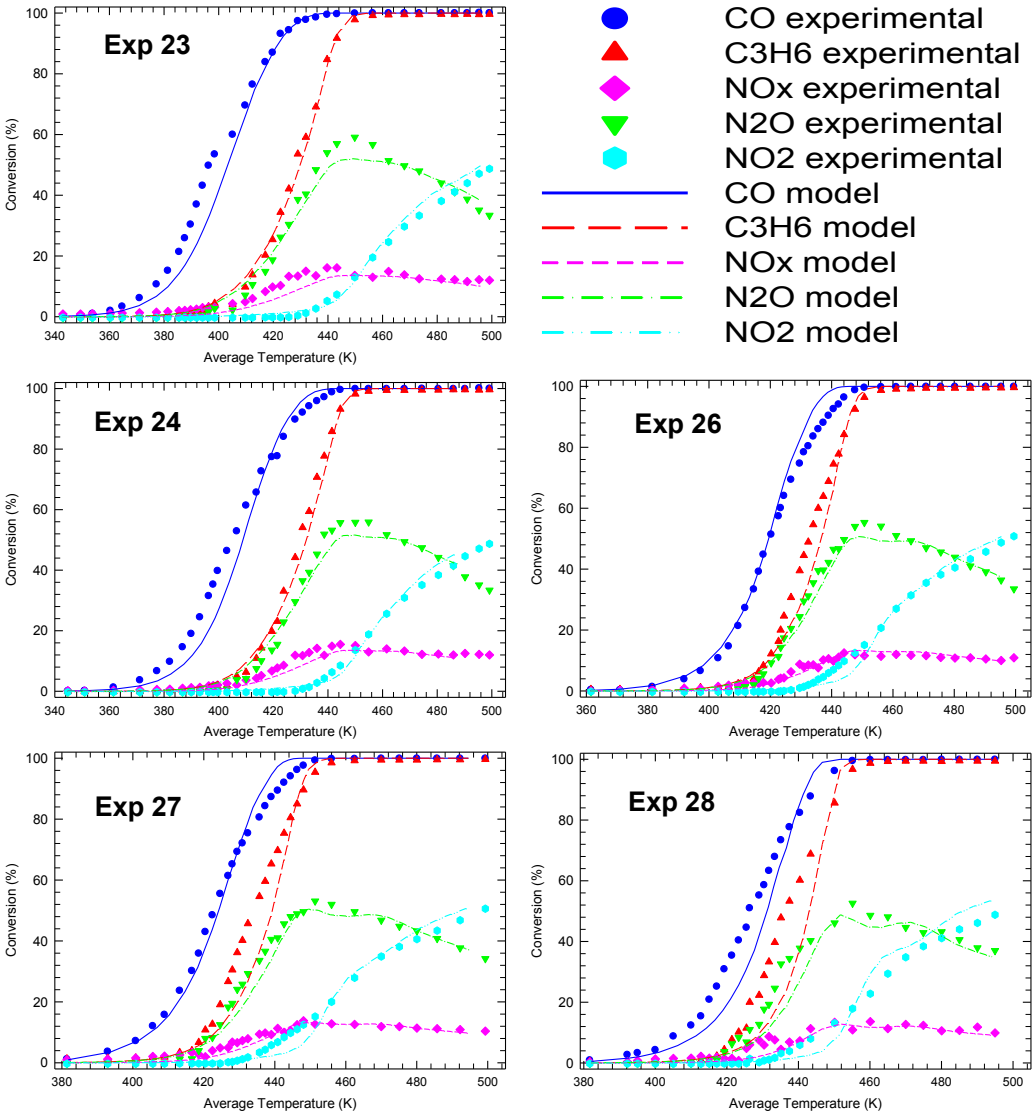


**Figure 72:** Optimization of Exp 23-28 simultaneously for model C1b.

**Table 39:** Value of the parameters and residuals for the modelling of CO, $C_3H_6$ and NO mixture when optimizing 5 experiments simultaneously for Model C1b

| Parameter | | Exp 23 | Exp 24 | Exp 26 | Exp 27 | Exp 28 |
|---|---|---|---|---|---|---|
| $k_1$ | $A_1$ | 328,385,900 | | | | |
| | $E_1$ | 50,556 | | | | |
| $k_2$ | $A_2$ | 560 | | | | |
| | $E_2$ | 0 | | | | |
| $k_3$ | $A_3$ | 69,782,931 | | | | |
| | $E_3$ | 77,149 | | | | |
| $k_4$ | $A_4$ | 2,169,484 | | | | |
| | $E_4$ | 98,633 | | | | |
| $K_5$ | $B_5$ | 352 | | | | |
| | $H_5$ | -2,835 | | | | |
| $K_6$ | $B_6$ | 1,363 | | | | |
| | $H_6$ | -2,008 | | | | |
| $K_8$ | $B_8$ | 6,848 | | | | |
| | $H_8$ | -1,383 | | | | |
| $K_9$ | $B_9$ | 0.40 | | | | |
| | $H_9$ | 160,107 | | | | |
| $K_{10}$ | $B_{10}$ | 93 | | | | |
| | $H_{10}$ | -51,813 | | | | |
| $k_{11}$ | $A_{11}$ | 2,136 | | | | |
| | $E_{11}$ | 0 | | | | |
| Residual | | 50 | 44 | 68 | 67 | 93 |
| Total residual | | 321 | | | | |

Experiments 29 – 33 have more variation in all of the reactants. When these five experiments were optimized together the fit was observed to be less satisfactory. The graphs are shown in Figure 73, and the parameters in Table 40.

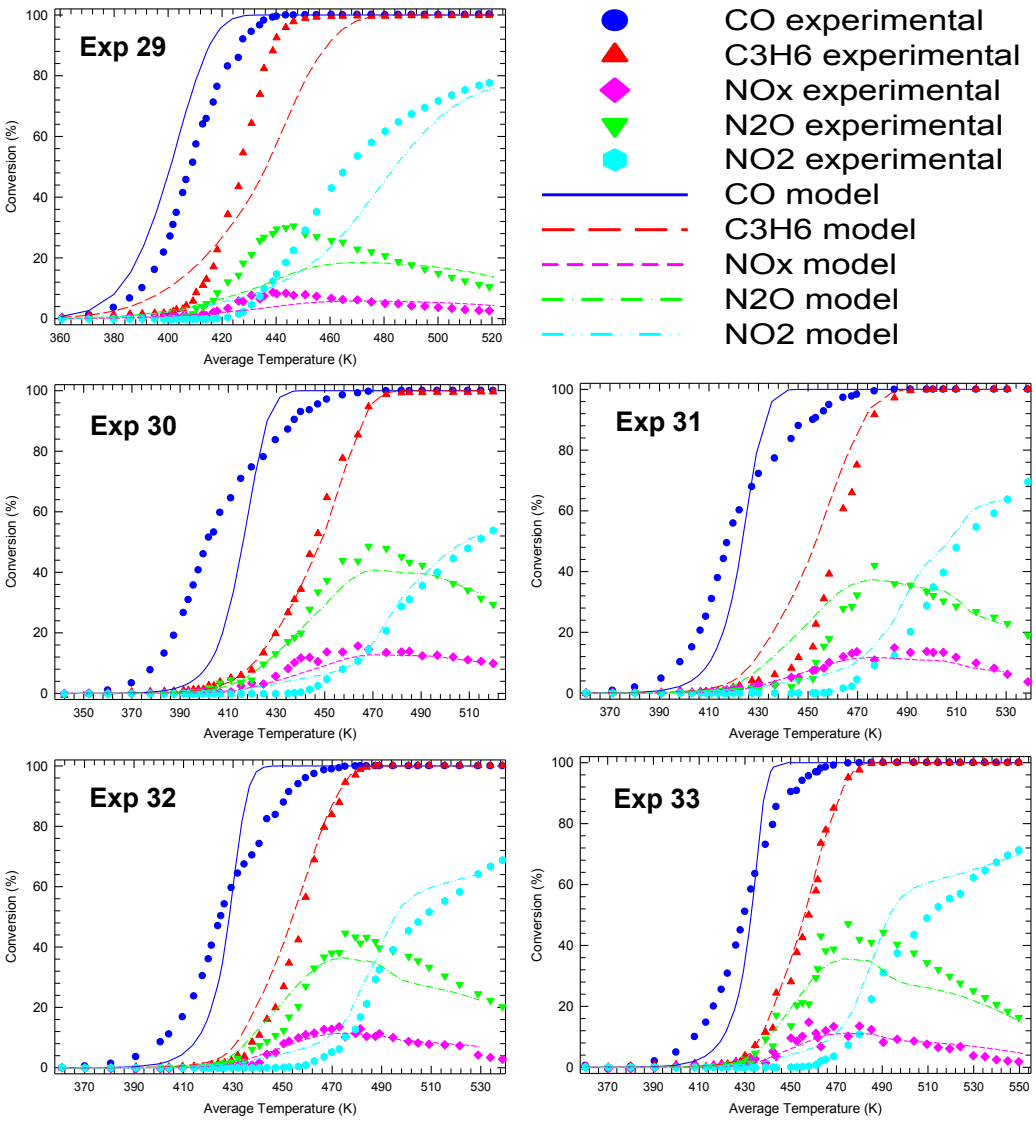


**Figure 73:** Optimization of Exp 29-33 simultaneously for model C1b.

**Table 40:** Value of the parameters and residuals for the modelling of CO, C3H6 and NO mixture when optimizing 5 experiments simultaneously for Model C1b

| Parameter | | Exp 29 | Exp 30 | Exp 31 | Exp 32 | Exp 33 |
|---|---|---|---|---|---|---|
| $k_1$ | $A_1$ | 966,314,588 | | | | |
| | $E_1$ | 102,114 | | | | |
| $k_2$ | $A_2$ | 390 | | | | |
| | $E_2$ | 0 | | | | |
| $k_3$ | $A_3$ | 33,980,589 | | | | |
| | $E_3$ | 63,379 | | | | |
| $k_4$ | $A_4$ | 2,576,906 | | | | |
| | $E_4$ | 58,865 | | | | |
| $K_5$ | $B_5$ | 1.68 | | | | |
| | $H_5$ | -3,521 | | | | |
| $K_6$ | $B_6$ | 857 | | | | |
| | $H_6$ | -2,000 | | | | |
| $K_8$ | $B_8$ | 6,848 | | | | |
| | $H_8$ | -1,264 | | | | |
| $K_9$ | $B_9$ | 0.16 | | | | |
| | $H_9$ | 120,704 | | | | |
| $K_{10}$ | $B_{10}$ | 50 | | | | |
| | $H_{10}$ | -55,438 | | | | |
| $k_{11}$ | $A_{11}$ | 1,242 | | | | |
| | $E_{11}$ | 0 | | | | |
| Residual | | 491 | 340 | 299 | 164 | 124 |
| Total residual | | 1,418 | | | | |

The final step for Model C1b was is to optimize all 10 experiments simultaneously. The results are shown in Figures 74 and 75, and the parameters are given in Table 41.

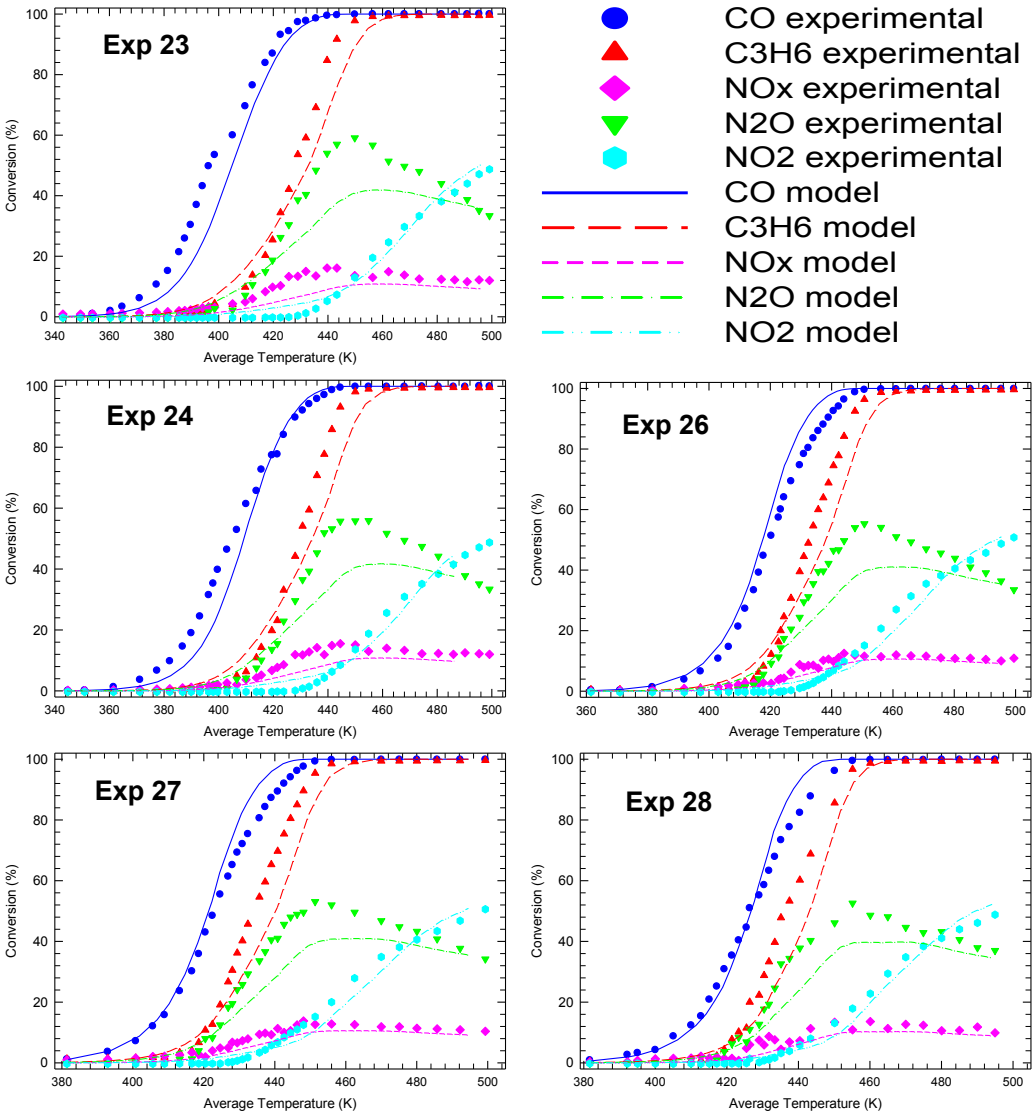


**Figure 74:** Experiments 23-28 when optimizing experiments 23-33 altogether for Model C1b.

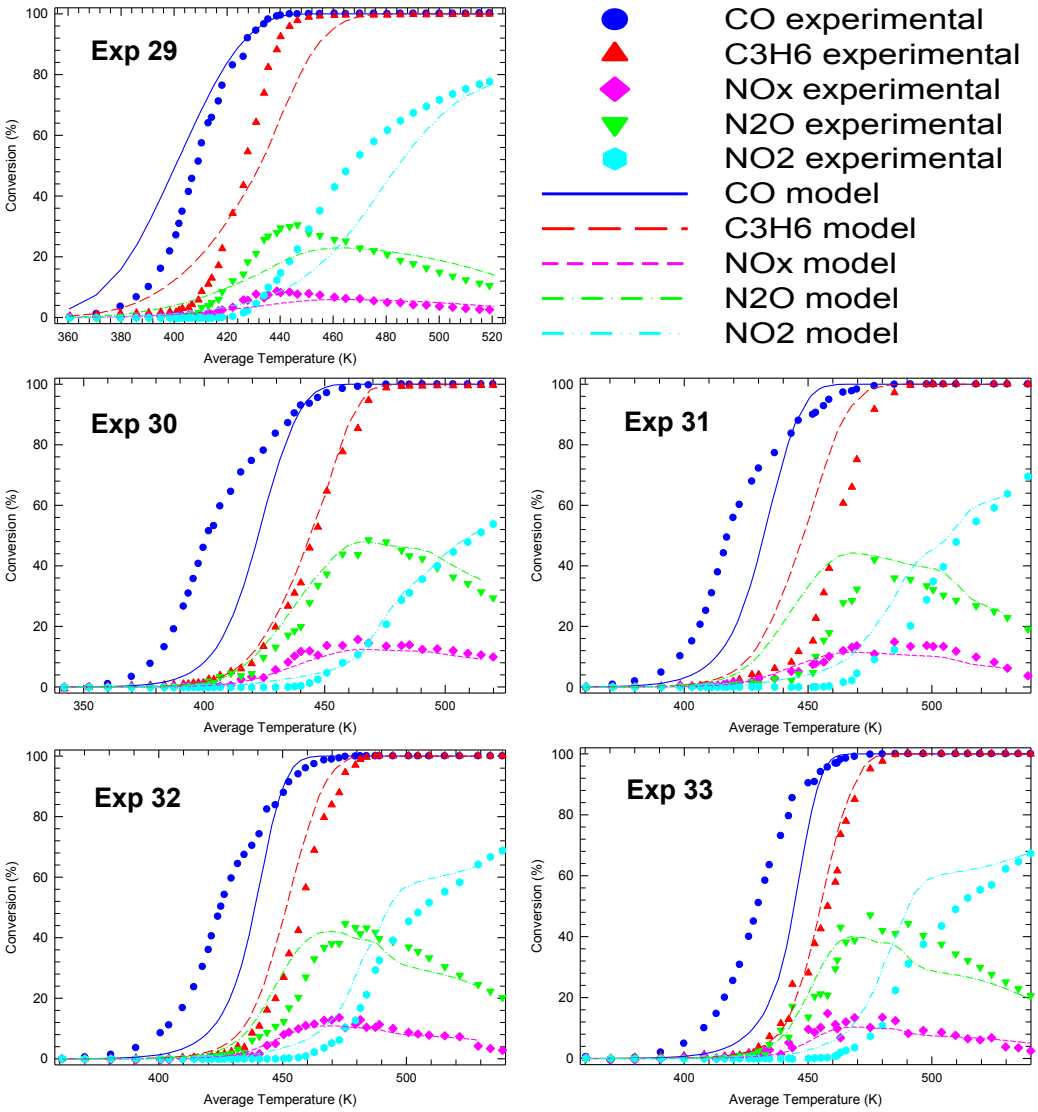


**Figure 75:** Experiments 29-33 when optimizing experiments 23-33 altogether for Model C1b.

**Table 41:** Value of the parameters and residuals for the modelling of CO, $C_3H_6$ and NO mixture when optimizing all 10 experiments simultaneously for Model C1b

| Parameter | | Exp 23 | Exp 24 | Exp 26 | Exp 27 | Exp 28 | Exp 29 | Exp 30 | Exp 31 | Exp 32 | Exp 33 |
|---|---|---|---|---|---|---|---|---|---|---|---|
| $k_1$ | $A_1$ | 174,913,128 | | | | | | | | | |
| | $E_1$ | 58,825 | | | | | | | | | |
| $k_2$ | $A_2$ | 422 | | | | | | | | | |
| | $E_2$ | 0 | | | | | | | | | |
| $k_3$ | $A_3$ | 31,059,025 | | | | | | | | | |
| | $E_3$ | 64,258 | | | | | | | | | |
| $k_4$ | $A_4$ | 1,675,798 | | | | | | | | | |
| | $E_4$ | 70,178 | | | | | | | | | |
| $K_5$ | $B_5$ | 74 | | | | | | | | | |
| | $H_5$ | -3,193 | | | | | | | | | |
| $K_6$ | $B_6$ | 734 | | | | | | | | | |
| | $H_6$ | -2,000 | | | | | | | | | |
| $K_8$ | $B_8$ | 4,511 | | | | | | | | | |
| | $H_8$ | -1,359 | | | | | | | | | |
| $K_9$ | $B_9$ | 0.47 | | | | | | | | | |
| | $H_9$ | 105,341 | | | | | | | | | |
| $K_{10}$ | $B_{10}$ | 50 | | | | | | | | | |
| | $H_{10}$ | -55,438 | | | | | | | | | |
| $k_{11}$ | $A_{11}$ | 1,629 | | | | | | | | | |
| | $E_{11}$ | 0 | | | | | | | | | |
| Residual | | 159 | 146 | 168 | 165 | 117 | 351 | 430 | 668 | 381 | 414 |
| Total residual | | 2,999 | | | | | | | | | |

**Model C4b**

The same procedure was followed for Model C4b. The results obtained from the optimization of experiments 23 – 28 are shown in Figure 76, with the parameters in Table 42. The results for the optimization of experiments 29 – 33 are shown in Figure 77, with the parameters given in Table 43.

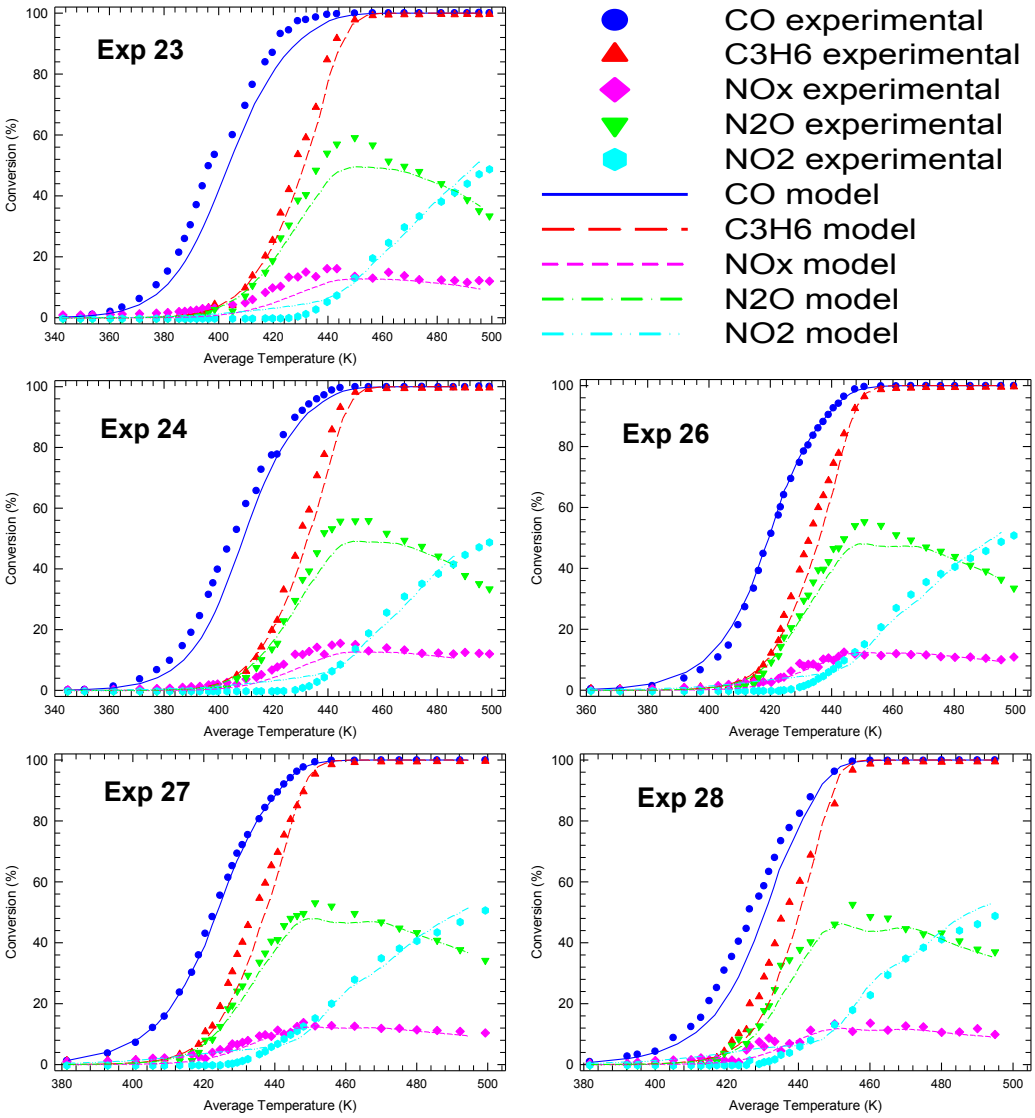


**Figure 76:** Optimization of Exp 23-28 simultaneously for Model C4b.

**Table 42:** Value of the parameters and residuals for the modelling of CO, C3H6 and NO mixture when optimizing 5 experiments simultaneously for Model C4b

| Parameter | | Exp 23 | Exp 24 | Exp 26 | Exp 27 | Exp 28 |
|---|---|---|---|---|---|---|
| $k_1$ | $A_1$ | 47,086,646 | | | | |
| | $E_1$ | 50,000 | | | | |
| $k_2$ | $A_2$ | 546 | | | | |
| | $E_2$ | 0 | | | | |
| $k_3$ | $A_3$ | 20,536,205 | | | | |
| | $E_3$ | 110,571 | | | | |
| $k_4$ | $A_4$ | 19,418 | | | | |
| | $E_4$ | 100,000 | | | | |
| $K_5$ | $B_5$ | 138 | | | | |
| | $H_5$ | -2,000 | | | | |
| $K_6$ | $B_6$ | 1.65 | | | | |
| | $H_6$ | -2,709 | | | | |
| $K_8$ | $B_8$ | 3.13 | | | | |
| | $H_8$ | -13,228 | | | | |
| $K_9$ | $B_9$ | 0.28 | | | | |
| | $H_9$ | 195,873 | | | | |
| $K_{10}$ | $B_{10}$ | 1,963 | | | | |
| | $H_{10}$ | -60,000 | | | | |
| $k_{11}$ | $A_{11}$ | 2,121 | | | | |
| | $E_{11}$ | 0 | | | | |
| Residual | | 63 | 43 | 38 | 33 | 39 |
| Total residual | | 214 | | | | |

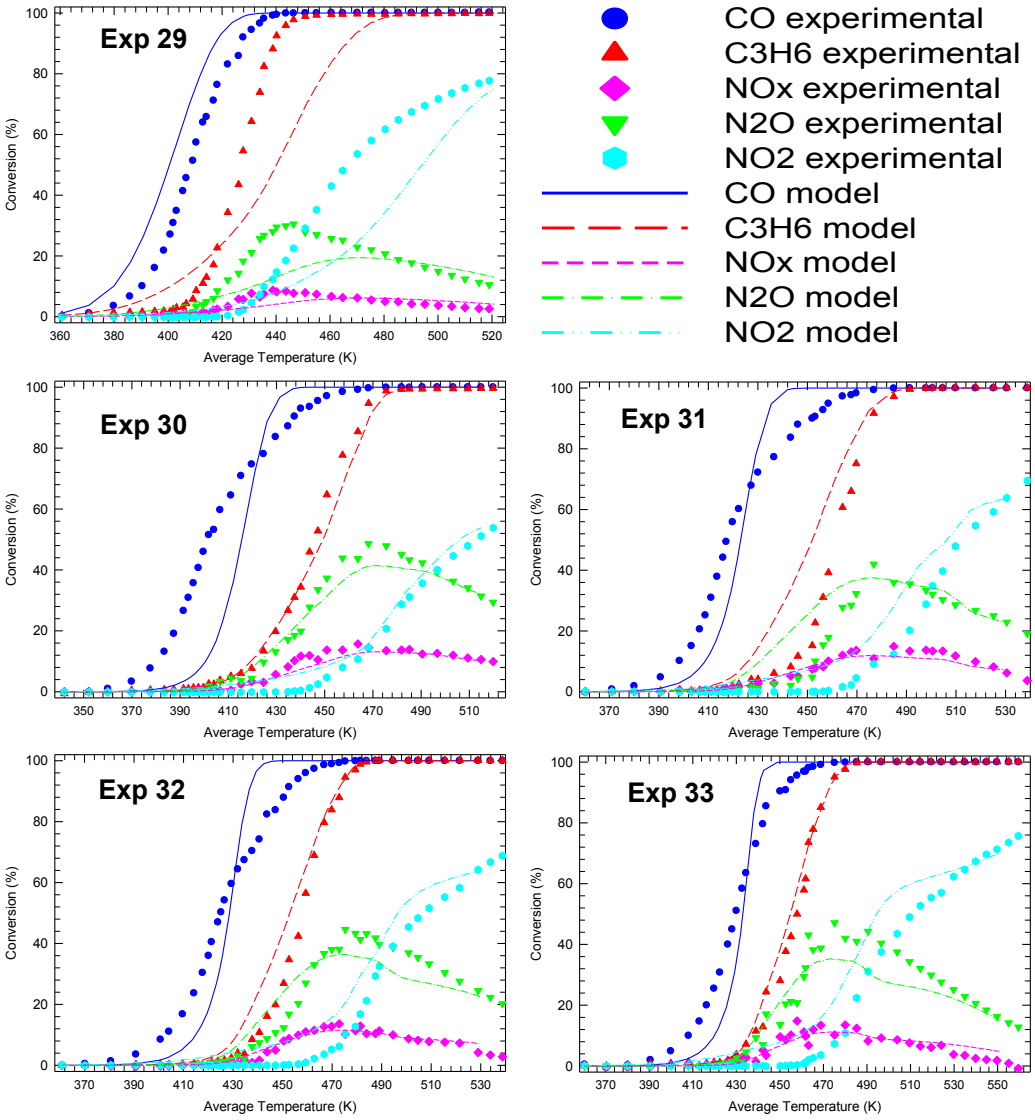


**Figure 77:** Optimization of Exp 29-33 simultaneously for Model C4b.

**Table 43:** Value of the parameters and residuals for the modelling of CO, $C_3H_6$ and NO mixture when optimizing 5 experiments simultaneously for Model C4b

| Parameter | | Exp 29 | Exp 30 | Exp 31 | Exp 32 | Exp 33 |
|---|---|---|---|---|---|---|
| $k_1$ | $A_1$ | 484,437,993 | | | | |
| | $E_1$ | 89,851 | | | | |
| $k_2$ | $A_2$ | 475 | | | | |
| | $E_2$ | 0 | | | | |
| $k_3$ | $A_3$ | 20,536,205 | | | | |
| | $E_3$ | 60,327 | | | | |
| $k_4$ | $A_4$ | 21,163 | | | | |
| | $E_4$ | 100,000 | | | | |
| $K_5$ | $B_5$ | 1.81 | | | | |
| | $H_5$ | -6,172 | | | | |
| $K_6$ | $B_6$ | 548 | | | | |
| | $H_6$ | -2,115 | | | | |
| $K_8$ | $B_8$ | 5,323 | | | | |
| | $H_8$ | -1,172 | | | | |
| $K_9$ | $B_9$ | 0.12 | | | | |
| | $H_9$ | 115,111 | | | | |
| $K_{10}$ | $B_{10}$ | 1,963 | | | | |
| | $H_{10}$ | -41,401 | | | | |
| $k_{11}$ | $A_{11}$ | 1,497 | | | | |
| | $E_{11}$ | 0 | | | | |
| Residual | | 662 | 310 | 334 | 184 | 144 |
| Total residual | | 1,632 | | | | |

The results found when optimizing all 10 experiments simultaneously are shown in Figures 78 and 79, with the parameters given in Table 44.

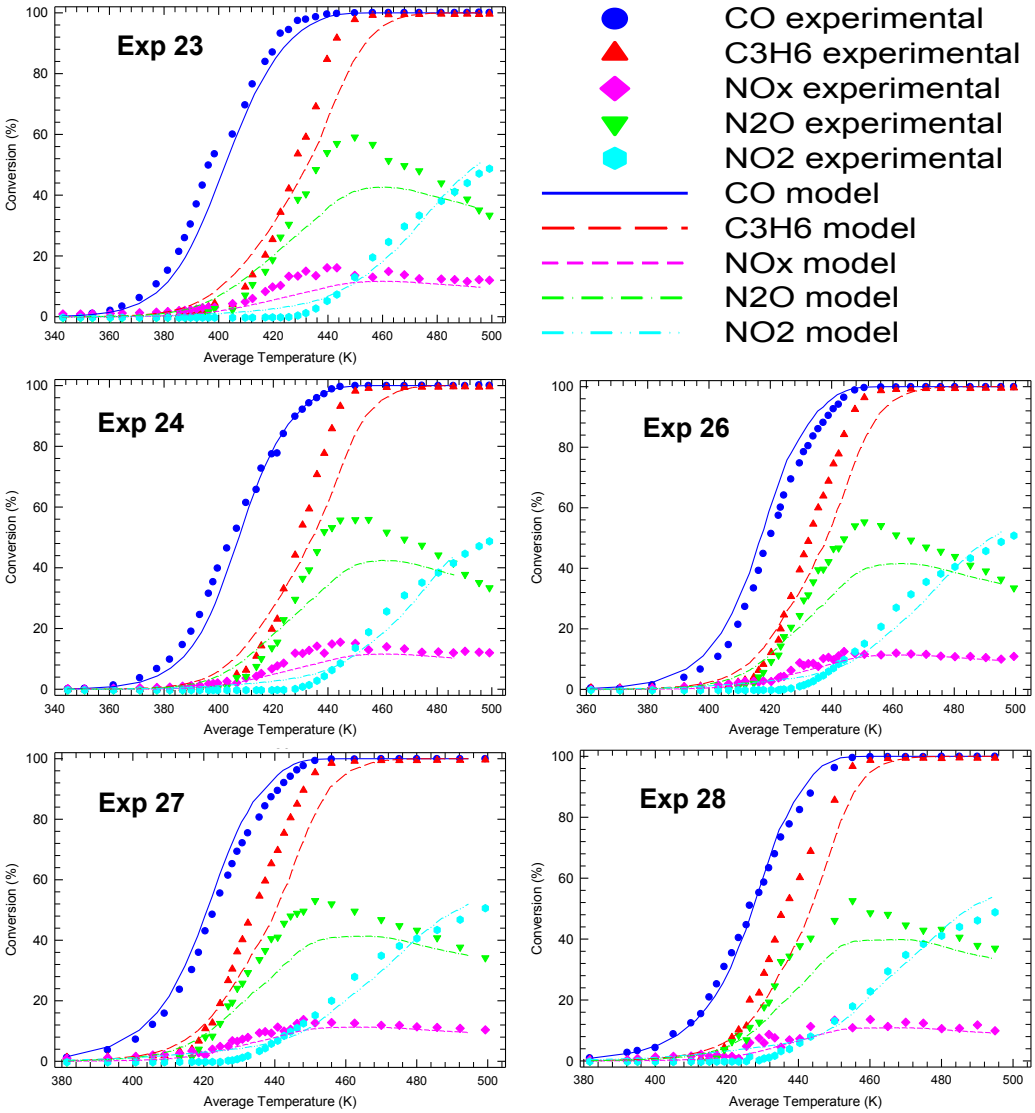


**Figure 78:** Experiments 23-28 when optimizing experiments 23-33 altogether for Model C4b.

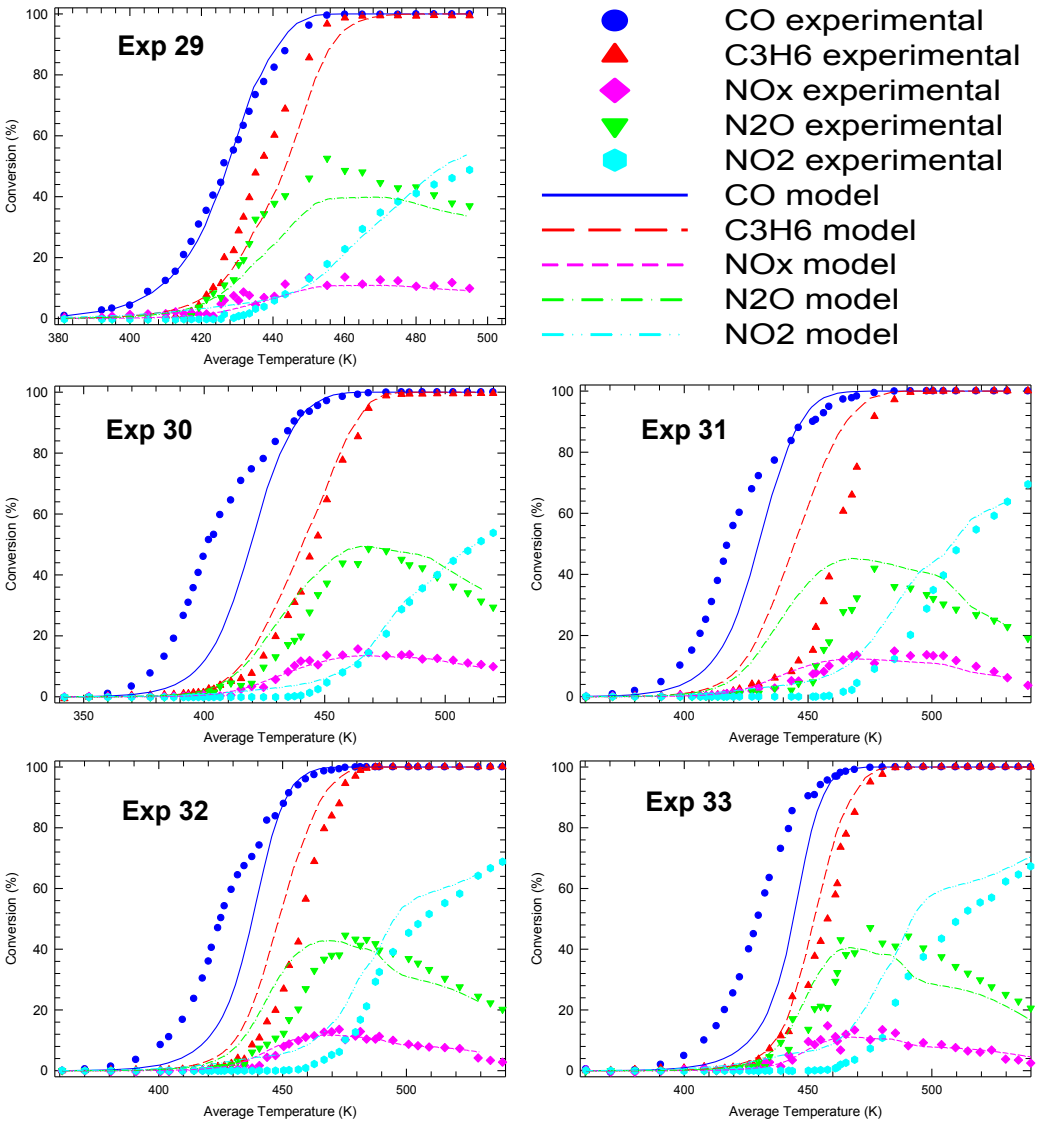


**Figure 79:** Experiments 29-33 when optimizing experiments 23-33 altogether for Model C4b.

**Table 44:** Value of the parameters and residuals for the modelling of CO, $C_3H_6$ and NO mixture when optimizing all 10 experiments simultaneously for Model C4b

| Parameter | | Exp 23 | Exp 24 | Exp 26 | Exp 27 | Exp 28 | Exp 29 | Exp 30 | Exp 31 | Exp 32 | Exp 33 |
|---|---|---|---|---|---|---|---|---|---|---|---|
| $k_1$ | $A_1$ | 92,581,510 | | | | | | | | | |
| | $E_1$ | 50,030 | | | | | | | | | |
| $k_2$ | $A_2$ | 477 | | | | | | | | | |
| | $E_2$ | 0 | | | | | | | | | |
| $k_3$ | $A_3$ | 20,536,205 | | | | | | | | | |
| | $E_3$ | 63,696 | | | | | | | | | |
| $k_4$ | $A_4$ | 21,163 | | | | | | | | | |
| | $E_4$ | 100,000 | | | | | | | | | |
| $K_5$ | $B_5$ | 72 | | | | | | | | | |
| | $H_5$ | -2,563 | | | | | | | | | |
| $K_6$ | $B_6$ | 58 | | | | | | | | | |
| | $H_6$ | -3,459 | | | | | | | | | |
| $K_8$ | $B_8$ | 5,323 | | | | | | | | | |
| | $H_8$ | -1,172 | | | | | | | | | |
| $K_9$ | $B_9$ | 0.15 | | | | | | | | | |
| | $H_9$ | 132,104 | | | | | | | | | |
| $K_{10}$ | $B_{10}$ | 2,891 | | | | | | | | | |
| | $H_{10}$ | -59,094 | | | | | | | | | |
| $k_{11}$ | $A_{11}$ | 1,748 | | | | | | | | | |
| | $E_{11}$ | 0 | | | | | | | | | |
| Residual | | 135 | 143 | 179 | 161 | 93 | 491 | 382 | 740 | 405 | 416 |
| Total residual | | 3,145 | | | | | | | | | |

**Model C5b**

Finally, the same procedure was followed for Model C5b. The results obtained from the optimization of experiments 23 – 28 are shown in Figure 80, with the parameters in Table 45. The results for the optimization of experiments 29 – 33 are shown in Figure 81, with the parameters given in Table 46.

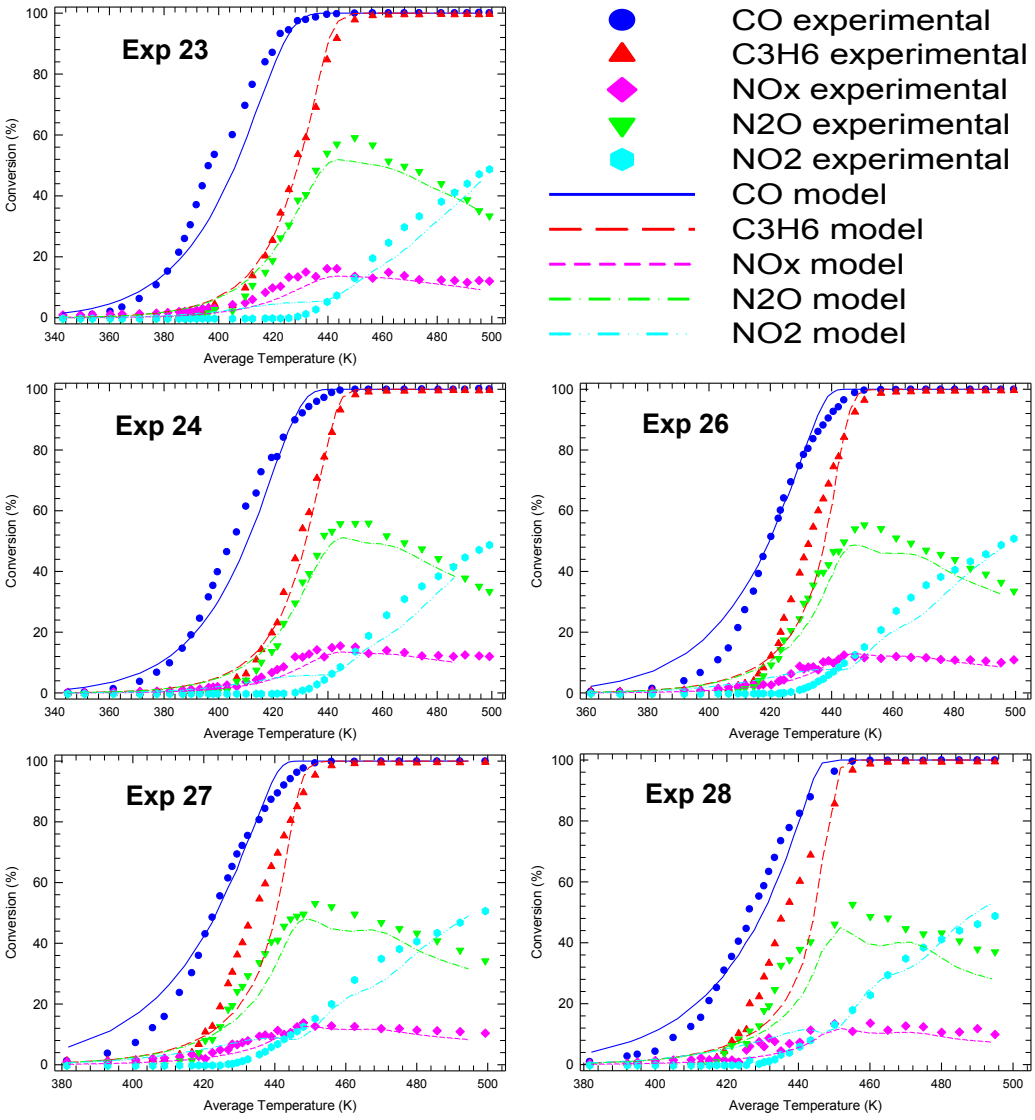


**Figure 80:** Optimization of Exp 23-28 simultaneously for Model C5b.

**Table 45:** Value of the parameters and residuals for the modelling of CO, C3H6 and NO mixture when optimizing 5 experiments simultaneously for Model C5b

| Parameter | | Exp 23 | Exp 24 | Exp 26 | Exp 27 | Exp 28 |
|---|---|---|---|---|---|---|
| $k_1$ | $A_1$ | 623,213,678 | | | | |
| | $E_1$ | 62,658 | | | | |
| $k_2$ | $A_2$ | 632 | | | | |
| | $E_2$ | 0 | | | | |
| $k_3$ | $A_3$ | 114,444,437 | | | | |
| | $E_3$ | 75,684 | | | | |
| $k_4$ | $A_4$ | 450,333,961 | | | | |
| | $E_4$ | 99,805 | | | | |
| $K_5$ | $B_5$ | 2,161 | | | | |
| | $H_5$ | -8,615 | | | | |
| $K_6$ | $B_6$ | 1,727 | | | | |
| | $H_6$ | -2,256 | | | | |
| $K_8$ | $B_8$ | 6,564 | | | | |
| | $H_8$ | -1,048 | | | | |
| $K_9$ | $B_9$ | 0.66 | | | | |
| | $H_9$ | 128,778 | | | | |
| $K_{10}$ | $B_{10}$ | 109 | | | | |
| | $H_{10}$ | -59,969 | | | | |
| $k_{11}$ | $A_{11}$ | 2,398 | | | | |
| | $E_{11}$ | 0 | | | | |
| Residual | | 80 | 63 | 111 | 124 | 144 |
| Total residual | | 522 | | | | |

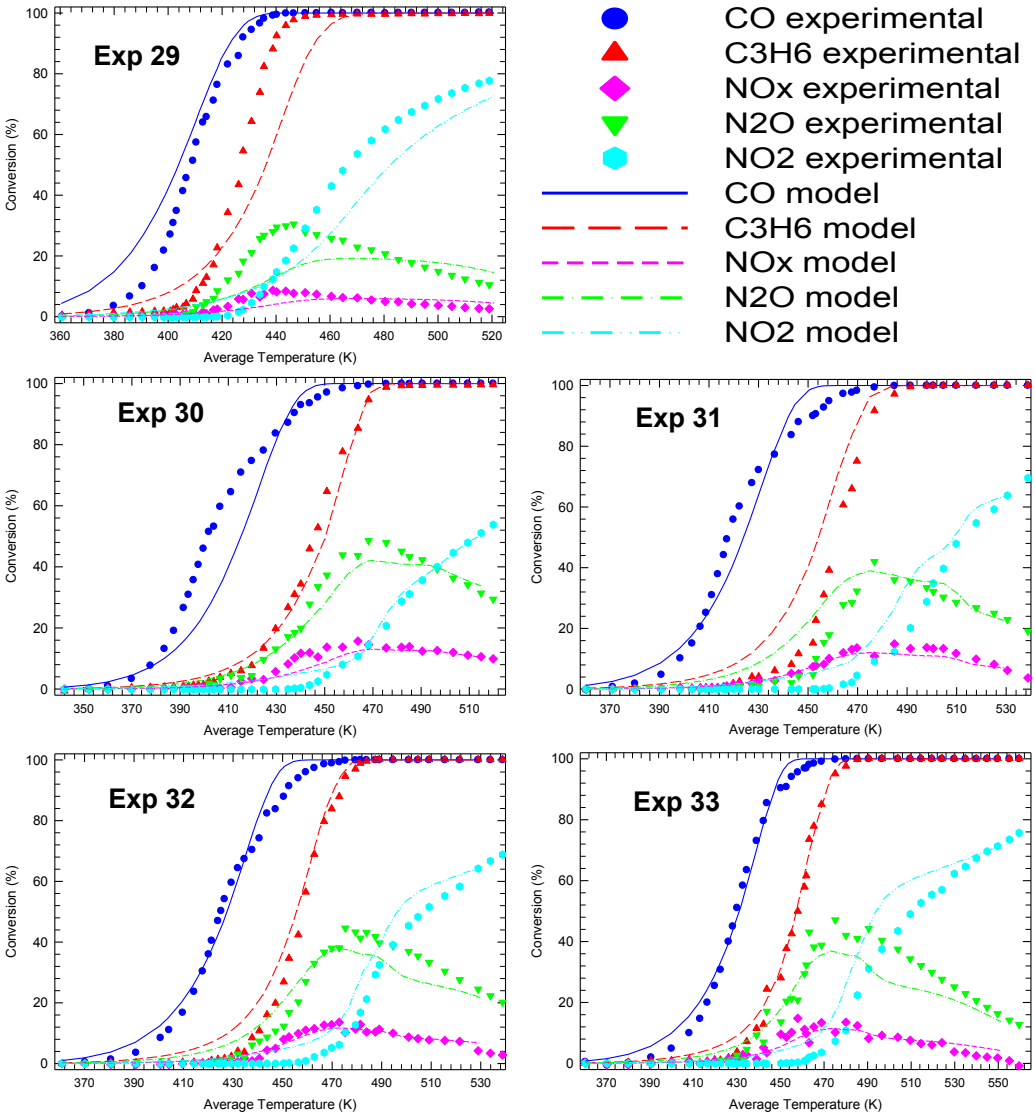


**Figure 81:** Optimization of Exp 29-33 simultaneously for Model C5b.

**Table 46:** Value of the parameters and residuals for the modelling of CO, C3H6 and NO mixture when optimizing 5 experiments simultaneously for Model C5b

| Parameter | | Exp 29 | Exp 30 | Exp 31 | Exp 32 | Exp 33 |
|---|---|---|---|---|---|---|
| $k_1$ | $A_1$ | 575,011,156 | | | | |
| | $E_1$ | 66,593 | | | | |
| $k_2$ | $A_2$ | 403 | | | | |
| | $E_2$ | 0 | | | | |
| $k_3$ | $A_3$ | 50,865,731 | | | | |
| | $E_3$ | 57,831 | | | | |
| $k_4$ | $A_4$ | 4,707,182 | | | | |
| | $E_4$ | 46,194 | | | | |
| $K_5$ | $B_5$ | 1,206 | | | | |
| | $H_5$ | -7,157 | | | | |
| $K_6$ | $B_6$ | 2,086 | | | | |
| | $H_6$ | -2,000 | | | | |
| $K_8$ | $B_8$ | 3,200 | | | | |
| | $H_8$ | -10,356 | | | | |
| $K_9$ | $B_9$ | 0.12 | | | | |
| | $H_9$ | 130,854 | | | | |
| $K_{10}$ | $B_{10}$ | 1.00 | | | | |
| | $H_{10}$ | -59,960 | | | | |
| $k_{11}$ | $A_{11}$ | 1,298 | | | | |
| | $E_{11}$ | 0 | | | | |
| Residual | | 321 | 129 | 200 | 63 | 62 |
| Total residual | | 775 | | | | |

The final set of plots for Model C5b shows the results of optimizing the ten experiments together. The graphs are shown in Figures 82 and 83, with the parameter values given in Table 47. From the residual, it can be seen that when fitting the ten experiments together, the best result was obtained with Model C5b.

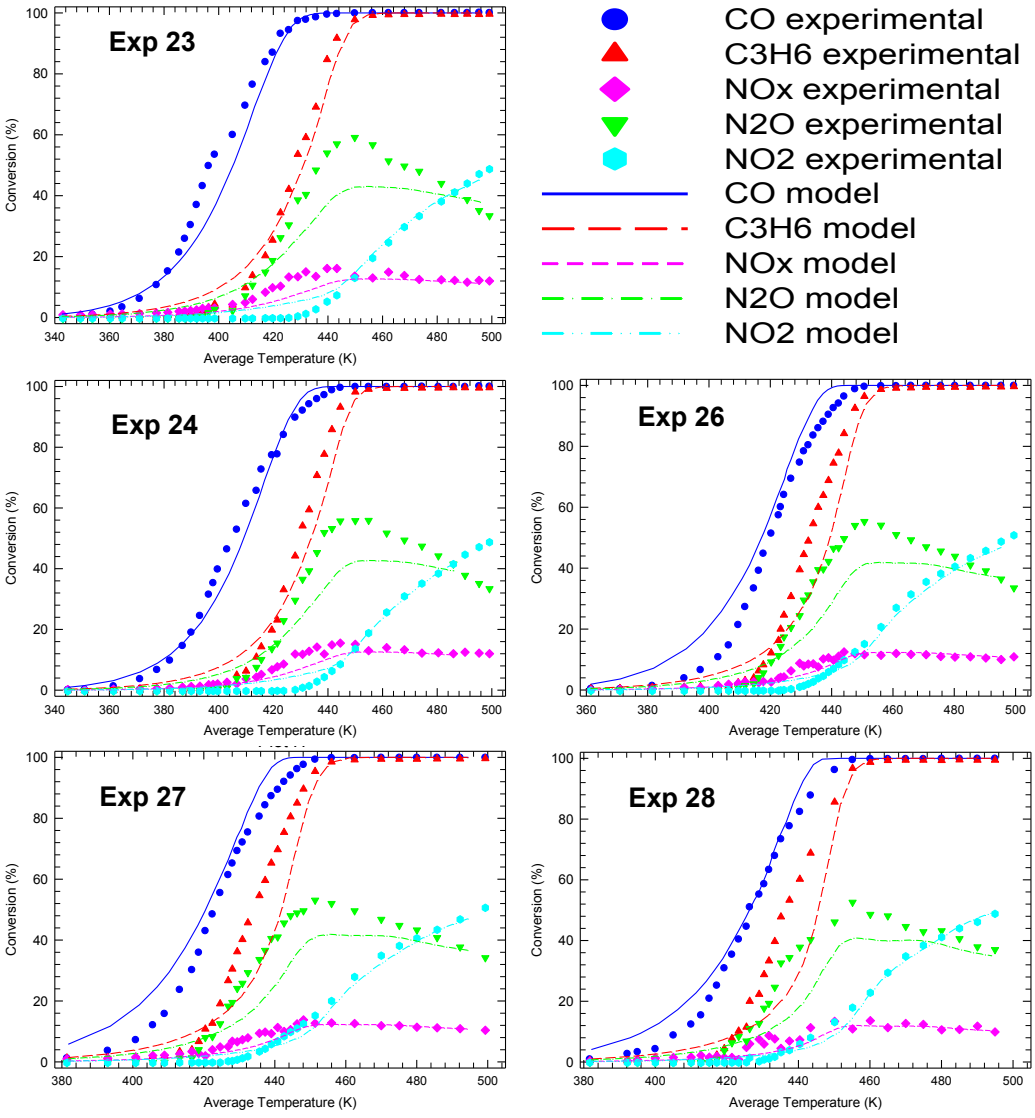


**Figure 82:** Experiments 23-28 when optimizing experiments 23-33 altogether for Model C5b.

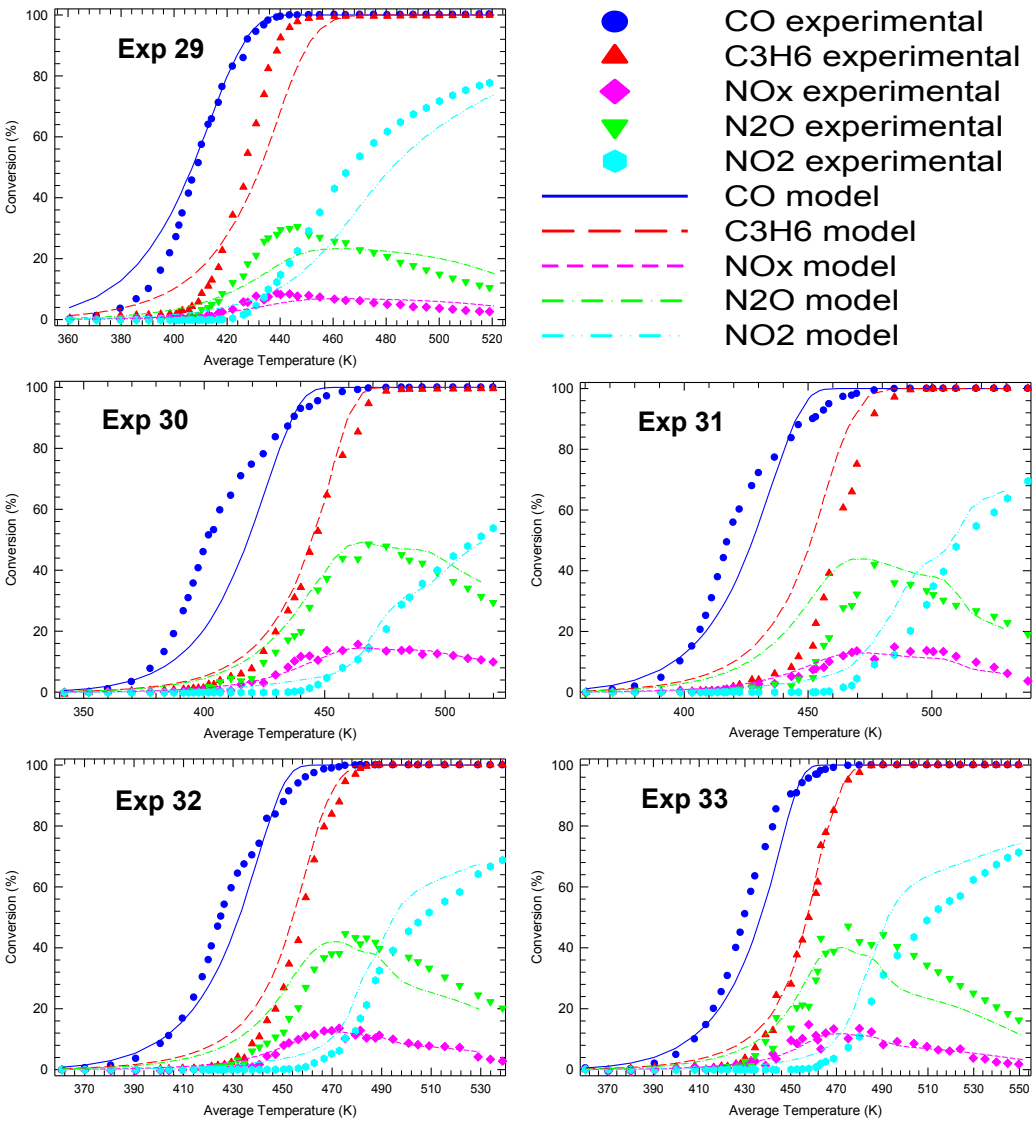


**Figure 83:** Experiments 29-33 when optimizing experiments 23-33 altogether for Model C5b.

**Table 47:** Value of the parameters and residuals for the modelling of CO, $C_3H_6$ and NO mixture when optimizing all 10 experiments simultaneously for Model C5b

| Parameter | | Exp 23 | Exp 24 | Exp 26 | Exp 27 | Exp 28 | Exp 29 | Exp 30 | Exp 31 | Exp 32 | Exp 33 |
|---|---|---|---|---|---|---|---|---|---|---|---|
| $k_1$ | $A_1$ | 575,011,156 | | | | | | | | | |
| | $E_1$ | 67,766 | | | | | | | | | |
| $k_2$ | $A_2$ | 483 | | | | | | | | | |
| | $E_2$ | 0 | | | | | | | | | |
| $k_3$ | $A_3$ | 72,892,769 | | | | | | | | | |
| | $E_3$ | 58,092 | | | | | | | | | |
| $k_4$ | $A_4$ | 5,129,917 | | | | | | | | | |
| | $E_4$ | 56,878 | | | | | | | | | |
| $K_5$ | $B_5$ | 1,668 | | | | | | | | | |
| | $H_5$ | -9,880 | | | | | | | | | |
| $K_6$ | $B_6$ | 1,930 | | | | | | | | | |
| | $H_6$ | -2,012 | | | | | | | | | |
| $K_8$ | $B_8$ | 4,124 | | | | | | | | | |
| | $H_8$ | -1,120 | | | | | | | | | |
| $K_9$ | $B_9$ | 0.19 | | | | | | | | | |
| | $H_9$ | 129,517 | | | | | | | | | |
| $K_{10}$ | $B_{10}$ | 1.00 | | | | | | | | | |
| | $H_{10}$ | -59,193 | | | | | | | | | |
| $k_{11}$ | $A_{11}$ | 1,637 | | | | | | | | | |
| | $E_{11}$ | 0 | | | | | | | | | |
| Residual | | 108 | 100 | 191 | 208 | 181 | 195 | 226 | 375 | 118 | 112 |
| Total residual | | 1,815 | | | | | | | | | |

The best overall result was obtained with model C5b. The predictive ability of this model was then tested, using the parameters of Table 47, to determine if it

would give good fits for the experiments of in the range 1-19. The graphs are shown in Figures 84 – 88, and the residuals in the accompanying tables.

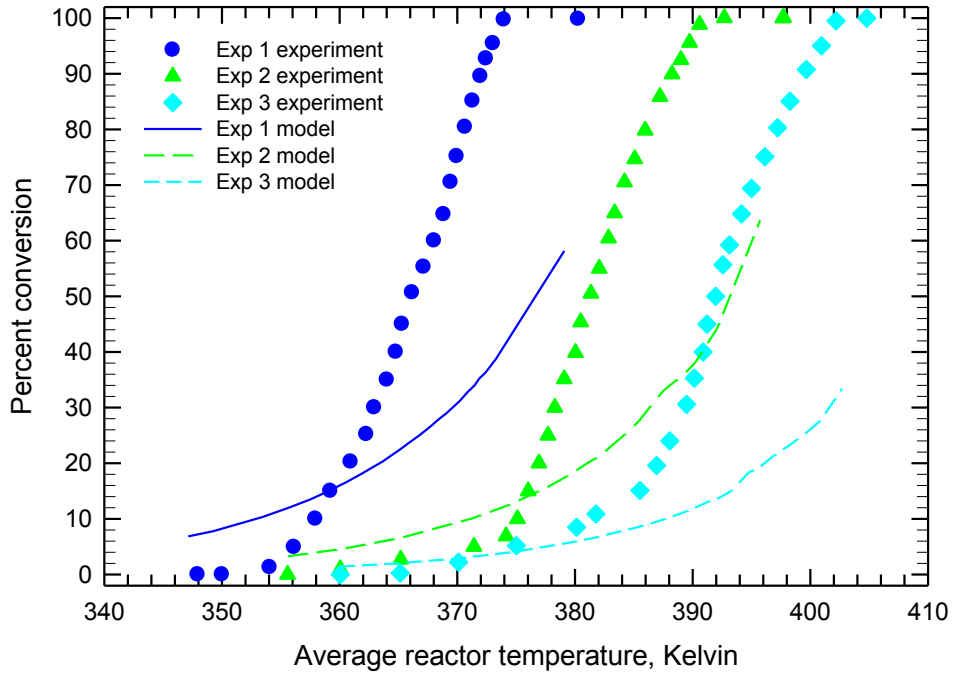


**Figure 84:** Plot of the CO experiments when using parameters of Table 47.

**Table 48:** Residual values of CO experiments when using parameters of Table 47

| | Exp 1 | Exp 2 | Exp 3 |
|---|---|---|---|
| Residual | 1,197 | 1,327 | 1,742 |

The predicted conversions are far from the experimental results.

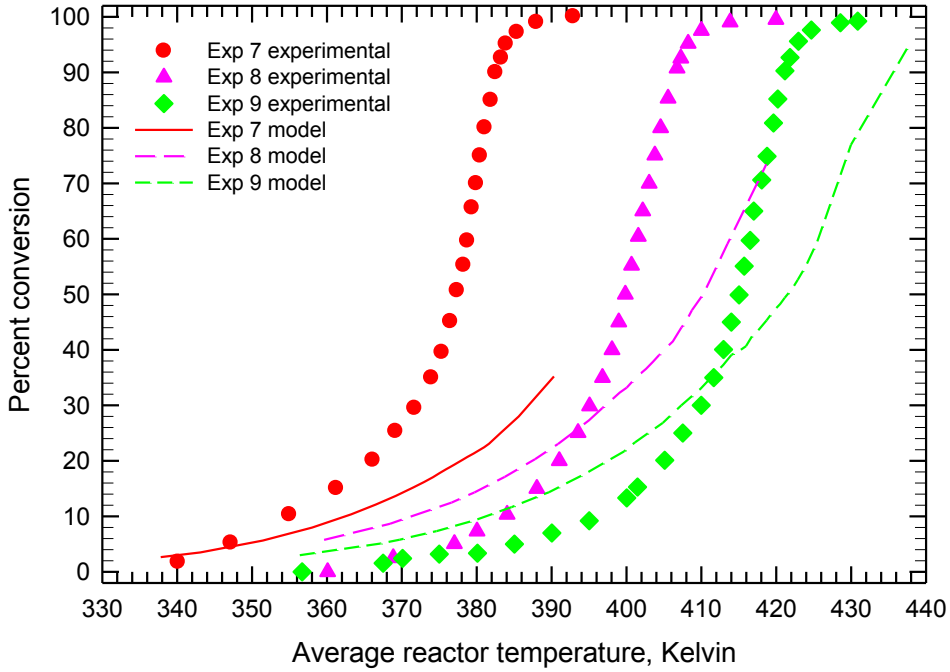


**Figure 85:** Plot of the $C_3H_6$ experiments when using parameters of Table 47.

**Table 49:** Residual values of $C_3H_6$ experiments when using parameters of Table 47

| | Exp 7 | Exp 8 | Exp 9 |
|---|---|---|---|
| Residual | 2,122 | 760 | 416 |

As with the CO oxidation, the predictions are not good

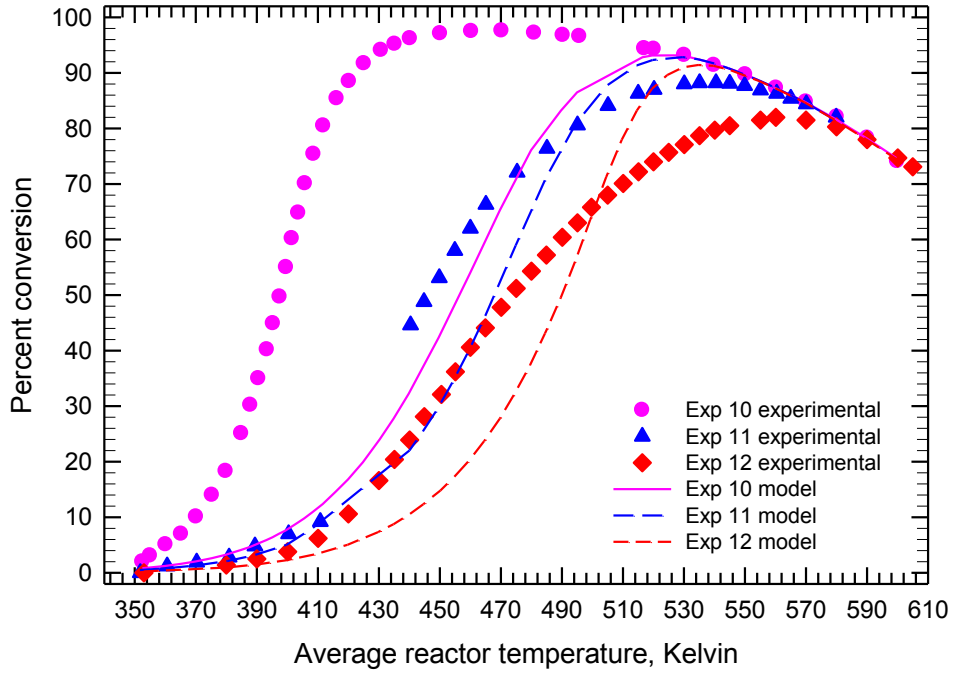


**Figure 86:** Plot of the NO experiments when using parameters of Table 47.

**Table 50:** Residual values NO experiments when using parameters of Table 47

| | Exp 10 | Exp 11 | Exp 12 |
|---|---|---|---|
| Residual | 1,536 | 117 | 131 |

Experiment 11 has a relatively small residual, although overall the fit is also not good.

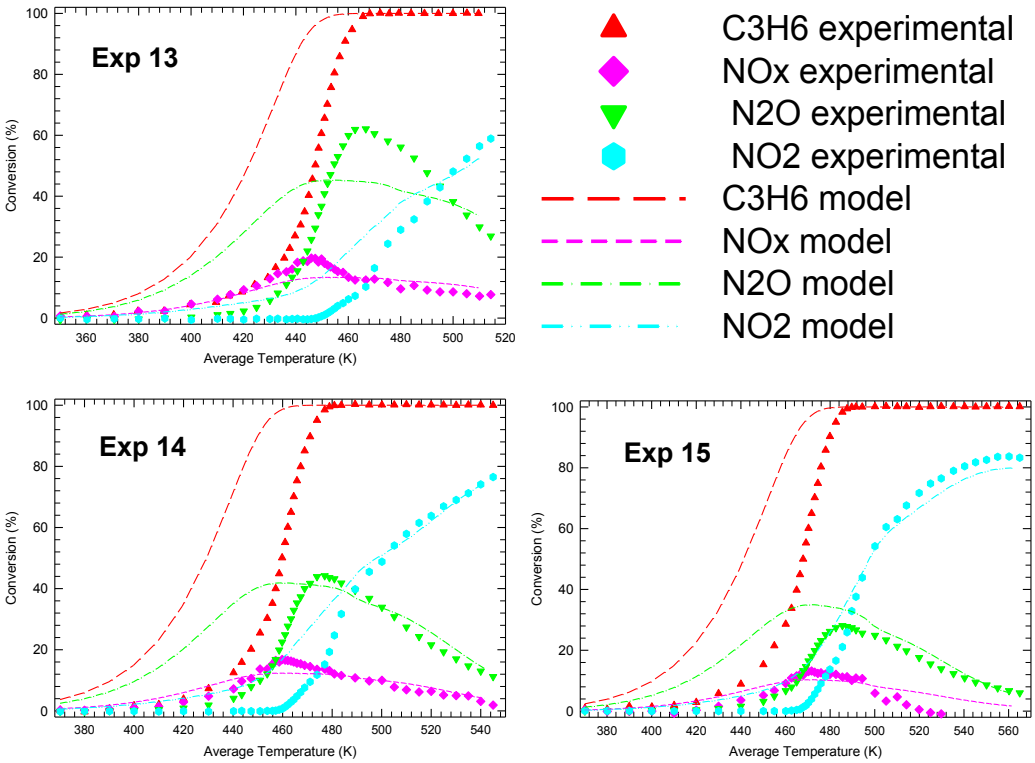


**Figure 87:** Plots of the $C_3H_6$ and NO oxidation experiments when using parameters of Table 47.

**Table 51:** Residual values $C_3H_6$ and NO oxidation experiments when using parameters of Table 47

| | Exp 13 | Exp 14 | Exp 15 |
|---|---|---|---|
| Residual | 1,402 | 1,355 | 840 |

The $NO_X$ and $NO_2$ curves are the best, but overall the result is not satisfactory.

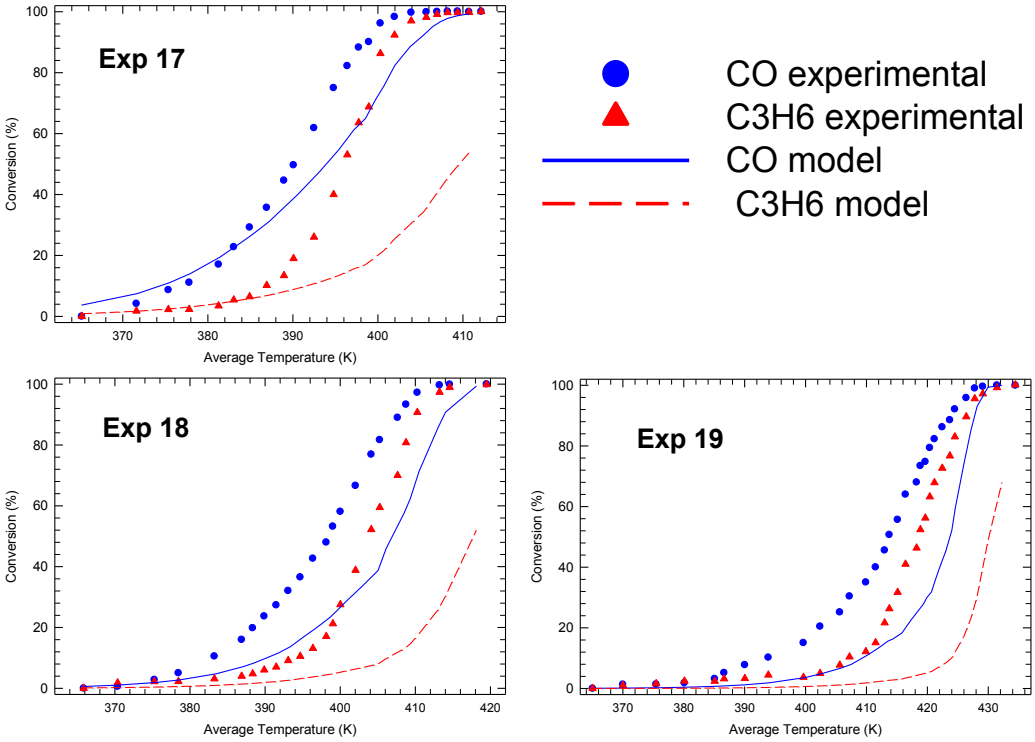


**Figure 88:** Plots of the CO and $C_3H_6$ oxidation experiments when using parameters of Table 47.

**Table 52:** Residual values CO and $C_3H_6$ oxidation experiments when using parameters of Table 47

| | Exp 17 | Exp 18 | Exp 19 |
|---|---|---|---|
| Residual | 1,747 | 1,773 | 2,285 |

The predictions are not acceptable.

The fact that the model parameters obtained for the fitting of experiments 23-33 could not reproduce the earlier experiments is consistent with the earlier comparisons. As a final effort, all 25 used experiments were used to fit the parameters. The plots obtained in this case are illustrated in Figures 89 – 95, with the parameter values and residuals listed in Tables 53 and 54 respectively.

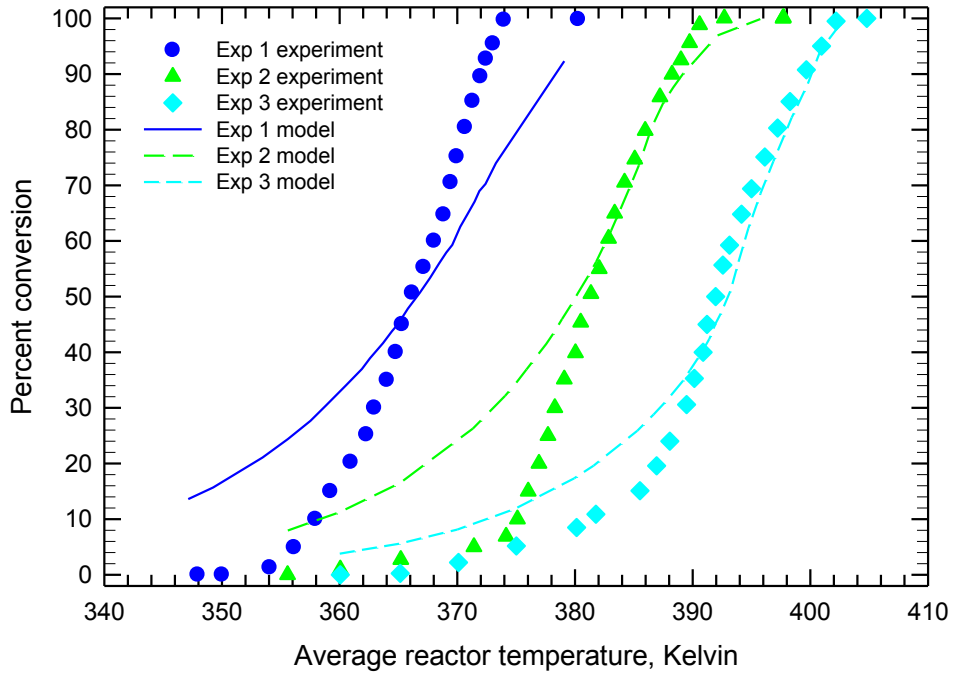


**Figure 89:** Plot of the CO experiments when optimizing experiments 1-33.

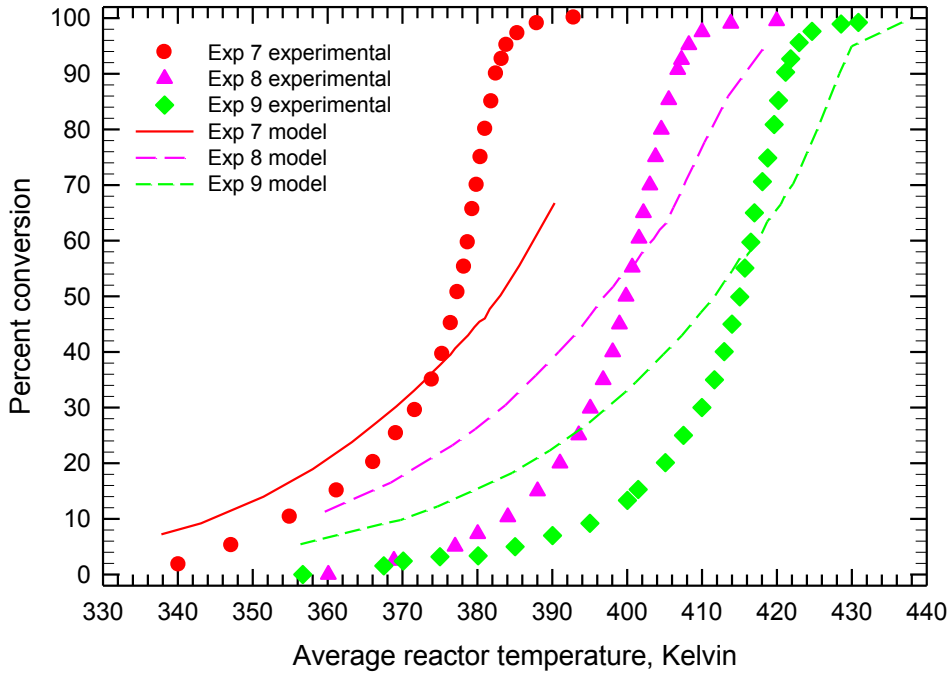


**Figure 90:** Plot of the $C_3H_6$ experiments when optimizing experiments 1-33.

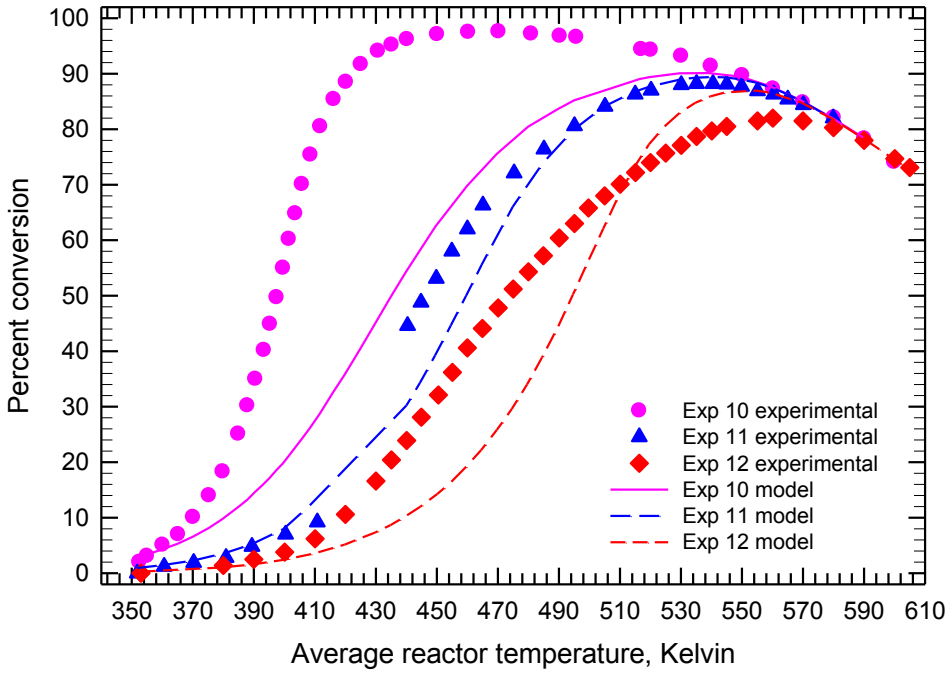


**Figure 91:** Plot of the NO experiments when optimizing experiments 1-33.

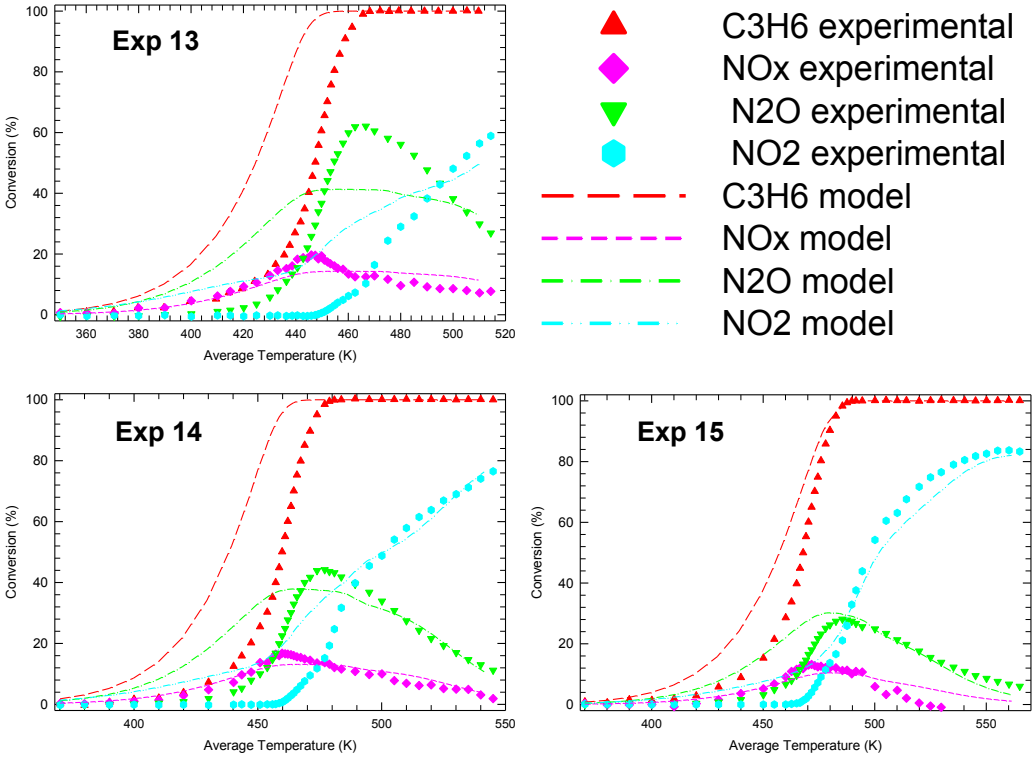


**Figure 92:** Plots of the $C_3H_6$ and NO experiments when optimizing experiments 1-33.

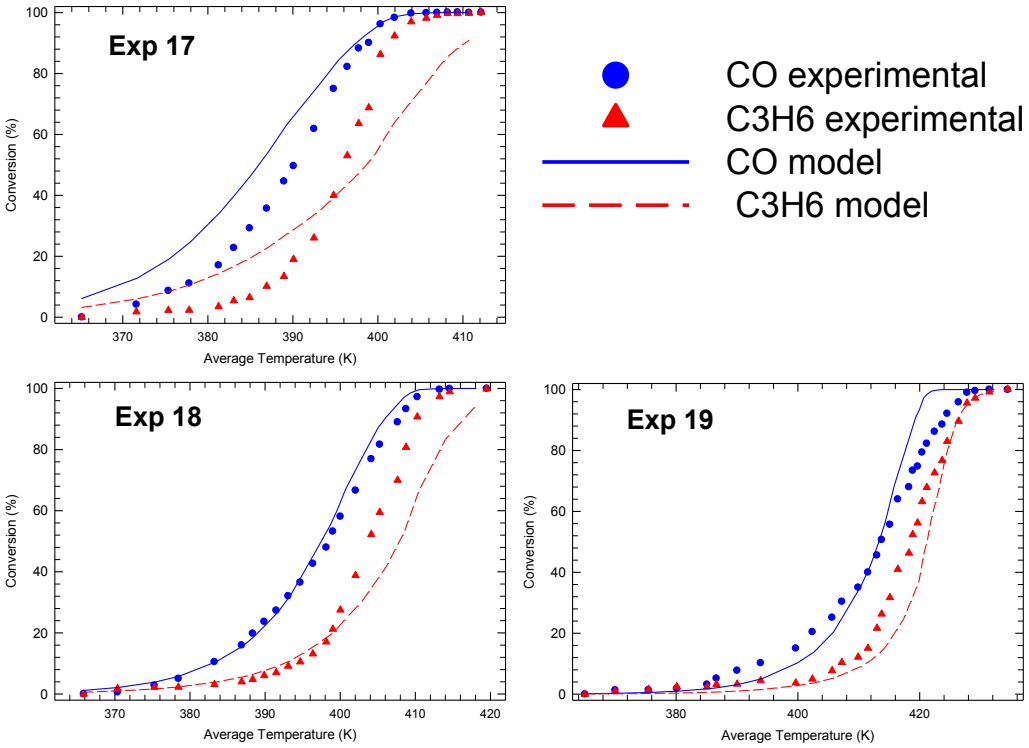


**Figure 93:** Plots of the CO and $C_3H_6$ experiments when optimizing experiments 1-33.

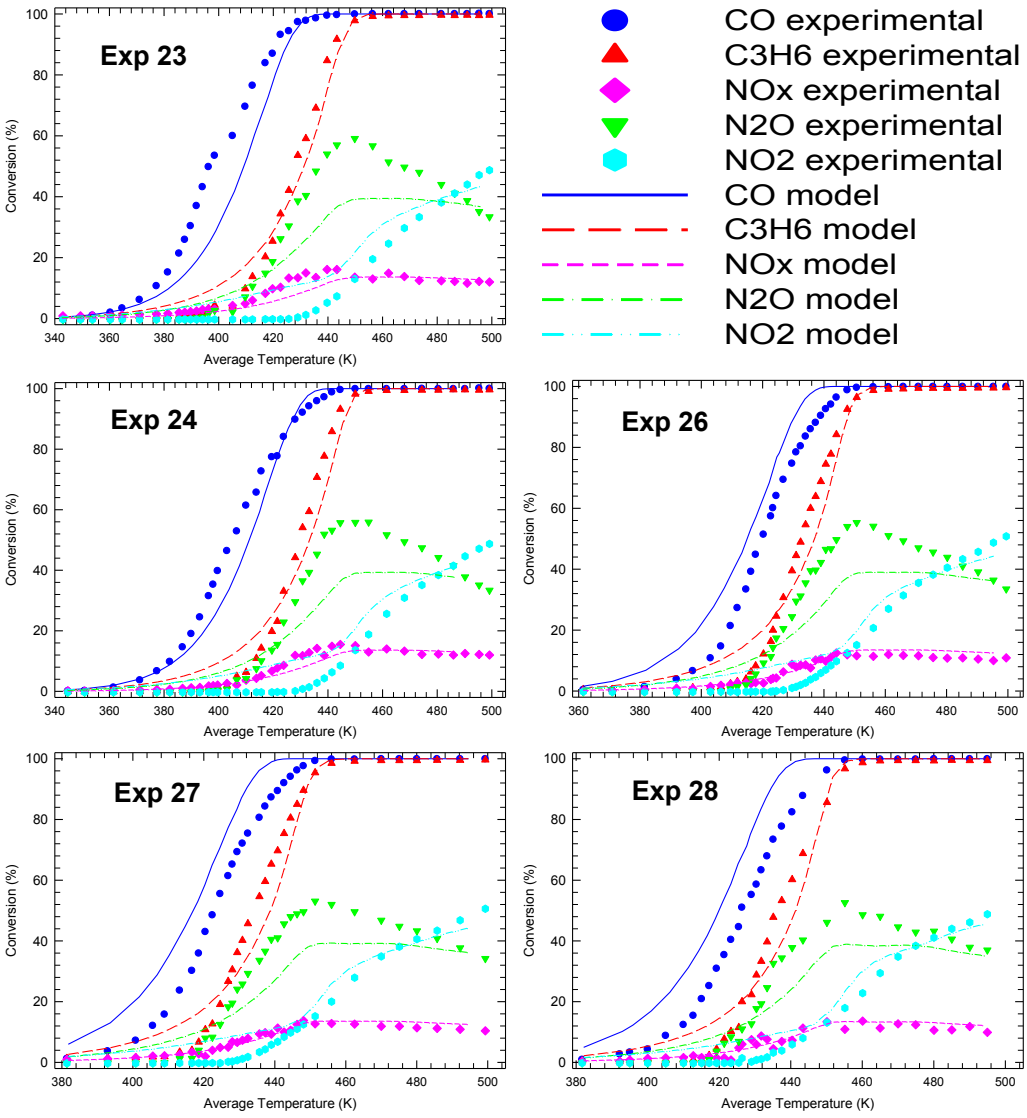


**Figure 94:** Plots of experiments 23-28 of the CO, $C_3H_6$ and NO set, when optimizing experiments 1-33.

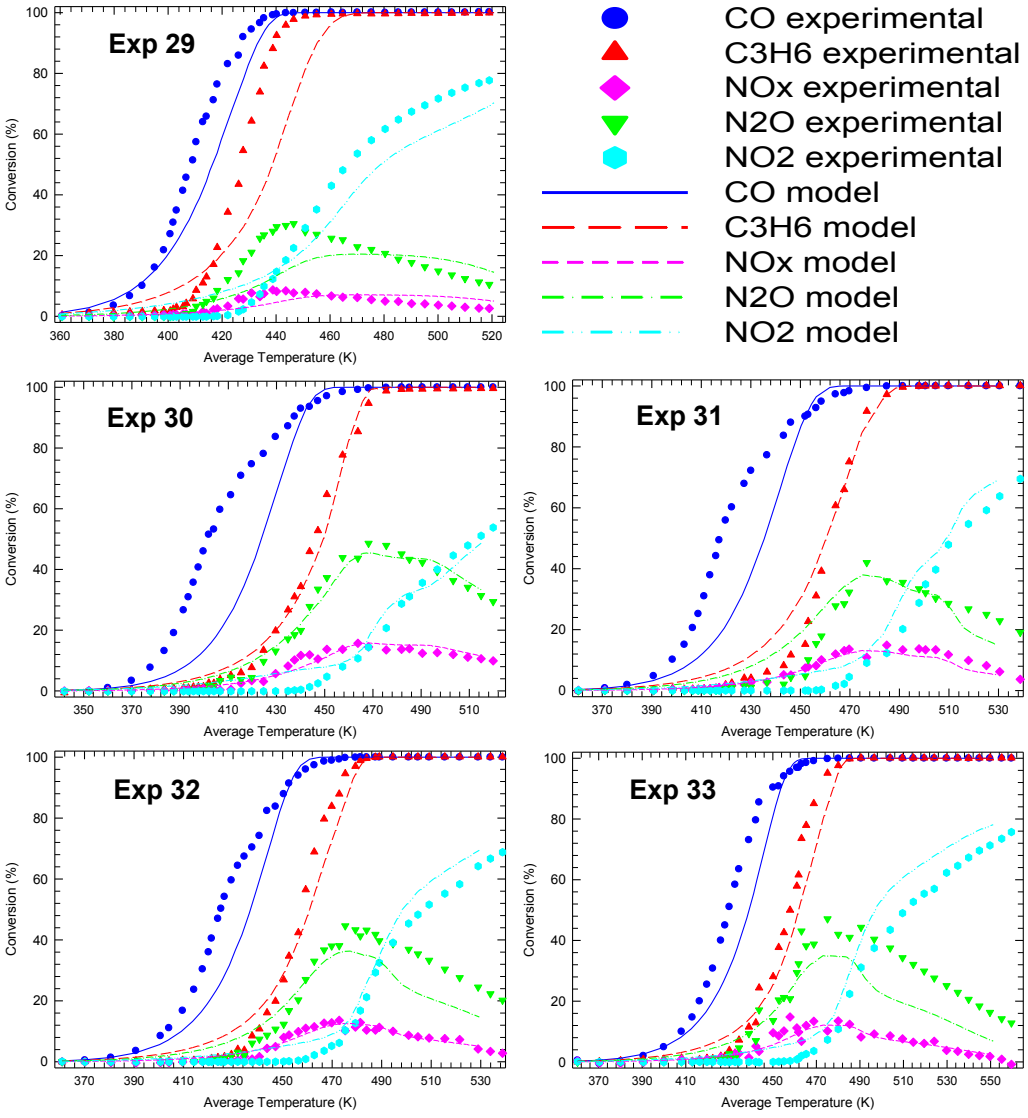


**Figure 95:** Plots of experiments 29-33 of the CO, $C_3H_6$ and NO set, when optimizing experiments 1-33.

**Table 53:** Value of the parameters and total residual for the modelling of CO, $C_3H_6$ and NO experiments, when optimizing all 25 experiments (1-33) simultaneously for Model C5b

| Parameter | | All Exp |
|---|---|---|
| $k_1$ | $A_1$ | 1,210,500,806 |
| | $E_1$ | 73,615 |
| $k_2$ | $A_2$ | 546 |
| | $E_2$ | 0 |
| $k_3$ | $A_3$ | 143,910,193 |
| | $E_3$ | 50,031 |
| $k_4$ | $A_4$ | 20,767,504 |
| | $E_4$ | 35,793 |
| $K_5$ | $B_5$ | 1,217 |
| | $H_5$ | -9,071 |
| $K_6$ | $B_6$ | 3,078 |
| | $H_6$ | -2,004 |
| $K_8$ | $B_8$ | 10,477 |
| | $H_8$ | -11,211 |
| $K_9$ | $B_9$ | 0.06 |
| | $H_9$ | 163,428.00 |
| $K_{10}$ | $B_{10}$ | 1.00 |
| | $H_{10}$ | -22,147.40 |
| $k_{11}$ | $A_{11}$ | 1,576 |
| | $E_{11}$ | 0 |
| Total Residual | | 8,828 |

**Table 54:** Residual values of the 25 experiments when optimizing them all simultaneously

| Experiment | Residual Value |
|---|---|
| Exp 1 | 237 |
| Exp 2 | 138 |
| Exp 3 | 73 |
| Exp 7 | 758 |
| Exp 8 | 242 |
| Exp 9 | 182 |
| Exp 10 | 796 |
| Exp 11 | 39 |
| Exp 12 | 131 |
| Exp 13 | 1,432 |
| Exp 14 | 967 |
| Exp 15 | 232 |
| Exp 17 | 342 |
| Exp 18 | 135 |
| Exp 19 | 147 |
| Exp 23 | 235 |
| Exp 24 | 184 |
| Exp 26 | 294 |
| Exp 27 | 339 |
| Exp 28 | 400 |
| Exp 29 | 362 |
| Exp 30 | 353 |
| Exp 31 | 333 |
| Exp 32 | 235 |
| Exp 33 | 241 |

The plots and values show that even though the fits are not that good, the improvement is evident when optimizing all the experiments simultaneously comparing to the previous case.

## 4.3. Summary and Discussion of Results

In the preceding sections the results and some discussion was presented for the modeling of the ignition curves for the platinum diesel oxidation catalyst. In this section some additional discussion and summary of the findings is made.

The first observation applies to all of the experimental and simulation results, and addresses the methods of model construction, which in turns is a reflection of the mechanistic meaning of the model. The nature of the experiments was indeed chosen to test this hypothesis, which is as follows. If a model for a mixture of reactants is valid (in a mechanistic sense), then it should be equally valid for any sub-set of the mixture. Thus, if the model is able to predict the performance when CO, $C_3H_6$ and NO are all present, then it should equally be able to predict the result when, for example, only NO and $C_3H_6$ are present, or indeed, for CO alone. Although it was possible to build models that were able to predict any combination or permutation of the reactants with a reasonable if not perfect accuracy, these models did not all have a common set of parameters. This observation has ramifications for model development. Any new catalyst formulation requires a new set of kinetic model parameters, and to determine these values it is desirable to do as few experiments as possible. The preferred practice when building a kinetic model (or indeed, a multi-parameter model) is to conduct a set of experiments that will allow the determination of each parameter separately or, failing that, as few parameters as possible. The idea would be, in the context of the DOC model, to determine the parameters for CO, $C_3H_6$ and NO in separate sets of experiments, and then to determine the parameters that result from interactions. This approach will clearly not work

with the model selected. If we consider the experiments with CO and $C_3H_6$, it was seen that when the parameters obtained from the CO and $C_3H_6$ alone experiments were applied to the mixture, the results were not acceptable, and could not be made so by adjustment of the interaction parameter proposed by Voltz [1]. Furthermore, when the results obtained from modeling the mixture were used to predict the individual results, the fit was again not acceptable. However, when modeling all of the experiments together, a reasonable fit was obtained. This could point to the fact that three experiments are not sufficient to determine the parameters with sufficient uniqueness to allow the stepwise approach to model building.

If we then consider the other mixtures, especially the full set of reactants; we see that it was not possible to find a set of parameters that was able to predict the results of all of the experiments with reasonable accuracy. Ideally, this would be a good target to achieve, which would suggest that models with a different form than those considered here might give a better result.

In the remainder of this section, each set of simulations will be discussed to see what has been learned. Considering the experiments performed with CO alone, it was seen that if only one experimental ignition curve was optimized, then it was seen that it was very easy to obtain a very good fit using the Voltz [1] type model. This same behavior was observed with other reactants, and when the oxidation of NO was studied, it was not possible for a single ignition curve to discriminate among the different models tested. Thus at least three curves were used in each subsequent optimization study. For the CO and $C_3H_6$ oxidations, either single or in a combination, it was not possible to achieve an acceptable fit for the Voltz [1] model using the literature values, either in the numerator or the denominator of the rate expression. As mentioned earlier, some other workers have indicated that they have used the Voltz [1] values in their models, although in most cases it appears that only a couple of ignition curves are used, and for a complex mixture with many other parameters in the model. Overall, it is

suggested that when optimizing ignition curves, all parameters should be allowed to vary. When the CO and $C_3H_6$ ignition curves (3 experiments) were optimized, including the interaction parameter in the Voltz [1] model give an improvement in the residual value, but it is not deemed to be necessary to include it to get a reasonable fit. Overall, we can conclude that the Voltz [1] model is an acceptable choice for the oxidation of CO and $C_3H_6$ mixtures, provided that all parameters are allowed to adjust. The results obtained on mixtures should not be extrapolated to experiments where a single reaction is used. The Voltz [1] model should not be considered to represent the reaction mechanism, but rather viewed as an empirical model.

Turning to the NO oxidation, the common literature models were tested for their ability to fit the data. The models proposed by Bhatia [4] (both in standard and modified form) and by Hauff [5] gave the best fit for the data, especially at low NO concentrations. This observation disagrees with those of Hauptmann et al. [24], who had previously compared common literature models for this reaction. When $C_3H_6$ was added to the reactor along with NO, several interesting features were observed. The first is that $C_3H_6$ inhibits the oxidation of NO, and vice versa. This observation was expected, because it had been seen before by Pandya [2], but interestingly was not included by Hauff et al. [5] in their model. The major new observation was the relatively large amount of $N_2O$ produced. Although the production of $N_2O$ has been reported by many researchers, especially over three way catalysts, there do not appear to have been any efforts to model its production. For this work, it was assumed that the $N_2O$ is a partial reduction product formed by the reaction between NO and $C_3H_6$ (or partial oxidation products of same). In this work, the formation of $N_2O$ was modelled using the same general method as that followed for the reduction reaction between NO and $C_3H_6$, which was the approach used by Pandya [2], who in turn based his work on the ideas proposed by Ansell et al. [26]) This method seems to work reasonably well, although at low NO concentrations the discrepancy

between experiment and model is the largest. The remaining observation was that when the reduction reaction between $NO_2$ and $C_3H_6$ was included (albeit in a simplistic way) the overall fit was improved. The reaction between $NO_2$ and $C_3H_6$ is expected to be fast, so the approach used here was felt to be reasonable.

For modelling the complete mixture, only the best models that worked for the other components were considered. Even though the parameter values for the models of mixtures did not necessarily work for the individual reactants, or pairs of them, it was felt that it was best to use at least the best form of the model. As discussed earlier, the proposed model for the DOC seems to work reasonable well for the mixtures, with the most difficult curve to fit being the $N_2O$ formation. Overall, it was concluded that the best fit was obtained with a modified version of the model proposed by Hauff et al [5].

As an overall observation of all the models and the optimization work, it can be concluded that the global model approach can work when applied to a relatively large data set. Clearly the model as proposed does not include all of the interactions present in the complete mixture. If it is desired to have a single model capable of fitting both mixtures and single or dual component experiments, some modifications to the model proposed here will have to be made.

# 5 Conclusions and Recommendations

In this work, an optimization study was performed to discriminate among various global kinetic models for the diesel oxidation catalyst, using the Voltz [1] type and other literature models as the starting point. The main conclusions can be summarized as follows:

(1) The original Voltz [1] model as proposed for CO and $C_3H_6$ oxidation is able to model the ignition curves for these mixtures fairly well. The interaction parameter that they used to fit higher concentrations of reactants gives a better fit, but is not considered essential. The presence or absence of the additional temperature in the denominator does not make any noticeable difference in the ability of the model to predict the results. If it is desired that the model is able to fit results for CO and $C_3H_6$ individually and together, then it is necessary to all of the experimental data when determining the coefficients. Finally, all of the parameters in the model must be allowed to adjust to obtain an acceptable result.

(2) The oxidation of NO alone was found to be best correlated using models proposed by Bhatia et al. [4] and Hauff et al. [5]. When $C_3H_6$ was included with the NO, it was observed that considerable amounts of $N_2O$ were formed. Modelling the formation of $N_2O$ in a manner similar to that used for the reduction of NO to $N_2$ (as originally proposed by Ansell et al. [26]) is reasonable, although some modifications to the model might offer the opportunity for improvement.

(3) Modelling the complete mixture representing the diesel oxidation catalyst can be achieved to a reasonable level of accuracy using a global Voltz [1] type model, although some improvements might lead to a better fit. The primary area of improvement is the formation of the $N_2O$. The proposed model for the DOC is not able to fit acceptable well the

experiments for the complete mixture as well as the single and double reactant experiments. An improved model would need to be developed if this is the desired goal.

Considering some recommendations for future work, a number of items might be interesting for further study. In point form, these are:

(1) Try to improve the overall model by considering some additional interaction parameters. This should be done with care, since the addition of parameters adds considerably to the complexity of the problems, and also to the time required to achieve a solution. Particular attention should be paid to the formation of $N_2O$.
(2) In future studies, it is recommended that experiments be performed with the sub-mixture of CO and NO, especially if a general model (capable of predicting both mixture and single component conversions) is desired.
(3) More variability should be included for the $C_3H_6$ and NO concentrations, particularly for the full mixture experiments.
(4) The form of the model, and any subsequent variations to it, should be tested on other catalysts, possibly with bi-metallic catalysts of Pt and Pd, so ascertain its generality.
(5) The model should be tested on real engine exhaust data. Although data were collected during the course of this work, the model was not tested against them. The data are given in the Appendix.

# 6 References

[1] S.E. Voltz, C.R. Morgan, Liederma.D, S.M. Jacob, Kinetic study of carbon-monoxide and propylene oxidation on platinum catalyst, Industrial & Engineering Chemistry Product Research and Development, 12 (1973) 294-301.
[2] A. Pandya, J. Mmbaga, R.E. Hayes, W. Hauptmann, M. Votsmeier, Global Kinetic Model and Parameter Optimization for a Diesel Oxidation Catalyst, Topics in Catalysis, 52 (2009) 1929-1933.
[3] S.S. Mulla, N. Chen, W.N. Delgass, W.S. Epling, F.H. Ribeiro, NO2 inhibits the catalytic reaction of NO and O-2 over Pt, Catalysis Letters, 100 (2005) 267-270.
[4] D. Bhatia, R.W. McCabe, M.P. Harold, V. Balakotaiah, Experimental and kinetic study of NO oxidation on model Pt catalysts, Journal of Catalysis, 266 (2009) 106-119.
[5] K. Hauff, U. Tuttlies, G. Eigenberger, U. Nieken, A global description of DOC kinetics for catalysts with different platinum loadings and aging status, Applied Catalysis B-Environmental, 100 (2010) 10-18.
[6] HealthCanada, Health effects of air pollution, in, 2006.
[7] R.S. Carel, Chapter 3: Health Aspects of Air Pollution, in: E. Sher (Ed.) Handbook of Air Pollution from Internal Combustion Engines: Pollutant Formation and Control, 1998.
[8] W. Epling, I. Nova, J. Szanyi, A. Yezerets, Diesel emissions control catalysis, Catalysis Today, 151 (2010) 201-201.
[9] S.S. Mulla, N. Chen, L. Cumaranatunge, G.E. Blau, D.Y. Zemlyanov, W.N. Delgass, W.S. Epling, F.H. Ribeiro, Reaction of NO and O-2 to NO2 on Pt: Kinetics and catalyst deactivation, Journal of Catalysis, 241 (2006) 389-399.
[10] J. Perez-Ramirez, F. Kapteijn, K. Schoffel, J.A. Moulijn, Formation and control of N2O in nitric acid production - Where do we stand today?, Applied Catalysis B-Environmental, 44 (2003) 117-151.
[11] J.B. Heywood, Chapter 1: Motor Vehicle Emissions Control: Past Achievements, Future Prospects, in: E. Sher (Ed.) Handbook of Air Pollution from Internal Combustion Engines: Pollutant Formation and Control, 1998.
[12] R.M. Heck, R.J. Farrauto, S.T. Gulati, Catalytic Air Pollution Control: Commercial Technology, 3erd edition ed., 2009.
[13] DieselNet, Emissions Standards: Canada: On-Road Vehicles, in, 2007.
[14] W.A. Majewski, M.K. Khair, Diesel Emissions and Their Control, SAE International, Warrendale, PA, 2006.
[15] E. Sher, Chapter 2: Environmental Aspects of Air Pollution, in: E. Sher (Ed.) Handbook of Air Pollution from Internal Combustion Engines: Pollutant Formation and Control, 1998.
[16] S. Hochgreb, Chapter 6: Combustion-Related Emissions in SI Engines, in: E. Sher (Ed.) Handbook of Air Pollution from Internal Combustion Engines: Pollutant Formation and Control, 1998.

[17] G. Hawley, Chapter 10: Combustion-Related Emissions in CI Engines, in: E. Sher (Ed.) Handbook of Air Pollution from Internal Combustion Engines: Pollutant Formation and Control, 1998.
[18] S. Henningsen, Chapter 14: Air Pollution fron Large Two-Stroke Diesel Engines and Technologics to Control It, in: E. Sher (Ed.) Handbook of Air Pollution from Internal Combustion Engines: Pollutant Formation and Control, 1998.
[19] A. Rusell, W.S. Epling, Diesel Oxidation Catalyst, in, Submitted to Catalysis Review, 2011.
[20] S. Salomons, R.E. Hayes, M. Votsmeier, A. Drochner, H. Vogel, S. Malmberg, J. Gieshoff, On the use of mechanistic CO oxidation models with a platinum monolith catalyst, Applied Catalysis B-Environmental, 70 (2007) 305-313.
[21] S.H. Oh, J.C. Cavendish, L.L. Hegedus, Mathematical-modeling of catalytic-converter lightoff - single-pellet studies, Aiche Journal, 26 (1980) 935-943.
[22] S.H. Oh, J.C. Cavendish, Transients of monolithic catalytic-converters - Response to step changes in feedstream temperature as related to controlling automobile emissions, Industrial & Engineering Chemistry Product Research and Development, 21 (1982) 29-37.
[23] S.H. Oh, J.C. Cavendish, Mathematical-modeling of catalytic-converter lightoff .3. prediction of vehicle exhaust emissions and parametric analysis, Aiche Journal, 31 (1985) 943-949.
[24] W. Hauptmann, A. Drochner, H. Vogel, M. Votsmeier, J. Gieshoff, Global kinetic models for the oxidation of NO on platinum under lean conditions, Topics in Catalysis, 42-43 (2007) 157-160.
[25] C.S. Sampara, E.J. Bissett, M. Chmielewski, D. Assanis, Global kinetics for platinum diesel oxidation catalysts, Industrial & Engineering Chemistry Research, 46 (2007) 7993-8003.
[26] G.P. Ansell, P.S. Bennett, J.P. Cox, J.C. Frost, P.G. Gray, A.M. Jones, R.R. Rajaram, A.P. Walker, M. Litorell, G. Smedler, The development of a model capable of predicting diesel lean NOx catalyst performance under transient conditions, Applied Catalysis B-Environmental, 10 (1996) 183-201.

# Appendix

## Testing a catalytic converter at the University of Alberta

It was intended to test the model developed using the synthetic gas mixtures with some exhaust gas data generated from a real engine. For this purpose, measurements were taken at the Mechanical Engineering Department in the University Of Alberta, under the supervision of Dr. David Checkel and with the assistance of graduate students Jason Boddez and Dallin Bullock.

The catalyst used was a 400 CPSI (channels per square inch), 2" diameter, 8 cm length, which gave approximately 9.9 cubic inch space volume. The target Gas Hourly Space Velocity (GHSV) was initially set to be around 40,000 $h^{-1}$ although the actual value depended on the engine operating conditions. The catalyst block was cut from the same unit as the test cores used at the University of Waterloo. Twenty six thermocouples were used to measure the axial and radial temperature profiles in the catalyst, as illustrated in Figure A1 and Table A1. The converter was installed on the single cylinder research engine.

Preliminary investigations were carried out on the engine to test the effect of the compression ratio (CR), the coefficient of variance of the indicated mean effective pressure (COV_IMEP), the pulse width (PW), the spark timing at a determined crank angle Before Top Dead Center (BTDC) and the ratio between the mass of air and the mass of fuel (Lambda).Lambda, which determines whether the engine is working in a lean (value larger than 1), stoichiometric (1) or rich (value smaller than 1) environments, was varied and tested to the limits, to observe the range of difference between the quantity for each gas produced.
During the process, it was determined that the engine would not be able to handle diesel fuel. Therefore, in order to get results a little closer to diesel exhaust, it was concluded that at least a liquid fuel would have to be used for future the tests.

Initially, problems with air in the pump generated pressure fluctuations that cause inconsistency on the results. After being repaired, good temperature curves were obtained, but the temperature was not sufficiently high to initiate conversion. Furthermore, there was deemed to be insufficient oxygen in the exhaust because of the lambda setting. To solve this problem, the solution was to insulate the lines in order to increase the temperature in 20-30 degree Celsius and to add up to a 10% of oxygen, which is still within the model range.

To improve the procedure, it was also decided to pre-heat the system previous to start the actual tests. The pre-heating process was carried using natural gas. The results of these changes showed that small conversions were obtained and some productions of $CO_2$. The temperature of the thermocouples that showed the lowest and the highest temperature values, at the peak of the

process, averaged 622K, which should be within the right range. But still the conversions were not satisfactory.

Following the less than satisfactory results obtained up to this point, a Homogeneous Charge Compression Ignition (HCCI) operating mode was set. The HCCI combustion system seemed to be a feasible solution since it runs at a similar efficiency to the diesel engine, and it is characterized by low emissions of NOx and PM but high production of CO and HC. [1]

**Table A1: Thermocouple distribution**

| Thermocouple | Axial Location |
|---|---|
| 1 | 20 mm |
| 2 | 20 mm |
| 3 | 20 mm |
| 4 | 20 mm |
| 5 | 20 mm |
| 6 | 20 mm |
| 7 | 20 mm |
| 8 | 20 mm |
| 9 | 20 mm |
| 10 | 10 mm |
| 11 | 60 mm |
| 12 | 60 mm |
| 13 | 60 mm |
| 14 | 60 mm |
| 15 | 60 mm |
| 16 | 60 mm |
| 17 | 60 mm |
| 18 | 60 mm |
| 19 | 60 mm |
| 20 | 30 mm |
| 21 | 40 mm |
| 22 | 50 mm |
| 23 | 70 mm |
| 24 | 75 mm |
| 25 | upstream |
| 26 | downstream |

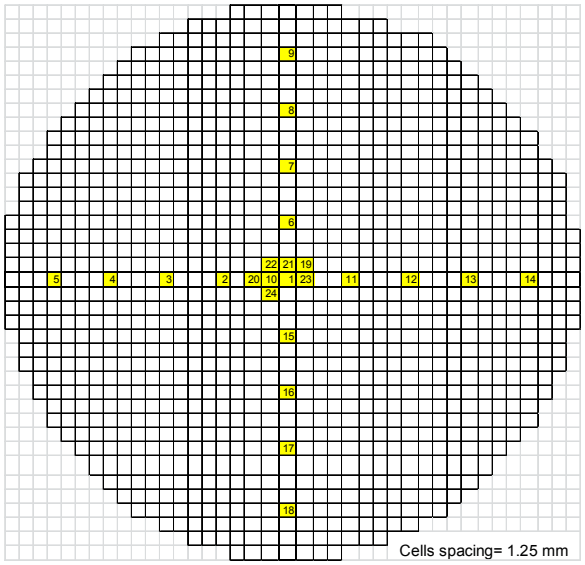


**Figure A1: Thermocouples distribution**

The tests done with the HCCI mode are described in the following. (cycles are taken every 0.3 seconds) :

Date: 2010_06_02
Operating Mode: HCCI with n-heptane port injected
Purpose: Initial numbers for catalyst testing using n-heptane. Run with EGR of 0%, except in operation points 13 and 14, where EGR ~ 2%.
Comments: *All the graphs show HC related to the ppm 'y' axis (right hand), and since **NOx** is so small **was** just **left** with **the % 'y' axis** (left hand) even though that number represent its ppm's (in the Emissions graphs).*

1. Motoring tests to adjust for n-heptane operation
2. Short hot motoring test at final CR.

3. Initial operating point. Table 2 specifies some of the operation conditions at this operation point. Figure 2 shows the emissions patterns, and table 3 the respective average of the concentrations. At this point NOx/NO sensor is measuring **NOx** emissions. These results were taken from **downstream** (after catalyst).

**Table A2: Average operation conditions at point number 3.**

| Air M.F. (g/s) | Liquid Fuel M.F. (mg/s) | Lambda | Compression Ratio | Liquid PI PW (ms) | Cat. Space Vol. Flow (exchanges/hr) |
|---|---|---|---|---|---|
| 4.5009 | 101.084734 | 2.94687 | 6.2287 | 8.3 | 78,844.5 |

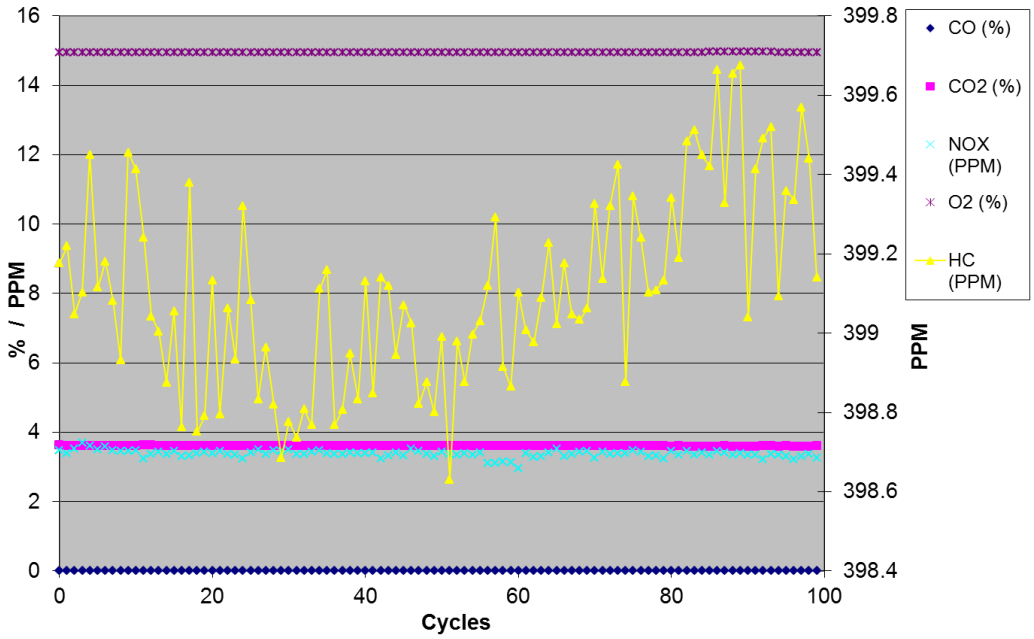


**Figure A2: Emissions at operation point number 3.**

**Table A3: Average concentrations shown at Figure A2.**

| CO (%) | CO2 (%) | HC (PPM) | NOX (PPM) | O2 (%) |
|---|---|---|---|---|
| 0.01063 | 3.6052 | 399.107 | 3.373859 | 14.9495 |

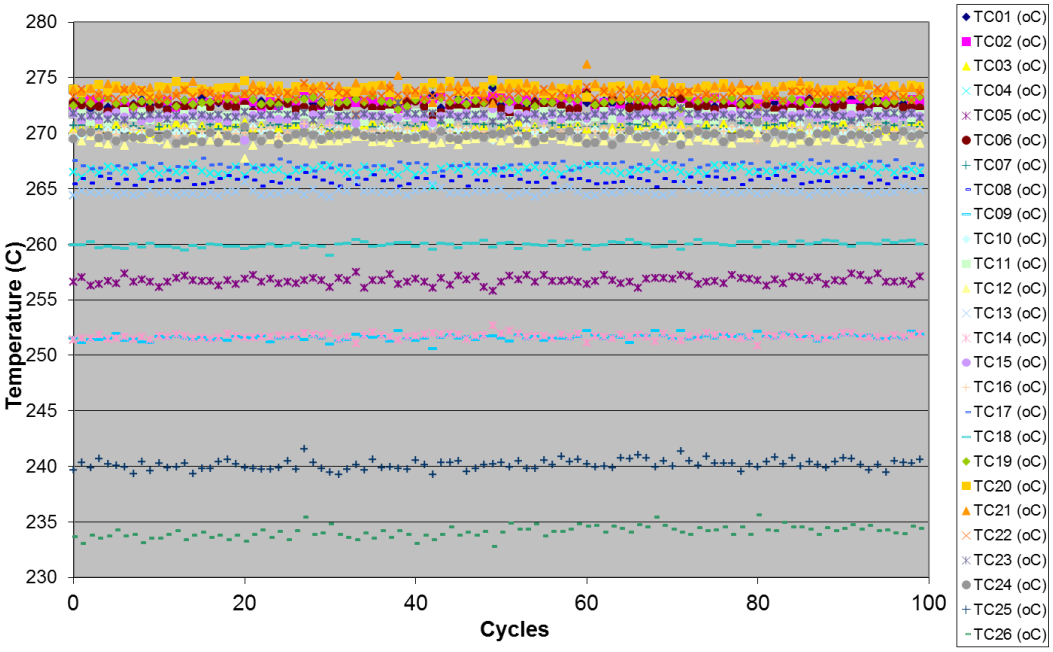


**Figure A3: Thermocouples temperature profile at operation point number 3.**

4. Same as 3, but upstream. Table A4 specifies some of the operation conditions at this operation point. Figure A4 shows the emissions patterns, and Table A5 the respective average of the concentrations. At this point NOx/NO sensor is measuring NOx emissions. These results were taken from **upstream** (before the catalyst).

**Table A4: Average operation conditions at point number 4.**

| Air M.F. (g/s) | Liquid Fuel M.F. (mg/s) | Lambda | Compression Ratio | Liquid PI PW (ms) | Cat. Space Vol. Flow (exchanges/hr) |
|---|---|---|---|---|---|
| 4.51656 | 102.6658 | 2.91508 | 6.228734 | 8.3 | 79,124.99 |

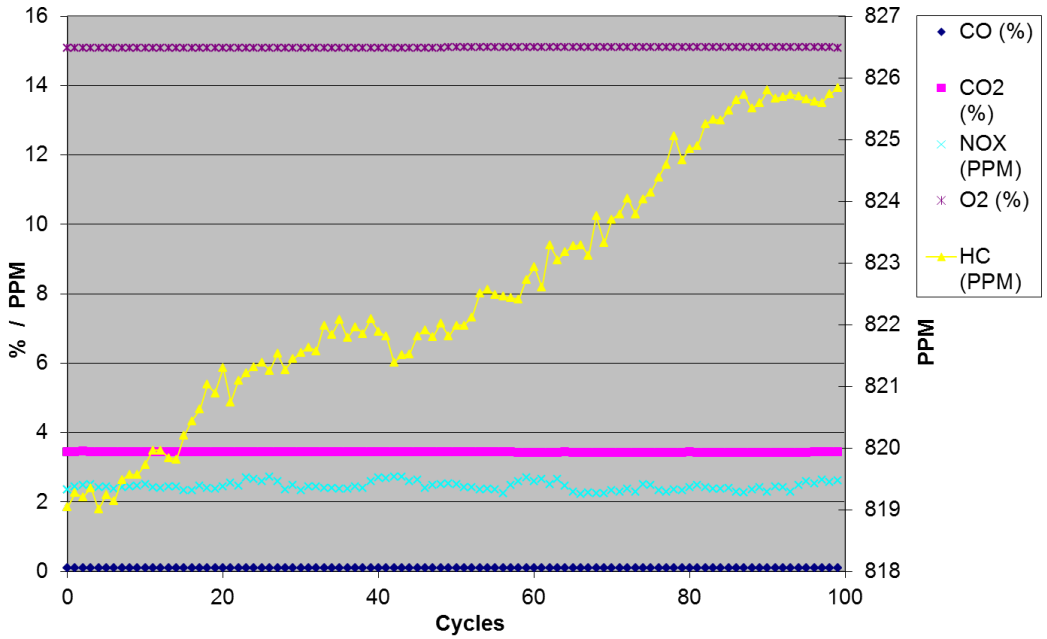


**Figure A4: Emissions at operation point number 4.**

**Table A5: Average concentrations shown at Figure A4.**

| CO (%) | CO2 (%) | HC (PPM) | NOX (PPM) | O2 (%) |
|---|---|---|---|---|
| 0.093356 | 3.429031 | 822.5188 | 2.449236 | 15.09252 |

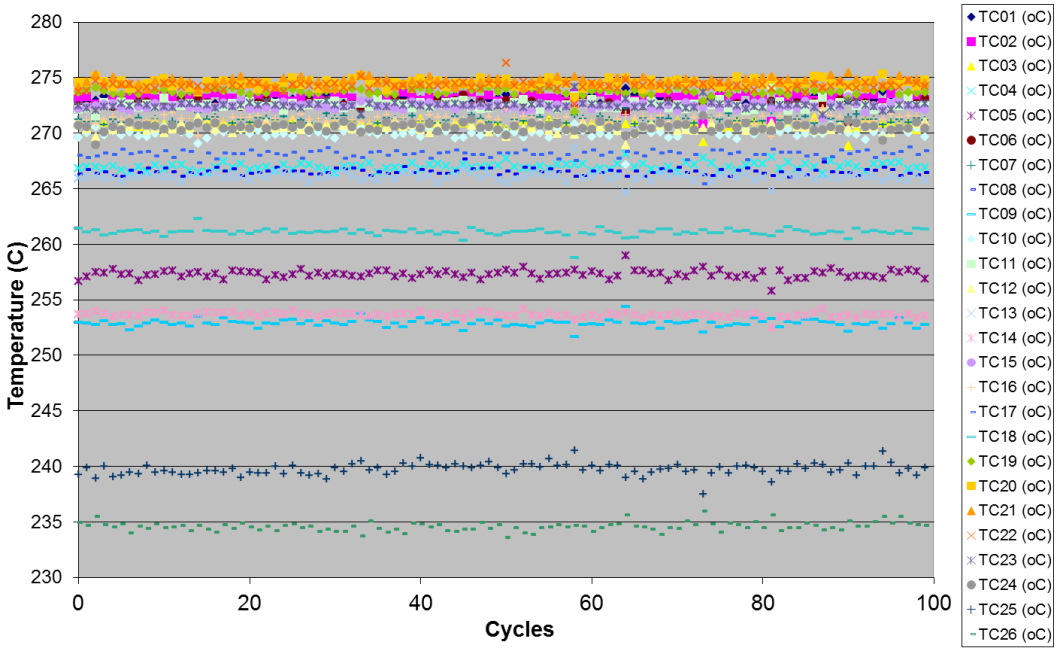


**Figure A5: Thermocouples temperature profile at operation point number 4.**

Discussion of tests 3-4: From **upstream** to **downstream**: **HC**, even though it isn't stable, it decreases almost a half. **NOx**, increases. **$CO_2$** increases but it is almost imperceptible. **$O_2$** and **CO**, you can barely notice that they decrease.

5. Leaner. Table A6 specifies some of the operation conditions at this operation point. Figure A6 shows the emissions patterns, and Table A7 the respective average of the concentrations. At this point NOx/NO sensor is measuring **NOx** emissions. These results were taken from **upstream** (before the catalyst).

**Table A6: Average operation conditions at point number 5.**

| Air M.F. (g/s) | Liquid Fuel M.F. (mg/s) | Lambda | Compression Ratio | Liquid PI PW (ms) | Cat. Space Vol. Flow (exchanges/hr) |
|---|---|---|---|---|---|
| 4.522823 | 96.1295 | 3.19102 | 6.228734 | 8 | 79,201.08 |

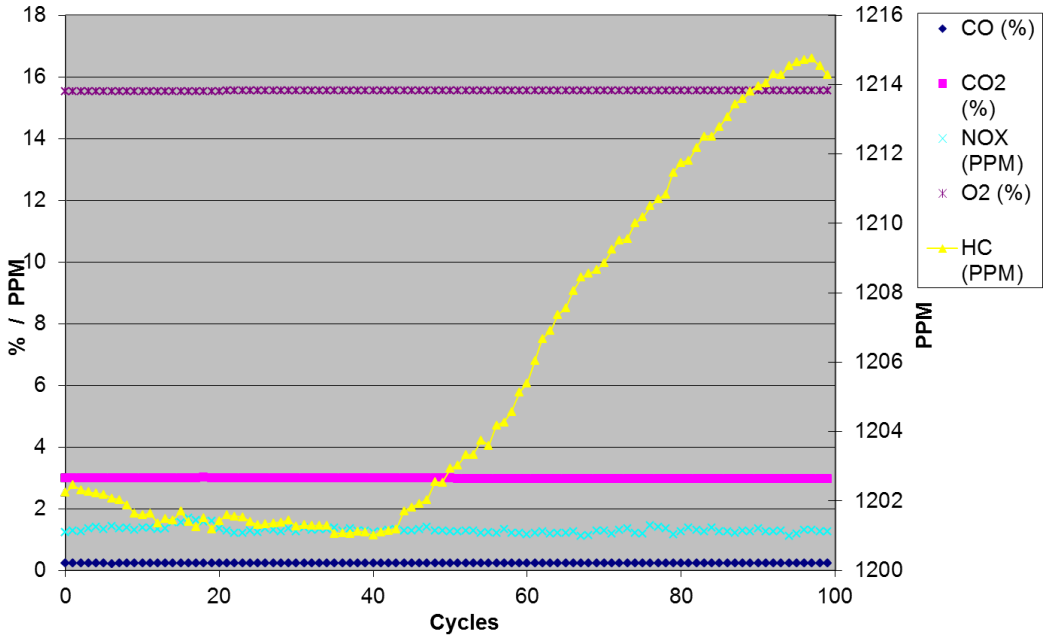


**Figure A6: Emissions at operation point number 5.**

**Table A7: Average concentrations shown at Figure A6.**

| CO (%) | CO2 (%) | HC (PPM) | NOX (PPM) | O2 (%) |
|---|---|---|---|---|
| 0.227211 | 2.980215 | 1205.63 | 1.302282 | 15.5493 |

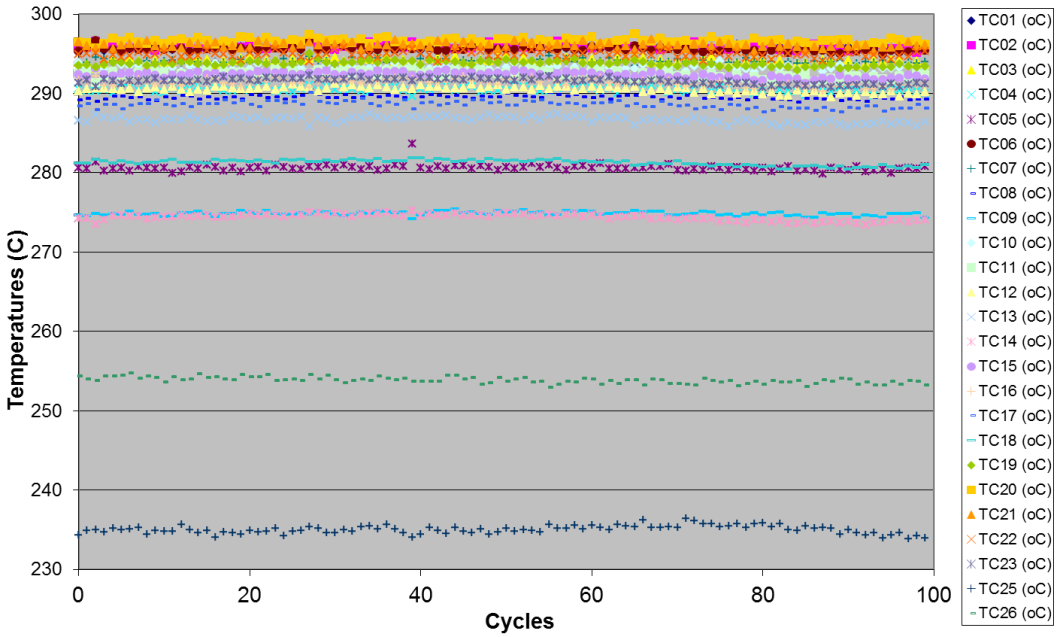


**Figure A7: Thermocouples temperature profile at operation point number 5.**

6. Table A8 specifies some of the operation conditions at this operation point. Figure A8 shows the emissions patterns and Table A9 the respective average of the concentrations. At this point NOx/NO sensor is measuring **NOx** emissions. These results were taken from **downstream** (after catalyst).

**Table A8: Average operation conditions at point number 6.**

| Air M.F. (g/s) | Liquid Fuel M.F. (mg/s) | Lambda | Compression Ratio | Liquid PI PW (ms) | Cat. Space Vol. Flow (exchanges/hr) |
|---|---|---|---|---|---|
| 4.500751 | 97.5155 | 3.039091 | 6.228734 | 8 | 78,823.91 |

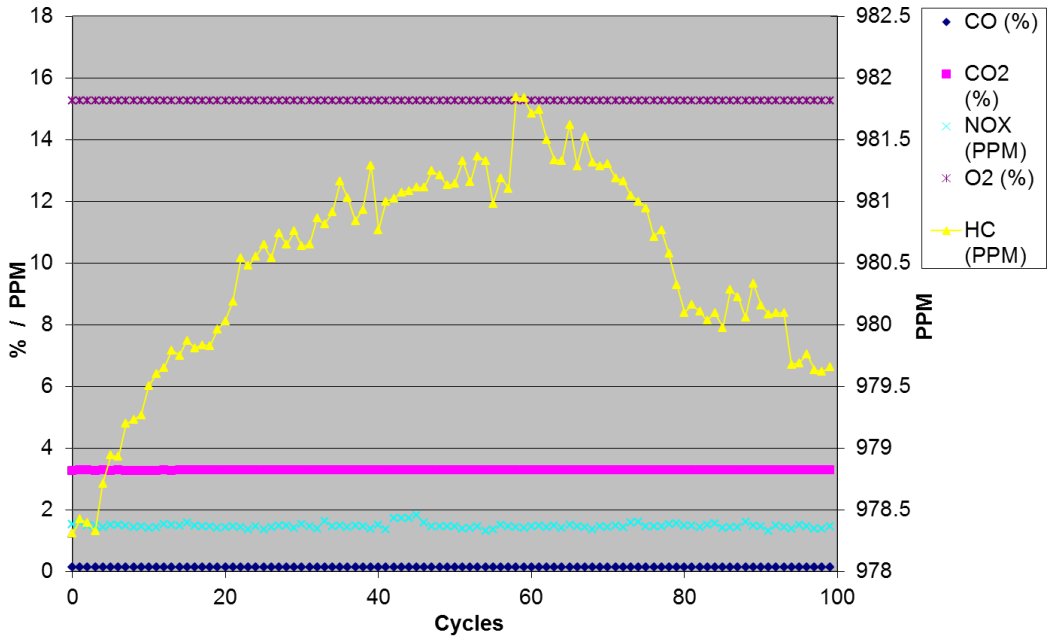


**Figure A8: Emissions at operation point number 6.**

**Table A9: Average concentrations shown at Figure A8.**

| CO (%) | CO2 (%) | HC (PPM) | NOX (PPM) | O2 (%) |
|---|---|---|---|---|
| 0.131264 | 3.279294 | 980.4704 | 1.467129 | 15.25485 |

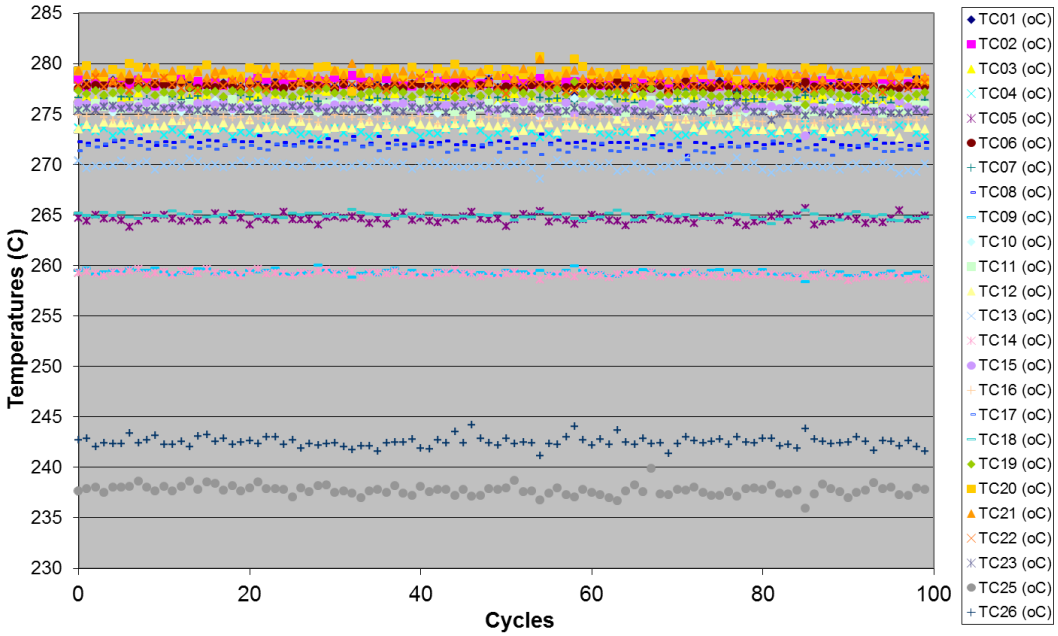


**Figure A9: Thermocouples temperature profile at operation point number 6.**

Discussion of tests 5-6: From **upstream** to **downstream**: **HC**, even though it is very unstable, you can see that decreases from 1210 to 980 ppm. **NOx**, seems to increase but it is almost imperceptible. **$CO_2$** increases a little bit. **$O_2$** and **CO**, you can barely notice it but they decrease.

7. Same as 6, but upstream. Table A10 specifies some of the operation conditions at this operation point. Figure A10 shows the emissions pattern, and Table A11 the respective average of the concentrations. At this point NOx/NO sensor is measuring **NOx** emissions. These results were taken from **upstream** (before the catalyst).

**Table A10: Average operation conditions at point number 7.**

| Air M.F. (g/s) | Liquid Fuel M.F. (mg/s) | Lambda | Compression Ratio | Liquid PI PW (ms) | Cat. Space Vol. Flow (exchanges/hr) |
|---|---|---|---|---|---|
| 4.503461 | 97.54924 | 3.039811 | 6.228734 | 8 | 78,871.25 |

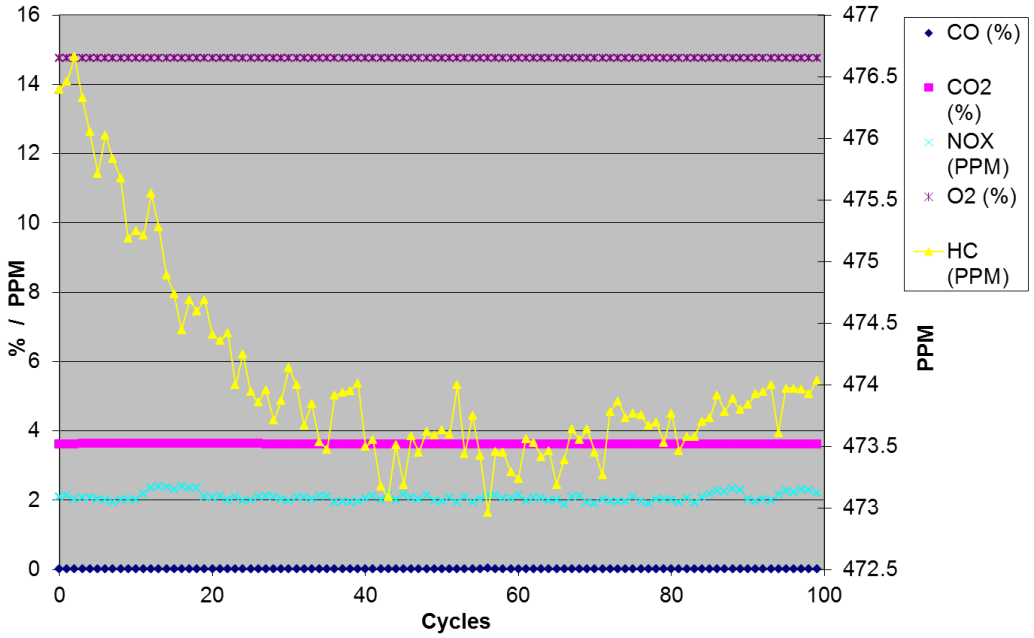


**Figure A10: Emissions at operation point number 7.**

**Table A11: Average concentrations shown at Figure A10.**

| CO (%) | CO2 (%) | HC (PPM) | NOX (PPM) | O2 (%) |
|---|---|---|---|---|
| 0.022299 | 3.618784 | 474.0554 | 2.080714 | 14.75661 |

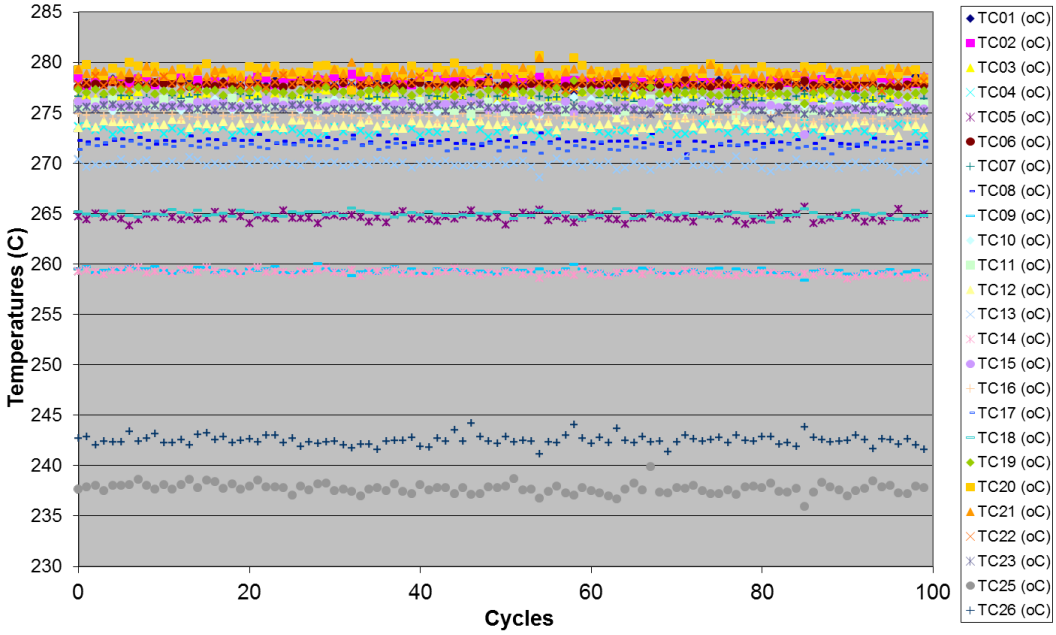


**Figure A11: Thermocouples temperature profile at operation point number 7.**

8. Table A12 specifies some of the operation conditions at this operation point. Figure A12 shows the emissions patterns and Table A13 the respective average of the concentrations. At this point NOx/NO sensor is measuring NOx emissions. These results were taken from upstream (before the catalyst).

**Table A12: Average operation conditions at point number 8.**

| Air M.F. (g/s) | Liquid Fuel M.F. (mg/s) | Lambda | Compression Ratio | Liquid PI PW (ms) | Cat. Space Vol. Flow (exchanges/hr) |
|---|---|---|---|---|---|
| 4.114797 | 99.62999 | 2.719577 | 6.228734 | 8 | 72,117.26 |

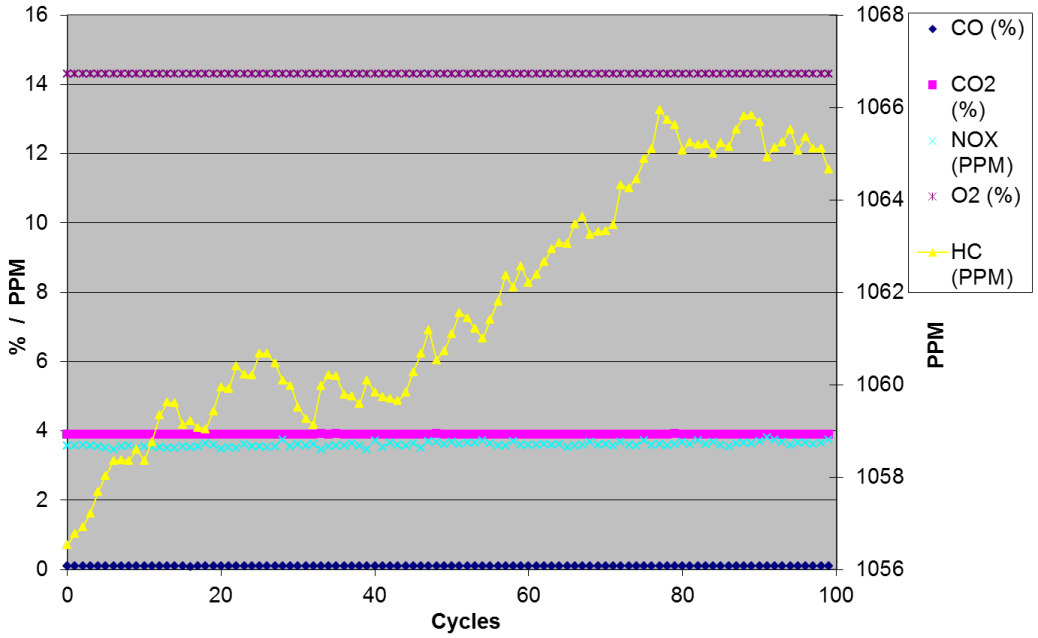


**Figure A12: Emissions at operation point number 8.**

**Table A13: Average concentrations shown at Figure A12.**

| CO (%) | CO2 (%) | HC (PPM) | NOX (PPM) | O2 (%) |
|---|---|---|---|---|
| 0.089272 | 3.895903 | 1,061.692 | 3.59672 | 14.29634 |

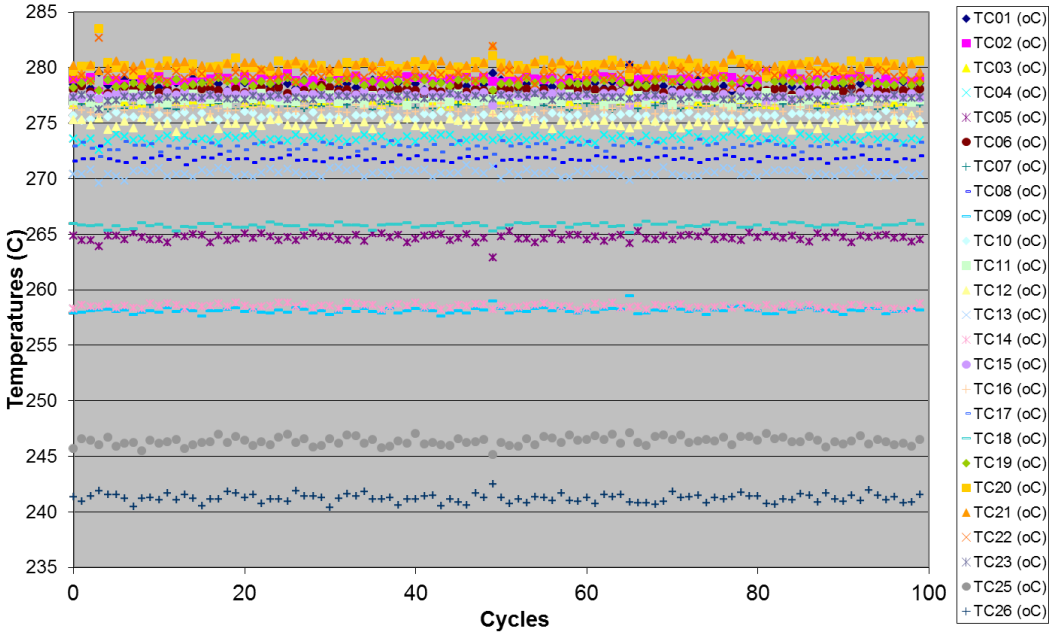


**Figure A13: Thermocouples temperature profile at operation point number 8.**

9. Same as 8, but downstream. Table A14 specifies some of the operation conditions at this operation point. Figure A14 shows the emissions patterns and Table A15 the respective average of the concentrations. At this point NOx/NO sensor is measuring **NOx** emissions. These results were taken from **downstream** (after catalyst).

**Table A14: Average operation conditions at point number 9.**

| Air M.F. (g/s) | Liquid Fuel M.F. (mg/s) | Lambda | Compression Ratio | Liquid PI PW (ms) | Cat. Space Vol. Flow (exchanges/hr) |
|---|---|---|---|---|---|
| 4.112486 | 99.46304 | 2.723068 | 6.228734 | 8 | 72,076.2 |

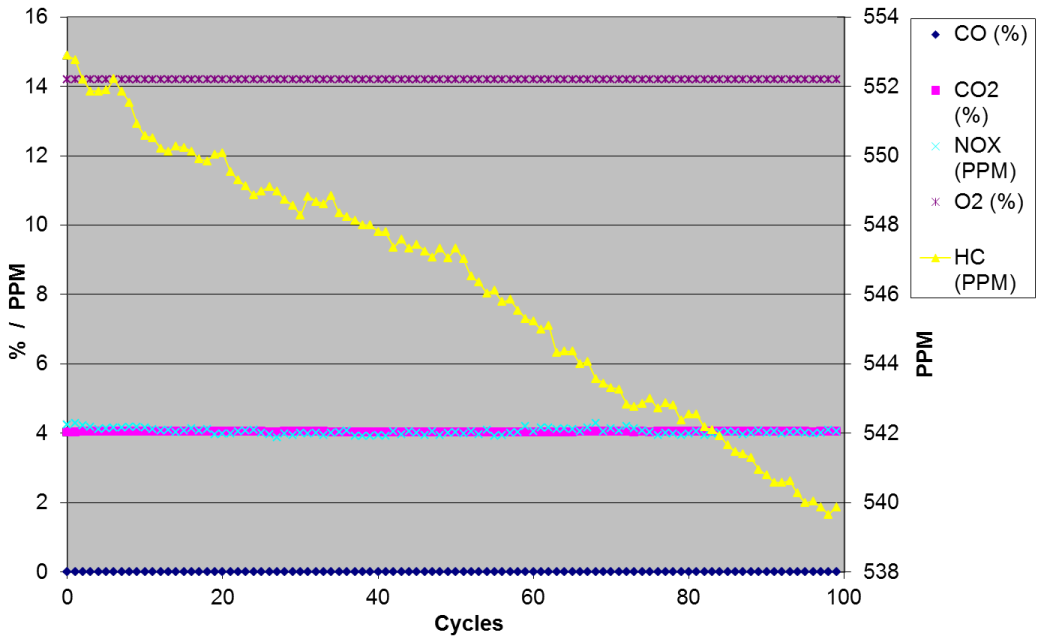


**Figure A14: Emissions at operation point number 8.**

**Table A15: Average concentrations shown at Figure A14.**

| CO (%) | CO2 (%) | HC (PPM) | NOX (PPM) | O2 (%) |
|---|---|---|---|---|
| 0.013624 | 4.039668 | 546.2544 | 4.047981 | 14.20363 |

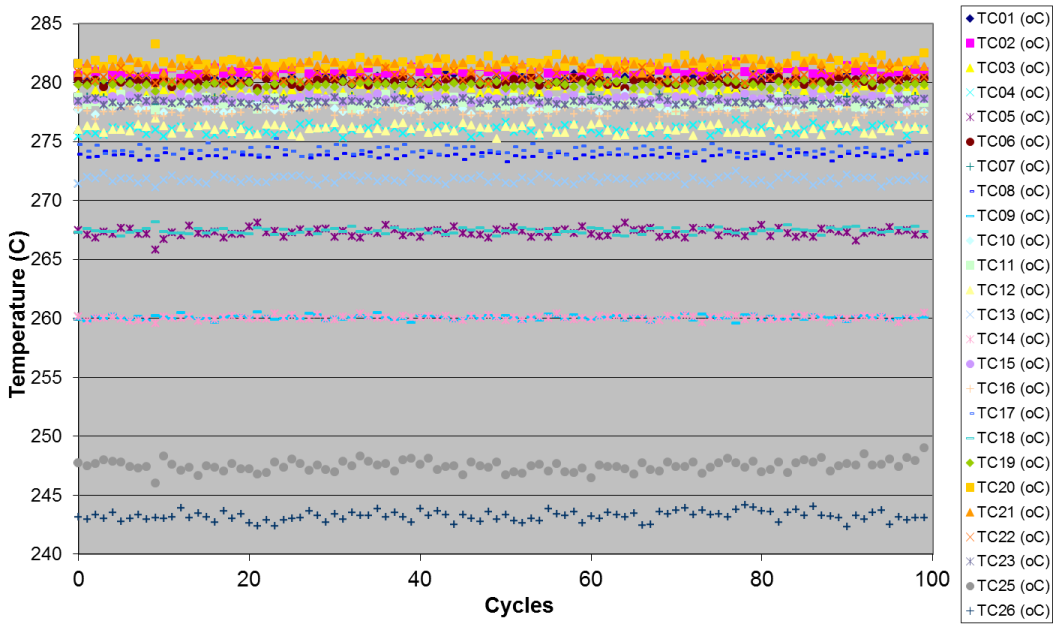


**Figure A15: Thermocouples temperature profile at operation point number 9.**

Discussion of tests 8-9: From **upstream** to **downstream**: **HC**, even though it is very unstable, you can see that decreases from 1060 to 548 ppm. **NOx**, increases. **$CO_2$** seems to be the same. **$O_2$** and **CO**, you can barely notice but they decrease.

10. Table A16 specifies some of the operation conditions at this operation point. Figure A16 shows the emissions patterns and Table A17 the respective average of the concentrations. At this point NOx/NO sensor is measuring **NOx** emissions. These results were taken from **downstream** (after catalyst).

**Table A16: Average operation conditions at point number 10.**

| Air M.F. (g/s) | Liquid Fuel M.F. (mg/s) | Lambda | Compression Ratio | Liquid PI PW (ms) | Cat. Space Vol. Flow (exchanges/hr) |
|---|---|---|---|---|---|
| 4.053208 | 113.1049 | 2.359578 | 6.228734 | 8.9 | 71,113.19 |

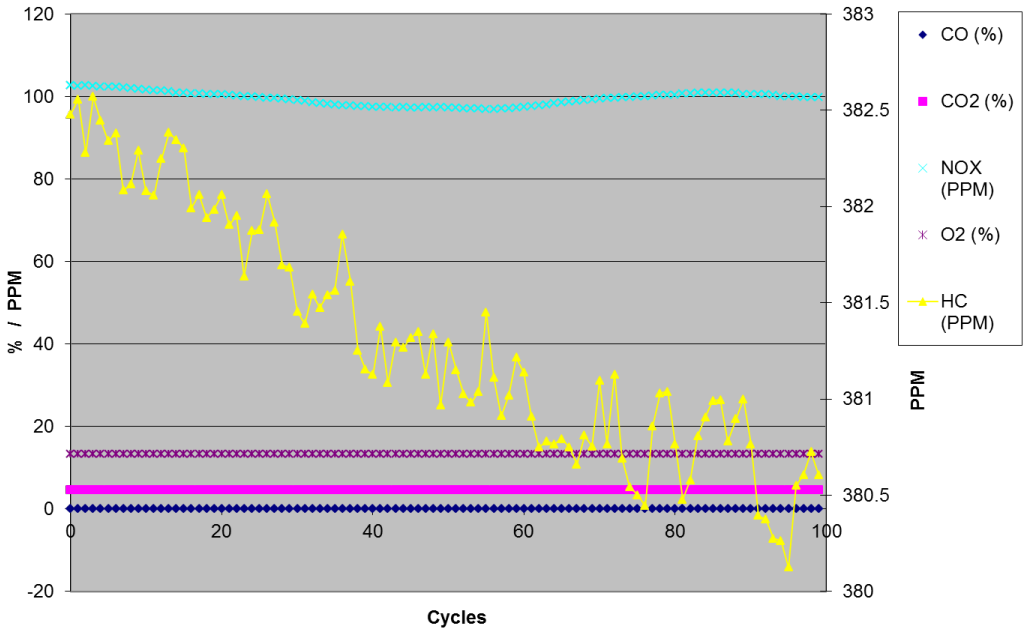


**Figure A16: Emissions at operation point number 10.**

**Table A17: Average concentrations shown at Figure A16.**

| CO (%) | CO2 (%) | HC (PPM) | NOX (PPM) | O2 (%) |
|---|---|---|---|---|
| 0.001024 | 4.685715 | 381.3098 | 99.49993 | 13.37042 |

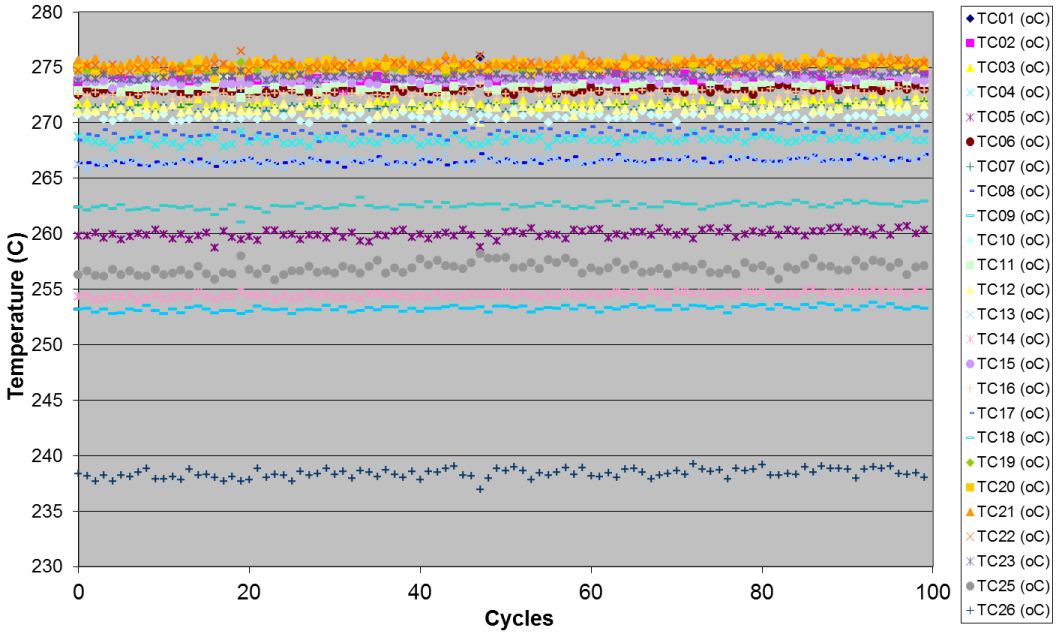


**Figure A17: Thermocouples temperature profile at operation point number 10.**

11. Same as 10, but upstream. Table A18 specifies some of the operation conditions at this operation point. Figure A18 shows the emissions patterns and Table A19 the respective average of the concentrations. At this point NOx/NO sensor is measuring **NOx** emissions. These results were taken from **upstream** (before the catalyst).

**Table A18: Average operation conditions at point number 11.**

| Air M.F. (g/s) | Liquid Fuel M.F. (mg/s) | Lambda | Compression Ratio | Liquid PI PW (ms) | Cat. Space Vol. Flow (exchanges/hr) |
|---|---|---|---|---|---|
| 4.055682 | 111.4619 | 2.396799 | 6.228734 | 8.9 | 71,147.98 |

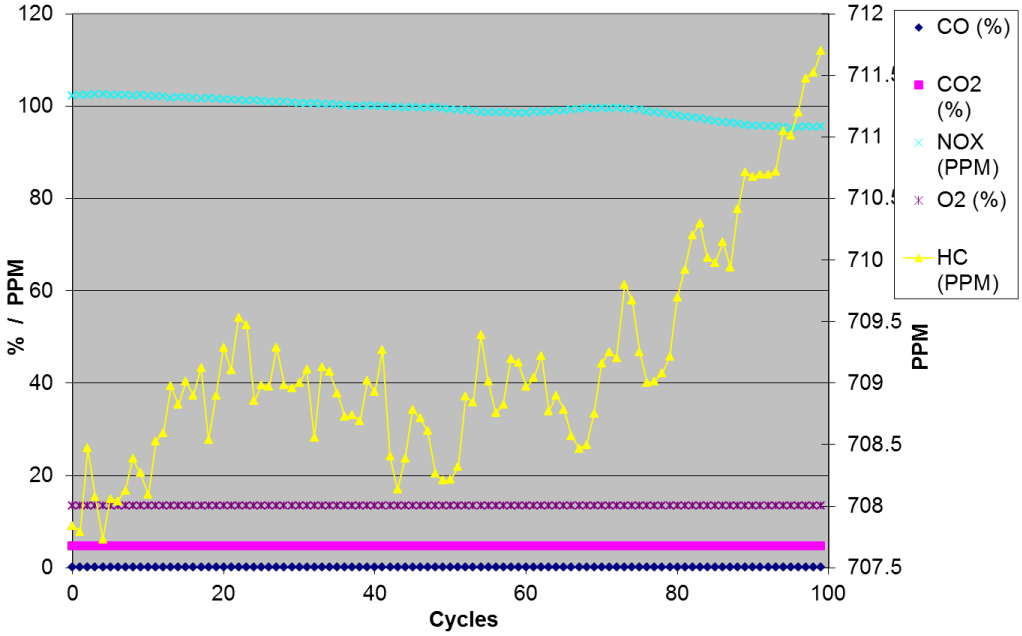


**Figure A18 : Emissions at operation point number 11.**

**Table A19: Average concentrations shown at Figure A18.**

| CO (%) | CO2 (%) | HC (PPM) | NOX (PPM) | O2 (%) |
|---|---|---|---|---|
| 0.031844 | 4.631391 | 709.1573 | 99.50456 | 13.39963 |

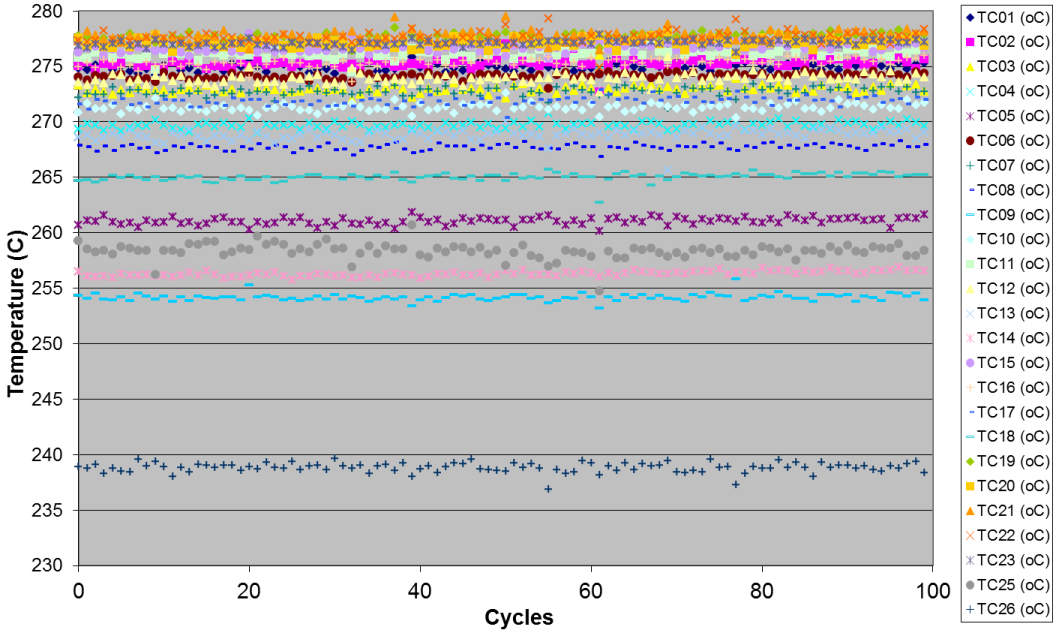


**Figure A19: Thermocouples temperature profile at operation point number 11.**

Discussion of tests 12-11: From **upstream** to **downstream**: **HC**, even though it is still very unstable, you can see that decreases from 710 to 381 ppm. **NOx**, is unstable but close to 100 ppm in both cases. **$CO_2$** is hard to see whether it changes or not. **$O_2$** and **CO** is hard to see if they change.

12. Table A20 specifies some of the operation conditions at this operation point. Figure A20 shows the emissions patterns and Table A21 the respective average of the concentrations. At this point NOx/NO sensor is measuring **NOx** emissions. These results were taken from **downstream** (after catalyst).

**Table A20: Average operation conditions at point number 12.**

| Air M.F. (g/s) | Liquid Fuel M.F. (mg/s) | Lambda | Compression Ratio | Liquid PI PW (ms) | Cat. Space Vol. Flow (exchanges/hr) |
|---|---|---|---|---|---|
| 2.858743 | 117.6387 | 1.601088 | 6.228734 | 9.3 | 50,347.08 |

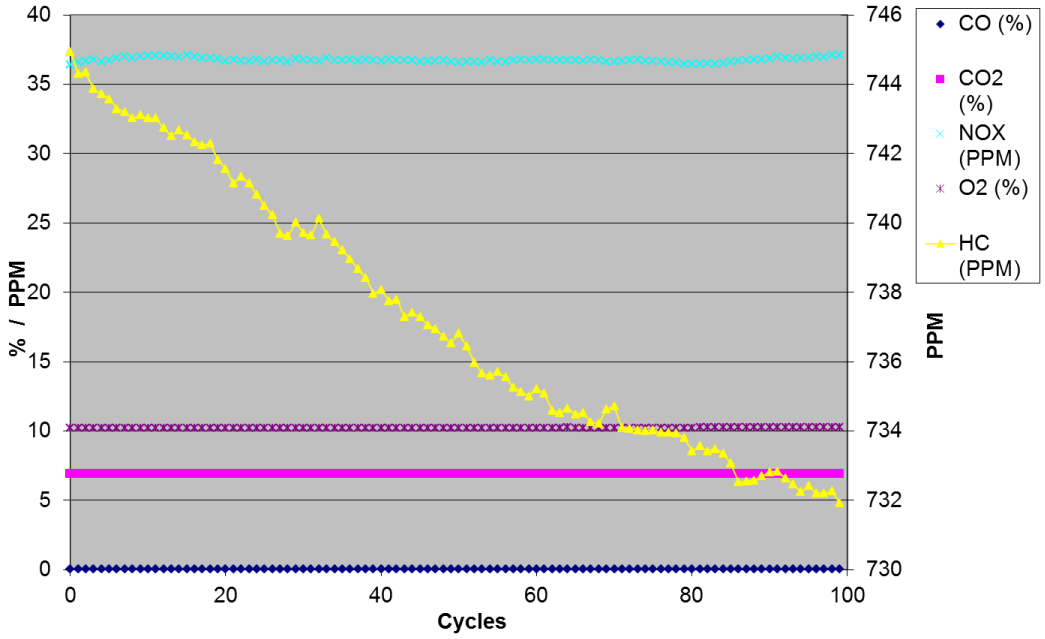


**Figure A20: Emissions at operation point number 12.**

**Table A21: Average concentrations shown at Figure A20.**

| CO (%) | CO2 (%) | HC (PPM) | NOX (PPM) | O2 (%) |
|---|---|---|---|---|
| 0.053099 | 6.919032 | 737.3169 | 36.75706 | 10.23644 |

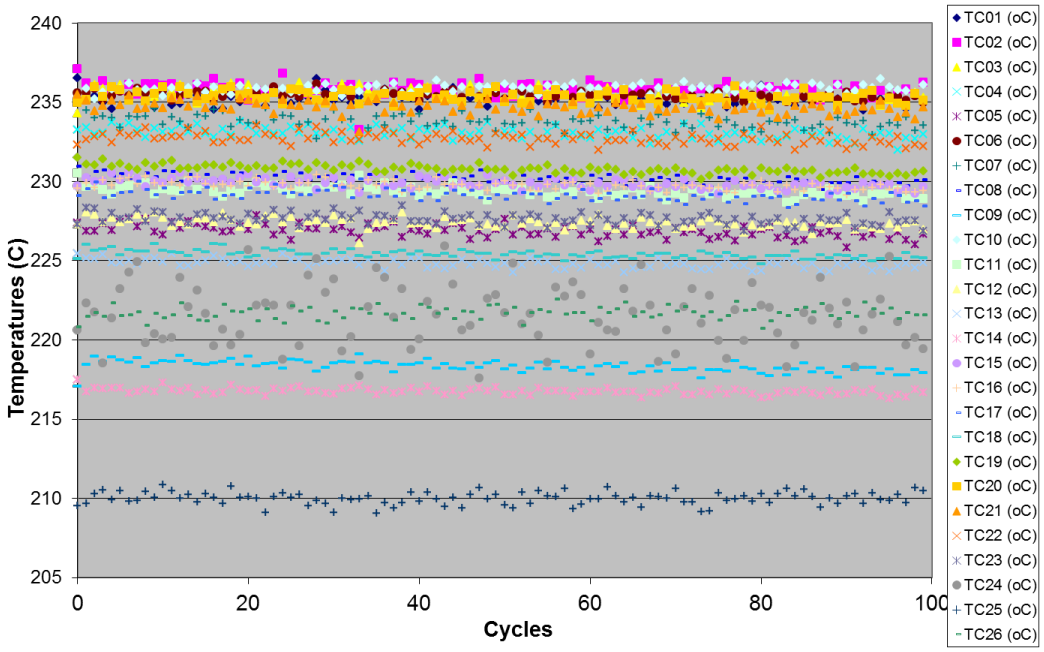


**Figure A21: Thermocouples temperature profile at operation point number 12.**

13. Table A22 specifies some of the operation conditions at this operation point. The EGR amount measured at ~2%. Figure A22 shows the emissions patterns and Table A23 the respective average of the concentrations. At this point NOx/NO sensor is measuring **NOx** emissions. These results were taken from **downstream** (after catalyst).

**Table A22: Average operation conditions at point number 13.**

| Air M.F. (g/s) | Liquid Fuel M.F. (mg/s) | Lambda | Compression Ratio | Liquid PI PW (ms) | Cat. Space Vol. Flow (exchanges/hr) |
|---|---|---|---|---|---|
| 2.703639 | 117.3941 | 1.516661 | 6.228734 | 9.3 | 47,646.35 |

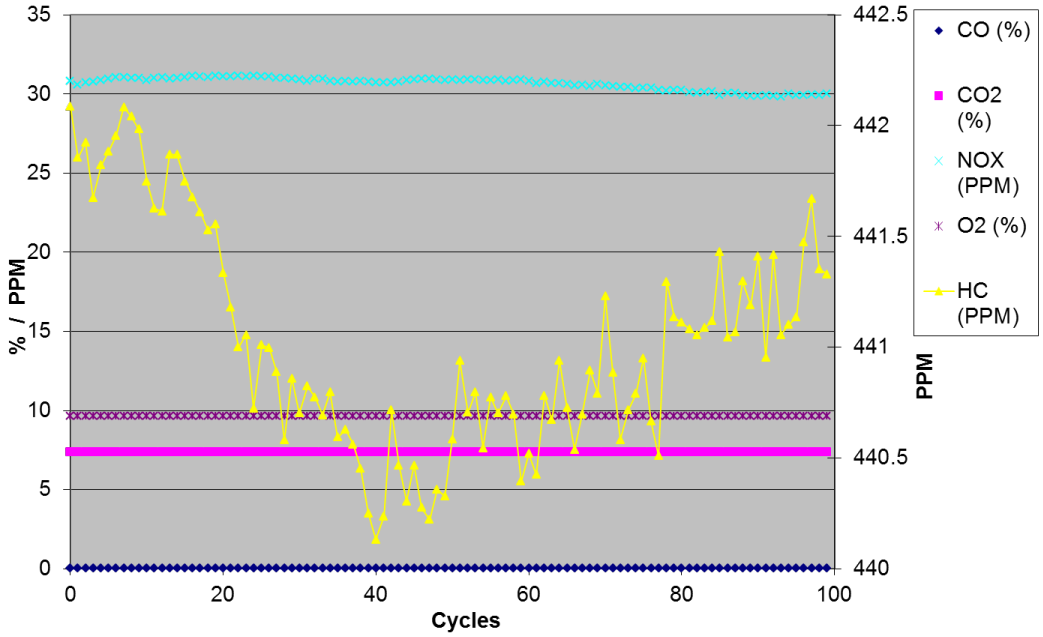


**Figure A22: Emissions at operation point number 13.**

**Table A23: Average concentrations shown at Figure A22.**

| CO (%) | CO2 (%) | HC (PPM) | NOX (PPM) | O2 (%) |
|---|---|---|---|---|
| 0.020009 | 7.36297 | 441.0259 | 30.65579 | 9.645207 |

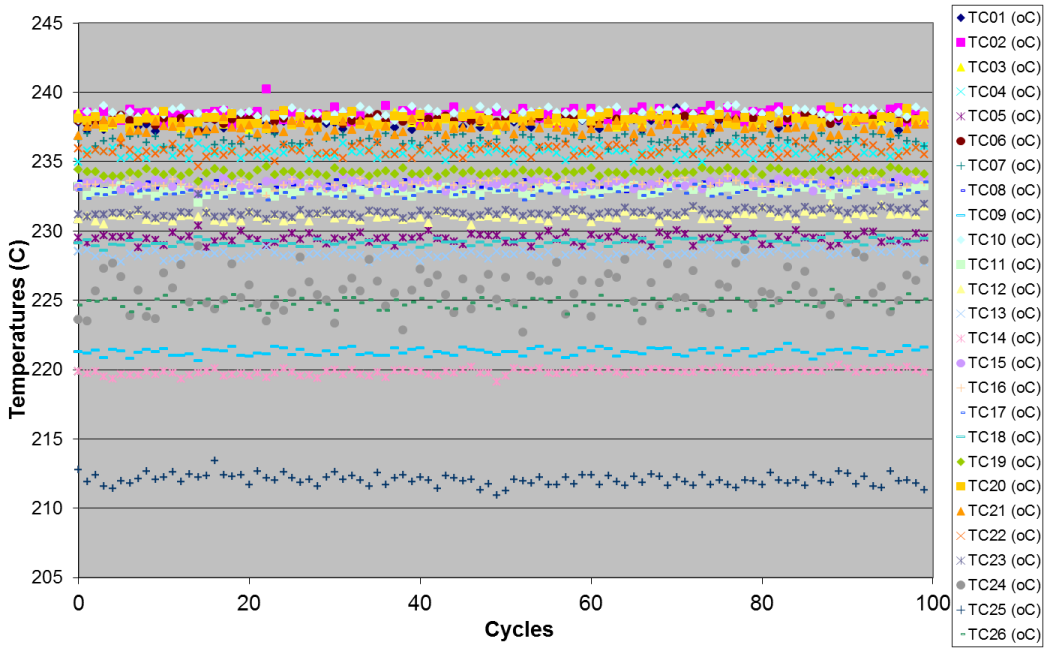


**Figure A23: Thermocouples temperature profile at operation point number 13.**

Discussion of tests 12-13: From **upstream** to **downstream**: **HC**, very unstable and decreases from about 738 to 441 ppm. **NOx**, decreases. **$CO_2$** increases a little bit. **$O_2$** presents a very small decrease and **CO** seems to be the same.

14. Same as 13, but upstream (EGR~2%). Table A24 specifies some of the operation conditions at this operation point. Figure A24 shows the emissions patterns and Table A25 the respective average of the concentrations. At this point NOx/NO sensor is measuring **NOx** emissions. These results were taken from **upstream** (before the catalyst).

**Table A24: Average operation conditions at point number 14.**

| Air M.F. (g/s) | Liquid Fuel M.F. (mg/s) | Lambda | Compression Ratio | Liquid PI PW (ms) | Cat. Space Vol. Flow (exchanges/hr) |
|---|---|---|---|---|---|
| 2.69816 | 118.4615 | 1.500805 | 6.228734 | 9.3 | 47,556.37 |

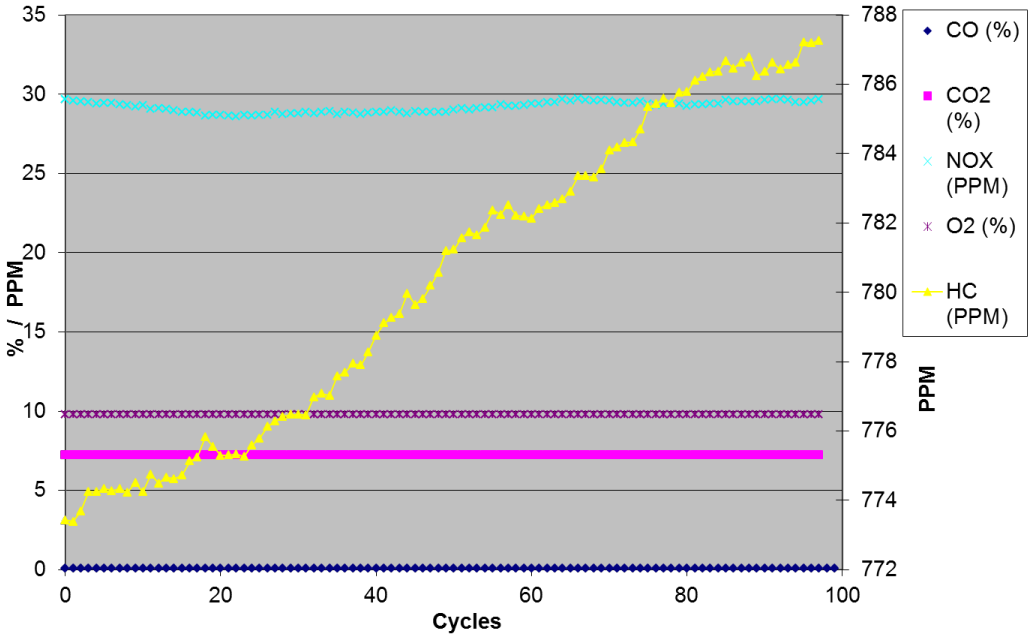


**Figure A24: Emissions at operation point number 14.**

**Table A25: Average concentrations shown at Figure 24.**

| CO (%) | CO2 (%) | HC (PPM) | NOX (PPM) | O2 (%) |
|---|---|---|---|---|
| 0.061505 | 7.226991 | 780.214 | 29.20351 | 9.78218 |

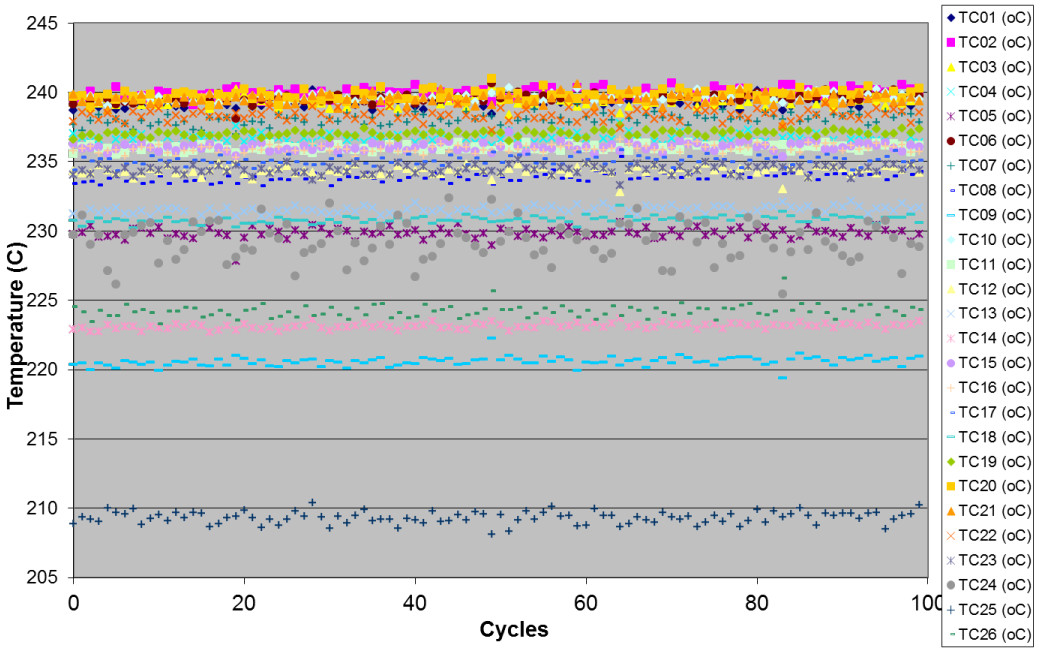


**Figure A25: Thermocouples temperature profile at operation point number 14.**

Note: There are some tests that were repeated, that's why it seems that there are upstream measurements that look like they do not have its corresponding downstream or vice versa.

**Date:** 2010-06-03
**Operating Mode:** HCCI with n-heptane port injected
**Purpose:** Catalyst testing. Run with EGR of 0%.
**Comments:** *Since HC and NOx are in ppm, their 'y' axis is the one at the right hand (unless specified different), and the % is the one at the left hand of the Emissions graphs.*

1. Hot motoring trace
2. Table A26 specifies some of the operation conditions at this operation point. Figure A26 shows the emissions patterns and Table A27 the respective average of the concentrations. At this point NOx/NO sensor is measuring **NOx** emissions. These results were taken from **upstream** (before the catalyst).

**Table A26: Average operation conditions at point number 2.**

| Air M.F. (g/s) | Liquid Fuel M.F. (mg/s) | Lambda | Compression Ratio | Liquid PI PW (ms) | Cat. Space Vol. Flow (exchanges/hr) |
|---|---|---|---|---|---|
| 3.961191 | 119.476 | 2.213919 | 6.14081 | 9.3 | 69,543.78 |

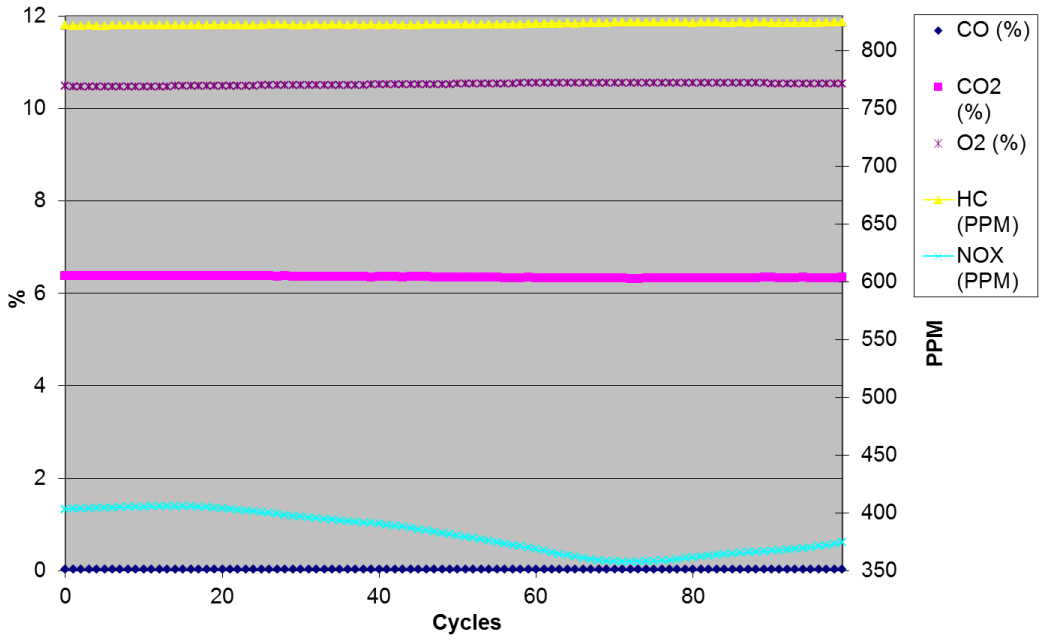


**Figure A26: Emissions at operation point number 2.**

**Table A27: Average concentrations shown at Figure A26.**

| CO (%) | CO2 (%) | HC (PPM) | NOX (PPM) | O2 (%) |
|---|---|---|---|---|
| 0.028358 | 6.350448 | 823.0027 | 382.1637 | 10.5189 |

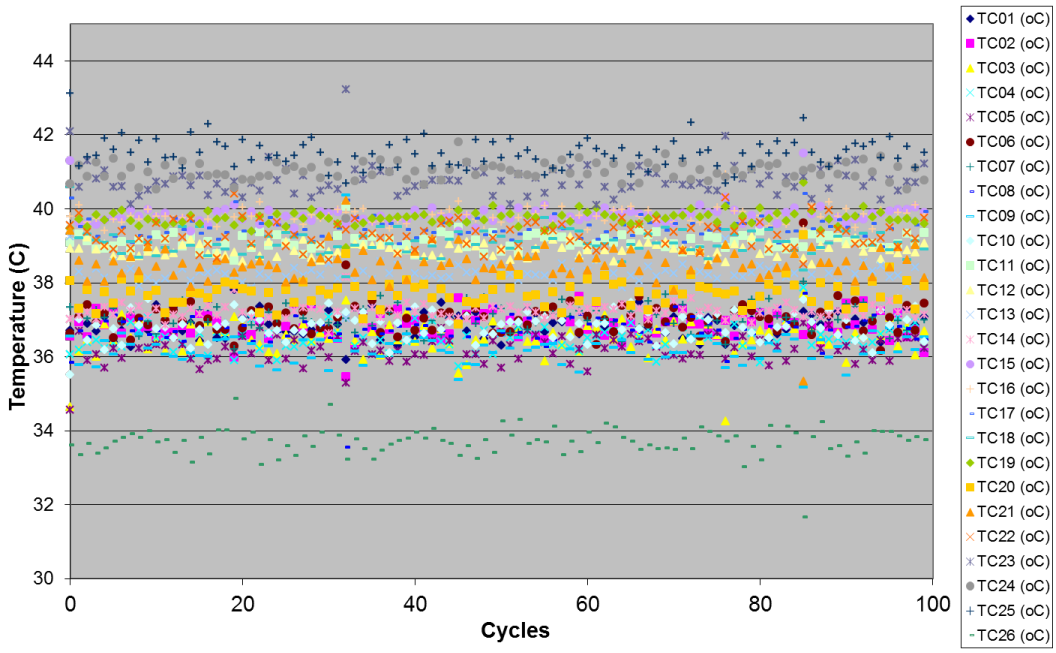


**Figure A27: Thermocouples temperature profile at operation point number 2.**

3. Transient test, switched from upstream to downstream catalyst emissions at approx. 100 cycles. Table A28 specifies some of the operation conditions at this operation point. Figure A28 shows the emissions patterns and Table A29 the respective average of the concentrations. At this point NOx/NO sensor is measuring **NOx** emissions.

**Table A28: Average operation conditions at point number 3.**

| | Air M.F. (g/s) | Liquid Fuel M.F. (mg/s) | Lambda | Compression Ratio | Liquid PI PW (ms) | Cat. Space Vol. Flow (exchanges/hr) |
|---|---|---|---|---|---|---|
| U | 3.977226 | 125.5501 | 2.147331 | 6.14081 | 9.3 | 69,853.44 |
| D | 4.017715 | 113.0589 | 2.444249 | 6.14081 | 9.3 | 70,495.24 |

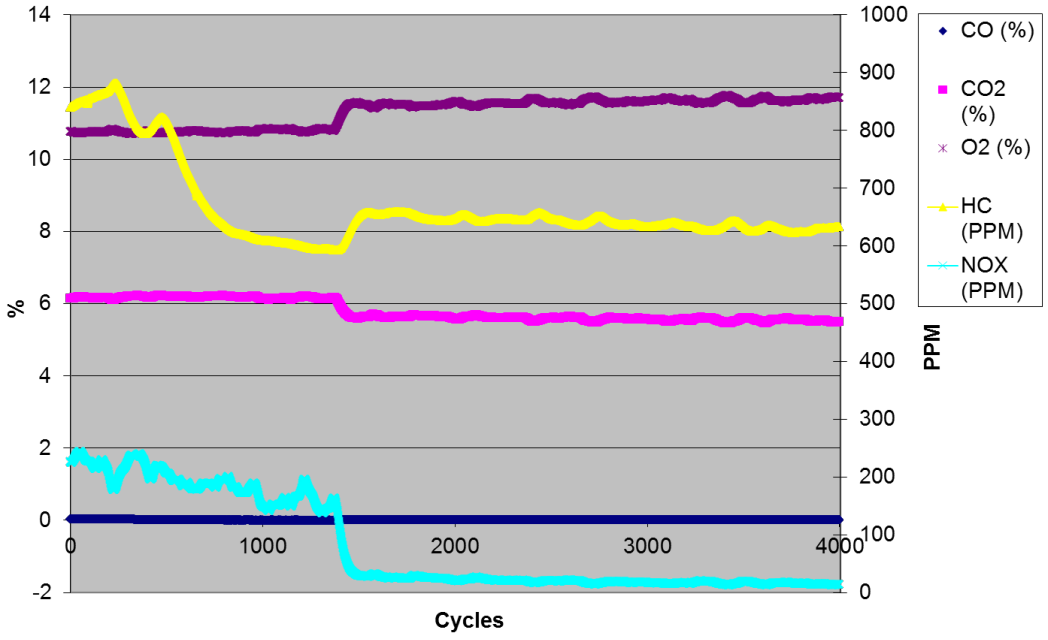


**Figure A28: Emissions at operation point number 3.**

**Table A29: Average concentrations shown at Figure A28.**

| | CO (%) | CO2 (%) | HC (PPM) | NOX (PPM) | O2 (%) |
|---|---|---|---|---|---|
| U | 0.027258 | 6.168389 | 847.4273 | 233.7385 | 10.73928 |
| D | 0.004123 | 5.782769 | 660.5993 | 75.73506 | 11.31128 |

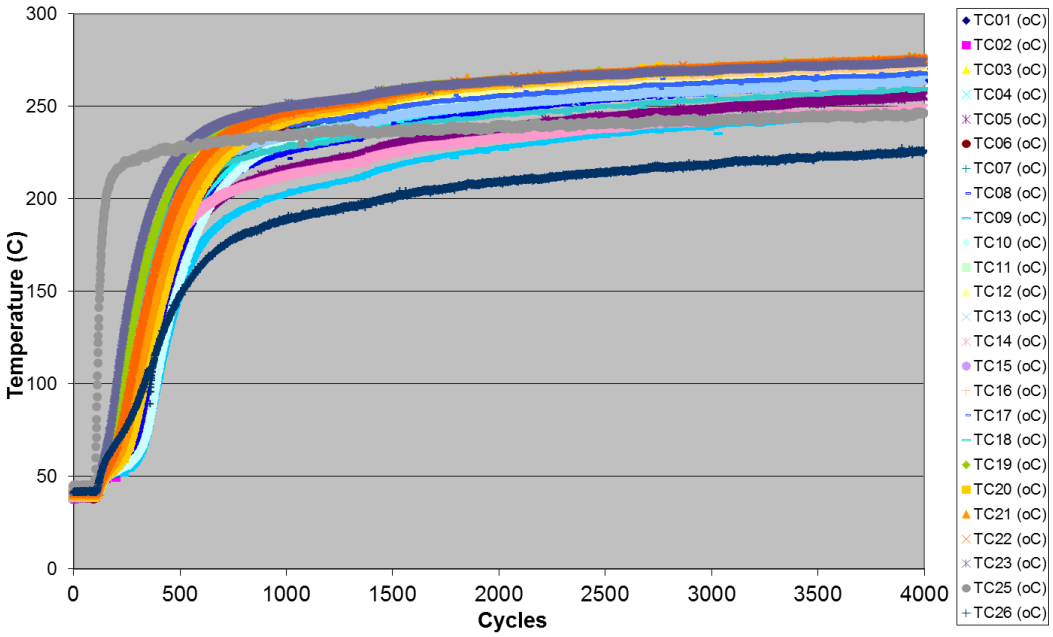


**Figure A29: Thermocouples temperature profile at operation point number 3.**

To see more in detail what happens with HC and NOx when the gases start passing through the catalyst, the next plot shows the 600 first cycles of the test, with the right hand "y" axis representing the PPM of HC and the left hand "y" axis the PPM of NOx and the rest of the gases in %.

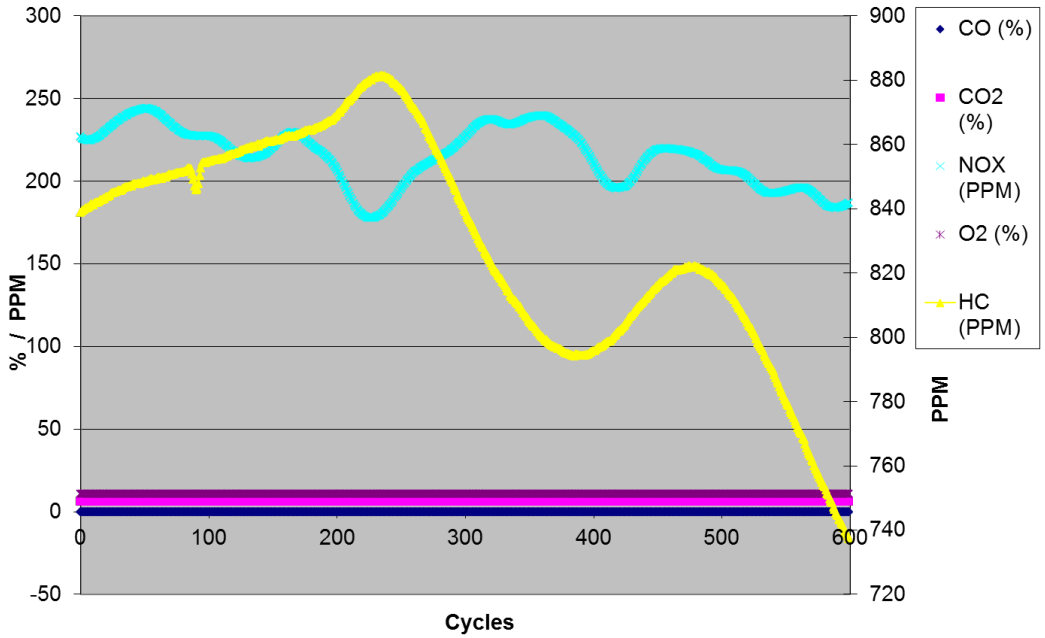


**Figure A30: Emissions at operation point number 3. Cycles 1-600.**

The emissions continue their patter after switching from upstream to downstream (probably because the catalyst is cold, so it isn't converting anything yet), even though they show a temporarily and short perturbation when this happens at 100 cycles. The pattern doesn't really change until about 250 cycles, that it is when the temperature achieves an average of about 100°C. That is when it seems to start showing some conversion, but only for **NOx** and **HC**, because **CO**, **$CO_2$** and **$O_2$** seem to be stable at the same amount all the time. That pattern keeps following almost the same path until cycle 1500 that seems to be the point where the catalyst average achieves 250°C, and suddenly all the emissions show changes. **NOx** decreases even more; **HC** increases (when before was decreasing); **$CO_2$** decreases; and **$O_2$** and **CO** increase.

4. Table A30 specifies some of the operation conditions at this operation point. Figure A31 shows the emissions patterns and Table A31 the respective average of the concentrations. At this point NOx/NO sensor is measuring **NOx** emissions. These results were taken from **upstream** (before the catalyst). Note that the engine must not have been at steady state before the transient test due to the fuel pressure was fluctuating during this test.

**Table A30: Average operation conditions at point number 4.**

| Air M.F. (g/s) | Liquid Fuel M.F. (mg/s) | Lambda | Compression Ratio | Liquid PI PW (ms) | Cat. Space Vol. Flow (exchanges/hr) |
|---|---|---|---|---|---|
| 4.063669 | 138.7016 | 2.336031 | 6.14081 | 9.3 | 71,424.16 |

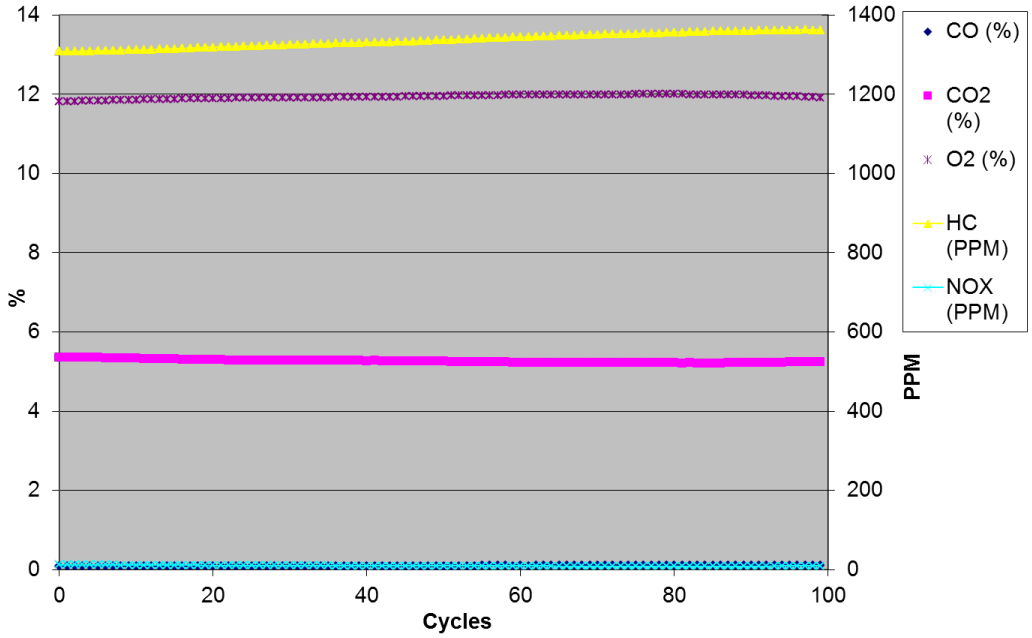


**Figure A31: Emissions at operation point number 4.**

**Table A31: Average concentrations shown at Figure A31.**

| CO (%) | CO2 (%) | HC (PPM) | NOX (PPM) | O2 (%) |
|---|---|---|---|---|
| 0.095821 | 5.26065 | 1,336.647 | 9.681643 | 11.93599 |

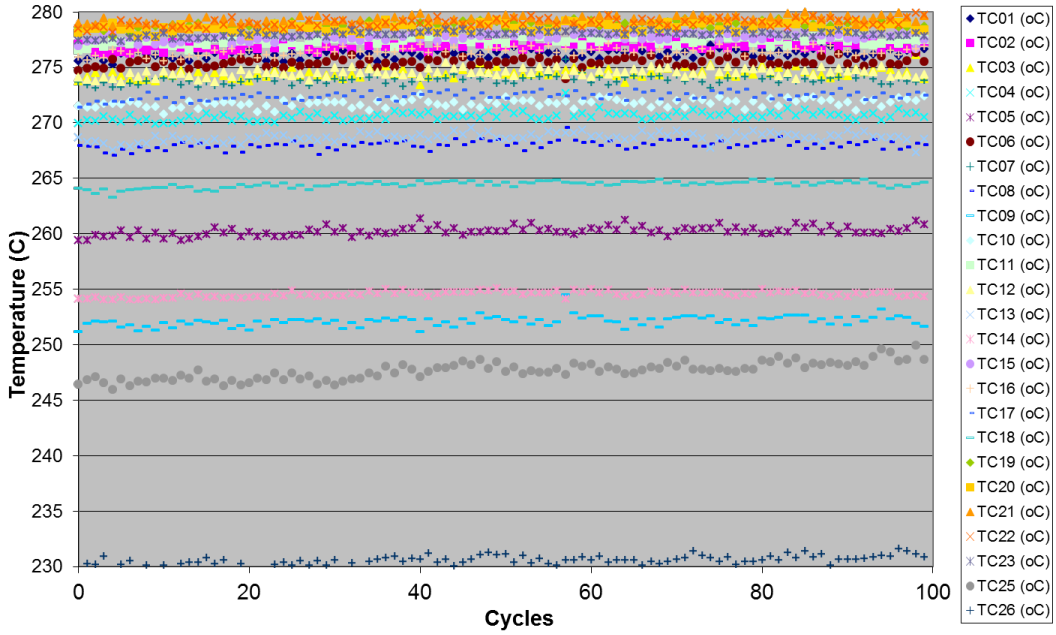


**Figure A32: Thermocouples temperature profile at operation point number 4.**

5. Same as 4, but downstream. Table A32 specifies some of the operation conditions at this operation point. Figure A33 shows the emissions patterns and Table A33 the respective average of the concentrations. At this point NOx/NO sensor is measuring **NOx** emissions. These results were taken from **downstream** (after catalyst). The fuel pressure is still seen fluctuating during this test.

**Table A32: Average operation conditions at point number 5.**

| Air M.F. (g/s) | Liquid Fuel M.F. (mg/s) | Lambda | Compression Ratio | Liquid PI PW (ms) | Cat. Space Vol. Flow (exchanges/hr) |
|---|---|---|---|---|---|
| 4.051222 | 156.4395 | 2.387328 | 6.14081 | 9.3 | 71,296.85 |

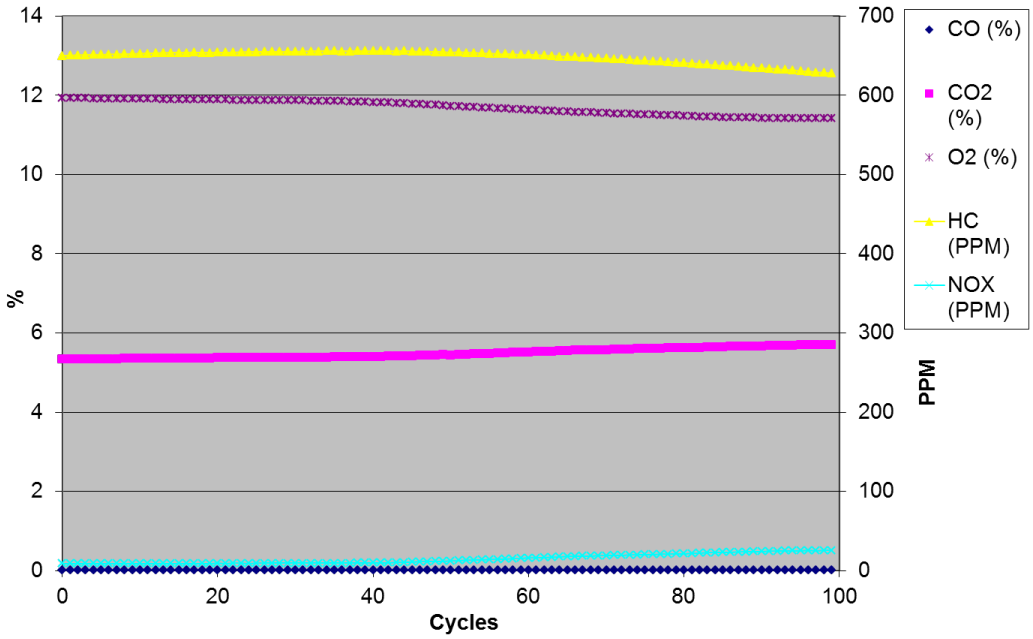


**Figure A33: Emissions at operation point number 5.**

**Table A33: Average concentrations shown at Figure A33.**

| CO (%) | CO2 (%) | HC (PPM) | NOX (PPM) | O2 (%) |
|---|---|---|---|---|
| 0.009143 | 5.48067 | 648.4198 | 14.65084 | 11.698 |

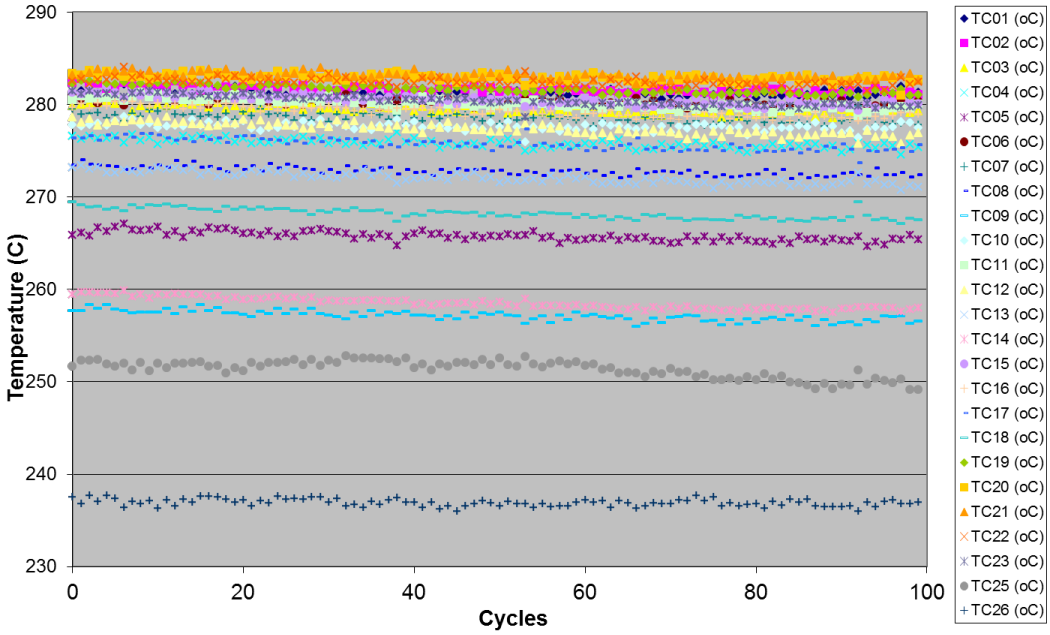


**Figure A34: Thermocouples temperature profile at operation point number 5.**

Discussion of tests 4-5: From **upstream** to **downstream**: **HC**, decreases to almost a half. **NOx**, seems to increase at the end. **$CO_2$** increases but just a bit at the end. **$O_2$** looks the same and **CO** decreases in a very small amount at the end.

6. Repeating operation point number 4. Table A34 specifies some of the operation conditions at this operation point. Figure A35 shows the emissions patterns and Table A35 the respective average of the concentrations. At this point NOx/NO sensor is measuring **NOx** emissions. These results were taken from **upstream** (before the catalyst).

**Table A34: Average operation conditions at point number 6.**

| Air M.F. (g/s) | Liquid Fuel M.F. (mg/s) | Lambda | Compression Ratio | Liquid PI PW (ms) | Cat. Space Vol. Flow (exchanges/hr) |
|---|---|---|---|---|---|
| 3.935746 | 119.1868 | 2.175787 | 6.14081 | 9.3 | 69,099.46 |

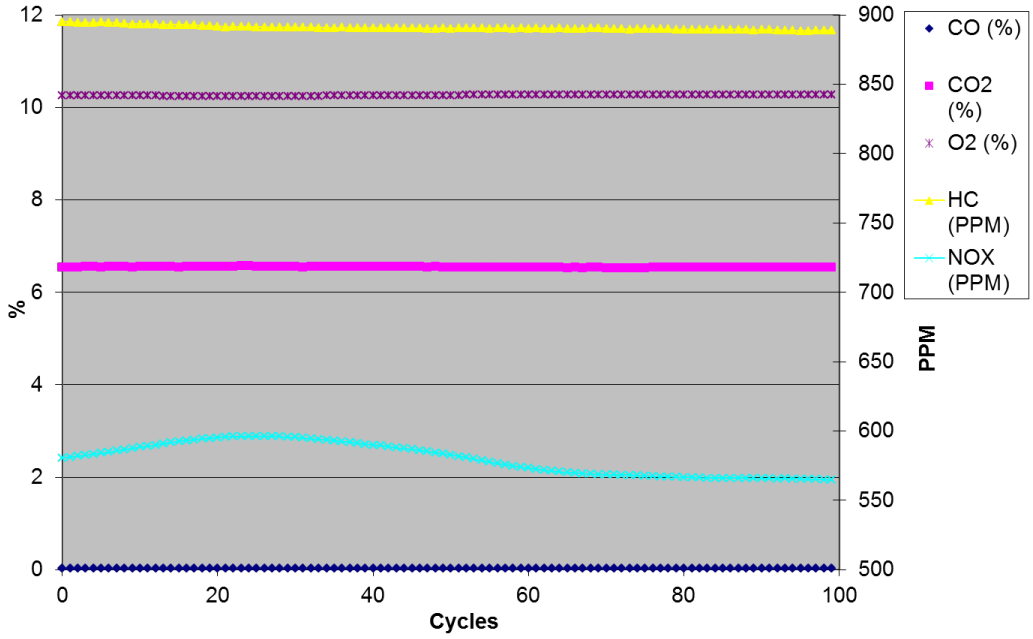


**Figure A35: Emissions at operation point number 6.**

**Table A35: Average concentrations shown at Figure 35.**

| CO (%) | CO2 (%) | HC (PPM) | NOX (PPM) | O2 (%) |
|---|---|---|---|---|
| 0.026783 | 6.544032 | 890.9186 | 579.9445 | 10.25969 |

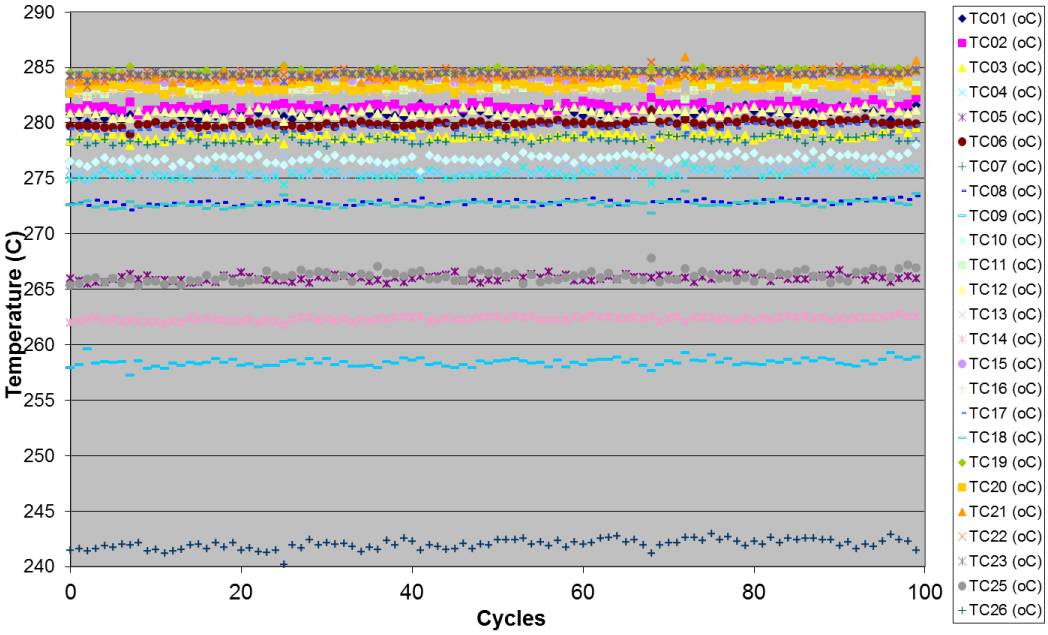


**Figure A36: Thermocouples temperature profile at operation point number 6.**

7. Repeating operation point number 5. Table A36 specifies some of the operation conditions at this operation point. Figure A37 shows the emissions patterns and Table A37 the respective average of the concentrations. At this point NOx/NO sensor is measuring **NOx** emissions. These results were taken from **downstream** (after catalyst).

**Table A36: Average operation conditions at point number 7.**

| Air M.F. (g/s) | Liquid Fuel M.F. (mg/s) | Lambda | Compression Ratio | Liquid PI PW (ms) | Cat. Space Vol. Flow (exchanges/hr) |
|---|---|---|---|---|---|
| 3.933181 | 119.1174 | 2.175673 | 6.14081 | 9.3 | 69,054.47 |

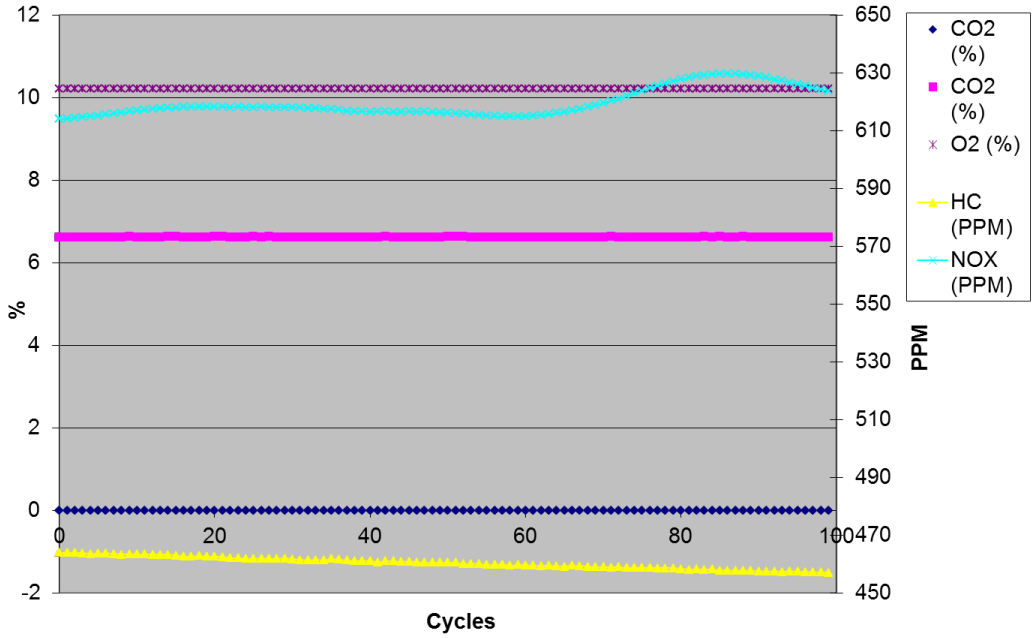


**Figure A37: Emissions at operation point number 7.**

**Table A37: Average concentrations shown at Figure A37.**

| CO (%) | CO2 (%) | HC (PPM) | NOX (PPM) | O2 (%) |
|---|---|---|---|---|
| -0.00333 | 6.619959 | 460.4568 | 619.5466 | 10.21037 |

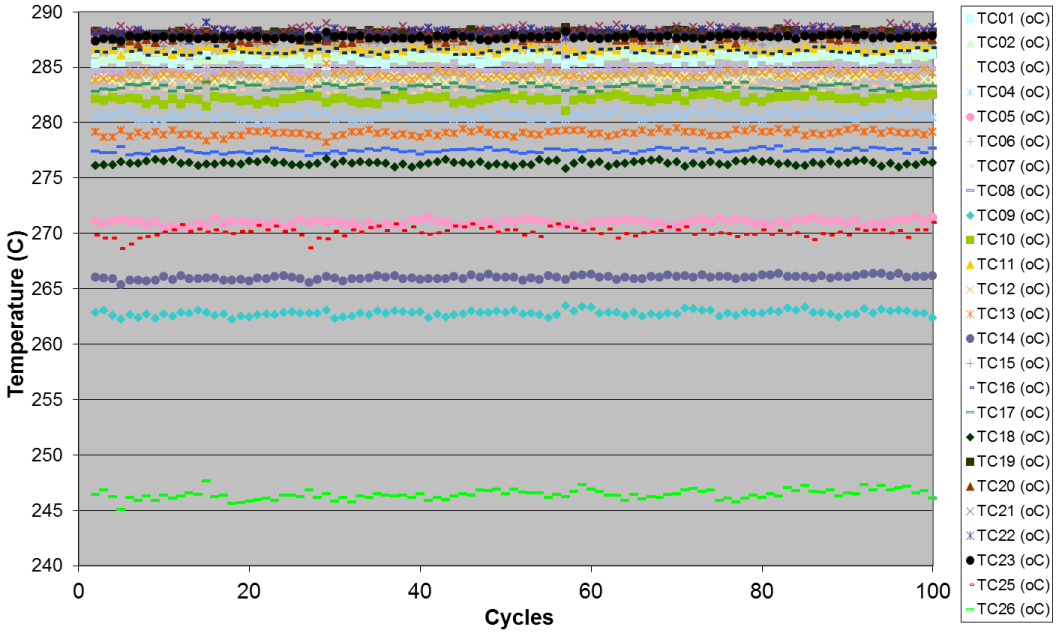


**Figure A38: Thermocouples temperature profile at operation point number 7.**

Discussion of tests 6-7: From **upstream** to **downstream**: **HC** decreases to almost a half. **NOx** increases. **$CO_2$** almost looks the same. **$O_2$** and **CO**, look the same as well.

8. Same operating conditions. Table A38 specifies some of the operation conditions at this operation point. Figure A39 shows the emissions patterns and Table A39 the respective average of the concentrations. At this point NOx/NO sensor is measuring **NOx** emissions during the first 100 cycles, and the second hundred measuring **NO**. These results were taken from **upstream** (before the catalyst).

**Table A38: Average operation conditions at point number 8.**

| | Air M.F. (g/s) | Liquid Fuel M.F. (mg/s) | Lambda | Compression Ratio | Liquid PI PW (ms) | Cat. Space Vol. Flow (exchanges/hr) |
|---|---|---|---|---|---|---|
| NOx | 3.94199 | 118.842 | 2.18662 | 6.14081 | 9.3 | 69,206.47 |
| NO | 3.94367 | 118.390 | 2.19612 | 6.14081 | 9.3 | 69,233.34 |

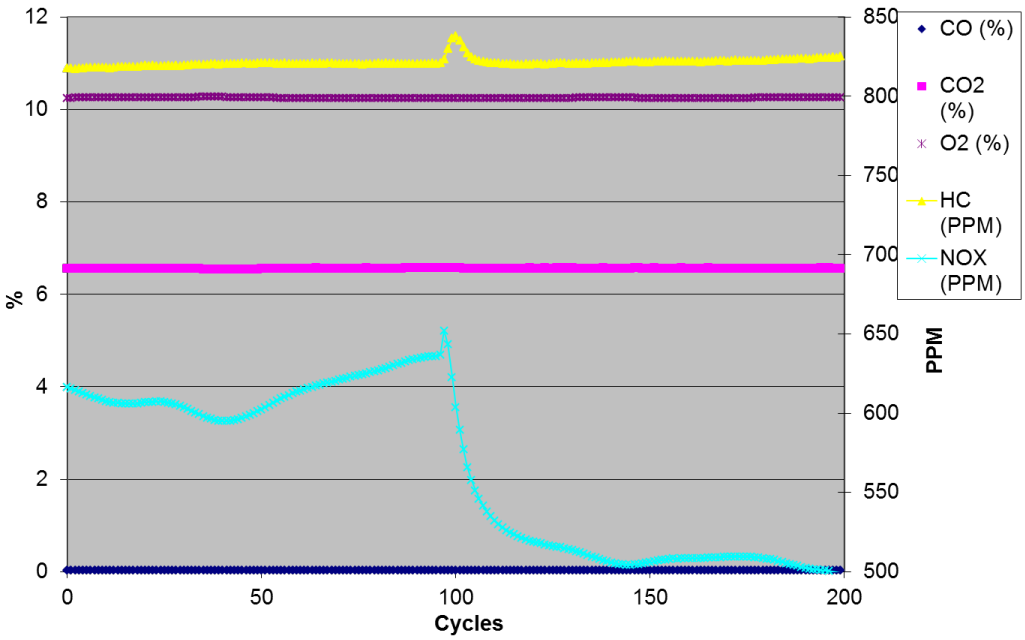


**Figure A39: Emissions at operation point number 8.**

**Table A39: Average concentrations shown at Figure A39.**

| | CO (%) | CO2 (%) | HC (PPM) | NOX (PPM) | O2 (%) |
|---|---|---|---|---|---|
| NOx | 0.025572 | 6.554984 | 820.3911 | 613.6471 | 10.2489 |
| NO | 0.025747 | 6.560631 | 822.1501 | 514.3106 | 10.24783 |

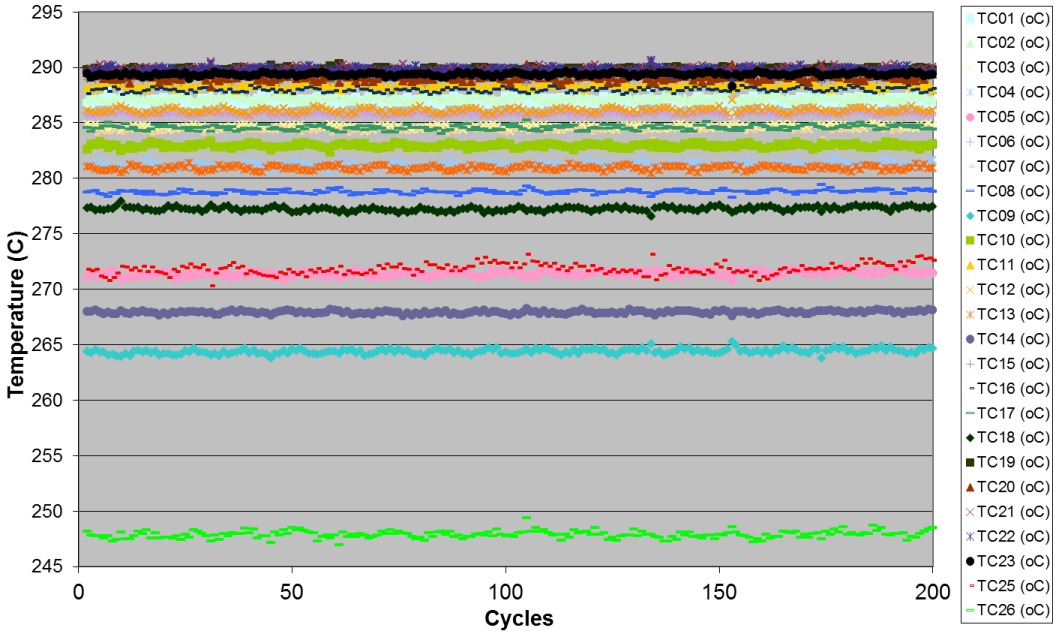


**Figure A40: Thermocouples temperature profile at operation point number 8.**

9. Same as 8, but now from downstream. Table A36 specifies some of the operation conditions at this operation point. Figure A37 shows the emissions patterns and Table A37 the respective average of the concentrations. At this point NOx/NO sensor is measuring **NOx** emissions during the first 100 cycles, and the second hundred measuring **NO**. These results were taken from **downstream** (after catalyst).

**Table A40: Average operation conditions at point number 9.**

| | Air M.F. (g/s) | Liquid Fuel M.F. (mg/s) | Lambda | Compression Ratio | Liquid PI PW (ms) | Cat. Space Vol. Flow (exchanges/hr) |
|---|---|---|---|---|---|---|
| NOx | 3.9423 | 118.114 | 2.1983 | 6.14081 | 9.3 | 69,209.17 |
| NO | 3.9425 | 118.392 | 2.1941 | 6.14081 | 9.3 | 69,213.8 |

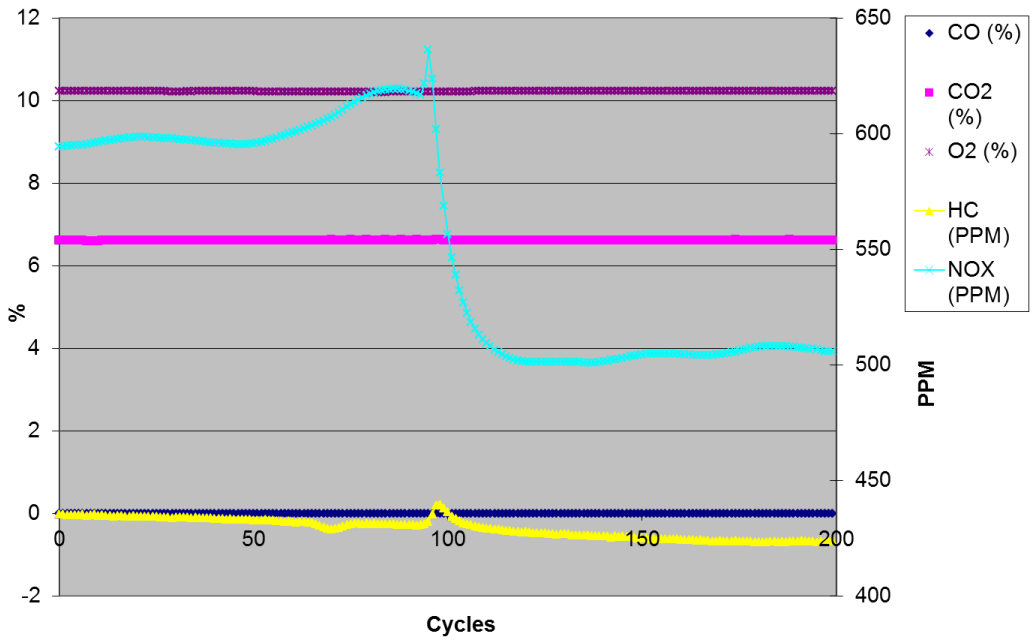


**Figure A41: Emissions at operation point number 9.**

**Table A41: Average concentrations shown at Figure A41.**

| | CO (%) | CO2 (%) | HC (PPM) | NOX (PPM) | O2 (%) |
|---|---|---|---|---|---|
| NOx | -0.00333 | 6.614021 | 433.0743 | 602.0554 | 10.21734 |
| NO | -0.00333 | 6.613966 | 425.8058 | 506.2441 | 10.22792 |

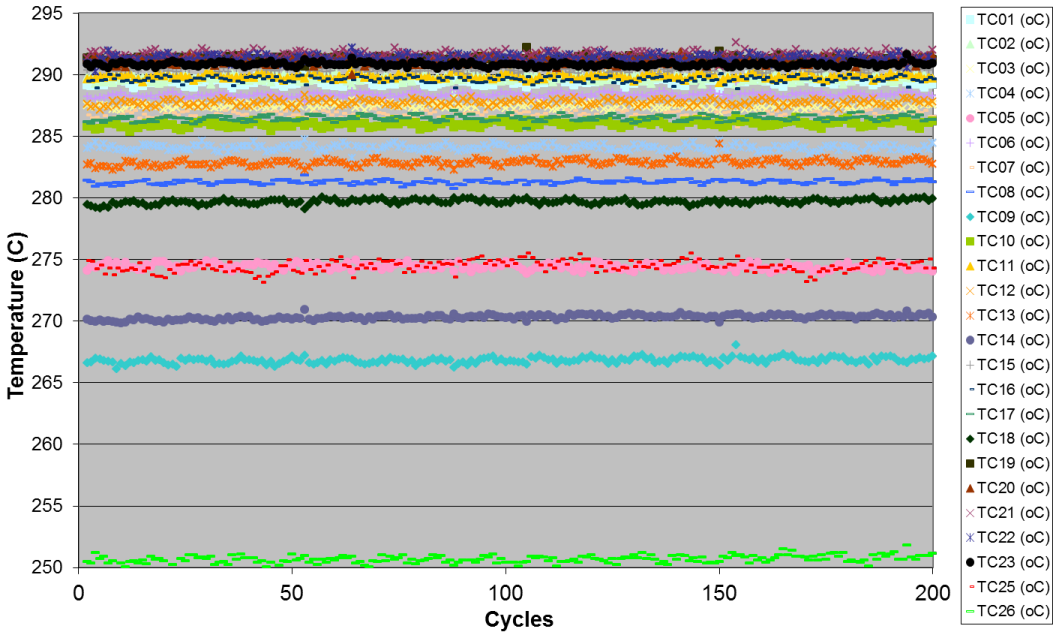


**Figure A42: Thermocouples temperature profile at operation point number 9.**

Discussion of tests 8-9: From **upstream** to **downstream**: **HC**, decreases 400 ppm. **NOx** and NO don't change. **$CO_2$** looks the same. **$O_2$** and **CO**, don't seem to change.

10. The system was cooled down and now. Hot motoring test when heating up.
11. Initial mode is switched to HCCI when getting close to cycle 100. Table A42 specifies some of the operation conditions at this operation point. Figure A43 shows the emissions patterns and Table A43 the respective average of the concentrations. The division for the operation conditions and emissions concentrations is done in the cycles 1-100 and 150-200 due the variability of cycles 100-150. At this point NOx/NO sensor is measuring **NOx** emissions. These results were taken from **upstream** (before the catalyst).

**Table A42: Average operation conditions at point number 11.**

| | Air M.F. (g/s) | Liquid Fuel M.F. (mg/s) | Lambda | Compression Ratio | Liquid PI PW (ms) | Cat. Space Vol. Flow (exchanges/hr) |
|---|---|---|---|---|---|---|
| Initial | 3.857 | 0 | 10.431 | 6.161705 | 4.2821 | 70,686.23 |
| HCCI | 4.251 | 0 | - | 6.161705 | 8.9 | 73,943.06 |

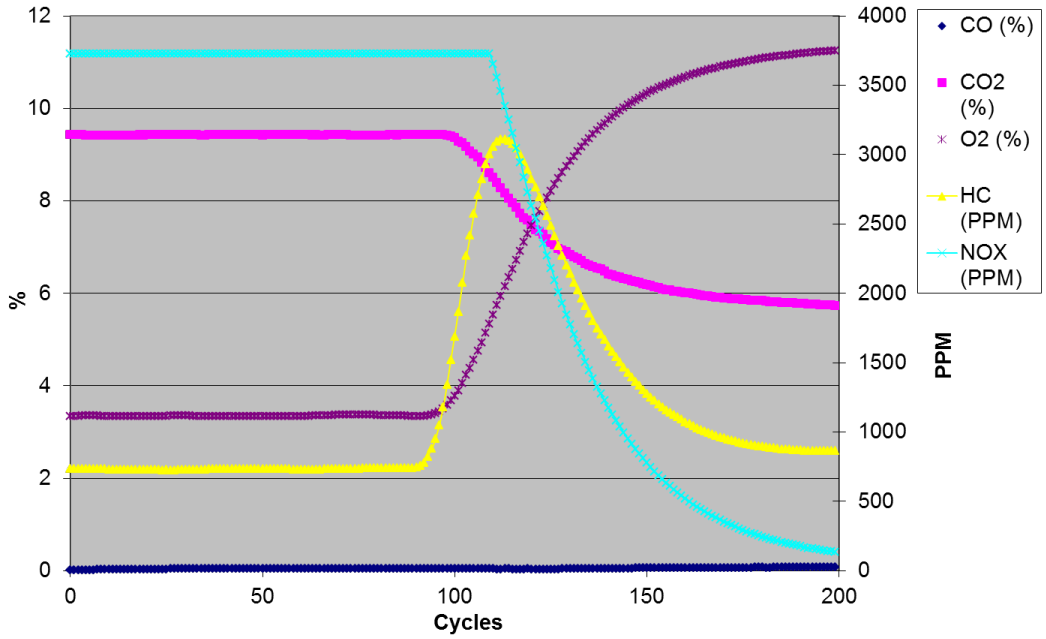


**Figure A43: Emissions at operation point number 11.**

**Table A43: Average concentrations shown at Figure A43.**

| | CO (%) | CO2 (%) | HC (PPM) | NOX (PPM) | O2 (%) |
|---|---|---|---|---|---|
| Initial | 0.036783 | 9.42152 | 768.7268 | 3,726.457 | 3.361589 |
| HCCI | 0.065341 | 5.885885 | 965.3366 | 340.8325 | 10.94206 |

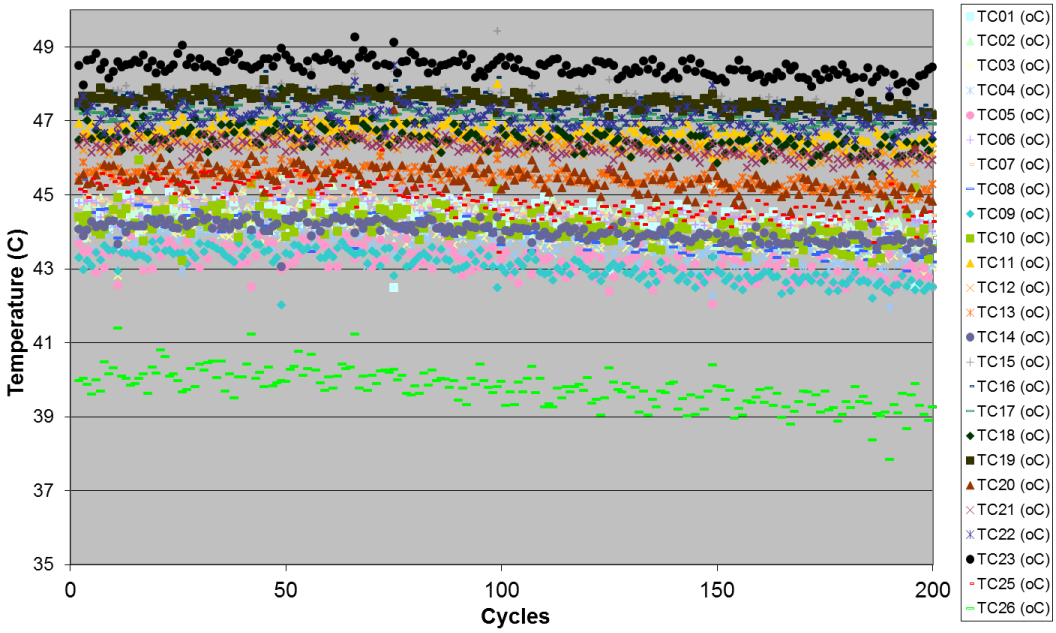


**Figure A44: Thermocouples temperature profile at operation point number 11.**

12. Table A44 specifies some of the operation conditions at this operation point. Figure A45 shows the emissions patterns and Table A45 the respective average of the concentrations. At this point NOx/NO sensor is measuring **NOx** emissions during the first 100 cycles, and the second hundred measuring **NO**. These results were taken from **upstream** (before the catalyst).

**Table A44: Average operation conditions at point number 12.**

| Air M.F. (g/s) | Liquid Fuel M.F. (mg/s) | Lambda | Compression Ratio | Liquid PI PW (ms) | Cat. Space Vol. Flow (exchanges/hr) |
|---|---|---|---|---|---|
| 4.275737 | 129.9964 | 2.169554 | 6.161705 | 10 | 75,071.23 |

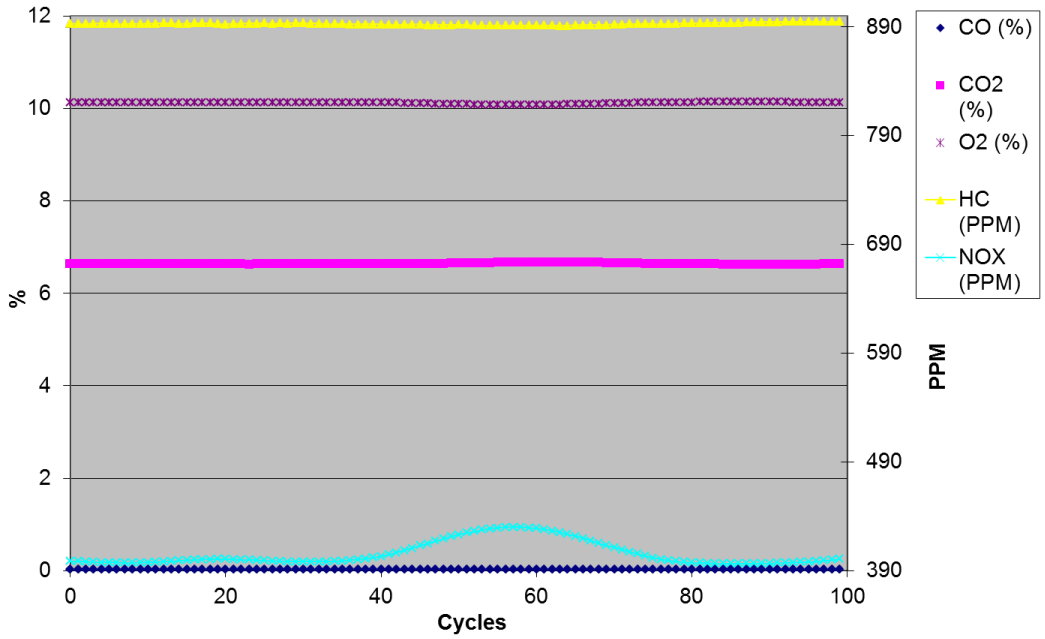


**Figure A45: Emissions at operation point number 12.**

**Table A45: Average concentrations shown at Figure A45.**

| CO (%) | CO2 (%) | HC (PPM) | NOX (PPM) | O2 (%) |
|---|---|---|---|---|
| 0.03161 | 6.63926 | 892.8034 | 405.5598 | 10.11885 |

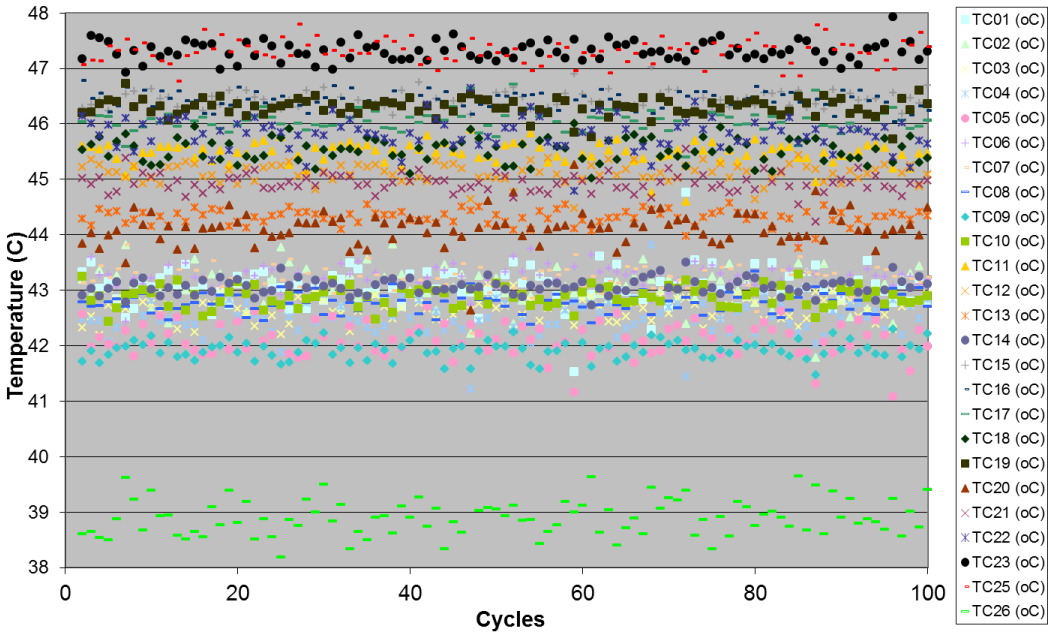


**Figure A46: Thermocouples temperature profile at operation point number 12.**

13. Transient test. These results started from **upstream** and **NOx** emissions during the first 100 cycles, and the second hundred measuring **NO**. At 200 cycles, the measures were changed to **downstream**, but still measuring **NO**, and at 2000 cycles, it was switched back to **NOx**. Tables A46 and A47 specify some of the operation conditions at this operation point. Figure A47 shows the emissions patterns, and Tables A48 and A49 the respective average of the concentrations.

**Table A46: Average operation conditions at point number 13 during upstream conditions.**

| | Air M.F. (g/s) | Liquid Fuel M.F. (mg/s) | Lambda | Compression Ratio | Liquid PI PW (ms) | Cat. Space Vol. Flow (exchanges/hr) |
|---|---|---|---|---|---|---|
| NOx | 4.2953 | 129.82 | 2.1792 | 6.161705 | 10 | 75,412.1 |
| NO | 4.2977 | 129.98 | 2.1795 | 6.161705 | 10 | 75,453.97 |

**Table A47: Average operation conditions at point number 13 during downstream conditions.**

| | Air M.F. (g/s) | Liquid Fuel M.F. (mg/s) | Lambda | Compression Ratio | Liquid PI PW (ms) | Cat. Space Vol. Flow (exchanges/hr) |
|---|---|---|---|---|---|---|
| NO | 4.29768 | 129.529 | 2.1870 | 6.161705 | 10 | 75,450.93 |
| NOx | 4.30258 | 129.197 | 2.1964 | 6.161705 | 10 | 75,534.53 |

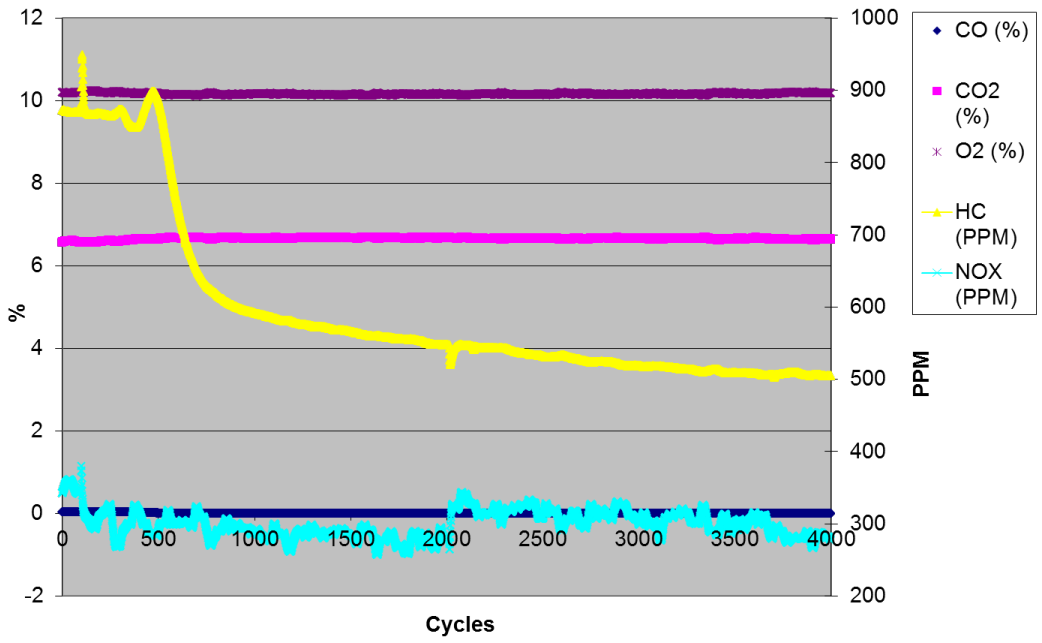


**Figure A47: Emissions at operation point number 13.**

**Table A48: Average concentrations shown at Figure A47 during upstream conditions.**

| | CO (%) | CO2 (%) | HC (PPM) | NOX (PPM) | O2 (%) |
|---|---|---|---|---|---|
| NOx | 0.032805 | 6.588112 | 869.7724 | 351.2543 | 10.18545 |
| NO | 0.033032 | 6.57155 | 874.9805 | 307.0326 | 10.2152 |

**Table A49: Average concentrations shown at Figure A47 during downstream conditions.**

| | CO (%) | CO2 (%) | HC (PPM) | NOX (PPM) | O2 (%) |
|---|---|---|---|---|---|
| NO | 0.004594 | 6.66094 | 646.5849 | 289.2215 | 10.1523 |
| NOx | -0.00023 | 6.654147 | 521.8786 | 306.384 | 10.15727 |

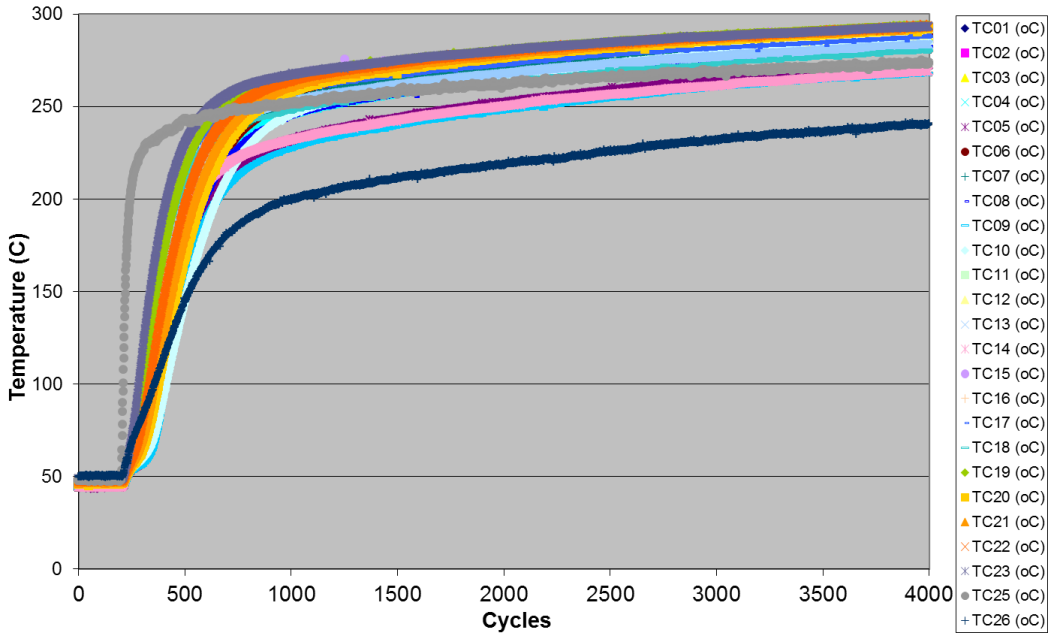


**Figure A48: Thermocouples temperature profile at operation point number 13.**

To see in more detail what happens with HC and NOx when the gases start passing through the catalyst, the next plot shows the 600 first cycles of the test, with the right hand "y" axis representing the PPM of HC and NOx and the left hand "y" axis the rest of the gases in %.

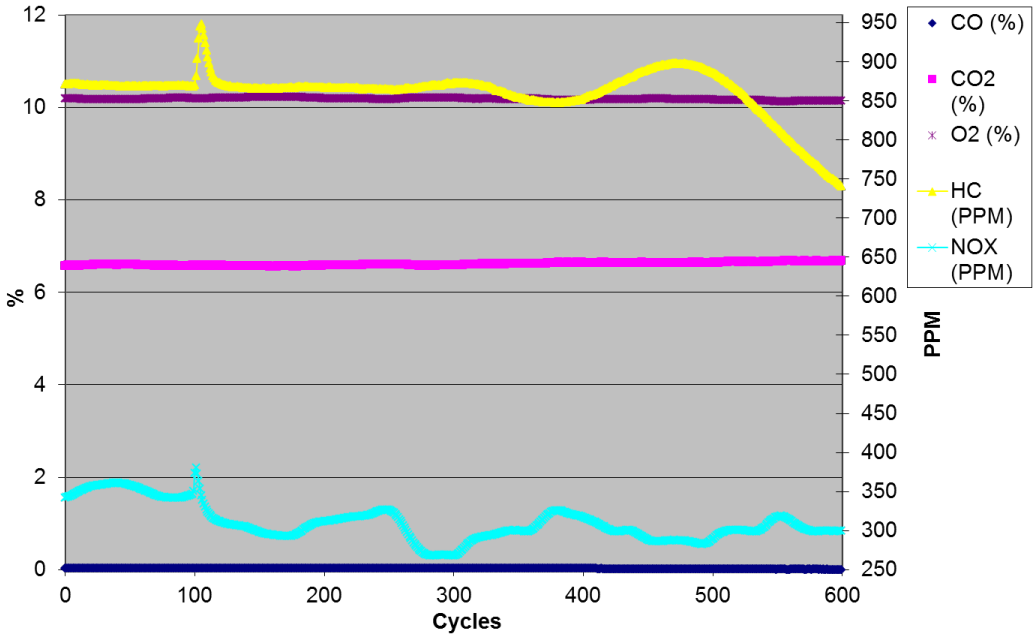


**Figure A49: Emissions at operation point number 13. Cycles 1-600.**

Here we can notice when the sensor was switch from **NOx** to **NO** at 100 cycles, but you can't notice the change from upstream to downstream. We start seeing some conversion of **HC** just at cycle 500, that's when the temperature in the catalyst had an average of about 200. At cycle 750, when the temperature average is about 250°C, the pattern of conversion of **HC** gets slower, but keep converting at about the same rate for the rest of the test. At 2000 cycle it can be notice the change from **NO** to **NOx** readings, and you can see that the amount increases, but that at the end seems to show some conversion. It can be seen that throughout the test, the amount of $\mathbf{CO_2}$ increases a little bit, but it's a little harder to notice, even though it seems to happen, that $\mathbf{O_2}$ and **CO** actually decrease.

14. Table A50 specifies some of the operation conditions at this operation point. Figure A50 shows the emissions patterns and Table A51 the respective average of the concentrations. At this point NOx/NO sensor is measuring **NOx** emissions during the first 100 cycles, and the second hundred measuring **NO**. These results were taken from **upstream** (before the catalyst).

**Table A50: Average operation conditions at point number 14.**

| | Air M.F. (g/s) | Liquid Fuel M.F. (mg/s) | Lambda | Compression Ratio | Liquid PI PW (ms) | Cat. Space Vol. Flow (exchanges/hr) |
|---|---|---|---|---|---|---|
| NOx | 4.0827 | 128.7 | 2.0891 | 6.161705 | 10 | 71,706.94 |
| NO | 4.0902 | 129.4 | 2.0823 | 6.161705 | 10 | 71,840.03 |

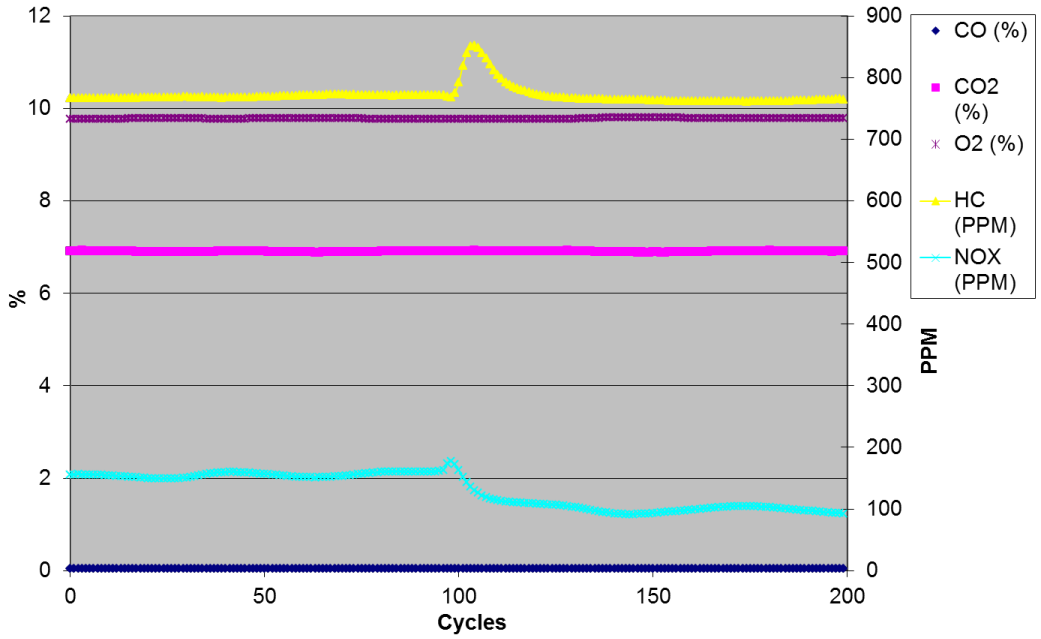


**Figure A50: Emissions at operation point number 14.**

**Table A51: Average concentrations shown at Figure A50.**

| | CO (%) | CO2 (%) | HC (PPM) | NOX (PPM) | O2 (%) |
|---|---|---|---|---|---|
| NOx | 0.044919 | 6.903726 | 769.8377 | 156.0254 | 9.778306 |
| NO | 0.044897 | 6.907197 | 772.8205 | 102.9864 | 9.783265 |

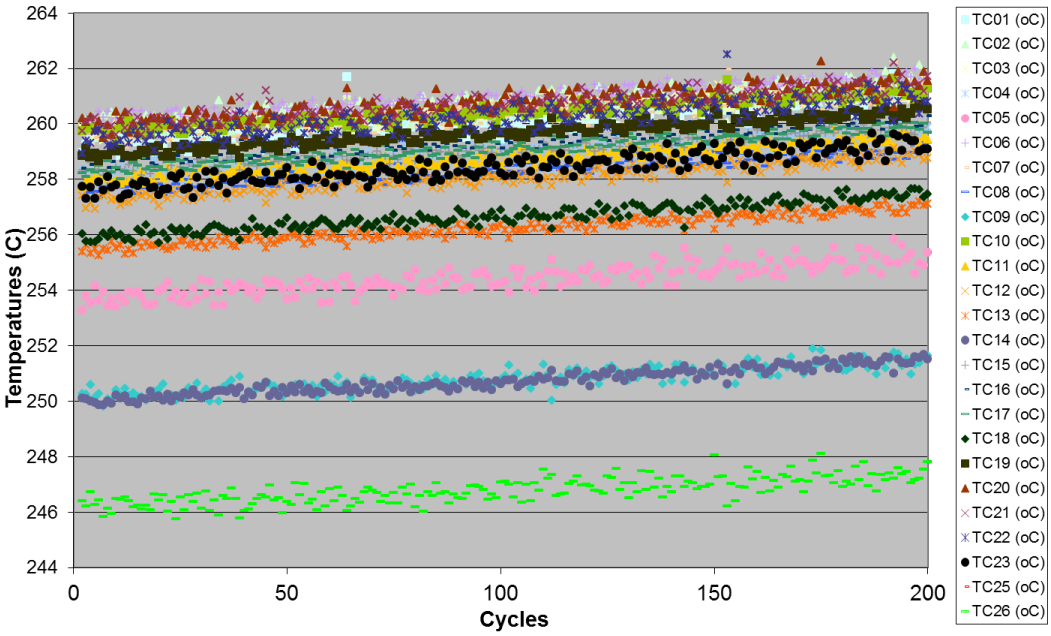


**Figure A51: Thermocouples temperature profile at operation point number 14.**

15. Same as 14, but downstream emissions. Table A52 specifies some of the operation conditions at this operation point. Figure A52 shows the emissions patterns and Table A53 the respective average of the concentrations. At this point NOx/NO sensor is measuring **NOx** emissions during the first 100 cycles, and the second hundred measuring **NO**. These results were taken from **downstream** (after catalyst).

**Table A52: Average operation conditions at point number 15.**

| | Air M.F. (g/s) | Liquid Fuel M.F. (mg/s) | Lambda | Compression Ratio | Liquid PI PW (ms) | Cat. Space Vol. Flow (exchanges/hr) |
|---|---|---|---|---|---|---|
| NOx | 4.075 | 127.24 | 2.1102 | 6.161705 | 10 | 71,580.59 |
| NO | 4.083 | 129.20 | 2.0837 | 6.161705 | 10 | 71,721.58 |

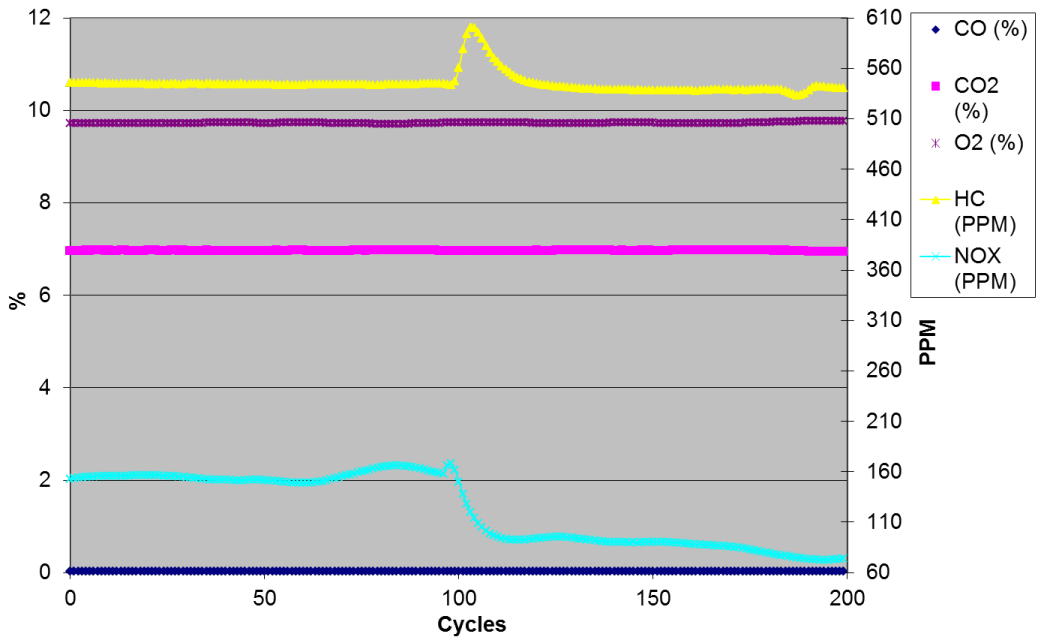


**Figure A52: Emissions at operation point number 15.**

**Table A53: Average concentrations shown at Figure A52.**

| | CO (%) | CO2 (%) | HC (PPM) | NOX (PPM) | O2 (%) |
|---|---|---|---|---|---|
| NOx | 0.022436 | 6.968003 | 544.5259 | 155.7358 | 9.724411 |
| NO | 0.022256 | 6.967225 | 545.4072 | 91.21611 | 9.736131 |

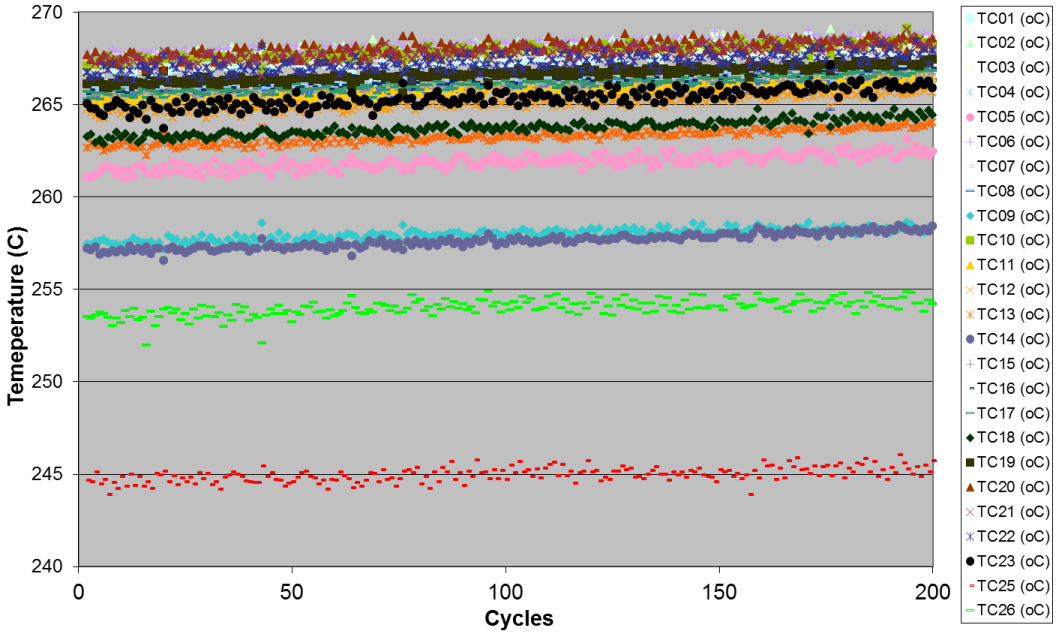


**Figure A53: Thermocouples temperature profile at operation point number 15.**

Discussion of tests 14-15: From **upstream** to **downstream**: **HC**, decreases from 760 to 530 ppm. The amount of **NOx** seems to be almost the same in both cases close to 150, but we can see a few amount of conversion of **NO** which goes from 100 to 70 ppm. **$CO_2$**, **$O_2$** and **CO**, seems to stay the same (no conversion).

Date: 2010_06_04
Operating Mode: HCCI with n-heptane port injected
Purpose: Catalyst testing. Run with EGR of 0%.
Comments: *Since HC and NOx are in ppm, their 'y' axis is the one at the right hand (unless specified different), and the % is the one at the left hand of the Emissions graphs.*

1. Hot motoring trace
2. Transient test. These results started from **upstream** and **NOx** emissions during the first 100 cycles, and the second hundred measuring **NO**. At 200 cycles, the measures were changed to **downstream**, but still measuring **NO**, and at 1000 cycles, it was switched back to **NOx**. Table A54 and A55 specify some of the operation conditions at this operation point. Figure A54 shows the emissions patterns, and Tables A56 and A57 the respective average of the concentrations.

**Table A54: Average operation conditions at point number 2 during upstream conditions.**

| | Air M.F. (g/s) | Liquid Fuel M.F. (mg/s) | Lambda | Compression Ratio | Liquid PI PW (ms) | Cat. Space Vol. Flow (exchanges/hr) |
|---|---|---|---|---|---|---|
| NOx | 4.2307 | 133.497 | 2.08704 | 6.285834 | 10.1 | 74,307.21 |
| NO | 4.2182 | 133.976 | 2.07293 | 6.285834 | 10.1 | 74,090.7 |

**Table A55: Average operation conditions at point number 2 during downstream conditions.**

| | Air M.F. (g/s) | Liquid Fuel M.F. (mg/s) | Lambda | Compression Ratio | Liquid PI PW (ms) | Cat. Space Vol. Flow (exchanges/hr) |
|---|---|---|---|---|---|---|
| NO | 4.0609 | 133.37 | 2.0050 | 6.285834 | 10.1 | 71,349.97 |
| NOx | 4.0274 | 133.05 | 1.9933 | 6.285834 | 10.1 | 70,764.78 |

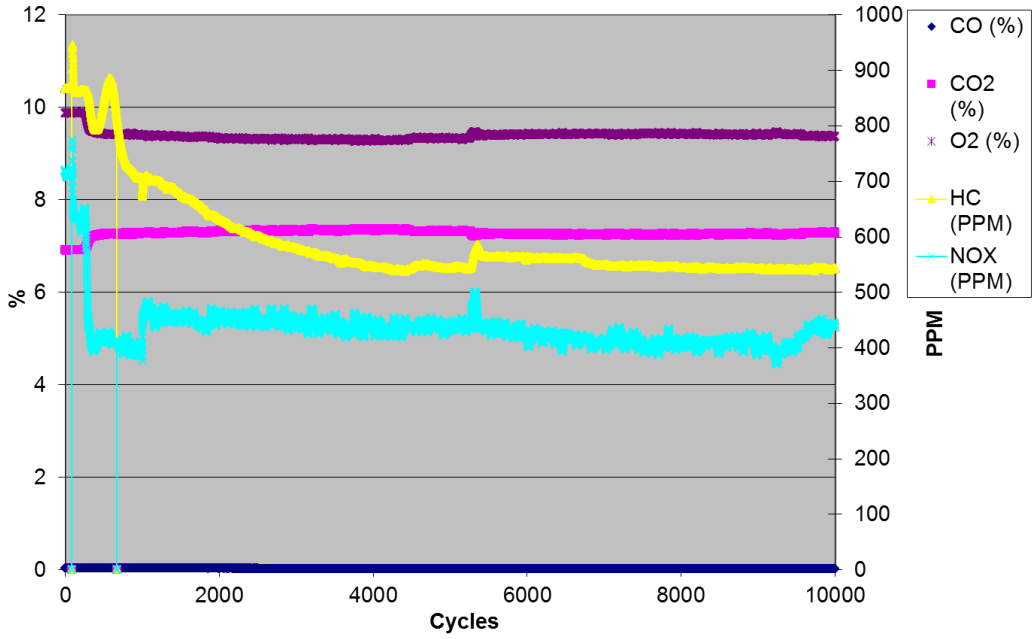


**Figure A54: Emissions at operation point number 2.**

**Table A56: Average concentrations shown at Figure A54 during upstream conditions.**

| | CO (%) | CO2 (%) | HC (PPM) | NOX (PPM) | O2 (%) |
|---|---|---|---|---|---|
| NOx | 0.043466 | 6.915655 | 870.7452 | 715.3133 | 9.874462 |
| NO | 0.042864 | 6.916612 | 866.7059 | 636.4777 | 9.881409 |

**Table A57: Average concentrations shown at Figure A54 during downstream conditions.**

| | CO (%) | CO2 (%) | HC (PPM) | NOX (PPM) | O2 (%) |
|---|---|---|---|---|---|
| NO | 0.039722 | 7.215545 | 797.5668 | 431.1999 | 9.47777 |
| NOx | 0.026358 | 7.289739 | 570.4054 | 430.1087 | 9.370795 |

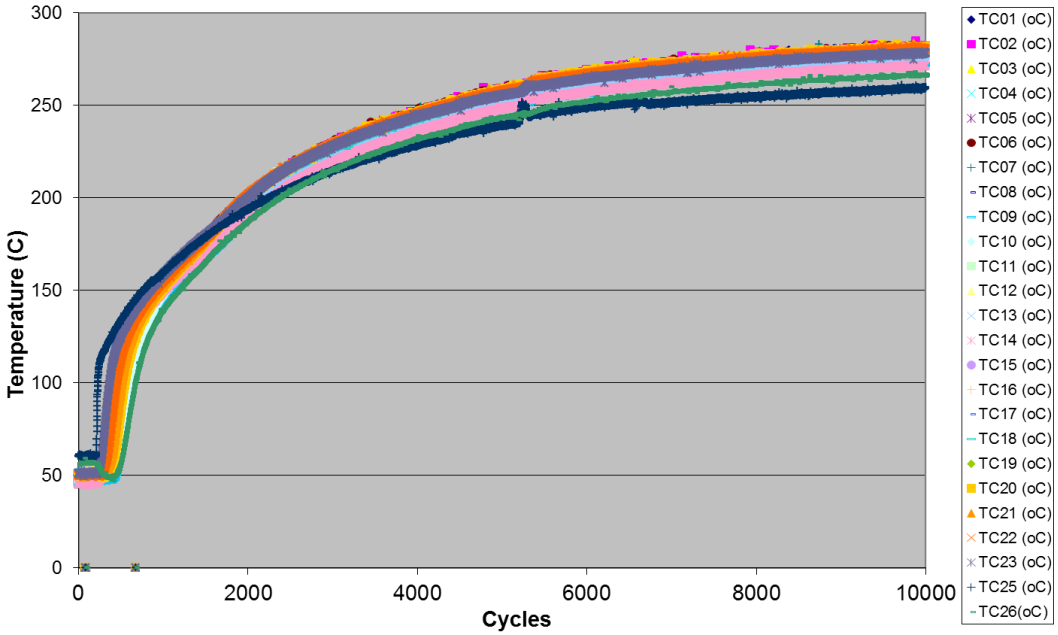


**Figure A55: Thermocouples temperature profile at operation point number 2.**

To see in more detail what happens with HC and NOx when the gases start passing through the catalyst, the next Figures A56 and A57 show the 1000 first cycles of the test, with the right hand "y" axis representing the PPM of HC and NOx and the left hand "y" axis the rest of the gases in %.

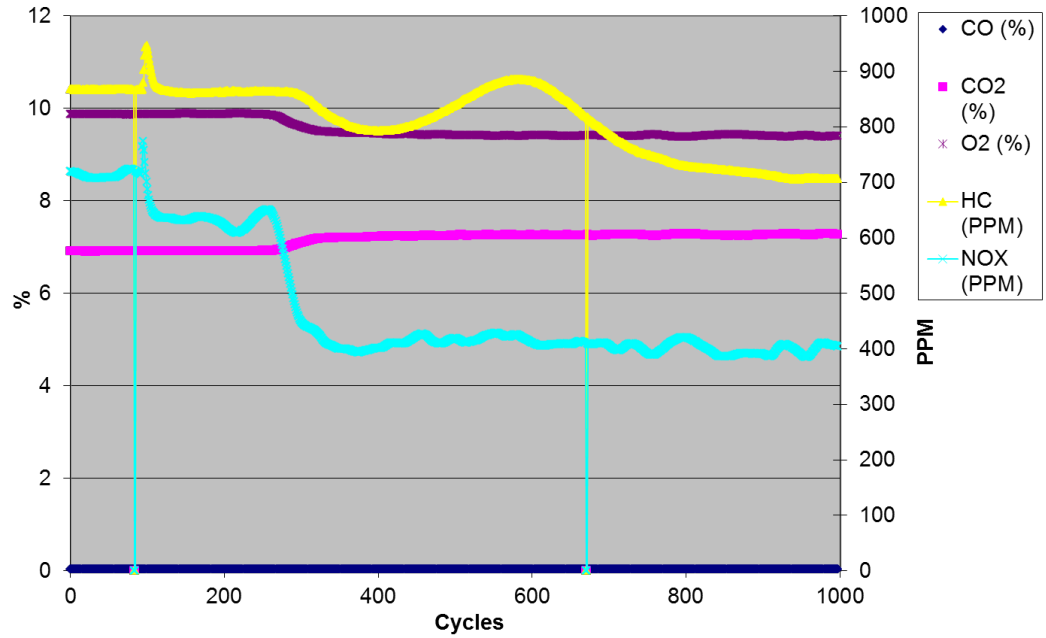


**Figure A56: Emissions at operation point number 2. Cycles 1-1000.**

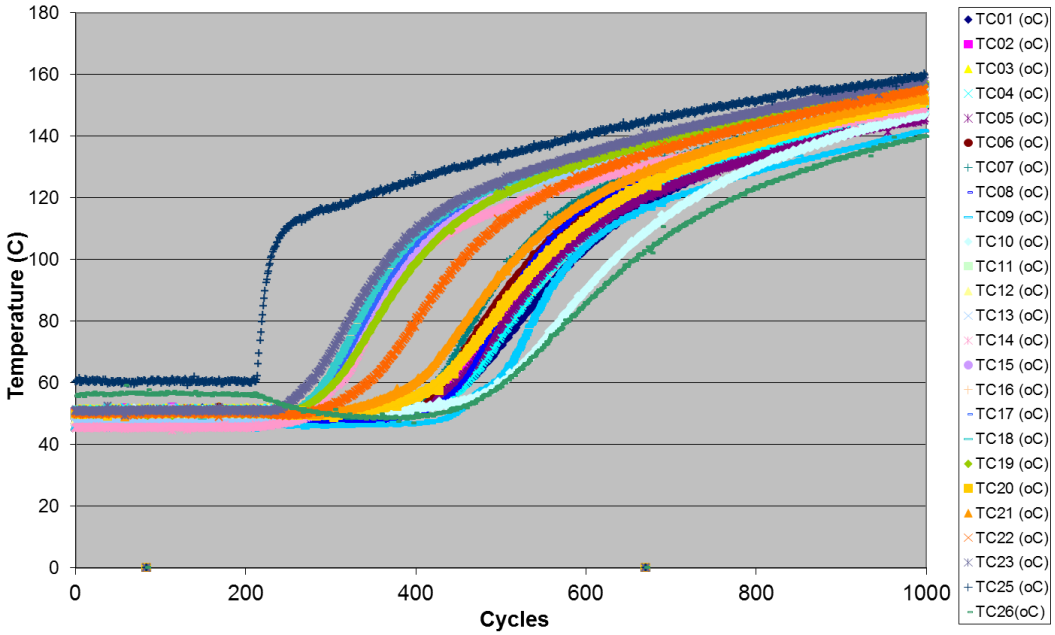


**Figure A57: Thermocouples temperature profile at operation point number 2. Cycles 1-1000.**

When the sensor is switched from NOx to NO (at cycle 100), we can see that the amount of NO is lower than NOx. It can be notice for almost all the gases except by CO, that the conversion starts close to the cycle 300, when the temperature average is about 60°C (downstream measurements started at cycle 200).

3. Upstream emissions at the same conditions as 2. First 100 cycles NOx, then NO. Table A52 specifies some of the operation conditions at this operation point. Figure A52 shows the emissions patterns and Table A53 the respective average of the concentrations. At this point NOx/NO sensor is measuring **NOx** emissions during the first 100 cycles, and the second hundred measuring **NO**. These results were taken from **upstream** (before the catalyst).

**Table A58: Average operation conditions at point number 3.**

| | Air M.F. (g/s) | Liquid Fuel M.F. (mg/s) | Lambda | Compression Ratio | Liquid PI PW (ms) | Cat. Space Vol. Flow (exchanges/hr) |
|---|---|---|---|---|---|---|
| NOx | 4.033 | 132.8 | 1.99922 | 6.285834 | 10.1 | 70,862.42 |
| NO | 4.041 | 132.7 | 2.00456 | 6.285834 | 10.1 | 71,009.87 |

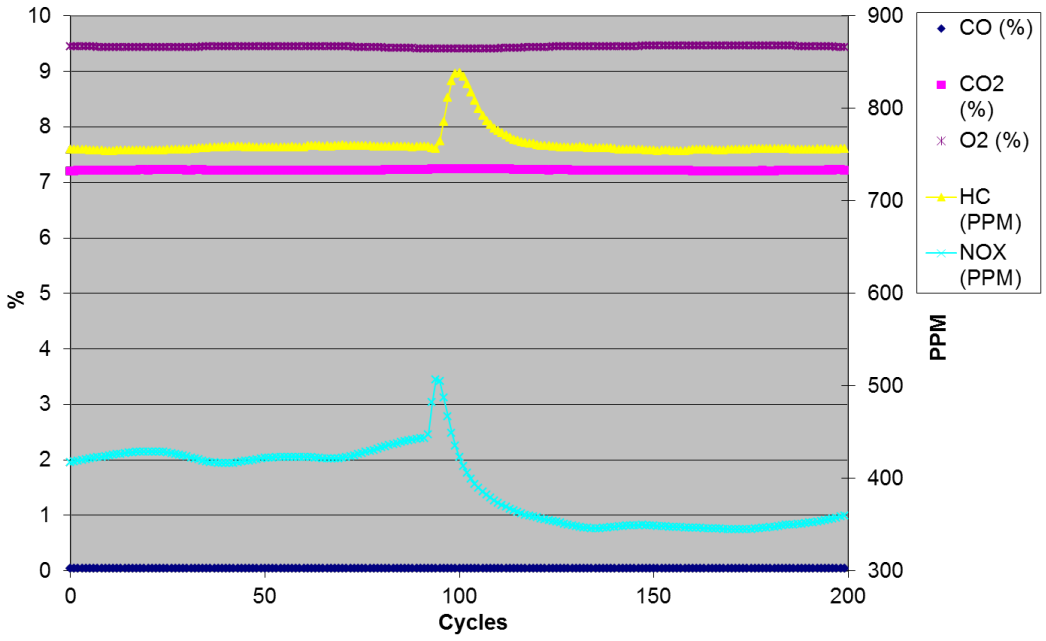


**Figure A58: Emissions at operation point number 3.**

**Table A59: Average concentrations shown at Figure A58.**

| | CO (%) | CO2 (%) | HC (PPM) | NOX (PPM) | O2 (%) |
|---|---|---|---|---|---|
| NOx | 0.044782 | 7.219118 | 760.6569 | 428.9406 | 9.43771 |
| NO | 0.044698 | 7.217559 | 761.5926 | 354.5865 | 9.450192 |

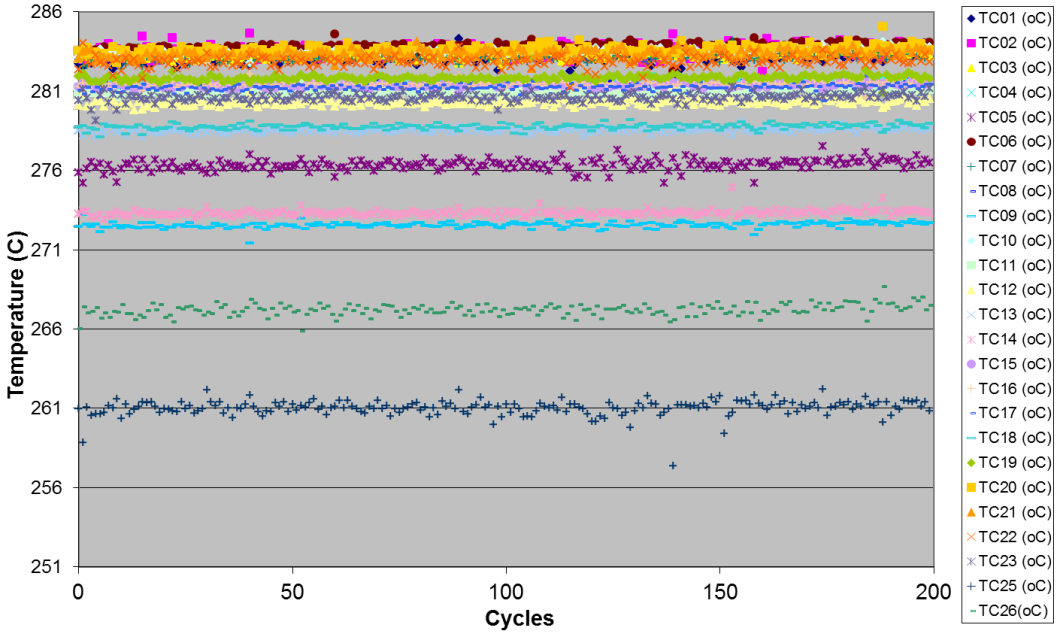


**Figure A59: Thermocouples temperature profile at operation point number 3.**

4. Hot motoring trace, after cooling down the engine.
5. Transient test, with no exhaust flow restrictions. These results started from **upstream** and **NOx** emissions during the first 100 cycles, and the second hundred measuring **NO**. At 200 cycles, the measures were changed to **downstream**, but still measuring **NO**, and at 1000 cycles, it was switched back to **NOx**. Tables A60 and A61 specify some of the operation conditions at this operation point. Figure A60 shows the emissions patterns, and Tables A62 and A63 the respective average of the concentrations.

**Table A60: Average operation conditions at point number 5 during upstream conditions.**

| | Air M.F. (g/s) | Liquid Fuel M.F. (mg/s) | Lambda | Compression Ratio | Liquid PI PW (ms) | Cat. Space Vol. Flow (exchanges/hr) |
|---|---|---|---|---|---|---|
| NOx | 4.764 | 121.52 | 2.5869 | 6.299199 | 9.5 | 83,529.6 |
| NO | 4.764 | 121.71 | 2.5833 | 6.299199 | 9.5 | 83,528.51 |

**Table A61: Average operation conditions at point number 5 during downstream conditions.**

| | Air M.F. (g/s) | Liquid Fuel M.F. (mg/s) | Lambda | Compression Ratio | Liquid PI PW (ms) | Cat. Space Vol. Flow (exchanges/hr) |
|---|---|---|---|---|---|---|
| NO | 4.770 | 121.3 | 2.5923 | 6.299199 | 9.5 | 83,646.5 |
| NOx | 4.778 | 120.5 | 2.6148 | 6.299199 | 9.5 | 83,774.39 |

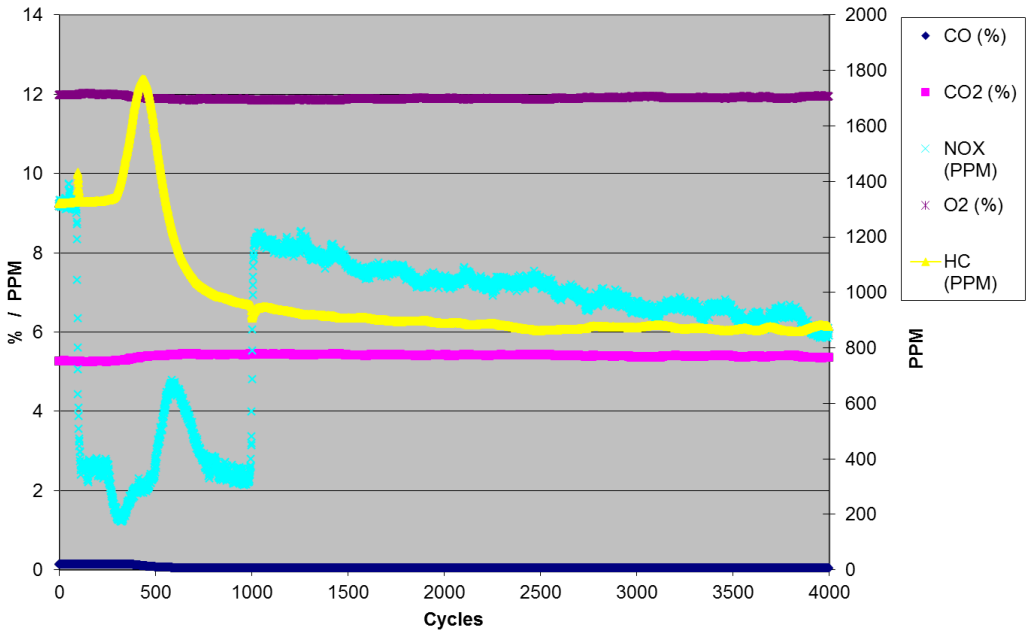


**Figure A60: Emissions at operation point number 5.**

**Table A62: Average concentrations shown at Figure A60 during upstream conditions.**

| | CO (%) | CO2 (%) | HC (PPM) | NOX (PPM) | O2 (%) |
|---|---|---|---|---|---|
| NOx | 0.140088 | 5.265802 | 1,326.873 | 9.000543 | 11.97782 |
| NO | 0.142401 | 5.250555 | 1,328.539 | 2.646566 | 12.00433 |

**Table A63: Average concentrations shown at Figure A60 during downstream conditions.**

| | CO (%) | CO2 (%) | HC (PPM) | NOX (PPM) | O2 (%) |
|---|---|---|---|---|---|
| NO | 0.074422 | 5.38504 | 1,246.722 | 2.719231 | 11.89925 |
| NOx | 0.041644 | 5.402821 | 885.3334 | 7.092501 | 11.89158 |

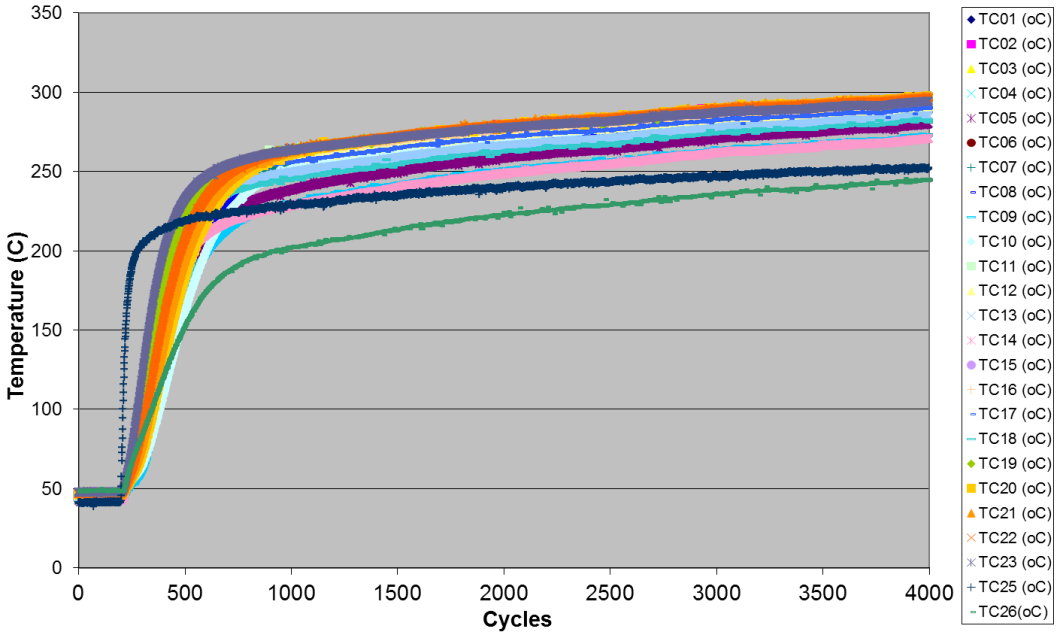


**Figure A61: Thermocouples temperature profile at operation point number 5.**

To see in more detail what happens with HC and NOx when the gases start passing through the catalyst, Figure A62 shows the 600 first cycles of the test, with the right hand “y” axis representing the PPM of HC and the left hand “y” axis the PPM of NOx and the rest of the gases in %.

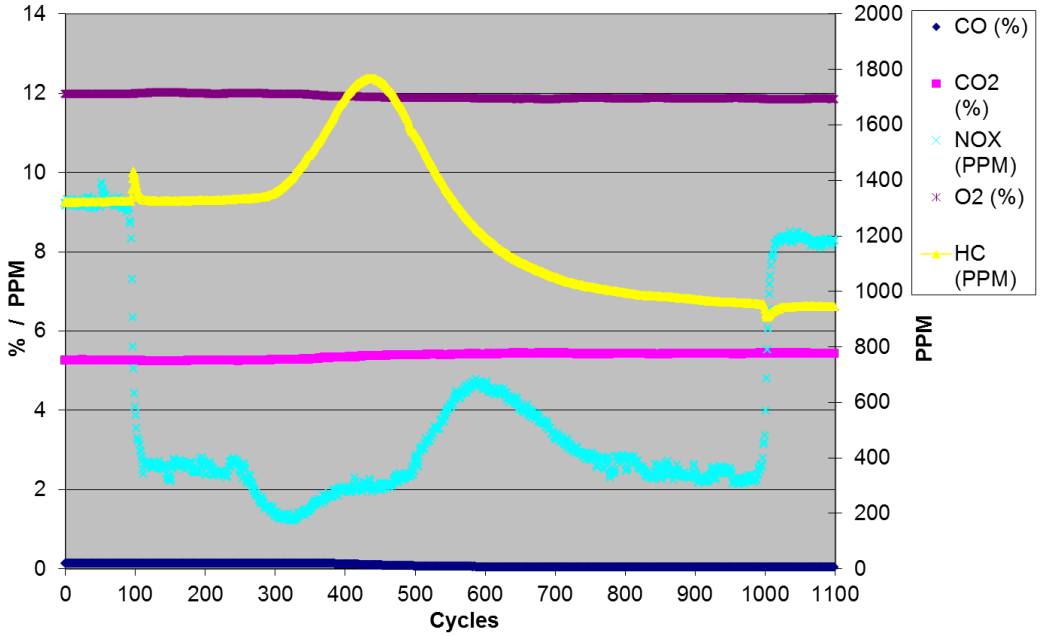


**Figure A62: Emissions at operation point number 5. Cycles 1-1100.**

When the sensor is switched from NOx to NO (at cycle 100), we can see that the amount of NO is lower than NOx, but in smaller amounts due that we are talking about 9 ppm to 3 ppm. The conversion pattern is not as obvious as test (3), but anyhow, you can notice the tendency of the curves towards the conversion.

6. Table A64 specifies some of the operation conditions at this operation point. Figure A63 shows the emissions patterns and Table A65 the respective average of the concentrations. At this point NOx/NO sensor is measuring **NOx** emissions during the first 100 cycles, and the second hundred measuring **NO**. These results were taken from **upstream** (before the catalyst).

**Table A64: Average operation conditions at point number 6.**

| | Air M.F. (g/s) | Liquid Fuel M.F. (mg/s) | Lambda | Compression Ratio | Liquid PI PW (ms) | Cat. Space Vol. Flow (exchanges/hr) |
|---|---|---|---|---|---|---|
| NOx | 4.6153 | 140.973 | 2.15917 | 6.299199 | 11.1 | 81,038.05 |
| NO | 4.6264 | 141.288 | 2.15871 | 6.299199 | 11.1 | 81,232.64 |

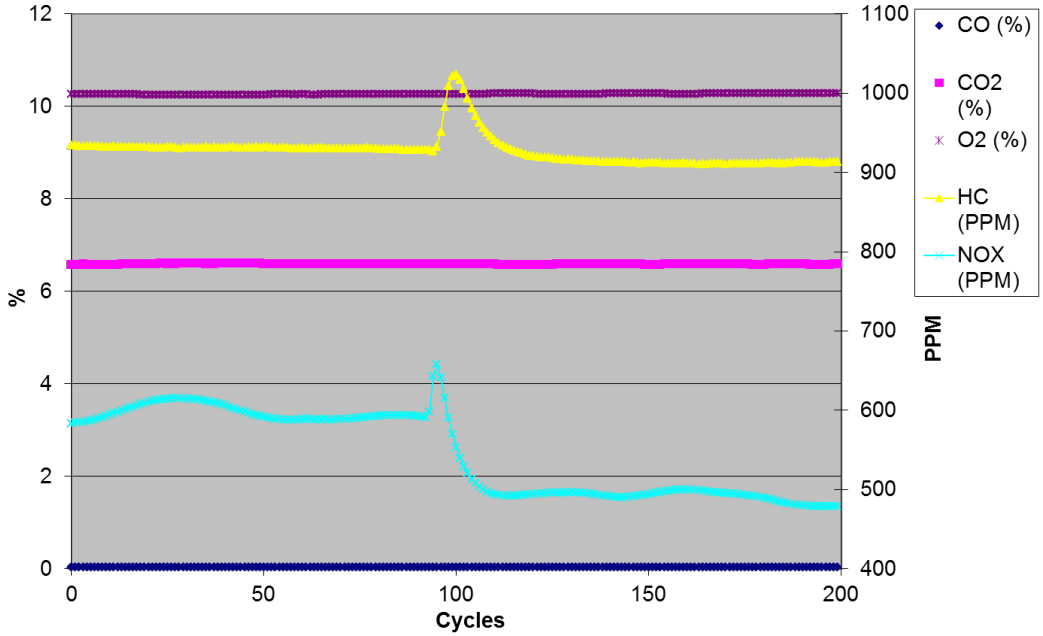


**Figure A63: Emissions at operation point number 6.**

**Table A65: Average concentrations shown at Figure A63.**

| | CO (%) | CO2 (%) | HC (PPM) | NOX (PPM) | O2 (%) |
|---|---|---|---|---|---|
| NOx | 0.033594 | 6.592788 | 934.7032 | 598.158 | 10.25862 |
| NO | 0.033286 | 6.586602 | 920.7733 | 493.7749 | 10.27735 |

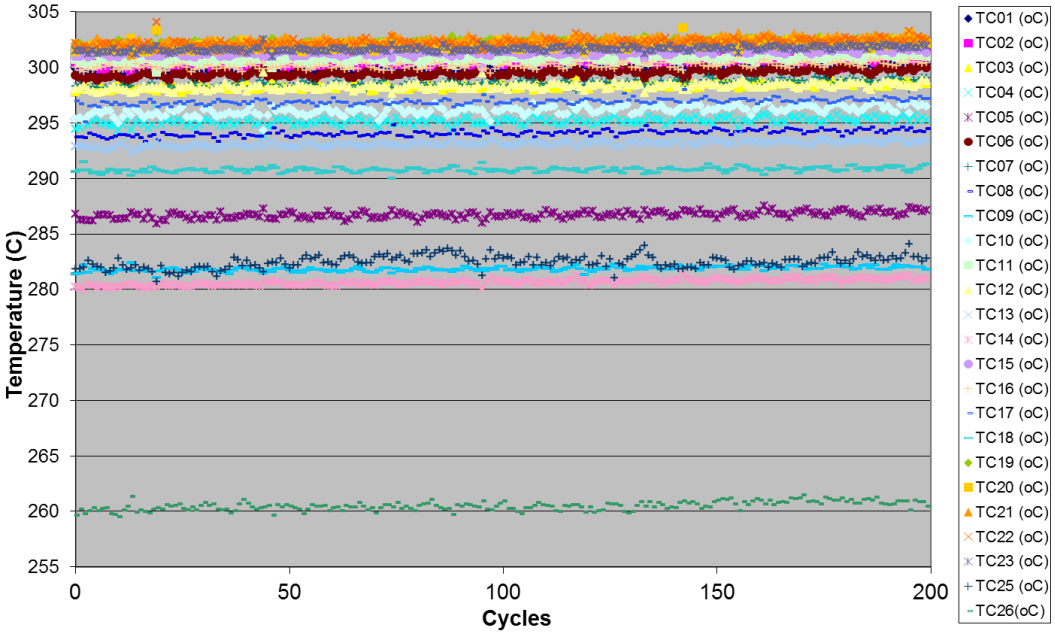


**Figure A64: Thermocouples temperature profile at operation point number 6.**

7. Same as 6, but downstream. Table A66 specifies some of the operation conditions at this operation point. Figure A65 shows the emissions patterns and Table A67 the respective average of the concentrations. At this point NOx/NO sensor is measuring **NOx** emissions during the first 100 cycles, and the second hundred measuring **NO**. These results were taken from **downstream** (after catalyst).

**Table A66: Average operation conditions at point number 7.**

| | Air M.F. (g/s) | Liquid Fuel M.F. (mg/s) | Lambda | Compression Ratio | Liquid PI PW (ms) | Cat. Space Vol. Flow (exchanges/hr) |
|---|---|---|---|---|---|---|
| NOx | 4.6343 | 141.142 | 2.1704 | 6.299199 | 11.1 | 81,368.33 |
| NO | 4.6348 | 140.441 | 2.18039 | 6.299199 | 11.1 | 81,374.8 |

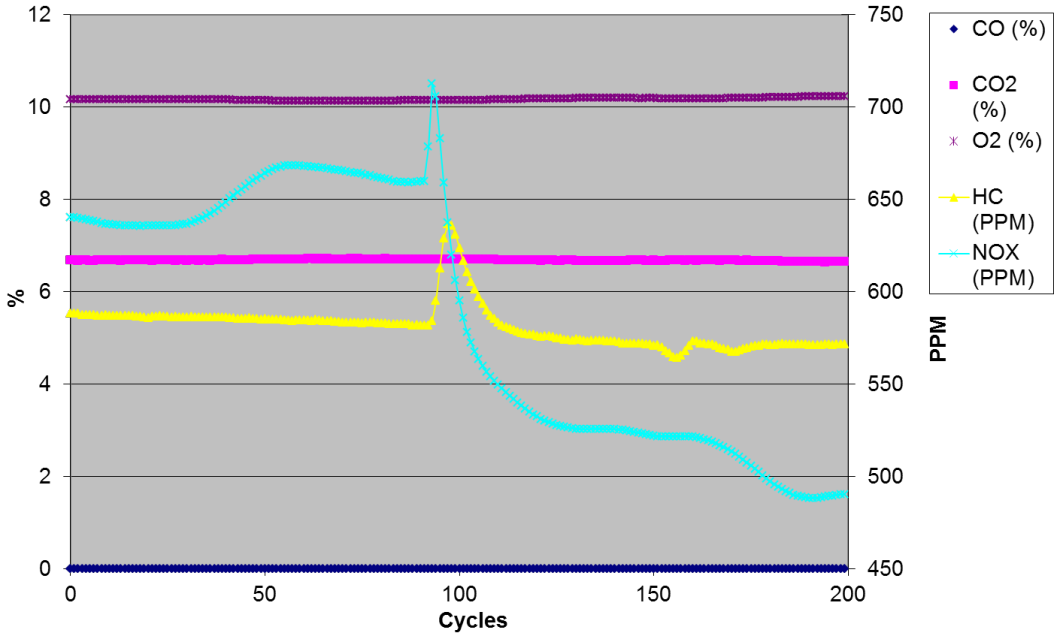


**Figure A65: Emissions at operation point number 7.**

**Table A67: Average concentrations shown at Figure A65.**

| | CO (%) | CO2 (%) | HC (PPM) | NOX (PPM) | O2 (%) |
|---|---|---|---|---|---|
| NOx | 0.004616 | 6.696872 | 586.6347 | 653.6959 | 10.15642 |
| NO | 0.004297 | 6.679741 | 576.5228 | 523.4883 | 10.1941 |

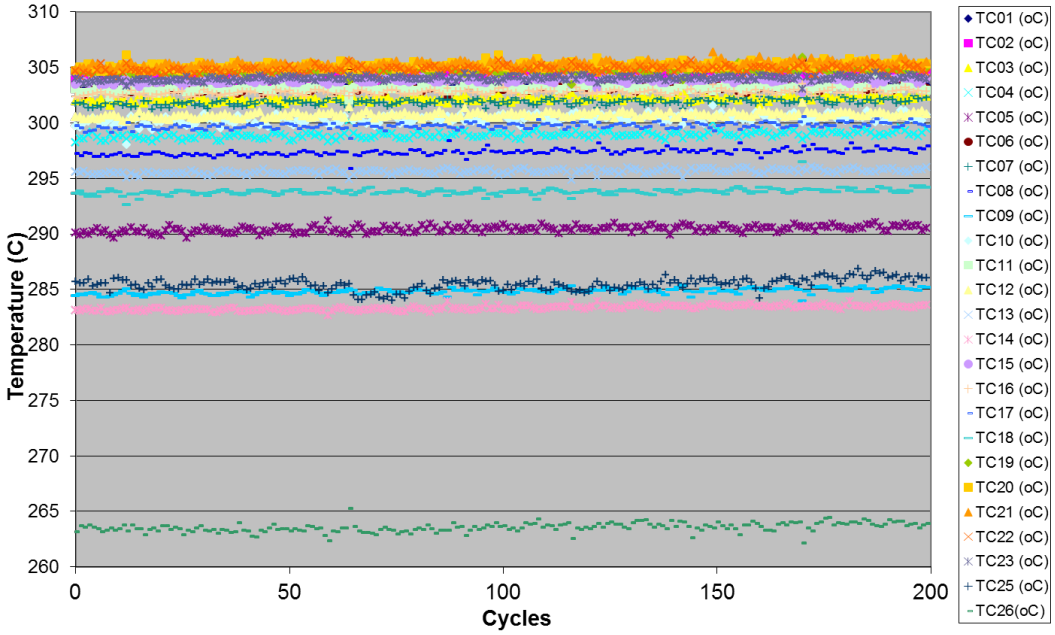


**Figure A66: Thermocouples temperature profile at operation point number 7.**

Discussion of tests 6-7: From **upstream** to **downstream**: **HC**, decreases from almost 900 ppm to 570 ppm. **NOx** seems to increase and **NO** is unstable, but at the end of the downstream is at the same level that at the upstream. **$CO_2$** increases but it is almost imperceptible. **$O_2$** and **CO** decrease in a very small amount.

8. Table A68 specifies some of the operation conditions at this operation point. Figure A67 shows the emissions patterns and Table A69 the respective average of the concentrations. At this point NOx/NO sensor is measuring **NOx** emissions during the first 100 cycles, and the second hundred measuring **NO**. These results were taken from **upstream** (before the catalyst).

**Table A68: Average operation conditions at point number 8.**

| | Air M.F. (g/s) | Liquid Fuel M.F. (mg/s) | Lambda | Compression Ratio | Liquid PI PW (ms) | Cat. Space Vol. Flow (exchanges/hr) |
|---|---|---|---|---|---|---|
| NOx | 3.4669 | 115.706 | 1.97656 | 6.299199 | 8.9 | 60,921.96 |
| NO | 3.4602 | 115.986 | 1.97116 | 6.299199 | 8.9 | 60,807.15 |

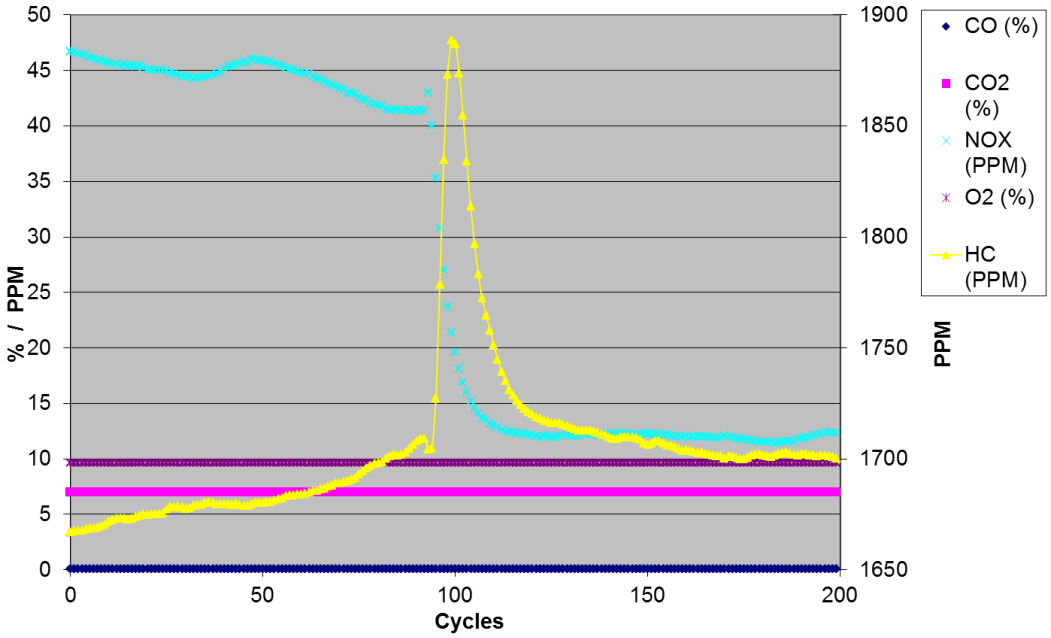


**Figure A67: Emissions at operation point number 8.**

**Table A69: Average concentrations shown at Figure A67.**

| | CO (%) | CO2 (%) | HC (PPM) | NOX (PPM) | O2 (%) |
|---|---|---|---|---|---|
| NOx | 0.083051 | 7.00677 | 1,692.364 | 43.27972 | 9.64445 |
| NO | 0.083366 | 7.011684 | 1,718.105 | 12.33772 | 9.647369 |

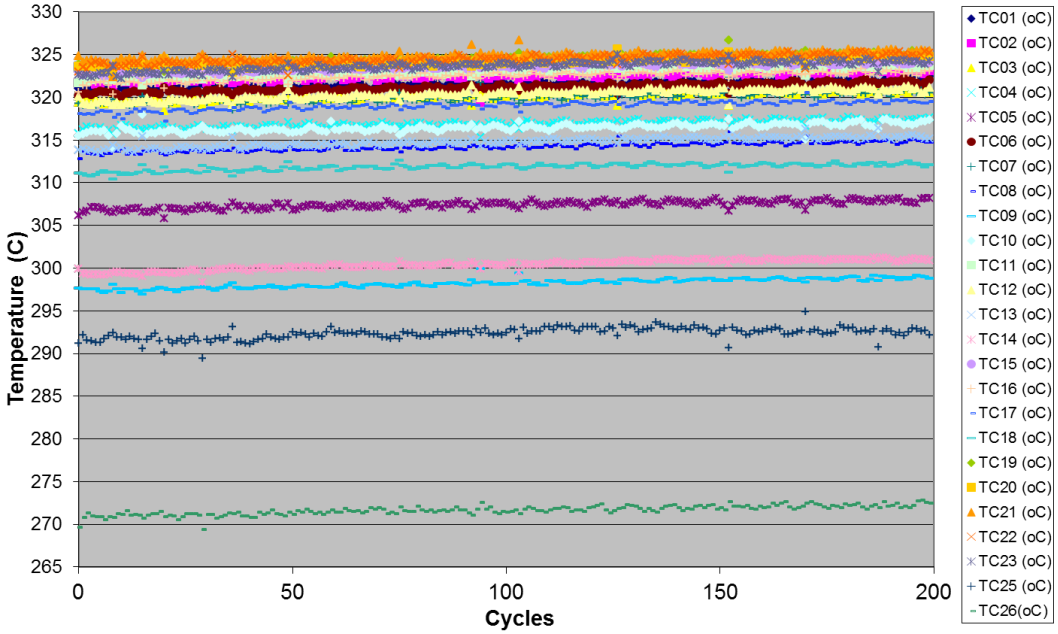


**Figure A68: Thermocouples temperature profile at operation point number 8.**

9. Same as 8, but downstream. Table A70 specifies some of the operation conditions at this operation point. Figure A69 shows the emissions patterns and Table A71 the respective average of the concentrations. At this point NOx/NO sensor is measuring **NOx** emissions during the first 100 cycles, and the second hundred measuring **NO**. These results were taken from **downstream** (after catalyst).

**Table A70: Average operation conditions at point number 9.**

| | Air M.F. (g/s) | Liquid Fuel M.F. (mg/s) | Lambda | Compression Ratio | Liquid PI PW (ms) | Cat. Space Vol. Flow (exchanges/hr) |
|---|---|---|---|---|---|---|
| NOx | 3.466 | 113.67 | 2.0163 | 6.299199 | 8.9 | 60,900.52 |
| NO | 3.472 | 113.59 | 2.0202 | 6.299199 | 8.9 | 61,004.44 |

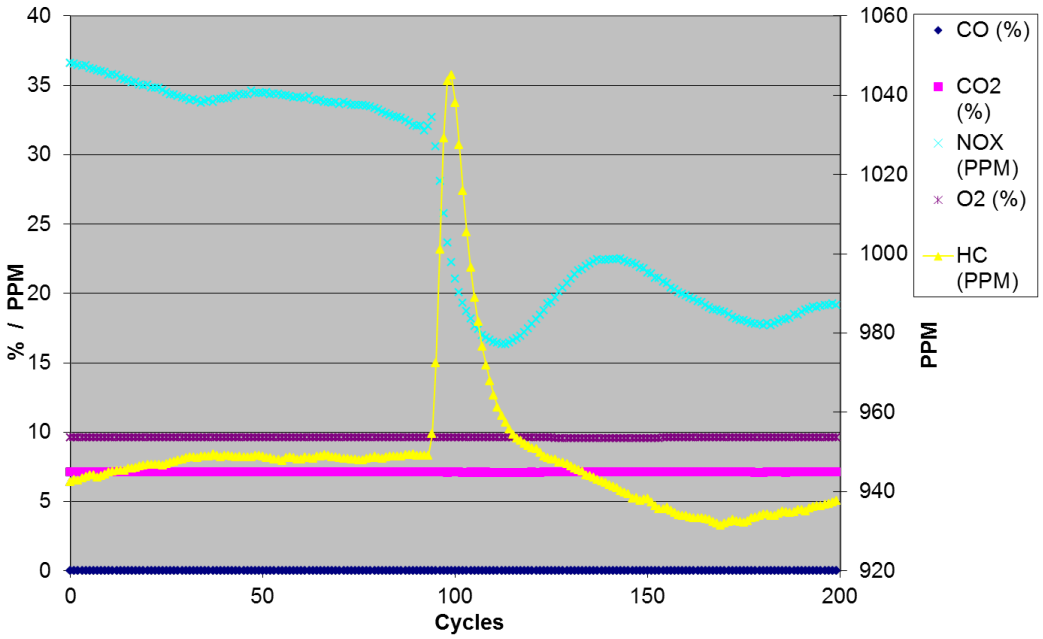


**Figure A69: Emissions at operation point number 9.**

**Table A71: Average concentrations shown at Figure A69.**

| | CO (%) | CO2 (%) | HC (PPM) | NOX (PPM) | O2 (%) |
|---|---|---|---|---|---|
| NOx | 0.023558 | 7.099255 | 952.1266 | 33.68679 | 9.595422 |
| NO | 0.024283 | 7.104652 | 944.8967 | 19.34439 | 9.596168 |

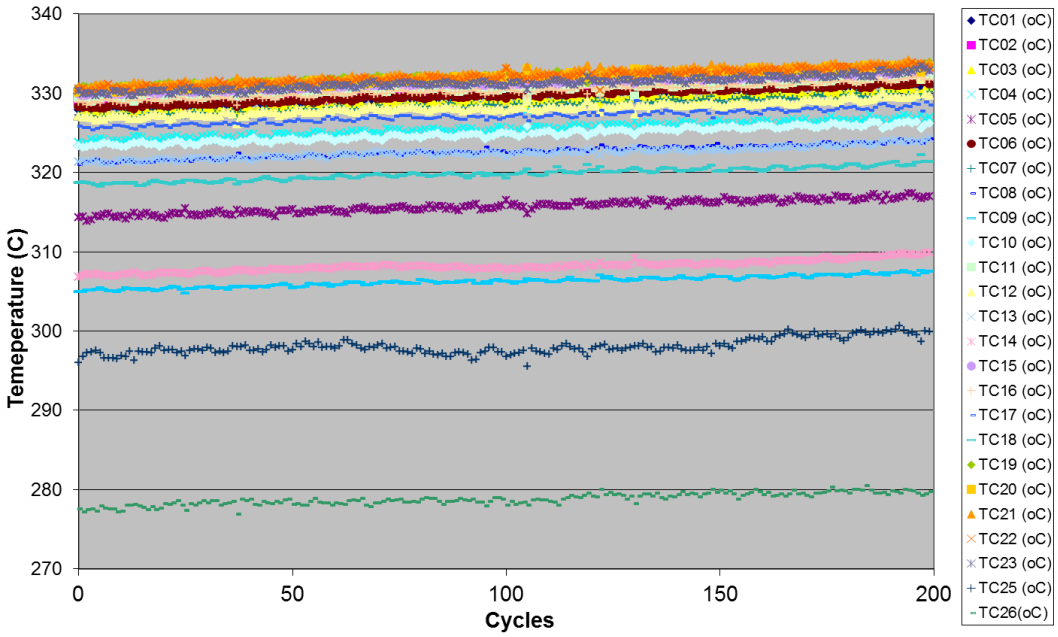


**Figure A70: Thermocouples temperature profile at operation point number 9.**

Discussion of tests 8-9: From **upstream** to **downstream**: **HC** decreases from almost 1680 ppm to about 940 ppm. **NOx**, decreases from 44 ppm to 34 ppm and **NO** increases from 12 ppm to 20 ppm. **$CO_2$** increases but it is almost imperceptible. **$O_2$** and **CO** decrease in a very small amount.

10. Table A72 specifies some of the operation conditions at this operation point. Figure A71 shows the emissions patterns and Table A73 the respective average of the concentrations. At this point NOx/NO sensor is measuring **NOx** emissions during the first 100 cycles, and the second hundred measuring **NO**. These results were taken from **upstream** (before the catalyst).

**Table A72: Average operation conditions at point number 10.**

| | Air M.F. (g/s) | Liquid Fuel M.F. (mg/s) | Lambda | Compression Ratio | Liquid PI PW (ms) | Cat. Space Vol. Flow (exchanges/hr) |
|---|---|---|---|---|---|---|
| NOx | 2.6338 | 117.25 | 1.495 | 6.299199 | 8.6 | 46,430.95 |
| NO | 2.6378 | 113.71 | 1.5318 | 6.299199 | 8.6 | 46,483.21 |

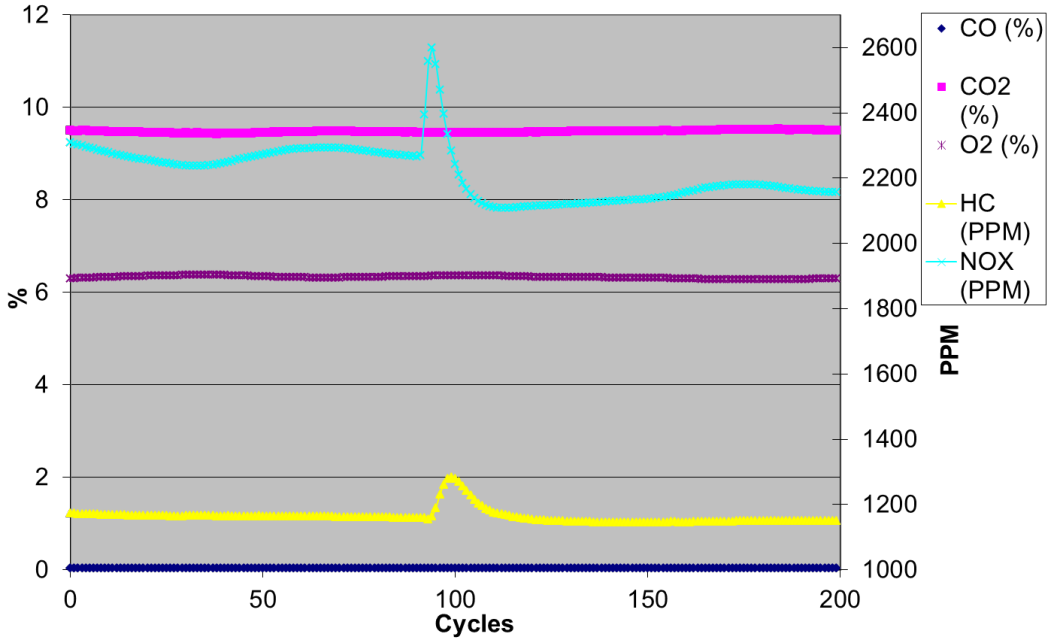


**Figure A71: Emissions at operation point number 10.**

**Table A73: Average concentrations shown at Figure A71.**

| | CO (%) | CO2 (%) | HC (PPM) | NOX (PPM) | O2 (%) |
|---|---|---|---|---|---|
| NOx | 0.037072 | 9.463089 | 1,170.19 | 2,285.108 | 6.345443 |
| NO | 0.037388 | 9.489766 | 1,156.764 | 2,145.493 | 6.313134 |

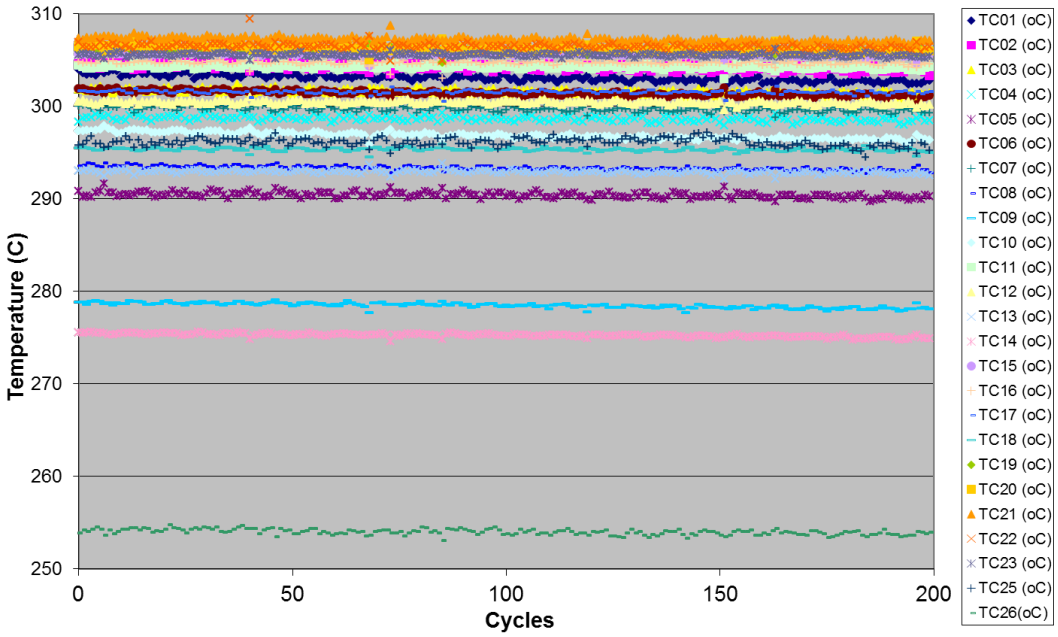


**Figure A72: Thermocouples temperature profile at operation point number 10.**

11. Same as 10, but downstream. Table A74 specifies some of the operation conditions at this operation point. Figure A73 shows the emissions patterns and Table A75 the respective average of the concentrations. At this point NOx/NO sensor is measuring **NOx** emissions during the first 100 cycles, and the second hundred measuring **NO**. These results were taken from **downstream** (after catalyst).

**Table A74: Average operation conditions at point number 11.**

| | Air M.F. (g/s) | Liquid Fuel M.F. (mg/s) | Lambda | Compression Ratio | Liquid PI PW (ms) | Cat. Space Vol. Flow (exchanges/hr) |
|---|---|---|---|---|---|---|
| NOx | 2.638 | 113.10 | 1.5450 | 6.299199 | 8.6 | 46,492.66 |
| NO | 2.629 | 113.30 | 1.5368 | 6.299199 | 8.6 | 46,342.22 |

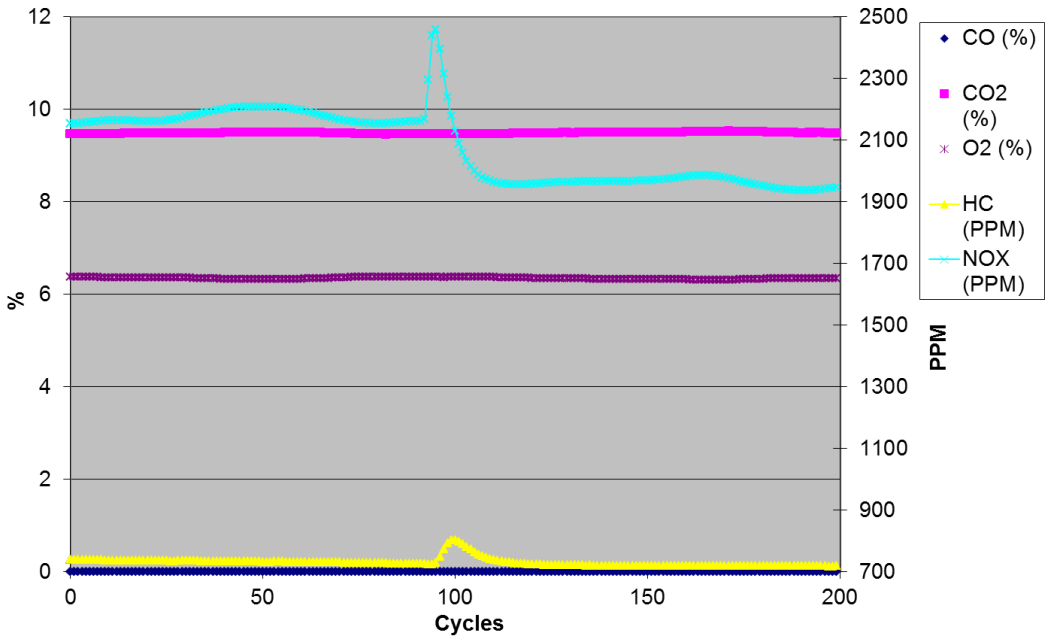


**Figure A73: Emissions at operation point number 11.**

**Table A75: Average concentrations shown at Figure A73.**

| | CO (%) | CO2 (%) | HC (PPM) | NOX (PPM) | O2 (%) |
|---|---|---|---|---|---|
| NOx | 0.010349 | 9.484303 | 736.2903 | 2,186.672 | 6.359571 |
| NO | 0.010332 | 9.499299 | 725.9808 | 1,967.346 | 6.34325 |

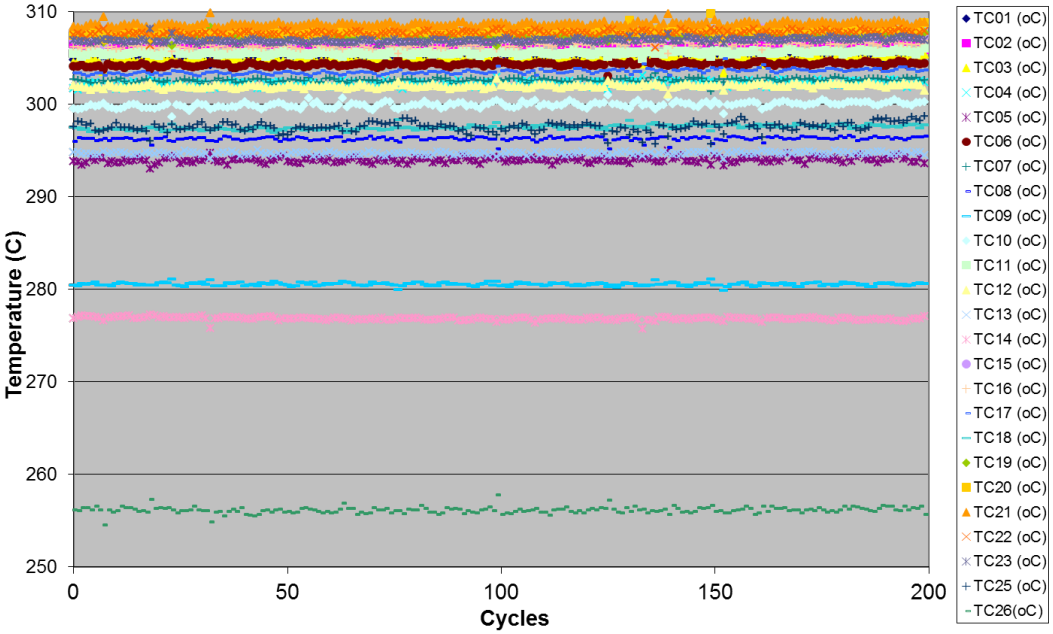


**Figure A74: Thermocouples temperature profile at operation point number 11.**

Discussion of tests 10-11: From **upstream** to **downstream**: **HC**, decreases from almost 1130 ppm to about 710 ppm. **NOx**, decreases from 2300 ppm to about 2200 ppm and **NO** decreases from 2190 ppm to 1940 ppm. **$CO_2$**, **$O_2$** and **CO** seem to be almost the same.

References

[1] M. Shahbakhti, A. Ghazimirsaied, C.R. Koch, Experimental study of exhaust temperature variation in a homogeneous charge compression ignition engine, Proceedings of the Institution of Mechanical Engineers Part D-Journal of Automobile Engineering, 224 (2010) 1177-1197.